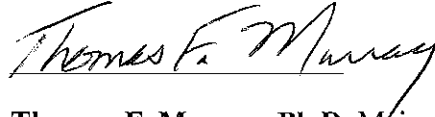


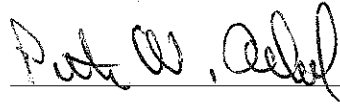


DISSERTATION APPROVED BY

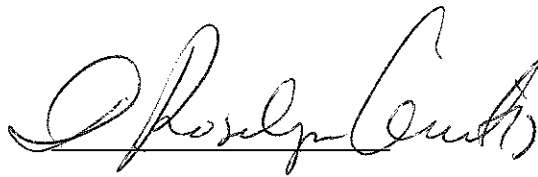
\_\_\_\_\_  
Date



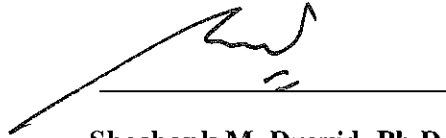
**Thomas F. Murray, Ph.D, Major Advisor**



**Peter W. Abel, Ph.D**



**Roselyn D. Cerutis, Ph.D**



**Shashank M. Dravid, Ph.D**



**Gail M. Jensen, Ph.D, Dean**

**INFLUENCE OF SODIUM CHANNEL ACTIVATION ON NMDA  
RECEPTOR-MEDIATED STRUCTURAL PLASTICITY**

**BY**

**JOJU GEORGE**

**A Dissertation Submitted to the Graduate Faculty of the Creighton University in  
Partial Fulfillment of the Requirements for the Degree of**

**DOCTOR OF PHILOSOPHY**

**Department of Pharmacology**

**Omaha, Nebraska**

**2010**

© 2010

**JOJU GEORGE**

**All Rights Reserved**

## ABSTRACT

Neuronal activity regulates morphology and connectivity of neurons during development. Many aspects of activity-dependent neuronal development such as dendritic arborization, spinogenesis and synaptogenesis are mediated via N-methyl D-aspartate receptor (NMDAR)-dependent signaling mechanisms. Inasmuch as neuronal activity involves activation of voltage-gated sodium channels (VGSCs) primarily, in this study, we used a sodium channel activator, brevetoxin-2 (PbTx-2) to mimic neuronal activity. Brevetoxins interact with binding site 5 on the  $\alpha$  subunit of VGSCs. PbTx-2 was found to increase intracellular sodium concentration ( $[Na^+]_i$ ) in immature cerebrocortical neurons above the critical threshold for upregulating NMDAR function. Hence PbTx-2 was used to explore the relationship between  $[Na^+]_i$  and NMDAR-dependent structural plasticity in developing cerebrocortical neurons. Exposure to PbTx-2 was found to sensitize immature neurons to NMDA-induced  $Ca^{2+}$  influx through a Src family kinase (SFK)-dependent pathway. The effects of PbTx-2 on upregulating NMDAR function did not involve depolarization of the neurons as explained by the modest membrane potential change in FMP (FLIPR<sup>®</sup> membrane potential) blue fluorescence assay and confirmed by the cell attached patch recordings. We found that chronic exposure to low concentration of PbTx-2 (30 nM) accelerated the appearance of spontaneous calcium oscillations in cerebrocortical neurons, which could be indicative of enhanced or accelerated functional network and synapse formation. Acute exposure to PbTx-2 increased cell surface expression of NR2B containing NMDARs and TrkB receptors (high affinity receptor for Brain-derived neurotrophic factor, BDNF) as observed in the surface biotinylation assay, demonstrating direct evidence for the ability of PbTx-2 to sensitize neurons for signaling

downstream of NMDAR and BDNF. Further, effects of PbTx-2 on various aspects of neuronal plasticity were investigated. We observed that treatment with PbTx-2 enhanced neurite outgrowth, dendritic arborization, spinogenesis and synaptogenesis. All the aspects of neuronal plasticity exhibited a biphasic concentration-response profile with 30 and 100 nM PbTx-2 having the most robust effect. Biphasic nature of these data can be explained by lower concentrations not sufficient enough to initiate signaling and higher concentrations resulting in internalization of VGSCs as shown in the whole cell binding assay. We also found that exposure to NMDA produced a neurite outgrowth response with similar hormetic profile suggesting engagement of similar signaling mechanisms in PbTx-2 and NMDA-induced neuronal morphogenesis. Pharmacological evaluation of PbTx-2 induced neuronal plasticity showed that it was mediated by signaling mechanisms downstream of NMDAR resulting in the activation of CaMKK (Calcium/calmodulin-dependent protein kinase kinase) and CaMKII (Calcium/calmodulin-dependent protein kinase II) pathway. The signaling mechanisms underlying PbTx-2 stimulated neuronal structural plasticity also involved activation of transcription factor CREB and initiation of further nuclear signaling events that resulted in increased BDNF gene expression. Also, PbTx-2 exposure was able to regulate actin dynamics locally by activation of Rho family GTPases, Rac and Cdc42. These findings suggest that the influence of a sodium channel activator on neuronal development involves NMDAR-mediated Calcium/calmodulin-dependent protein kinase (CaMK) signaling with downstream activation of CREB (Cyclic AMP response element binding protein)-dependent transcription of BDNF.

**Keywords:**

Activity- dependent plasticity, PbTx-2, VGSCs, NMDAR, BDNF, CaMKK, CaMKII, Rho family GTPases, spontaneous calcium oscillations, neurite outgrowth, dendritic arborization, spinogenesis, synaptogenesis.

## PREFACE

### PUBLICATIONS:

**Joju George**, Shashank Dravid, Anand, Prakash, Jun Xie, Jennifer Peterson, Sairam V. Jabba, Daniel G. Baden and Thomas F. Murray (2009) Sodium channel activation augments NMDA receptor function and promotes neurite outgrowth in immature cerebrocortical neurons. *Journal of Neuroscience*, 29 (10):3288-301.

**Joju George**, Karmel V. Headen, Afolabi Ogunleye, Greg A. Perry, Terrence Wilwerding, Lawrence C. Parrish, Timothy P. McVaney, John S. Mattson, and D. Roselyn Cerutis (2009) Lysophosphatidic acid signals through specific LPA receptor subtypes to control key regenerative responses of human gingival and periodontal ligament fibroblasts. *Journal of Periodontology*, 80 (8):1338-47.

Zhengyu Cao, **Joju George**, William H. Gerwick , Daniel G. Baden , Jon D. Rainier, Thomas F. Murray (2008) Influence of lipid soluble gating modifier toxins on sodium influx in neocortical neurons. *Journal of Pharmacology and Experimental Therapeutics*, 326 (2):604-13.

Zhengyu Cao, **Joju George**, Daniel G. Baden, Thomas F. Murray (2007) Brevetoxin-induced phosphorylation of Pyk2 and Src in murine neocortical neurons involves distinct signaling pathways. *Brain Research*, 1184:17-27.

## **PUBLISHED ABSRACTS:**

**Joju George** and Thomas F. Murray (2010) Sodium channel activator-induced neuronal development is NMDA receptor dependent and involves a  $\text{Ca}^{2+}$ /calmodulin kinase (CaMK)-CREB-BDNF signaling pathway. *FASEB Journal*, 770.11.

Thomas F. Murray, Eric Busse, **Joju George** (2009) Voltage-gated sodium channel activators with differing efficacies stimulate neurite outgrowth in cerebrocortical neurons Location. *Nanosymposium*, Society for neuroscience, 9.9.

**Joju George** and Thomas F. Murray (2009) Sodium channel activation modulates synchronized calcium oscillations and neuronal morphology in immature cerebrocortical neurons. *FASEB Journal*, 23:946.1

**Joju George**, Zhengyu Cao and Thomas F Murray (2008) Brevetoxin sensitizes immature cerebrocortical neurons to NMDA receptor signaling through activation of voltage-gated sodium channels. *FASEB Journal*, 22:721.6.

D. Roselyn Cerutis, **Joju George**, Karmel V. Headen, Stephanie A. Brady, Nancy A. Schulte, Myron L. Toews, Lawrence C. Parrish, Timothy P. McVaney, Terry M. Wilwerding and John S. Mattson (2008) Lysophosphatidic acid receptor subtype-specific regulation of human oral fibroblast healing responses. *FASEB Journal*, 22:805.10.

Thomas F. Murray, Jun Xie, Jennifer Peterson, **Joju George**, Daniel G. Baden (2007) Brevetoxin activation of voltage-gated sodium channels stimulates neurite outgrowth in immature cerebrocortical neurons. Society for Neuroscience, 34.13/E9

**DEDICATION**

**To**

**My Beloved Family**

## **ACKNOWLEDGEMENTS**

I would like to thank Dr. Thomas F. Murray for providing me this great opportunity to work under his guidance. His constant inspiration and constructive suggestions kept me encouraged and focused throughout my studies. I would like to thank all the members of Murray lab, past and present for all the help rendered to me. I wish to express my sincere thanks to all my committee members for giving me advices and great suggestions at every stage of my research. I will always remember the staff of the Department of Pharmacology with gratitude. Finally I express my deep love and warmest thanks to my wife Lakshmi and our bundles of joy, Ankit and Ritvik.

# TABLE OF CONTENTS

	<b>Page</b>
<b>ACKNOWLEDGEMENTS .....</b>	<b>ix</b>
<b>LIST OF TABLES.....</b>	<b>xi</b>
<b>LIST OF FIGURES.....</b>	<b>xii</b>
<b>CHAPTER</b>	
<b>1. INTRODUCTION AND REVIEW OF LITERATURE.....</b>	<b>1</b>
<b>2. SODIUM CHANNEL ACTIVATION AUGMENTS NMDA RECEPTOR FUNCTION AND PROMOTES NEURITE OUTGROWTH IN IMMATURE CEREBROCORTICAL NEURONS.....</b>	<b>52</b>
<b>3. INTRACELLULAR SODIUM REGULATION OF NMDA RECEPTOR- DEPENDENT NEURONAL PLASTICITY.....</b>	<b>77</b>
<b>4. SUMMARY AND CONCLUSIONS.....</b>	<b>168</b>

## LIST OF TABLES

	Page
<b>Table 1: Receptor sites on sodium channels.....</b>	<b>30</b>
<b>Table 2.2: EC<sub>50</sub> and 95% confidence intervals derived from the NMDA concentration-response in the presence and absence of 30 nM PbTx-2 .....</b>	<b>56</b>

## LIST OF FIGURES

	Page
<b>Figure 1: Stages of morphological differentiation of neurons.....</b>	<b>3</b>
<b>Figure 2: Filopodia formation and spinogenesis.....</b>	<b>6</b>
<b>Figure 3: Structure of NMDA receptors.....</b>	<b>12</b>
<b>Figure 4: Structure of Voltage-gated sodium channels.....</b>	<b>29</b>
<b>Figure 2.1: NMDA-induced excitotoxicity in immature cerebrocortical neurons</b> <b>.....</b>	<b>55</b>
<b>Figure 2.2: PbTx-2 augments NMDA-induced Ca<sup>2+</sup> influx in immature</b> <b>cerebrocortical neurons as a function of culture age.....</b>	<b>56</b>
<b>Figure 2.3: Effect of 30 nM PbTx-2 on NMDA-induced Ca<sup>2+</sup> influx in immature</b> <b>cerebrocortical neurons.....</b>	<b>57</b>
<b>Figure 2.4: Pharmacological evaluation of PbTx-2-induced potentiation of</b> <b>NMDA-induced Ca<sup>2+</sup> influx in DIV-2 cerebrocortical neurons.....</b>	<b>57</b>
<b>Figure 2.5: PbTx-2 increases intracellular sodium levels in DIV-2 cerebrocortical</b> <b>neurons.....</b>	<b>58</b>
<b>Figure 2.6: PbTx-2-evoked change in membrane potential in DIV-2</b>	



<b>Figure 2.S7: Schematic diagram for pathways involved in PbTx-2 stimulation of neurite outgrowth.....</b>	<b>76</b>
<b>Figure 3.1: PbTx-2 enhanced neurite outgrowth exhibits a hormetic profile similar to the NMDA response.....</b>	<b>143</b>
<b>Figure 3.2: PbTx-2-induced Ca<sup>2+</sup> influx and pharmacological evaluation in cerebrocortical neurons.....</b>	<b>144</b>
<b>Figure 3.3: Influence of PbTx-2 on cell surface channel and receptor expression .....</b>	<b>147</b>
<b>Figure 3.4: PbTx-2 exposure enhances dendritic arborization.....</b>	<b>152</b>
<b>Figure 3.5: PbTx-2 enhances spinogenesis by stimulating increased filopodia formation.....</b>	<b>154</b>
<b>Figure 3.6: Ontogeny of spontaneous Ca<sup>2+</sup> oscillations in cerebrocortical neurons.....</b>	<b>155</b>
<b>Figure 3.7: PbTx-2 exposure accelerated the emergence of spontaneous Ca<sup>2+</sup> oscillations.....</b>	<b>156</b>
<b>Figure 3.8: Effect of PbTx-2 on formation of synapses in cerebrocortical neuron cultures.....</b>	<b>158</b>

<b>Figure 3.9: Signaling mechanisms underlying PbTx-2-induced neuronal</b>	
<b>plasticity.....</b>	<b>163</b>
<b>Figure 3.10: PbTx-2-induced concentration-dependent activation of CREB</b>	
<b>(Ser133) and pharmacological evaluation of CREB phosphorylation.</b>	
<b>.....</b>	<b>164</b>
<b>Figure 3.11: PbTx-2 increases BDNF mRNA expression in a time and</b>	
<b>concentration-dependent manner.....</b>	<b>165</b>
<b>Figure 3.12: Involvement of Rho family GTPases.....</b>	<b>167</b>

## CHAPTER 1

### INTRODUCTION AND REVIEW OF LITERATURE:

#### A. Neuronal development:

Neuronal development is a very complex process. Once the neurons are formed, they undergo morphological differentiation to become mature neurons. The morphological property a neuron acquires is tightly correlated to its neuronal function. Different types of neuronal populations exhibit distinct morphological characteristics based on their function. This type-specific morphology appears to be specified by genetic programs (Jan and Jan, 2003). The morphological differentiation process begins shortly after the neurons become postmitotic and proceeds through distinguishable stages. These stages include initiation or growth cone formation, lengthening or neurite outgrowth, axon differentiation, dendritic branching or arborization, spine formation or spinogenesis and establishment of neuronal connectivity or synapse formation (synaptogenesis) (Fig. 1). Although these stages may overlap with one another, the sequence of events is very distinct in the process of dendritogenesis. Although the initial dendritic growth is relatively slow, further dendritic extension is a very fast process. Subsequently, the molecular guidance mechanisms establish polarity and distinguish axon from dendritic processes which initiates axonal differentiation. Dendritic arborization is a very dynamic process which includes branch addition, elimination and stabilization of the dendritic arbor. The development of dendritic arbor occurs with high rate of branch addition and retraction while stabilization process occurs over a long period of time. Although mature

neurons show a very low branch turnover under basal conditions, they preserve some degree of plasticity (Wong and Ghosh, 2002; Chen and Ghosh, 2005; Redmond, 2008)

Stages in dendritic arbor development are regulated by both an intrinsic genetic program and a wide variety of extracellular signals, either globally at the whole-cell level or locally in dendrites (Urbanska et al., 2008). Transcription factors play a pivotal role by their effects on the intrinsic genetic program. The developmental studies in *Drosophila melanogaster* neurons revealed the identification of various autonomously acting transcription factors, such as hamlet, Cut, Abrupt, spineless, etc in the process of dendritogenesis. In mammalian nervous system, less is known about similar transcription factors which determine dendritic patterning independently from extracellular signaling cues. Neurogenin2 (Ngn2), a basic helix-loop-helix factor that defines a specific pattern of dendritic arborization in pyramidal neurons in cerebral cortex (Hand et al., 2005) and Dlx homeobox transcription factors regulate dendritic branching in cortical interneurons (Cobos et al., 2007). Studies show that extracellular cues have an overwhelming influence on dendritic development. Depending on the developmental stage, a combination of diffusible or guidance cues, cell contacts and neuronal activity were shown to control dendritic arborization and plasticity (McAllister, 2000; Wong and Ghosh, 2002). Among the diffusible cues the important ones are brain-derived neurotrophic factor (BDNF), agrin, semaphoring 3A, Slit, reelin, bone morphogenetic protein family members and cpg15. Among cell contacts, the cell-cell interacting surface proteins like N-cadherin, EphrinB, Notch, cell adhesion moleculeL1 are some of the important factors regulating dendritic growth and branching. However, it is becoming increasingly apparent that neuronal activity has a profound influence on multiple aspects

of dendritic development. The effects of neuronal activity on dendritic development are mediated by intracellular calcium signals, and recent studies indicate that calcium-induced signaling events have both cytoplasmic and nuclear targets (Chen and Ghosh, 2005).

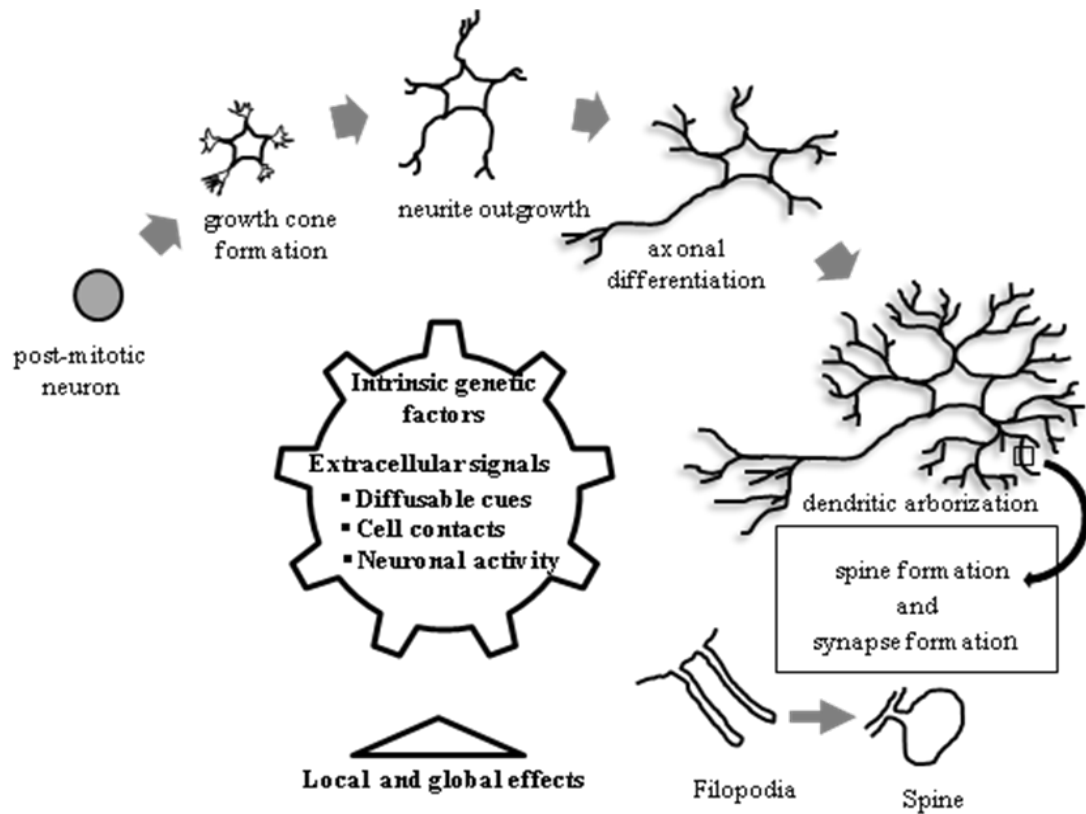


**Fig. 1** Stages of morphological differentiation of neurons.

## **B. Influence of activity on neuronal structural plasticity:**

### **(i) Activity-dependent dendritic growth and branching:**

The influence of neuronal activity on dendritic arborization has been demonstrated in several studies using activity deprivation experiments. Blockade or attenuation of activity leads to long lasting deficits in dendritic arborization. In xenopus, light-induced visual activity increases the growth of new dendritic branches and imparts stability in existing branches of tectal neurons (Sin et al., 2002). The exposure to an enriched environment or training on a motor-learning task has been reported to influence dendritic growth. Hippocampal neurons, but not neurons in the motor areas, from mice housed in an enriched environment showed larger dendritic trees and increased dendritic growth compared to littermates raised in standard or exercise cages (Faherty et al., 2003). It has been demonstrated in developing cerebellum that there is a precise relationship between afferent innervations and dendritic development. Afferent input by parallel fibers of granule cells is required for growth of purkinje cell dendrites into the molecular layer and experiments in which this input was disrupted, resulted in dramatic attenuation of purkinje cell arbors. Similar observation in other regions of developing nervous system indicate that afferent inputs have a considerable influence on dendritic development of their postsynaptic targets (Wong and Ghosh, 2002). Normal locomotor activity also appeared to be important for motor neuron dendrite elaboration (Inglis et al., 2000). Pharmacological blockade of spontaneous activity in *in vitro* slice cultures and in dissociated neurons caused decreased dendritic growth (Redmond et al., 2002).

## **(ii) Activity-dependent spine and synapse formation:**

Dendritic spines are specialized post synaptic protrusions with characteristic bulbous ending or spine heads at their tips. Spines are the sites of excitatory neurotransmission. Dendritic spines are first formed in early postnatal life, shaped up by animal's experience, and maintained into adulthood. Spines are very dynamic protrusions and they undergo morphological changes continuously throughout the life of an individual. Spines vary in their sizes and shapes and are classified as thin, stubby and mushroom. There is a strong correlation between size and shape of the spine head and strength of the synapse, presumably related to the higher levels of AMPA receptors in larger spines (Kasai et al., 2003). There is also evidence that it is the smaller weaker spines that preferentially undergo long-term potentiation (LTP), whereas larger spines are more stable and show less plasticity (Matsuzaki et al., 2004). Such observation have led to the idea that thin spines might represent 'plasticity spines' and large mushrooms' memory spines' (Kasai et al., 2003). Dendritic filopodia are the precursors of spines. They are highly motile, long, thin, headless and most often PSD-free protrusions abundantly present in developing neurons. Due to their highly motile nature, filopodia repeatedly make transient contacts with axons, however only a selected subset of these contacts is stabilized. After the formation of the stabilized contacts, the dendritic filopodia transform to functional spines and initiates the process of excitatory synapse formation (Tada and Sheng, 2006)

Though little is known about the molecular and cellular mechanisms underlying the formation and maintenance of dendritic filopodia, the transformation from filopodia to spines, and the physiological significance of dendritic filopodia, several functional

molecules have been recently identified, which regulate the formation of dendritic filopodia (Fig. 2). These molecules are classified as ‘accelerators’ and ‘brakes’. The accelerators include CaMKII, syndecan-2 and paralemmin-1, which enhance filopodia formation and further accelerate spine maturation, whereas ‘brakes’ slow spine maturation and sometimes even causing spine-to-filopodia reversion. Telencephalin is an important ‘brake’ molecule, which is a dendrite-associated adhesion molecule specifically expressed by spiny neurons in mammalian telencephalon (Yoshihara et al., 2009)

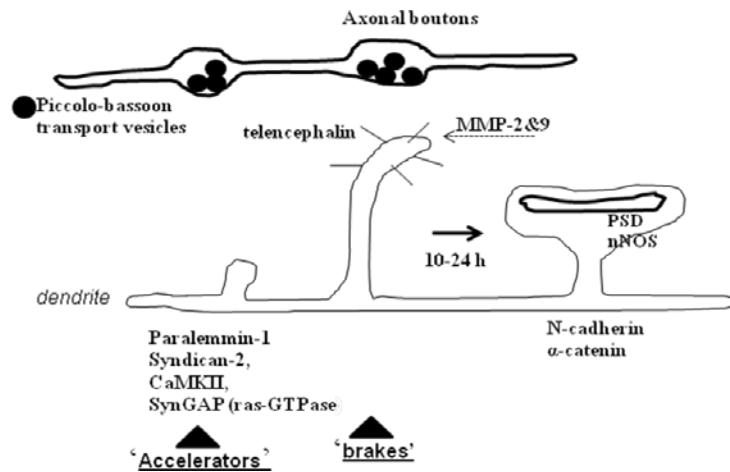


**Fig. 2** Filopodia formation and spinogenesis. ‘Accelerators’ initiate filopodia formation from the dendritic shaft and ‘brakes’ (e.g. Telencephalin) stabilize filopodia and facilitate filopodia to make transient contacts with axonal boutons. Transformation of filopodia to spines is triggered by exclusion of Telencephalin from the filopodial membrane via proteolytic cleavage (MMP-2 & 9), internalization, or lateral diffusion.

As discussed above in the process of synaptogenesis, highly motile filopodia make suitable and stable contact with axons through the generation of calcium transients and

independent of neurotransmitter release mechanisms (Lohmann and Bonhoeffer, 2008)

An adhesion molecule Telencephalin is abundant in dendritic filopodia but mostly excluded from spines. In filopodia these Telencephalins are bound with actin-binding proteins ( $\alpha$ -actinin and ERM (ezrin/radixin/moesin) family proteins) in dendritic shafts. Telencephalin enhances filopodia formation/maintenance and also spine-to-filopodia reversion. Recently, it has been demonstrated that Telencephalin induces dendritic filopodia formation through the cytoplasmic interaction with ERM family actin-binding proteins (Furutani et al., 2007) and that the extracellular region of Telencephalin is proteolytically cleaved by matrix metalloproteinase (MMP)-2 and -9 (Tian et al., 2007). Thus the filopodia to spine transition might be triggered by the exclusion of Telencephalin from the filopodial plasma membrane through proteolytic shedding, internalization, or lateral diffusion (Yoshihara et al., 2009). In young neurons, new spines and filopodia are produced at a high rate and seemingly in a random fashion. Studies show that adhesion molecules are the likely candidates contributing to the process of selecting presynaptic axonal partners by filopodia. Moreover, recent studies also show an important role of nitric oxide (NO). NO is produced at excitatory synapses by neuronal nitric oxide synthase (nNOS) which is brought to the synapse through its interaction with the second PDZ domain of PSD-95. Upon over expression of PSD-95, nNOS expression also increases and leads to the formation of spines that become innervated by multiple presynaptic partners (Nikonenko et al., 2008). During spine maturation process, the head size and volume of the spine increases. The enlargement of spine head size linked to increased dynamics of PSD proteins and the increase in spine volume closely correlate with the accumulation of additional AMPA receptors (Zito et al., 2009) and

reorganization of the actin cytoskeleton (Honkura et al., 2008). Our current understanding suggests the existence of two parallel tracks. One based on the growth of filopodia and predominantly active in early phases of development, where regulation of motility by molecules such as Ephrins and Telencephalin plays a critical role for the transformation into spine synapses. A second track, mostly observed in later development and mature brain, where protrusions grow directly as spines, most likely without initial PSD or partner, and for which activity and forms of plasticity such as LTP are probably key factors leading through trans-synaptic signaling, NO, adhesion molecules, Rho GTPases and certainly yet unrecognized partners, to the maturation and persistence of the new synapse (Yoshihara et al., 2009).

Several lines of evidence suggest that neuronal activity regulates spine morphology. LTP-inducing stimuli cause formation of new spines and enlargement of existing spines whereas long-term depression (LTD)-inducing stimuli cause shrinkage and/or retraction of spines (Tada and Sheng, 2006). Synaptic activity also influences the organelle content of spines. Synaptic stimulation can drive the translocation of mitochondria into spines; reciprocally, the morphogenesis of dendritic spines depends on the quantity and function of mitochondria in dendrites (Li et al., 2004). Although the conclusions are tentative, the current evidence indicates that spines might undergo complex changes in both shape and number over time after a novel experience, thereby relating dendritic spines to neuronal plasticity and long-term memory formation. The immediate changes that occur after stimulation are likely to involve the influx of AMPA receptors into the spine, which might be accompanied by changes in the volume and length of the spine to allow better linkage between the spine head and parent dendrite. This might result in the formation of

new spines—a process that normally takes several hours—or the pruning of existing ones. Spine pruning might also be associated with memory erasure, depotentiation or LTD (Segal, 2005).

**(iii) Spontaneous synchronized  $\text{Ca}^{2+}$  oscillations, a manifestation of neuronal connectivity:**

Neuronal populations such as cerebrocortical, hippocampal and spinal cord cells, exhibit synchronous spontaneous  $\text{Ca}^{2+}$  oscillations as a result of synchronous activation of a population of neurons in culture and *in vivo* during development. This can be demonstrated by calcium imaging using fluorescent  $\text{Ca}^{2+}$  indicator dyes. Imaging fluctuations in  $[\text{Ca}^{2+}]_i$  in embryonic neurons for extended periods *in vivo* and in culture reveals that neuronal cell bodies and growth cones can exhibit multiple spontaneous elevations of  $[\text{Ca}^{2+}]_i$  per hr, each of which lasts for  $10 \pm 30$  seconds. These studies reveal the existence of two types of intracellular  $\text{Ca}^{2+}$  transients,  $\text{Ca}^{2+}$  spikes and  $\text{Ca}^{2+}$  waves. Spikes depend on  $\text{Ca}^{2+}$  influx through voltage-gated channels and  $\text{Ca}^{2+}$  release from intracellular stores ( $\text{Ca}^{2+}$ -induced  $\text{Ca}^{2+}$  release via ryanodine receptors), and achieve a mean  $[\text{Ca}^{2+}]_i$  of  $\sim 500$  nM. Spikes have relatively rapid kinetics (mean duration approximately 10 s), and since they involve  $\text{Ca}^{2+}$ -dependent action potentials they are propagated throughout a neuron. In contrast to spikes,  $\text{Ca}^{2+}$  waves are kinetically slower (mean duration  $\sim 30$  s in growth cones), mediated by gap junctional diffusion of IP3 and do not involve action potentials for their generation (Spitzer et al., 2000). Formation of functional synapses and rhythmic release of neurotransmitters in a neuronal network have been demonstrated to be responsible for this synchronous oscillatory activity.

### **C. Transduction of neuronal activity via calcium-dependent signaling pathways:**

Activity-dependent neuronal development is primarily regulated by calcium dependent signaling events (Konur and Ghosh, 2005). Neuronal activity leads to changes in intracellular calcium levels through two mechanisms, (1) increase in cytosolic calcium by release of calcium from intracellular stores and (2) entry of extracellular calcium via plasma membrane calcium channels and calcium-permeable receptor channels. Calcium release from intracellular stores has been shown to act locally to stabilize already formed dendritic structure (Lohmann and Wong, 2005) and influence the mobility of dendrite filopodia (Lohmann et al., 2005). In contrast, influx of extracellular calcium plays a major role in transducing local as well as global signaling events that control dendritic arborization and spine formation (Wong and Ghosh, 2002; Redmond, 2008). Studies have shown that voltage-gated calcium channels (VGCC) and NMDA receptors are the major channels responsible for transducing neuronal activity into calcium influx mediated signaling cascades. The NMDARs have specifically been identified as key channels converting neuronal activity from pre-synaptic neuron into calcium influx in the post-synaptic neuron. Many of the effects of activity-dependent developmental plasticity of dendritic arbors and spines are mediated by NMDA receptors (Rajan and Cline, 1998; Cline, 2001; Lee et al., 2005; Ewald et al., 2008), a  $\text{Ca}^{2+}$  permeable ionotropic glutamate receptor that plays a central role in synaptic development, plasticity and synaptic transmission.

#### **D. NMDA receptors and their role in activity-dependent neuronal development:**

NMDARs are heteromeric complexes incorporating different subunits within a repertoire of three subtypes: NR1, NR2 and NR3. Most NMDARs are believed to assemble as tetramers, associating two NR1 and two NR2 subunits in a ‘dimer of dimers’ quaternary structure (Paoletti and Neyton, 2007). NMDAR subunits all share a common membrane topology. It is characterized by a large extracellular N-terminus, a membrane region comprising 3 transmembrane segments (TM1, 3 and 4) and a re-entrant pore loop (M2). There is an extracellular loop between TM3 and TM4, and a cytoplasmic ‘C’ terminus which varies in size depending upon the subunit and provides multiple sites of interaction with numerous intracellular proteins (Dingledine et al., 1999; Cull-Candy and Leszkiewicz, 2004). The N-terminal domain (NTD) contains binding sites for allosteric inhibitors such as  $Zn^{2+}$  and ifenprodil. The agonist binding domain (ABD) binds glycine in NR1 and NR3, whereas NR2 ABDs bind glutamate (Furukawa et al., 2005). The glycine sites on NMDAR are distinct from the inhibitory strychnine sensitive glycine receptor which mediates the neurotransmitter functions of glycine. The sequences of the regions lining the pore are highly conserved in NR2 subunits and accordingly, permeation properties (e.g. ionic selectivity), as well as the affinity for the pore blocking  $Mg^{2+}$  vary little among the different NR1/NR2 receptor subtypes. In contrast, inclusion of the NR3 subunit markedly decreases single channel conductance,  $Ca^{2+}$  permeability and  $Mg^{2+}$  block because of the presence of the positively charged amino acid arginine at the pore region (Cull-Candy and Leszkiewicz, 2004). pH is another important allosteric modulator of this receptor and the receptor activity is almost completely suppressed at pH less than 6.

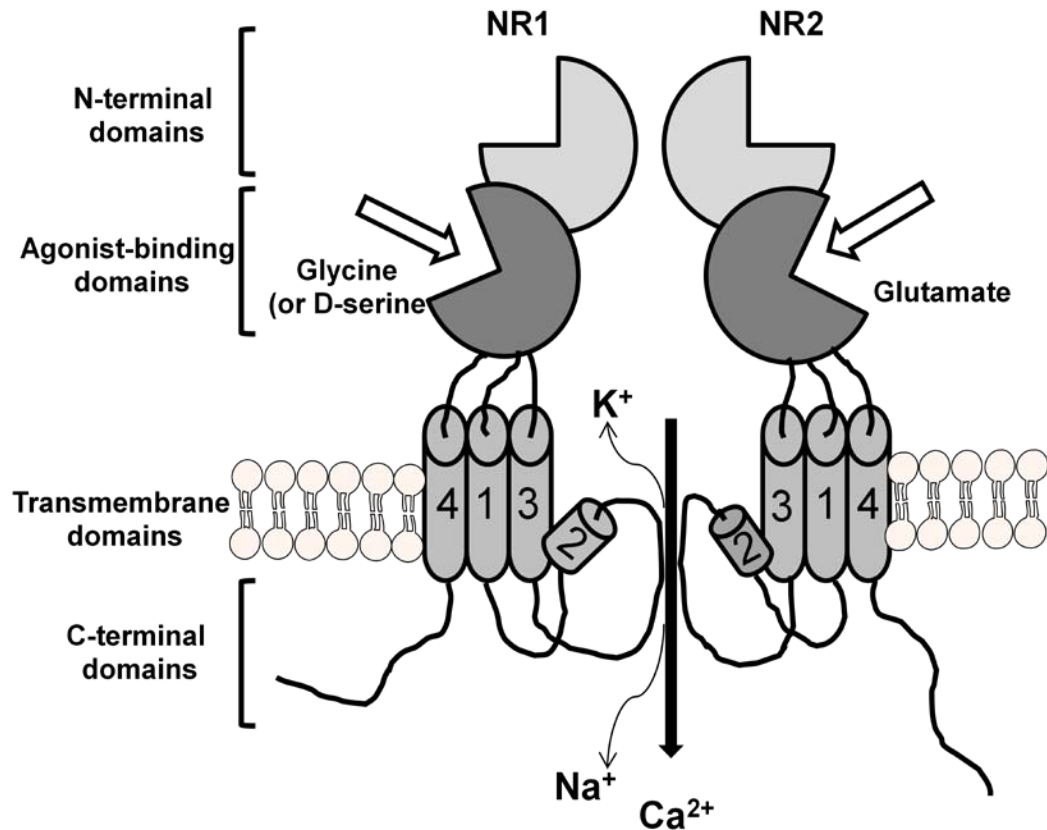


**Fig. 3** Structure of NMDA receptors.

**(i) Upregulatory mechanisms of NMDA receptor function:**

Src family kinases (SFKs) are found to be the main regulators of NMDARs and NMDA-dependent synaptic plasticity. Five members of SFKs—Src, Fyn, Yes, Lck and Lyn—are expressed throughout the CNS. All, except Lck, have been shown to be components of the NMDAR complex. These kinases share a common domain structure that includes the catalytic domain of Src homology (SH) 1 domain, the SH2 domain and the SH3 domain. The catalytic domain confers tyrosine kinase activity and contains the activation loop within which is a tyrosine residue (Y416) that is important for the regulation of kinase activity. Dephosphorylation of Y527 also leads to activation of SFKs. C-terminal Src

kinase and Csk homologous kinase are known to phosphorylate Y527. The phosphorylated Y527 interacts intramolecularly with the SH2 domain and thereby suppresses kinase activity. A protein tyrosine phosphatase, PTP $\alpha$  is found to selectively dephosphorylate Y527 in the regulatory domain of SFKs and thereby activate SFKs (Salter and Kalia, 2004).

SFK-mediated increase in NMDAR gating involves phosphorylation of tyrosine residues in the C-terminal domains of NMDAR subunits. The NR2A, NR2B and NR2D, but not NR1 subunits are mainly involved in tyrosine phosphorylation by SFKs. The C-terminal domains of NR2A and NR2B contain about 630 and 650 aminoacids, respectively, with each C-terminal tail containing 25 tyrosine residues. Three tyrosine phosphorylation sites on NR2A (Y1292, Y1325 and Y1387) have been identified as targets for Src-mediated phosphorylation. Y842 of NR2A is also phosphorylated and dephosphorylation of this residue may regulate the interaction of NMDAR with AP-2 adapter, a protein complex that is involved in clathrin-coated endocytic vesicle formation (Vissel et al., 2001). NR2B also contains three tyrosine phosphorylation sites (Y1252, Y1336 and Y1472), which are phosphorylated by Fyn, with Y1472 as the major phosphorylation site (Nakazawa et al., 2001; Takasu et al., 2002). Y1472 is within a tyrosine-based internalization motif (YEKL), which binds directly to the medium chain of AP-2 adapter (Roche et al., 2001; Lavezzari et al., 2003). Phosphorylation of NR2B Y1472 disrupts its binding to AP-2, thereby resulting in inhibition of NR2B-mediated endocytosis (Salter and Kalia, 2004; Chen and Roche, 2007).

The function of NMDARs is also regulated by Serine / Threonine phosphorylation. These Ser / Thr residues are the substrates for cAMP-dependent protein kinase (PKA),

protein kinase C (PKC), protein kinase B (PKB), CaMKII, Cyclin-dependent kinase-5 (Cdk5) and casein kinase II (CKII) (Chen and Roche, 2007). These kinases can regulate intracellular trafficking or channel properties of NMDA receptors, resulting in changes in synaptic strength underlying many forms of synaptic plasticity (Lee, 2006).

Ca<sup>2+</sup> calmodulin-dependent protein kinase kinase (CaMKK) has been demonstrated to be an upstream regulator of both Ca<sup>2+</sup> calmodulin-dependent protein kinase (CaMK) and mitogen activated protein kinase (MAPK) which are reported to be the key mediators of calcium dependent neurite outgrowth (Redmond et al., 2002). NMDAR-dependent CaMKK/CaMKI signaling cascades have been shown to regulate neurite/axonal outgrowth (Wayman et al., 2004), activity-dependent synaptogenesis (Saneyoshi et al., 2008), and Ca<sup>2+</sup>-dependent extracellular signal-regulated kinase (ERK) activation and dendritic outgrowth (Schmitt et al., 2004; Wayman et al., 2006). NMDARs therefore play a critical role in activity-dependent development and plasticity, dendritic arborization, spine morphogenesis, and synapse formation by stimulating these calcium-dependent signaling pathways (Rajan and Cline, 1998; Sin et al., 2002; West et al., 2002; Wong and Ghosh, 2002; Miller and Kaplan, 2003; Tolia et al., 2005; Ultanir et al., 2007).

**(ii) Intracellular sodium and regulation of NMDAR function :**

The electrical signals of neurons are fundamentally dependent on voltage-gated sodium channels, which are responsible for the rising phase of the action potential. Recent studies have indicated that changes in [Na<sup>+</sup>]<sub>i</sub> produced in the soma and dendrites as a result of neuronal activity may act as a signaling molecule and play a role in activity-dependent synaptic plasticity. It has been shown that synaptic stimulation causes [Na<sup>+</sup>]<sub>i</sub>

increments of 10 mM in dendrites and up to 35-40 mM in dendritic spines (Rose et al., 1999; Rose and Konnerth, 2001). In hippocampal neurons intracellular  $[\text{Na}^+]_i$  increments have been demonstrated to increase NMDAR-mediated whole cell currents and NMDAR single channel activity by increasing both channel open probability and mean open time (Yu and Salter, 1998). Using veratridine, these investigators demonstrated that influx of  $\text{Na}^+$  through a tetrodotoxin (TTX) sensitive VGSC was sufficient to produce potentiation of NMDAR channel activity. An increment of  $[\text{Na}^+]_i$  of only 10 mM was sufficient to produce significant augmentation of NMDA receptor currents (Yu and Salter, 1998; Yu, 2006). It has also been reported that increments of  $[\text{Na}^+]_i$  greater than 5 mM represent a critical threshold required to regulate NMDAR-mediated  $\text{Ca}^{2+}$  influx in primary cultures of hippocampal neurons (Xin et al., 2005). This  $[\text{Na}^+]_i$  mediated upregulation of NMDAR function has been shown to require Src kinase activation (Yu and Salter, 1998). Src family kinases act as a crucial point of convergence for signaling pathways that enhance NMDAR activity, and, by upregulating the function of NMDARs, Src activity controls the production of NMDAR-dependent synaptic potentiation and plasticity (Salter and Kalia, 2004). Although neuronal activity plays a profound role during development, very little is known about the relationship between  $[\text{Na}^+]_i$  and NMDAR signaling in the developing nervous system.

#### **E. Signaling mechanism of activity-dependent neuronal development:**

##### **(i) $\text{Ca}^{2+}$ / Calmodulin-kinase (CaMK) signaling pathways:**

Translation of neuronal activity into intracellular response is mainly mediated by  $\text{Ca}^{2+}$ -dependent signaling events. Many of these intracellular responses are mediated by

CaMKs, a family of serine / threonine protein kinases. CaMKs are activated via binding of Calcium/calmodulin ( $\text{Ca}^{2+}/\text{CaM}$ ) and subsequently they phosphorylate serine / threonine residues of target proteins to trigger downstream signaling events. Members of this family include, CaMKII, CaMKK, CaMKI and CaMKIV. The CaMKII is most highly expressed in neurons. There are four isoforms of CaMKII  $\alpha$ ,  $\beta$ ,  $\gamma$ , and  $\delta$ . All isoforms contain a highly conserved N-terminal catalytic domain, a regulatory domain as well as C-terminal domain. The regulatory domain contains the autoinhibitory domain, a calmodulin binding domain and the autophosphorylation sites. All isoforms are capable of homo-and hetero-multimerization via their C-terminal domains to form 300-700 kDa holoenzymes. Activation of CaMKII by  $\text{Ca}^{2+}/\text{CaM}$  allows intramolecular autophosphorylation of several sites, including Thr286, Thr305 and Thr306. Binding of  $\text{Ca}^{2+}/\text{calmodulin}$  disrupt the autoinhibitory interactions and allow substrates and ATP to gain access to the catalytic site. Simultaneous  $\text{Ca}^{2+}/\text{calmodulin}$  binding to adjacent subunits in a single holoenzyme results in the efficient *trans*-autophosphorylation of Thr286 in the autoinhibitory site (Colbran and Brown, 2004). Autophosphorylation of Thr286 has two primary consequences: (1) the subsequent dissociation of bound  $\text{Ca}^{2+}/\text{CaM}$  (i.e., when intracellular  $\text{Ca}^{2+}$  levels are reduced) is decreased by several orders of magnitude, thereby prolonging its activation, and (2) even after full dissociation of  $\text{Ca}^{2+}/\text{CaM}$ , the kinase retains partial (30-60%) activity (i.e.,  $\text{Ca}^{2+}$ -independent or constitutive /autonomous activity). Thus transient elevations of intracellular  $\text{Ca}^{2+}$  levels can result in prolonged CaMKII activity until dephosphorylation of Thr286 by protein phosphatases. The autophosphorylation of CaMKII at Thr286 has also been shown to promote and stabilize CaMKII binding to PSD whereas autophosphorylation of

Thr305/306 suppresses this interaction. Studies show that the interaction of CaMKII with the NR2B subunit of NMDAR facilitates the translocation of CaMKII to PSD following NMDAR activation (Wayman et al., 2008). Additionally, Thr305 or Thr306 is found to block binding of Ca<sup>2+</sup>/calmodulin and lock CaMKII in an inactive stage until these residues are dephosphorylated. The role of CaMKII $\alpha$  and  $\beta$  isoforms have been examined in dendritic growth and elaboration and the studies indicate that CaMKII $\alpha$  plays a role in stabilization of dendritic arbors in mature neurons whereas in young neurons, active CaMKII $\alpha$  leads to attenuation of dendritic arbors (Redmond, 2008). CaMKII $\beta$  specifically bind and bundles F-actin to promote dendritic branching and increased filopodia motility at DIV-3 hippocampal neurons (Fink et al., 2003).

CaMKK has two isoforms, namely  $\alpha$  and  $\beta$ . The  $\alpha$  isoform is mostly cytoplasmic whereas  $\beta$  isoform may also be nuclear. The primary substrates of CaMKK are CaMKI and CaMKIV because their phosphorylation and activation by CaMKK is very rapid whereas protein kinase B (PKB/Akt) which is a secondary substrate requires prolonged activation by CaMKK. Activation of CaMKI upon NMDAR stimulation occurs in less than 5 min, whereas PKB/Akt activation by CaMKK is maximal in about 60 min (Schmitt et al., 2005).

CaMKI also shows four different isoforms. The  $\alpha$  and  $\gamma$  isoforms are predominantly cytoplasmic, where the  $\gamma$  isoform is lipid modified and can associate with the Golgi and plasma membranes (Takemoto-Kimura et al., 2003). Plasma membrane localization of the  $\gamma$  isoform is probably important for the ability of this isoform to exert crosstalk with the Ras/ERK pathway (Wayman et al., 2006). CaMKI  $\alpha$  and  $\gamma$  isoforms have been

implicated in mediating dendritic growth and branching. It has been reported that a splice variant of the  $\beta$  isoform may be nuclear (Ueda et al., 1999).

CaMKIV is monomeric and the active CaMKIV is predominantly nuclear. CaMKIV expression is upregulated during the peak period of dendrite development and induces significant elaboration of dendrites (Redmond et al., 2002).

**(ii) PKB/Akt signaling pathway:**

Recent studies indicate that Akt (also known as Protein kinase B/PKB), a serine threonine kinase, plays an important role in several aspects of neurite outgrowth. The Akt-mediated neurite outgrowth has been shown to involve the signaling pathways glycogen synthase kinase (GSK)  $3\beta$ , peripherin, mammalian target of rapamycin (mTOR),  $\delta$ -catenin and Hsp27. There are three isoforms of Akt, Akt1, Akt2 and Akt3 and all these three isoforms possess an N-terminal pleckstrin homology (PH) domain, a kinase domain and C-terminal regulatory domain. One of the major upstream regulators of Akt, is phosphatidylinositol 3-kinase (PI3K), which on activation via tyrosine kinase or G protein-coupled receptors, facilitates the conversion of membrane phospholipid phosphatidylinositol (4, 5)-diphosphate (PIP<sub>2</sub>) to Phosphatidylinositol (3, 4, 5)-triphosphate (PIP<sub>3</sub>). The accumulation of PIP<sub>3</sub> promotes the translocation of Akt to the plasma membranes, where Akt binds to PIP<sub>3</sub> via its PH domain. Binding of Akt to PIP<sub>3</sub> leads to the phosphorylation of Akt at Thr308 and Ser473 by phosphoinositide-dependent kinase 1 and 2 respectively (Read and Gorman, 2009). As in neurite outgrowth, the PI3K-Akt-GSK pathway has been shown to regulate the early stages of dendrite formation in hippocampal neurons stimulated with hepatocyte growth factor (Lim and Walikonis,

2008). It has also been reported that the proline-rich inositol polyphosphatase (PiPP) hydrolyses PIP3 and negatively regulates Akt phosphorylation at Ser473. Increased phosphorylation of Akt at Ser473 and GSK3 $\beta$  at Ser9 occurred at the growth cone following targeted depletion of PiPP, indicating the spatial distribution of activated Akt-GSK signaling in neurite elongation (Ooms et al., 2006). Moreover, the Akt-mTOR pathway has been shown to be the primary mediator of PI3K regulated dendritic branching (Jaworski et al., 2005). The co-ordinated PI3K-Akt and Ras-MAPK signaling pathways have been shown to increase dendritic complexity in dissociated postnatal hippocampal CA1/CA3 neuronal cultures (Kumar et al., 2005). More recently, the interaction of a heat shock protein27 (Hsp27) with Akt has been reported to play a role in the maintenance of Akt activity in neuritogenesis.

**(iii) Ras-homologous guanosine triphosphatases (Rho GTPases)-mediated regulation of actin dynamics:**

Rho GTPases constitute a distinct family within the super family of Ras-related small GTPases that control the dynamics of the cytoskeleton and mediate the effects of multiple signals that regulate the growth and development of dendrites, dendritic spines, and axons. Rho GTPases function as binary molecular switches between an inactive GDP-bound state and an active GTP-bound state. Guanine nucleotide exchange factors (GEFs) facilitate the transition from the inactive GDP-bound state to the active GTP-bound state, whereas guanine nucleotide dissociation inhibitors and GTPase activator proteins act as negative regulators of Rho GTPase signaling. Twenty two mammalian genes encoding Rho GTPases have been described. The best characterized are members of the RhoA, Rac, and Cdc42 families. The activation of Rho, Rac, or Cdc42 leads to assembly of

contractile actin-myosin filaments, protrusive actin-rich lamellipodia, and protrusive actin-rich filopodia, respectively. RhoA inhibits growth of dendrites and axons via one of the major downstream effectors, Rho kinase, which phosphorylates and activates the myosin light chain and its kinase. Phosphorylation of myosin promotes its interaction with actin, leading to retraction of axonal and dendritic growth cones. In contrast, both Rac1 and Cdc42 facilitate dendritic and axonal growth via several transduction pathways. These include PAK (P21 kinase), which, via LIMK (Lin-11, Isl-2, Mec-3 kinase) inactivates the actin depolymerizing protein cofilin. Both Rac1 and Cdc42 activate the actin-related protein (Arp) 2/3 complex, which promotes actin nucleation and polymerization. Arp2/3 complex is activated by Cdc42 via N-WASP (wiskott-Aldrich syndrome protein) and by Rac1 via WAVE (WASP family Verprolin-homologous protein) (Jaffe and Hall, 2005; Benarroch, 2007).

**(iv) Activity-regulated transcriptional mechanisms:**

**(a) Activity-dependent transcription factors:**

Currently, five transcription factors have been identified that are responsive to neuronal activity and mediators of neuronal morphology. They are CREB (cyclic AMP-responsive element binding protein), NeuroD (neurogenic differentiation), NeuroD2, MEF2 (myocyte enhancer factor2) and Sp4. In addition to transcription factors, proteins that bind transcription factors including calcium-responsive transactivator (CREST), CREB-binding protein (CBP), and LIM domain only 4 (LMO4) are also activated in response to neuronal activity via calcium signaling (Redmond, 2008). CREB has been implicated in a number of biological functions, all of which depend on its ability to act as

a stimulus-induced transcription factor that can be activated by a variety of extracellular signals. In the brain, CREB mediates both activity-dependent synaptic plasticity and trophic factor-dependent neuronal survival. Consistent with its role as an activity-dependent transcription factor, CREB is phosphorylated at a serine critical for its function (Ser-133) in physiologically active brain areas during a wide range of behaviors. A number of signal transduction cascades initiated by either cytoplasmic or nuclear calcium have been shown to mediate CREB serine-133 phosphorylation in various neuronal cell lines and primary neuronal cultures. In CREB-dependent transcriptional mechanism, CREB sits prebound as a dimer to the cyclic-responsive element (CRE) in unstimulated cells. In response to neuronal stimulation and activation of CREB kinases, CREB is phosphorylated at serine-133, thereby binding it to CBP and recruiting this co-activator to the promoter. CBP recruits the polymerase complex onto promoters bound by serine-133 phosphorylated CREB, thereby activating transcriptional mechanisms (West et al., 2001). In the absence of extracellular stimuli, the presence of transcriptional repressors and relatively condensed chromatin conformation result in low levels of CRE-driven transcription from these promoters (Cohen and Greenberg, 2008). CBP possess endogenous histone acetyltransferase activity and catalyzes the acetylation of promoter-associated histones, disrupting the histone-DNA interactions and making the chromatin surrounding the transcriptional start site accessible to the transcriptional machinery (Bannister and Kouzarides, 1996). The phosphorylation of CREB at serine-142 and 143, in addition to serine-133, has been shown to be required for maximal, calcium-specific CREB-dependent gene expression in cortical neurons (Kornhauser et al., 2002). But these additional phosphorylation sites prevent CREB-CBP interactions, implicating CBP-

independent CREB function which is required for stimulus-dependent behavioral adaptations under some circumstances (Cohen and Greenberg, 2008). CREB is activated by a wide variety of stimuli and signaling pathways. CaMKs, including CaMKI, CaMKII and CaMKIV as well as Ras/MAPK signaling events play major roles in the activity-dependent nuclear phosphorylation of CREB at serine-133. In response to many stimuli, the activation of the Ras/MAPK/Rsk and CaMK pathways occur in concert, suggesting that these pathways may play cooperative roles in CREB activation. Studies of the kinetics of CREB phosphorylation have shown that CaMKs dominate the rapid phase of CREB phosphorylation after membrane depolarization, whereas Ras/MAPK pathway activation is slower and becomes the predominant CREB kinase at later times after stimulation (Dolmetsch et al., 2001; Wu et al., 2001). Although NeuroD and NeuroD2 transcription factors have been identified as activity-regulated transcription factors, the specific signaling mechanisms leading to their transcriptional activation and also their role in dendritic morphology are not yet determined. Another activity-regulated transcription factor, MEF2 was shown to play a role in differentiation of dendrite claws of cerebellar granule neurons. Activity via L-type VGCC and NMDA receptors activates and phosphorylates MEF2, but calcineurin, a calcium sensitive phosphatase subsequently dephosphorylates MEF2. After dephosphorylation MEF2 is acetylated. Once acetylated, MEF2 activates transcription. Both neuronal activity and acetylated MEF2 attenuated dendritic claw differentiation (Redmond, 2008). Recently, a zinc finger transcription factor, Sp4 has been shown to mediate activity-induced dendritic development of cerebellar granule neurons (Ramos et al., 2007).

**(b) Activity-regulated genes:**

The expression of C-fos and other immediate early genes in the hippocampus after seizures (Morgan et al., 1987), lead to the observation that genes can be activated following extracellular stimuli. Arc, one of the activity regulated genes, has been shown to be involved in regulating AMPA receptor-mediated transmission and AMPA receptor internalization. (Chowdhury et al., 2006; Rial Verde et al., 2006; Shepherd et al., 2006). One of the most intensively studied activity-regulated genes is Brain-derived neurotrophic factor (BDNF) (Ernfors et al., 1991; Isackson et al., 1991). BDNF was originally identified as a survival factor for peripheral neurons but was subsequently shown to be involved in regulating a number of attributes of neurons, including axonal and dendritic growth, the efficacy of synaptic transmission and synaptic plasticity (Lohof et al., 1993; Figurov et al., 1996; Kang and Schuman, 1996). Moreover, it was shown that BDNF expression was regulated by CREB-dependent transcription (Shieh et al., 1998; Tao et al., 1998).

The BDNF gene in rodents is composed of nine exons: exon I to VIII possess their own promoter and are associated by a splicing mechanism to exon IX, which is the only one to be translated into a protein. The combination of these different splicing forms with two alternative polyadenylation sites in the 3' untranslated region can give rise to multiple different pre-mRNA that are expressed in a developmentally regulated and tissue-specific manner (Aid et al., 2007). The level of BDNF mRNA transcription is positively regulated by neuronal activity (Zafra et al., 1990; Castren et al., 1992; Berninger et al., 1995; Tongiorgi, 2008). Studies have shown that the pre-pro-BDNF is synthesized and sequestered in the endoplasmic reticulum. The pro-BDNF then transits

the Golgi apparatus and accumulates in membrane stacks of the trans-Golgi network. Two types of secretory pathways exist. Secretion via the constitutive pathway does not rely on extracellular signals or any triggering events. In the regulated pathway, fusion of the secretory granules with the plasma membrane is triggered by an intracellular rise in  $\text{Ca}^{2+}$ . This  $\text{Ca}^{2+}$  rise can result from an influx through VGCC or NMDARs upon membrane depolarization or from activation of internal  $\text{Ca}^{2+}$  stores following the activation of metabotropic glutamatergic receptors. Activity-dependent dendritic BDNF release has been demonstrated in neuronal cultures. So far, at least three distinct signals subserving BDNF release has been directly identified: 1, tetanic stimulation of presynaptic glutamatergic fibers, 2) action potentials that propagate backwards into the dendrites, and 3) prolonged depolarization of the postsynaptic neurons. The BDNF release following tetanic stimulation has been seen to act locally to modulate the development and plasticity of stimulated synapses whereas BDNF release triggered by back-propagating action potentials influence the development and plasticity of stimulated and non-stimulated synapses (Kuczewski et al., 2009). Horch and Katz (2002) reported that the BDNF-induced dendritic branching is spatially restricted. BDNF acts through binding to two receptors: TrkB and p75. Binding to the high affinity tyrosine kinase receptor, TrkB, mediates most of the neuronal effects of BDNF. However, BDNF can also bind to a pan-neurotrophin receptor, p75, to influence cell death and, perhaps, to modulate the effects of the other neurotrophins. BDNF binding to TrkB induces receptor dimerization, phosphorylation, and activation of the intracellular tyrosine kinase domain (McAllister, 2002). BDNF-TrkB signaling has been shown to activate lipid-modified  $\text{CaMKI}\gamma$  that is colocalized in a lipid raft with Rac and its GEF, STEF. This signaling

pathway is postulated to enhance actin polymerization and thereby promote dendritic formation (Takemoto-Kimura et al., 2007). Surface expression of TrkB is also reported to be regulated by neuronal activity at multiple levels including increased insertion into the plasma membrane (Du et al., 2000) , enhanced endocytosis of BDNF-TrkB signaling complex, and activation of transcription of the TrkB gene (Nagappan and Lu, 2005).

Another activity-regulated gene, candidate plasticity gene-15 (cpg15/neuritin), has also been reported to enhance dendritic branch length in *Xenopus* tectal neurons (Nedivi, 1999) and promote neuritogenesis of hippocampal and cortical neurons in vitro (Naeve et al., 1997).

Wnt-2, a secretory protein, has an important role in mediating dendritic growth. After depolarization of hippocampal neurons, Wnt-2 expression increased dependent upon CREB signaling (Wayman et al., 2006). In general, Wnt signaling involves at least three different pathways, 1) the canonical or Wnt /  $\beta$ -catenin pathway regulates cell fate decisions and possibly synaptogenesis. Binding of Wnt to the Frizzled, a seven-pass transmembrane protein, and low-density lipoprotein receptor-related protein (LRP) 5 or LRP6 receptor complex activates Dishevelled, a cytoplasmic scaffold protein. Signaling through Frizzled receptor requires G-protein activation. Activation of Dishevelled results in the inhibition of glycogen synthase kinase 3 $\beta$  (GSK3 $\beta$ ) and accumulation of  $\beta$ -catenin in the cytoplasm. GSK3 $\beta$  enhanced phosphorylation of  $\beta$ -catenin leads to proteasome-mediated degradation of  $\beta$ -catenin via ubiquitination pathway, but inhibiting GSK3 $\beta$  enhances the levels of  $\beta$ -catenin. Translocation of  $\beta$ -catenin to the nucleus mediates transcription-dependent signaling events.  $\beta$ -catenin can also bind the intracellular domain of N-cadherin, as well as associate with  $\alpha$ -catenin, an actin binding protein, to stabilize

the dendritic cytoskeleton. (2) In the planar cell polarity pathway, Frizzled receptor functions through G-proteins to activate Dishevelled, which in turn, signals to Rho GTPases (Rho or Rac or both). Activation of Rac signals occur through the c-jun amino (N)-terminal kinase (JNK). Activation of Rho GTPases induces changes in the cytoskeleton. This pathway has been implicated in cell and tissue polarity and also in dendritic arborization. Binding of Wnt7b to frizzled signals through the Rac/JNK pathway and has been shown to stimulate dendritic arborization (Chang et al., 2003). (3) In the Wnt/calcium pathway, activation of Dishevelled induces the release of intracellular calcium and activation of protein kinase C (PKC) and CaMKII. This pathway has been implicated in cell fate and cell movement (Bamji, 2005; Ciani and Salinas, 2005). (Yu and Malenka, 2003) showed that Wnts are involved in activity-dependent dendritic growth through a transcription independent, adhesion-mediated branch of the canonical  $\beta$ -catenin pathway. Wayman et al (2006) reported that the activity-dependent dendritic arborization requires sequential activation of the NMDAR, CaMKK, CaMKI and MEK/ERK to enhance CREB-mediated transcription of Wnt-2. Wnt signaling has also been implicated in axon guidance mechanisms. Wnts induce axon remodeling by changing the organization and dynamics of the microtubules. In the cerebellum and spinal cord, Wnts inhibit axon extension but increase growth cone size and branching and also increases growth cone size in dorsal root ganglia neurons. Moreover, studies on the mossy fiber-granule cell synapse in the mouse cerebellum revealed a role for the canonical Wnt pathway in synapse formation. Wnt7A expression is at its highest when granule cells are contacted by mossy fiber axons, their presynaptic targets, which indicates that Wnt7A regulates the maturation of this synapse (Ciani and Salinas, 2005).

**(c) Activity-regulated microRNAs:**

Recent evidence points to a widespread role for neural microRNA (miRNA) at various stages of synaptic development, including dendritogenesis, synapse formation and synapse maturation (Schratt, 2009). It now appears that much of the genome is transcribed, and that many of the noncoding RNAs represent microRNAs that are processed to generate 20-30 nucleotide long fragments that can recognize and degrade endogenous mRNAs. Vo et al., 2005 reported that the CREB-regulated microRNA, miR132 can affect neuronal morphogenesis. miR132 suppresses translation of p250GAP, thereby stimulating Rac1 and dendritic outgrowth. Klein and colleagues reported that the same microRNA can regulate MECP2 expression (Klein et al., 2005). It has also been reported that miRNA-134 can regulate dendritic spine development through the inhibition of LimK1 (Schratt et al., 2006). These findings show that neuronal activity can influence the abundance of specific mRNAs by regulating microRNA expression (Qiu and Ghosh, 2008).

**F. Voltage-gated sodium channels:**

Voltage-gated sodium channels are critical elements of action potential initiation and propagation in excitable cells because they are responsible for the initial depolarization of the membrane (Catterall et al., 2003). When the cell membrane is depolarized by a few millivolts, sodium channels activate and inactivate within milliseconds. Influx of sodium ions through the integral membrane proteins comprising the channel depolarizes the membrane further and initiates the rising phase of the action potential (Yu and Catterall, 2003). Sodium channels consists of a pore forming  $\alpha$  subunit (~260 kDa) associated with

one or more  $\beta$  subunits (~33-36 kDa). The sodium channels in the adult central nervous system contain  $\beta 1$  (or  $\beta 3$ ) and  $\beta 3$  subunits whereas sodium channels in adult skeletal muscle have only the  $\beta 1$  subunit. The pore forming  $\alpha$  subunit is sufficient for functional expression, but the kinetics and voltage dependence of channel gating are modified by the  $\beta$  subunits (Catterall et al., 2005). Nine  $\alpha$  subunits ( $\text{Na}_v1.1\text{-Na}_v1.9$ ) have been functionally characterized and a tenth related isoform ( $\text{Na}_x$ ) may also function as a sodium channel. The primary sequence predicts that the sodium channel  $\alpha$  subunit folds into four domains (I-IV), which are similar to one another and contain six  $\alpha$ -helical transmembrane segments (S1-S6) and an additional pore loop located between the S5 and S6 segments. The pore loops line the outer narrow entry to the pore whereas the S5 and S6 segments line the inner wider exit from the pore. The S4 segments in each domain contain positively charged amino acid residues at every third position. These residues serve as gating charges and move across the membrane to initiate channel activation in response to depolarization of the membrane. The short intracellular loop connecting homologous domains III and IV serves as the inactivation gate, folding into the channel structure and blocking the pore from the inside during sustained depolarization of the membrane (Yu and Catterall, 2003; Catterall et al., 2005; Docherty and Farmer, 2009).



At least six distinct receptor sites for neurotoxins and one receptor site for local anesthetics and related drugs have been identified (Cestele and Catterall, 2000) and summarized in the table below,

Receptor Site	Toxin or Drug	Domains
Neurotoxin receptor site 1	Tetrodotoxin, saxitoxin, $\mu$ -conotoxin	IS5-S6, IIS5-S6, IIIS5-S6, IVS5-S6
Neurotoxin receptor site 2	Veratridine, batrachotoxin, grayanotoxin	IS6, IVS6
Neurotoxin receptor site 3	$\alpha$ -Scorpion toxins, sea anemone toxins	IS5-IS6, IVS3-S4, IVS5-S6
Neurotoxin receptor site 4	$\beta$ -Scorpion toxins	IIS1-S2, IIS3-S4
Neurotoxin receptor site 5	Brevetoxins, ciguatoxins	IS6, IVS5
Neurotoxin receptor site 6	$\delta$ -conotoxins	Not established
Local anesthetic receptor site	Local anesthetic drugs, antiarrhythmic drugs, antiepileptic drugs	IS6, IIIS6, IVS6

**Table 1** Receptor sites on sodium channels (Adapted from Catterall et al., 2003)

**G. Brevetoxin (PbTx-2), a voltage-gated sodium channel activator:**

Brevetoxins (PbTx) are potent lipid soluble cyclic polyether neurotoxins produced by the marine dinoflagellate *Karenia brevis*, an organism linked to toxic ‘red tide’ blooms that occur periodically in the Gulf of Mexico along the west coast of Florida, as well as the coastline of Texas (Baden, 1989). Blooms of *Karenia brevis* are known to cause massive fish kills and marine mammal mortalities and have been implicated in toxicity in humans resulting from the ingestion of contaminated shellfish or inhalation of brevetoxin-containing aerosols in sea spray (Pierce et al., 2005). Brevetoxins are classified based on their ring system as either decacyclic brevetoxin A or undecacyclic brevetoxin B. All toxins possess four common features: An A-ring electrophile of some type, in most cases a five or six –membered ring lactone (“head”), a relatively rigid four-ring region thought to be involved in binding at the  $\alpha$  subunit of VGSC (“rigid region”), a several-ring “spacer” region that separates the binding region from the activity region and a side chain (“tail”region). Brevetoxin-2 (PbTx-2), the most prominent member of the

brevetoxin B family, consists of 11 *trans*-fused ether rings condensed in a ladder shape (cylinder, ~30 (long) x 6 Å (diameter)), 23 stereogenic centers, and three C=C double bonds (Baden et al., 2005; Michelliza et al., 2007).

Brevetoxins are known to interact specifically with site 5 on the  $\alpha$ -subunit of VGSCs (Poli et al., 1986) and are thought to orient ‘head-down’ into the channel (Gawley et al., 1992), intercalating between the  $\alpha$ -helices of domains III and IV of the VGSC (Trainer et al., 1994), with the lactone A-ring inward towards the cytoplasm and the tail region pointed outwards towards the extracellular region. Brevetoxins exert their biological activity by binding with high affinity ( $K_d=1.6$  nM,  $B_{max}=1.9$  pmol per mg protein) to the  $\alpha$  subunit of VGSCs (Poli et al., 1986).

All natural brevetoxins have four distinct activities that alter the normal closed (C)-open (O)-inactivation (I) triad of VGSCs: (1) the activation potential is shifted to more negative potentials, favoring a C $\rightarrow$ O allosteric change at normal resting potential; (2) a longer mean open time, which can be influenced by a number of factors, but which results in the channel being in the open configuration longer; (3) an induction of sodium ion subconductance states and (4) an inhibition of inactivation O $\rightarrow$ I (Baden DG-2005).

#### **H. Objective of the study:**

The primary long range objective of this project is to elucidate the mechanisms by which the sodium channel activators influence neuronal development in cerebrocortical neurons. More specifically, the effects of sodium channel activation on neurite outgrowth, dendritic arborization and synaptogenesis will be investigated to explore the relationship between  $[Na^+]_i$  and NMDAR-dependent neuronal development. Understanding the role of

$[\text{Na}^+]_i$  in activity-dependent regulation of neuronal development offers a promising avenue for therapeutic intervention in the treatment of neurological disorders such as stroke and traumatic brain injury.

**Rationale:**

Neuronal activity regulates the morphology and connectivity of neurons during development. The mechanisms by which neurons decode neuronal activity into activation of signaling pathways that regulate morphological complexity are unclear. These pathways are reported to involve local (modulation of actin dynamics) as well as global (activation of nuclear signaling and gene transcription) signaling mechanisms (Wong and Ghosh, 2002). Investigations in this area have revealed the involvement of CaMKs and MAPKs in mediating activity-dependent increases in dendritic complexity. Elevation of intracellular sodium in soma and dendrites as a result of neuronal activity may act as a signaling molecule that plays a role in activity-dependent synaptic plasticity. Even though different lines of evidence indicate  $[\text{Na}^+]_i$  may act as a signaling molecule, very little is known about its involvement in activity-dependent neuronal development. We reasoned that  $[\text{Na}^+]_i$  may act as a positive regulator of developmental plasticity by upregulating NMDAR channel activity in immature cerebrocortical neurons. In the present project, we are using a sodium channel activator, brevetoxin (PbTx-2) to manipulate  $[\text{Na}^+]_i$  in immature murine cerebrocortical neurons in an effort to mimic the influence of neuronal activity. Brevetoxins interact with neurotoxin site 5 on the  $\alpha$ -subunit of voltage-gated sodium channels (Catterall and Gainer, 1985; Poli et al., 1986) and augment sodium influx through VGSCs by shifting the activation potential to more negative values,

increasing the mean open time of the channel and inhibiting channel inactivation (Jeglitsch et al., 1998).

**Central Hypothesis:**

Our central hypothesis is that sodium channel activators are capable of mimicking activity-dependent regulation of neuronal development by upregulating NMDAR signaling pathways. Upregulation of NMDAR signaling pathways influence neuronal growth and plasticity. We have recently shown that an array of sodium channel gating modifiers produce  $[Na^+]_i$  increments that are of sufficient magnitude to increase NMDAR channel activity (Cao et al., 2008). Voltage-gated sodium channel activators may represent a novel pharmacologic strategy to regulate neuronal plasticity through a NMDAR and Src family kinase-dependent mechanism.

**Specific Hypotheses:**

- I. Sodium channel activation augments NMDA receptor function and promotes neurite outgrowth in immature murine cerebrocortical neurons.

**Specific aims:**

1. Investigate the mechanisms underlying the influence of  $[Na^+]_i$  on NMDA receptor signaling in immature cerebrocortical neurons.
2. Characterize the mechanisms underlying VGSC influence on neurite outgrowth.

**II.** Sodium channel activation regulates spontaneous  $\text{Ca}^{2+}$  oscillations, spinogenesis and synaptogenesis in cerebrocortical neurons.

**Specific aims:**

3. Determine the temporal correlation between synchronous  $\text{Ca}^{2+}$  oscillations, spinogenesis and synaptogenesis in cerebrocortical neurons.
4. Delineate the signaling pathways involved in PbTx-2 regulation of spinogenesis and synaptogenesis.

**Significance:**

- Dendritic abnormalities are the most consistent anatomical correlates of mental retardation including Fragile X, fetal alcohol, Down's and Rett syndromes (Kaufmann and Moser, 2000). Delineating the pathways underlying neurite outgrowth and synaptic connectivity will broaden our understanding of neurotrophic signaling to provide insight into strategies for future therapeutic interventions.
- Normal cognitive processing, i.e. learning and memory consolidation, require structural remodeling of synaptic connections. This remodeling is commonly manifested as changes in dendritic arborization and alterations in the size, shape and density of dendritic spines. Inasmuch as spines represent sites for excitatory synaptic inputs, modification of spine properties translates into changes in the efficacy of synaptic communication. In understanding the molecular mechanisms involved in these processes, one may be able to develop therapies to treat psychiatric disorders.
- NMDAR hypofunction and schizophrenia. Disturbances in neuronal connectivity, particularly in glutamatergic synaptic connections, underlie schizophrenia and associated disorders. Neuropathological studies with autopsied brains from

schizophrenic individuals have reported reduced numbers of dendritic spines (Glantz and Lewis, 2000). Some studies have reported that there is a reduction in the glutamate receptor binding in the prefrontal cortex of individuals with schizophrenia. In general, NMDAR hypofunction has emerged as a major hypothesis for the incidence of schizophrenia with compelling evidence to support it. As the direct acting NMDA agonists can be excitotoxic, our investigation of upregulating the NMDAR function by the increments in  $[Na^+]_i$  provides a novel alternative method for the discovery of drugs to treat NMDAR hypofunction disorders.

- Stroke: Many of the mechanisms that underlie recovery after stroke are similar to those involved with plasticity in the intact brain. The stroke recovery mechanisms follow similar rules to those that hold during the development of nervous system and experience-dependent plasticity. Although the dendrites in the penumbra are damaged after a stroke event, they can partially recover their structure during reperfusion and the surviving neurons in the peri-infarct cortex, which is situated at the border of an infarct that has sufficient blood perfusion, undergo active structural and functional remodeling after stroke and sow the seeds for recovery. These neurons are spontaneously active owing to the transient loss of inhibition and increased glutamatergic transmission. This facilitates axonal sprouting and synaptogenesis in the peri-infarct area leading to remapping of function from damaged areas to surviving tissue. After stroke, cortical remapping is both activity-dependent and based on competition. The local environment might be altered after stroke to allow residually active stroke-affected inputs to compete effectively for making new connections compared to the intact tissues. Thus, a critical period of heightened neuroplasticity

exists in stroke patients implying the existence of a critical window within which rehabilitation has to be initiated so as to regain the maximum function. After development, stroke is a second, limited period of increased expression of genes and proteins that are important for neuronal growth, synaptogenesis and the proliferation of dendritic spines (Murphy and Corbett, 2009). We have shown that activation of VGSCs enhance NMDAR function and thereby promote different aspects of neuronal structural plasticity. As the direct acting NMDAR agonists are potentially excitotoxic, our current investigation reports a novel alternative method to upregulate NMDAR function by activating the voltage gated sodium channels and thereby increasing the  $[Na^+]_i$  above a critical threshold for enhancing NMDAR function.

## **References:**

- Aid T, Kazantseva A, Piirsoo M, Palm K, Timmusk T (2007) Mouse and rat BDNF gene structure and expression revisited. *J Neurosci Res* 85:525-535.
- Baden DG (1989) Brevetoxins: unique polyether dinoflagellate toxins. *FASEB J* 3:1807-1817.
- Baden DG, Bourdelais AJ, Jacocks H, Michelliza S, Naar J (2005) Natural and derivative brevetoxins: historical background, multiplicity, and effects. *Environ Health Perspect* 113:621-625.
- Bamji SX (2005) Cadherins: actin with the cytoskeleton to form synapses. *Neuron* 47:175-178.
- Bannister AJ, Kouzarides T (1996) The CBP co-activator is a histone acetyltransferase. *Nature* 384:641-643.
- Benarroch EE (2007) Rho GTPases: role in dendrite and axonal growth, mental retardation, and axonal regeneration. *Neurology* 68:1315-1318.
- Berninger B, Marty S, Zafra F, da Penha Berzaghi M, Thoenen H, Lindholm D (1995) GABAergic stimulation switches from enhancing to repressing BDNF expression in rat hippocampal neurons during maturation in vitro. *Development* 121:2327-2335.
- Boiko T, Rasband MN, Levinson SR, Caldwell JH, Mandel G, Trimmer JS, Matthews G (2001) Compact myelin dictates the differential targeting of two sodium channel isoforms in the same axon. *Neuron* 30:91-104.

- Cao Z, George J, Gerwick WH, Baden DG, Rainier JD, Murray TF (2008) Influence of lipid soluble gating modifier toxins on sodium influx in neocortical neurons. *J Pharmacol Exp Ther.*
- Castren E, Zafra F, Thoenen H, Lindholm D (1992) Light regulates expression of brain-derived neurotrophic factor mRNA in rat visual cortex. *Proc Natl Acad Sci U S A* 89:9444-9448.
- Catterall WA, Gainer M (1985) Interaction of brevetoxin A with a new receptor site on the sodium channel. *Toxicon* 23:497-504.
- Catterall WA, Goldin AL, Waxman SG (2003) International Union of Pharmacology. XXXIX. Compendium of voltage-gated ion channels: sodium channels. *Pharmacol Rev* 55:575-578.
- Catterall WA, Perez-Reyes E, Snutch TP, Striessnig J (2005) International Union of Pharmacology. XLVIII. Nomenclature and structure-function relationships of voltage-gated calcium channels. *Pharmacol Rev* 57:411-425.
- Cestele S, Catterall WA (2000) Molecular mechanisms of neurotoxin action on voltage-gated sodium channels. *Biochimie* 82:883-892.
- Chang L, Jones Y, Ellisman MH, Goldstein LS, Karin M (2003) JNK1 is required for maintenance of neuronal microtubules and controls phosphorylation of microtubule-associated proteins. *Dev Cell* 4:521-533.
- Chen BS, Roche KW (2007) Regulation of NMDA receptors by phosphorylation. *Neuropharmacology* 53:362-368.
- Chen Y, Ghosh A (2005) Regulation of dendritic development by neuronal activity. *J Neurobiol* 64:4-10.

- Chowdhury S, Shepherd JD, Okuno H, Lyford G, Petralia RS, Plath N, Kuhl D, Huganir RL, Worley PF (2006) Arc/Arg3.1 interacts with the endocytic machinery to regulate AMPA receptor trafficking. *Neuron* 52:445-459.
- Ciani L, Salinas PC (2005) WNTs in the vertebrate nervous system: from patterning to neuronal connectivity. *Nat Rev Neurosci* 6:351-362.
- Cline HT (2001) Dendritic arbor development and synaptogenesis. *Curr Opin Neurobiol* 11:118-126.
- Cobos I, Borello U, Rubenstein JL (2007) Dlx transcription factors promote migration through repression of axon and dendrite growth. *Neuron* 54:873-888.
- Cohen S, Greenberg ME (2008) Communication between the synapse and the nucleus in neuronal development, plasticity, and disease. *Annu Rev Cell Dev Biol* 24:183-209.
- Colbran RJ, Brown AM (2004) Calcium/calmodulin-dependent protein kinase II and synaptic plasticity. *Curr Opin Neurobiol* 14:318-327.
- Cull-Candy SG, Leszkiewicz DN (2004) Role of distinct NMDA receptor subtypes at central synapses. *Sci STKE* 2004:re16.
- Dingledine R, Borges K, Bowie D, Traynelis SF (1999) The glutamate receptor ion channels. *Pharmacol Rev* 51:7-61.
- Docherty RJ, Farmer CE (2009) The pharmacology of voltage-gated sodium channels in sensory neurones. *Handb Exp Pharmacol*:519-561.
- Dolmetsch RE, Pajvani U, Fife K, Spotts JM, Greenberg ME (2001) Signaling to the nucleus by an L-type calcium channel-calmodulin complex through the MAP kinase pathway. *Science* 294:333-339.

- Du J, Feng L, Yang F, Lu B (2000) Activity- and Ca(2+)-dependent modulation of surface expression of brain-derived neurotrophic factor receptors in hippocampal neurons. *J Cell Biol* 150:1423-1434.
- Ernfors P, Bengzon J, Kokaia Z, Persson H, Lindvall O (1991) Increased levels of messenger RNAs for neurotrophic factors in the brain during kindling epileptogenesis. *Neuron* 7:165-176.
- Ewald RC, Van Keuren-Jensen KR, Aizenman CD, Cline HT (2008) Roles of NR2A and NR2B in the development of dendritic arbor morphology in vivo. *J Neurosci* 28:850-861.
- Faherty CJ, Kerley D, Smeyne RJ (2003) A Golgi-Cox morphological analysis of neuronal changes induced by environmental enrichment. *Brain Res Dev Brain Res* 141:55-61.
- Figurov A, Pozzo-Miller LD, Olafsson P, Wang T, Lu B (1996) Regulation of synaptic responses to high-frequency stimulation and LTP by neurotrophins in the hippocampus. *Nature* 381:706-709.
- Fink CC, Bayer KU, Myers JW, Ferrell JE, Jr., Schulman H, Meyer T (2003) Selective regulation of neurite extension and synapse formation by the beta but not the alpha isoform of CaMKII. *Neuron* 39:283-297.
- Furukawa H, Singh SK, Mancusso R, Gouaux E (2005) Subunit arrangement and function in NMDA receptors. *Nature* 438:185-192.
- Furutani Y, Matsuno H, Kawasaki M, Sasaki T, Mori K, Yoshihara Y (2007) Interaction between telencephalin and ERM family proteins mediates dendritic filopodia formation. *J Neurosci* 27:8866-8876.

- Gawley RE, Rein KS, Kinoshita M, Baden DG (1992) Binding of brevetoxins and ciguatoxin to the voltage-sensitive sodium channel and conformational analysis of brevetoxin B. *Toxicon* 30:780-785.
- Glantz LA, Lewis DA (2000) Decreased dendritic spine density on prefrontal cortical pyramidal neurons in schizophrenia. *Arch Gen Psychiatry* 57:65-73.
- Hand R, Bortone D, Mattar P, Nguyen L, Heng JI, Guerrier S, Boutt E, Peters E, Barnes AP, Parras C, Schuurmans C, Guillemot F, Polleux F (2005) Phosphorylation of Neurogenin2 specifies the migration properties and the dendritic morphology of pyramidal neurons in the neocortex. *Neuron* 48:45-62.
- Honkura N, Matsuzaki M, Noguchi J, Ellis-Davies GC, Kasai H (2008) The subspine organization of actin fibers regulates the structure and plasticity of dendritic spines. *Neuron* 57:719-729.
- Horch HW, Katz LC (2002) BDNF release from single cells elicits local dendritic growth in nearby neurons. *Nat Neurosci* 5:1177-1184.
- Inglis FM, Zuckerman KE, Kalb RG (2000) Experience-dependent development of spinal motor neurons. *Neuron* 26:299-305.
- Isackson PJ, Huntsman MM, Murray KD, Gall CM (1991) BDNF mRNA expression is increased in adult rat forebrain after limbic seizures: temporal patterns of induction distinct from NGF. *Neuron* 6:937-948.
- Jaffe AB, Hall A (2005) Rho GTPases: biochemistry and biology. *Annu Rev Cell Dev Biol* 21:247-269.
- Jan YN, Jan LY (2003) The control of dendrite development. *Neuron* 40:229-242.

- Jaworski J, Spangler S, Seeburg DP, Hoogenraad CC, Sheng M (2005) Control of dendritic arborization by the phosphoinositide-3'-kinase-Akt-mammalian target of rapamycin pathway. *J Neurosci* 25:11300-11312.
- Jeglitsch G, Rein K, Baden DG, Adams DJ (1998) Brevetoxin-3 (PbTx-3) and its derivatives modulate single tetrodotoxin-sensitive sodium channels in rat sensory neurons. *J Pharmacol Exp Ther* 284:516-525.
- Kang H, Schuman EM (1996) A requirement for local protein synthesis in neurotrophin-induced hippocampal synaptic plasticity. *Science* 273:1402-1406.
- Kaplan MR, Cho MH, Ullian EM, Isom LL, Levinson SR, Barres BA (2001) Differential control of clustering of the sodium channels Na(v)1.2 and Na(v)1.6 at developing CNS nodes of Ranvier. *Neuron* 30:105-119.
- Kasai H, Matsuzaki M, Noguchi J, Yasumatsu N, Nakahara H (2003) Structure-stability-function relationships of dendritic spines. *Trends Neurosci* 26:360-368.
- Kaufmann WE, Moser HW (2000) Dendritic anomalies in disorders associated with mental retardation. *Cereb Cortex* 10:981-991.
- Klein ME, Impey S, Goodman RH (2005) Role reversal: the regulation of neuronal gene expression by microRNAs. *Curr Opin Neurobiol* 15:507-513.
- Konur S, Ghosh A (2005) Calcium signaling and the control of dendritic development. *Neuron* 46:401-405.
- Kornhauser JM, Cowan CW, Shaywitz AJ, Dolmetsch RE, Griffith EC, Hu LS, Haddad C, Xia Z, Greenberg ME (2002) CREB transcriptional activity in neurons is regulated by multiple, calcium-specific phosphorylation events. *Neuron* 34:221-233.

- Kuczewski N, Porcher C, Lessmann V, Medina I, Gaiarsa JL (2009) Activity-dependent dendritic release of BDNF and biological consequences. *Mol Neurobiol* 39:37-49.
- Kumar V, Zhang MX, Swank MW, Kunz J, Wu GY (2005) Regulation of dendritic morphogenesis by Ras-PI3K-Akt-mTOR and Ras-MAPK signaling pathways. *J Neurosci* 25:11288-11299.
- Lavezzari G, McCallum J, Lee R, Roche KW (2003) Differential binding of the AP-2 adaptor complex and PSD-95 to the C-terminus of the NMDA receptor subunit NR2B regulates surface expression. *Neuropharmacology* 45:729-737.
- Lee HK (2006) Synaptic plasticity and phosphorylation. *Pharmacol Ther* 112:810-832.
- Lee LJ, Lo FS, Erzurumlu RS (2005) NMDA receptor-dependent regulation of axonal and dendritic branching. *J Neurosci* 25:2304-2311.
- Li Z, Okamoto K, Hayashi Y, Sheng M (2004) The importance of dendritic mitochondria in the morphogenesis and plasticity of spines and synapses. *Cell* 119:873-887.
- Lim CS, Walikonis RS (2008) Hepatocyte growth factor and c-Met promote dendritic maturation during hippocampal neuron differentiation via the Akt pathway. *Cell Signal* 20:825-835.
- Lohmann C, Wong RO (2005) Regulation of dendritic growth and plasticity by local and global calcium dynamics. *Cell Calcium* 37:403-409.
- Lohmann C, Bonhoeffer T (2008) A role for local calcium signaling in rapid synaptic partner selection by dendritic filopodia. *Neuron* 59:253-260.
- Lohmann C, Finski A, Bonhoeffer T (2005) Local calcium transients regulate the spontaneous motility of dendritic filopodia. *Nat Neurosci* 8:305-312.

- Lohof AM, Ip NY, Poo MM (1993) Potentiation of developing neuromuscular synapses by the neurotrophins NT-3 and BDNF. *Nature* 363:350-353.
- Matsuzaki M, Honkura N, Ellis-Davies GC, Kasai H (2004) Structural basis of long-term potentiation in single dendritic spines. *Nature* 429:761-766.
- McAllister AK (2000) Cellular and molecular mechanisms of dendrite growth. *Cereb Cortex* 10:963-973.
- McAllister AK (2002) Bdnf. *Curr Biol* 12:R310.
- Michelliza S, Abraham WM, Jacocks HM, Schuster T, Baden DG (2007) Synthesis, modeling, and biological evaluation of analogues of the semisynthetic brevetoxin antagonist beta-naphthoyl-brevetoxin. *Chembiochem* 8:2233-2239.
- Miller FD, Kaplan DR (2003) Signaling mechanisms underlying dendrite formation. *Curr Opin Neurobiol* 13:391-398.
- Morgan JI, Cohen DR, Hempstead JL, Curran T (1987) Mapping patterns of c-fos expression in the central nervous system after seizure. *Science* 237:192-197.
- Murphy TH, Corbett D (2009) Plasticity during stroke recovery: from synapse to behaviour. *Nat Rev Neurosci* 10:861-872.
- Naeve GS, Ramakrishnan M, Kramer R, Hevroni D, Citri Y, Theill LE (1997) Neuritin: a gene induced by neural activity and neurotrophins that promotes neuritogenesis. *Proc Natl Acad Sci U S A* 94:2648-2653.
- Nagappan G, Lu B (2005) Activity-dependent modulation of the BDNF receptor TrkB: mechanisms and implications. *Trends Neurosci* 28:464-471.
- Nakazawa T, Komai S, Tezuka T, Hisatsune C, Umemori H, Semba K, Mishina M, Manabe T, Yamamoto T (2001) Characterization of Fyn-mediated tyrosine

- phosphorylation sites on GluR epsilon 2 (NR2B) subunit of the N-methyl-D-aspartate receptor. *J Biol Chem* 276:693-699.
- Nedivi E (1999) Molecular analysis of developmental plasticity in neocortex. *J Neurobiol* 41:135-147.
- Nikonenko I, Boda B, Steen S, Knott G, Welker E, Muller D (2008) PSD-95 promotes synaptogenesis and multiinnervated spine formation through nitric oxide signaling. *J Cell Biol* 183:1115-1127.
- Ooms LM, Fedele CG, Astle MV, Ivetac I, Cheung V, Pearson RB, Layton MJ, Forrai A, Nandurkar HH, Mitchell CA (2006) The inositol polyphosphate 5-phosphatase, PIPP, is a novel regulator of phosphoinositide 3-kinase-dependent neurite elongation. *Mol Biol Cell* 17:607-622.
- Paoletti P, Neyton J (2007) NMDA receptor subunits: function and pharmacology. *Curr Opin Pharmacol* 7:39-47.
- Pierce RH, Henry MS, Blum PC, Hamel SL, Kirkpatrick B, Cheng YS, Zhou Y, Irvin CM, Naar J, Weidner A, Fleming LE, Backer LC, Baden DG (2005) Brevetoxin composition in water and marine aerosol along a Florida beach: Assessing potential human exposure to marine biotoxins. *Harmful Algae* 4:965-972.
- Poli MA, Mende TJ, Baden DG (1986) Brevetoxins, unique activators of voltage-sensitive sodium channels, bind to specific sites in rat brain synaptosomes. *Mol Pharmacol* 30:129-135.
- Qiu Z, Ghosh A (2008) A brief history of neuronal gene expression: regulatory mechanisms and cellular consequences. *Neuron* 60:449-455.

- Rajan I, Cline HT (1998) Glutamate receptor activity is required for normal development of tectal cell dendrites in vivo. *J Neurosci* 18:7836-7846.
- Ramos B, Gaudilliere B, Bonni A, Gill G (2007) Transcription factor Sp4 regulates dendritic patterning during cerebellar maturation. *Proc Natl Acad Sci U S A* 104:9882-9887.
- Read DE, Gorman AM (2009) Involvement of Akt in neurite outgrowth. *Cell Mol Life Sci* 66:2975-2984.
- Redmond L (2008) Translating neuronal activity into dendrite elaboration: signaling to the nucleus. *Neurosignals* 16:194-208.
- Redmond L, Kashani AH, Ghosh A (2002) Calcium regulation of dendritic growth via CaM kinase IV and CREB-mediated transcription. *Neuron* 34:999-1010.
- Rial Verde EM, Lee-Osbourne J, Worley PF, Malinow R, Cline HT (2006) Increased expression of the immediate-early gene *arc/arg3.1* reduces AMPA receptor-mediated synaptic transmission. *Neuron* 52:461-474.
- Roche KW, Standley S, McCallum J, Dune Ly C, Ehlers MD, Wenthold RJ (2001) Molecular determinants of NMDA receptor internalization. *Nat Neurosci* 4:794-802.
- Rose CR, Konnerth A (2001) NMDA receptor-mediated Na<sup>+</sup> signals in spines and dendrites. *J Neurosci* 21:4207-4214.
- Rose CR, Kovalchuk Y, Eilers J, Konnerth A (1999) Two-photon Na<sup>+</sup> imaging in spines and fine dendrites of central neurons. *Pflugers Arch* 439:201-207.
- Salter MW, Kalia LV (2004) Src kinases: a hub for NMDA receptor regulation. *Nat Rev Neurosci* 5:317-328.

- Saneyoshi T, Wayman G, Fortin D, Davare M, Hoshi N, Nozaki N, Natsume T, Soderling TR (2008) Activity-dependent synaptogenesis: regulation by a CaM-kinase kinase/CaM-kinase I/betaPIX signaling complex. *Neuron* 57:94-107.
- Schmitt JM, Wayman GA, Nozaki N, Soderling TR (2004) Calcium activation of ERK mediated by calmodulin kinase I. *J Biol Chem* 279:24064-24072.
- Schmitt JM, Guire ES, Saneyoshi T, Soderling TR (2005) Calmodulin-dependent kinase kinase/calmodulin kinase I activity gates extracellular-regulated kinase-dependent long-term potentiation. *J Neurosci* 25:1281-1290.
- Schratt G (2009) microRNAs at the synapse. *Nat Rev Neurosci* 10:842-849.
- Schratt GM, Tuebing F, Nigh EA, Kane CG, Sabatini ME, Kiebler M, Greenberg ME (2006) A brain-specific microRNA regulates dendritic spine development. *Nature* 439:283-289.
- Segal M (2005) Dendritic spines and long-term plasticity. *Nat Rev Neurosci* 6:277-284.
- Shepherd JD, Rumbaugh G, Wu J, Chowdhury S, Plath N, Kuhl D, Huganir RL, Worley PF (2006) Arc/Arg3.1 mediates homeostatic synaptic scaling of AMPA receptors. *Neuron* 52:475-484.
- Shieh PB, Hu SC, Bobb K, Timmusk T, Ghosh A (1998) Identification of a signaling pathway involved in calcium regulation of BDNF expression. *Neuron* 20:727-740.
- Sin WC, Haas K, Ruthazer ES, Cline HT (2002) Dendrite growth increased by visual activity requires NMDA receptor and Rho GTPases. *Nature* 419:475-480.
- Spitzer NC, Lautermilch NJ, Smith RD, Gomez TM (2000) Coding of neuronal differentiation by calcium transients. *Bioessays* 22:811-817.

- Tada T, Sheng M (2006) Molecular mechanisms of dendritic spine morphogenesis. *Curr Opin Neurobiol* 16:95-101.
- Takasu MA, Dalva MB, Zigmond RE, Greenberg ME (2002) Modulation of NMDA receptor-dependent calcium influx and gene expression through EphB receptors. *Science* 295:491-495.
- Takemoto-Kimura S, Terai H, Takamoto M, Ohmae S, Kikumura S, Segi E, Arakawa Y, Furuyashiki T, Narumiya S, Bito H (2003) Molecular cloning and characterization of CLICK-III/CaMKIgamma, a novel membrane-anchored neuronal Ca<sup>2+</sup>/calmodulin-dependent protein kinase (CaMK). *J Biol Chem* 278:18597-18605.
- Takemoto-Kimura S, Ageta-Ishihara N, Nonaka M, Adachi-Morishima A, Mano T, Okamura M, Fujii H, Fuse T, Hoshino M, Suzuki S, Kojima M, Mishina M, Okuno H, Bito H (2007) Regulation of dendritogenesis via a lipid-raft-associated Ca<sup>2+</sup>/calmodulin-dependent protein kinase CLICK-III/CaMKIgamma. *Neuron* 54:755-770.
- Tao X, Finkbeiner S, Arnold DB, Shaywitz AJ, Greenberg ME (1998) Ca<sup>2+</sup> influx regulates BDNF transcription by a CREB family transcription factor-dependent mechanism. *Neuron* 20:709-726.
- Tian L, Stefanidakis M, Ning L, Van Lint P, Nyman-Huttunen H, Libert C, Itohara S, Mishina M, Rauvala H, Gahmberg CG (2007) Activation of NMDA receptors promotes dendritic spine development through MMP-mediated ICAM-5 cleavage. *J Cell Biol* 178:687-700.

- Tolias KF, Bikoff JB, Burette A, Paradis S, Harrar D, Tavazoie S, Weinberg RJ, Greenberg ME (2005) The Rac1-GEF Tiam1 couples the NMDA receptor to the activity-dependent development of dendritic arbors and spines. *Neuron* 45:525-538.
- Tongiorgi E (2008) Activity-dependent expression of brain-derived neurotrophic factor in dendrites: facts and open questions. *Neurosci Res* 61:335-346.
- Trainer VL, Baden DG, Catterall WA (1994) Identification of peptide components of the brevetoxin receptor site of rat brain sodium channels. *J Biol Chem* 269:19904-19909.
- Ueda T, Sakagami H, Abe K, Oishi I, Maruo A, Kondo H, Terashima T, Ichihashi M, Yamamura H, Minami Y (1999) Distribution and intracellular localization of a mouse homologue of Ca<sup>2+</sup>/calmodulin-dependent protein kinase I $\beta$ 2 in the nervous system. *J Neurochem* 73:2119-2129.
- Ultanir SK, Kim JE, Hall BJ, Deerinck T, Ellisman M, Ghosh A (2007) Regulation of spine morphology and spine density by NMDA receptor signaling in vivo. *Proc Natl Acad Sci U S A* 104:19553-19558.
- Urbanska M, Blazejczyk M, Jaworski J (2008) Molecular basis of dendritic arborization. *Acta Neurobiol Exp (Wars)* 68:264-288.
- Vissel B, Krupp JJ, Heinemann SF, Westbrook GL (2001) A use-dependent tyrosine dephosphorylation of NMDA receptors is independent of ion flux. *Nat Neurosci* 4:587-596.

- Vo N, Klein ME, Varlamova O, Keller DM, Yamamoto T, Goodman RH, Impey S (2005) A cAMP-response element binding protein-induced microRNA regulates neuronal morphogenesis. *Proc Natl Acad Sci U S A* 102:16426-16431.
- Wayman GA, Lee YS, Tokumitsu H, Silva AJ, Soderling TR (2008) Calmodulin-kinases: modulators of neuronal development and plasticity. *Neuron* 59:914-931.
- Wayman GA, Impey S, Marks D, Saneyoshi T, Grant WF, Derkach V, Soderling TR (2006) Activity-dependent dendritic arborization mediated by CaM-kinase I activation and enhanced CREB-dependent transcription of Wnt-2. *Neuron* 50:897-909.
- Wayman GA, Kaech S, Grant WF, Davare M, Impey S, Tokumitsu H, Nozaki N, Banker G, Soderling TR (2004) Regulation of axonal extension and growth cone motility by calmodulin-dependent protein kinase I. *J Neurosci* 24:3786-3794.
- West AE, Griffith EC, Greenberg ME (2002) Regulation of transcription factors by neuronal activity. *Nat Rev Neurosci* 3:921-931.
- West AE, Chen WG, Dalva MB, Dolmetsch RE, Kornhauser JM, Shaywitz AJ, Takasu MA, Tao X, Greenberg ME (2001) Calcium regulation of neuronal gene expression. *Proc Natl Acad Sci U S A* 98:11024-11031.
- Westenbroek RE, Merrick DK, Catterall WA (1989) Differential subcellular localization of the RI and RII Na<sup>+</sup> channel subtypes in central neurons. *Neuron* 3:695-704.
- Wong RO, Ghosh A (2002) Activity-dependent regulation of dendritic growth and patterning. *Nat Rev Neurosci* 3:803-812.
- Wu GY, Deisseroth K, Tsien RW (2001) Activity-dependent CREB phosphorylation: convergence of a fast, sensitive calmodulin kinase pathway and a slow, less

- sensitive mitogen-activated protein kinase pathway. *Proc Natl Acad Sci U S A* 98:2808-2813.
- Xin WK, Kwan CL, Zhao XH, Xu J, Ellen RP, McCulloch CA, Yu XM (2005) A functional interaction of sodium and calcium in the regulation of NMDA receptor activity by remote NMDA receptors. *J Neurosci* 25:139-148.
- Yoshihara Y, De Roo M, Muller D (2009) Dendritic spine formation and stabilization. *Curr Opin Neurobiol* 19:146-153.
- Yu FH, Catterall WA (2003) Overview of the voltage-gated sodium channel family. *Genome Biol* 4:207.
- Yu X, Malenka RC (2003) Beta-catenin is critical for dendritic morphogenesis. *Nat Neurosci* 6:1169-1177.
- Yu XM (2006) The Role of Intracellular Sodium in the Regulation of NMDA-Receptor-Mediated Channel Activity and Toxicity. *Mol Neurobiol* 33:63-80.
- Yu XM, Salter MW (1998) Gain control of NMDA-receptor currents by intracellular sodium. *Nature* 396:469-474.
- Zafra F, Hengerer B, Leibrock J, Thoenen H, Lindholm D (1990) Activity dependent regulation of BDNF and NGF mRNAs in the rat hippocampus is mediated by non-NMDA glutamate receptors. *EMBO J* 9:3545-3550.
- Zito K, Scheuss V, Knott G, Hill T, Svoboda K (2009) Rapid functional maturation of nascent dendritic spines. *Neuron* 61:247-258.

Development/Plasticity/Repair

# Sodium Channel Activation Augments NMDA Receptor Function and Promotes Neurite Outgrowth in Immature Cerebrocortical Neurons

Joju George,<sup>1</sup> Shashank M. Dravid,<sup>1</sup> Anand Prakash,<sup>1</sup> Jun Xie,<sup>1,2</sup> Jennifer Peterson,<sup>3</sup> Sairam V. Jabba,<sup>1</sup> Daniel G. Baden,<sup>4</sup> and Thomas F. Murray<sup>1</sup><sup>1</sup>Department of Pharmacology, Creighton University School of Medicine, Omaha, Nebraska 68178, <sup>2</sup>Department of Biochemistry and Molecular Biology, Shanxi Medical University, Taiyuan 030001, China, <sup>3</sup>College of Veterinary Medicine, University of Georgia, Athens, Georgia 30602, and <sup>4</sup>Center for Marine Science, University of North Carolina at Wilmington, Wilmington, North Carolina 28409

A range of extrinsic signals, including afferent activity, affect neuronal growth and plasticity. Neuronal activity regulates intracellular  $\text{Ca}^{2+}$ , and activity-dependent calcium signaling has been shown to regulate dendritic growth and branching (Konur and Ghosh, 2005). NMDA receptor (NMDAR) stimulation of  $\text{Ca}^{2+}$ /calmodulin-dependent protein kinase signaling cascades has, moreover, been demonstrated to regulate neurite/axonal outgrowth (Wayman et al., 2004). We used a sodium channel activator, brevetoxin (PbTx-2), to explore the relationship between intracellular  $[\text{Na}^+]_i$  and NMDAR-dependent development. PbTx-2 alone, at a concentration of 30 nM, did not affect  $\text{Ca}^{2+}$  dynamics in 2 d *in vitro* cerebrocortical neurons; however, this treatment robustly potentiated NMDA-induced  $\text{Ca}^{2+}$  influx. The 30 nM PbTx-2 treatment produced a maximum  $[\text{Na}^+]_i$  of  $16.9 \pm 1.5$  mM, representing an increment of  $8.8 \pm 1.8$  mM over basal. The corresponding membrane potential change produced by 30 nM PbTx-2 was modest and, therefore, insufficient to relieve the voltage-dependent  $\text{Mg}^{2+}$  block of NMDARs. To unambiguously demonstrate the enhancement of NMDA receptor function by PbTx-2, we recorded single-channel currents from cell-attached patches. PbTx-2 treatment was found to increase both the mean open time and open probability of NMDA receptors. These effects of PbTx-2 on NMDA receptor function were dependent on extracellular  $\text{Na}^+$  and activation of Src kinase. The functional consequences of PbTx-2-induced enhancement of NMDAR function were evaluated in immature cerebrocortical neurons. PbTx-2 concentrations between 3 and 300 nM enhanced neurite outgrowth. Voltage-gated sodium channel activators may accordingly represent a novel pharmacologic strategy to regulate neuronal plasticity through an NMDA receptor and Src family kinase-dependent mechanism.

## Introduction

Neuronal activity plays a key role in the regulation of dendritic development (McAllister, 2000; Cline, 2001; Chen and Ghosh, 2005). Neuronal activity regulates intracellular  $\text{Ca}^{2+}$ , and activity-dependent calcium signaling has been shown to regulate dendritic growth and branching (Konur and Ghosh, 2005).  $\text{Ca}^{2+}$ /calmodulin-dependent protein kinases (CaMKs) and mitogen-activated protein kinase (MAPKs) appear to be key mediators of calcium-dependent neurite outgrowth (Redmond et al., 2002). CaMK kinase (CaMKK) has been demonstrated to be an upstream regulator of both CaMK- and MAPK-signaling pathways. NMDA receptor (NMDAR)-dependent CaMKK/calmodulin kinase I-signaling cascades have, moreover, been shown to regulate neurite/axonal outgrowth (Wayman et al., 2004), activity-dependent synaptogenesis (Saneyoshi et al., 2008), and

$\text{Ca}^{2+}$ -dependent extracellular regulated kinase activation and dendritic outgrowth (Schmitt et al., 2004; Wayman et al., 2006). NMDARs, therefore, play a critical role in activity-dependent development and plasticity, dendritic arborization, spine morphogenesis, and synapse formation by stimulating these calcium-dependent signaling pathways (Rajan and Cline, 1998; Sin et al., 2002; West et al., 2002; Wong and Ghosh, 2002; Miller and Kaplan, 2003; Tolia et al., 2005; Ultanir et al., 2007).

Recent studies have indicated that changes in intracellular sodium concentration ( $[\text{Na}^+]_i$ ) produced in the soma and dendrites as a result of neuronal activity may act as a signaling molecule and play a role in activity-dependent synaptic plasticity. It has been shown that synaptic stimulation causes  $[\text{Na}^+]_i$  increments of 10 mM in dendrites and of up to 35–40 mM in dendritic spines (Rose et al., 1999; Rose and Konnerth, 2001). In hippocampal neurons, intracellular  $[\text{Na}^+]_i$  increments have been demonstrated to increase NMDAR-mediated whole-cell currents and NMDAR single-channel activity by increasing both channel open probability and mean open time. This  $[\text{Na}^+]_i$ -mediated upregulation of NMDAR function has been shown to require Src kinase activation (Yu and Salter, 1998). Src family kinases act as a crucial point of convergence for signaling pathways that enhance

Received Dec. 22, 2008; revised Feb. 5, 2009; accepted Feb. 7, 2009.

This work was supported in part by National Institutes of Health Grants ES10594 (to D.G.B.) and NS053398 (to T.F.M.).

Correspondence should be addressed to Dr. Thomas F. Murray, Department of Pharmacology, Creighton University School of Medicine, Omaha, NE 68178. E-mail: tfmurray@creighton.edu.

DOI:10.1523/JNEUROSCI.6104-08.2009

Copyright © 2009 Society for Neuroscience 0270-6474/09/293288-14\$15.00/0

NMDAR activity, and, by upregulating the function of NMDARs, Src gates the production of NMDAR-dependent synaptic potentiation and plasticity (Salter and Kalia, 2004).

We reasoned that  $[Na^+]_i$  may act as a positive regulator of developmental plasticity in immature cerebrocortical neurons. In the present study, we used brevetoxin (PbTx-2), a voltage-gated sodium channel (VGSC) activator, to manipulate  $[Na^+]_i$  in immature murine cerebrocortical neurons. Brevetoxins interact with neurotoxin site 5 on the  $\alpha$ -subunit of VGSCs (Catterall and Gainer, 1985; Poli et al., 1986) and augment sodium influx through VGSCs by shifting the activation potential to more negative values, increasing the mean open time of the channel and inhibiting channel inactivation (Jeglitsch et al., 1998). Using immature cerebrocortical neurons, we now demonstrate that a VGSC activator elevates  $[Na^+]_i$  levels, enhances NMDA-induced  $Ca^{2+}$  influx, increases both NMDAR channel open probability and mean open time, and augments neurite outgrowth. These results provide direct evidence to support the hypothesis that NMDA receptor function is upregulated by elevated  $[Na^+]_i$ , which, in turn, promotes neurite outgrowth.

## Materials and Methods

### Materials

Trypsin, penicillin, streptomycin, heat-inactivated fetal bovine serum, horse serum, and soybean trypsin inhibitor were obtained from Atlanta Biologicals. Minimum essential medium, deoxyribonuclease, poly-L-lysine, poly-D-lysine hydrobromide, cytosine arabinoside, NMDA, protease inhibitor mixture, MK-801, D(-)-2-amino-5-phosphopentanoic acid (APV), and nifedipine were purchased from Sigma. Pluronic acid, fluo-3 acetoxyethyl ester (AM), and sodium-binding benzofuran isophthalate (SBFI)-AM were purchased from Invitrogen. 4-Amino-5-(4-chlorophenyl)-7-(t-butyl)pyrazolo[3, 4-d] pyrimidine (PP2), 4-amino-7-phenylpyrazol [3, 4-d] pyrimidine (PP3), and STO-609 were purchased from Calbiochem. ECL Plus kits were purchased from GE Healthcare. Neurobasal and B-27 supplement were purchased from Invitrogen. FLIPR (fluorometric imaging plate reader) membrane potential assay kit was purchased from Molecular Devices. Anti-phospho Src (416) and anti-Src antibodies were purchased from Cell Signaling Technology, rabbit anti-human protein gene product 9.5 (PGP 9.5) from AbD Serotec, and fluorescein (FITC) affiniPure goat anti-rabbit IgG from Jackson ImmunoResearch Laboratories. Brevetoxin-2 (PbTx-2) was isolated and purified from *Karina brevis* cultures at the Center for Marine Sciences at the University of North Carolina (Wilmington, NC).

### Methods

**Cerebrocortical neuron culture.** Primary cultures of cerebrocortical neurons were harvested from embryos of Swiss-Webster mice on embryonic day 16 and cultured as described previously (Cao et al., 2008). Cells were plated onto poly-L-lysine-coated 96-well (9 mm), clear-bottomed, black-well culture plates (Costar) at a density of  $1.5 \times 10^5$  cells per well, 24-well (15.6 mm) culture plates at a density of  $0.05 \times 10^6$  cells per well, 12-well (22 mm) culture plate (TPP-Midscience) at a density of  $1.8 \times 10^6$  cells per well or 6-well (35 mm) culture dishes at a density of  $4.5 \times 10^6$  cell per well, respectively, and incubated at 37°C in a 5% CO<sub>2</sub> and 95% humidity atmosphere. Cytosine arabinoside (10  $\mu$ M) was added to the culture medium on day 2 after plating to prevent proliferation of non-neuronal cells. The culture media was changed on days 4 and 7 using a serum-free growth medium containing neurobasal medium supplemented with B-27, 100 I.U./ml penicillin, 0.10 mg/ml streptomycin, and 0.2 mM L-glutamine. All animal use protocols were approved by the Institutional Animal Care and Use Committee.

**Excitotoxicity assays.** The growth medium of neurons grown on 12 well plates was collected and saved, and the neurons washed thrice in 1 ml of sterile filtered Locke's incubation buffer (154 mM NaCl, 5.6 mM KCl, 1.0 mM MgCl<sub>2</sub>, 2.3 mM CaCl<sub>2</sub>, 8.6 mM HEPES, 5.6 mM glucose, 0.1 mM glycine, pH 7.4). The neurons were then exposed to varying concentrations of NMDA in 1 ml of Locke's buffer for 2 h at 37°C in a 5% CO<sub>2</sub> and

95% humidity atmosphere. At the termination of NMDA exposure, the incubation medium was collected for later analysis of lactate dehydrogenase (LDH) activity, and the neurons were washed thrice in 1 ml of fresh Locke's buffer followed by replacement with previously collected growth medium that had been filtered and supplemented with 1.25 mg/ml D-glucose. The cell cultures were then incubated at 37°C in a 5% CO<sub>2</sub> and 95% humidity atmosphere. At 24 h after treatment exposure, the growth medium was collected and saved for analysis of LDH activity. The LDH activity was assayed according to a previously described method (Koh and Choi, 1987).

Neuronal injury was also assessed morphologically by exposing cerebrocortical neurons for 5 min to the vital dye fluorescein diacetate (5  $\mu$ g/ml). After 5 min incubation in dye, the neurons were washed three times in fresh Locke's buffer. Three random 20 $\times$  field images were taken per well. Uniform sector areas ( $n = 6$ ) were counted for viable neurons on each 20 $\times$  field image and were normalized to the number of viable neurons per area of the well.

**Immunocytochemistry.** To assess the influence of PbTx-2 on neuronal morphogenesis, cells grown on poly-lysine coated cover glass placed inside 24-well culture plates were used. PbTx-2 at concentrations ranging from 0.1 to 1000 nM were added to the culture medium at 3 h after plating. In some experiments, these concentrations of PbTx-2 were co-incubated with tetrodotoxin (TTX) (1  $\mu$ M), MK-801 (1  $\mu$ M), nifedipine (1  $\mu$ M), or STO-609 (2.6  $\mu$ M). Cultures were fixed for 20 min at room temperature at 15, 24, 40, or 108 h after plating using 4% paraformaldehyde in PBS. After fixation, neurons were blocked and permeabilized by incubation for 30 min with PBS containing 2% fetal bovine serum and 0.15% Triton X-100. The coverslips were then inverted onto 100  $\mu$ l droplets of blocking buffer containing the protein gene product 9.5 (anti-PGP 9.5) primary antibody for 60 min at room temperature or overnight at 4°C. After three successive washes in blocking buffer, coverslips were incubated with a secondary antibody [FITC (anti-rabbit IgG)] for 60 min at room temperature. Coverslips were washed and mounted on microscope slides and analyzed by fluorescence microscopy on an Olympus IX 71 inverted microscope with a Nikon camera. Digital images of individual neurons were captured and total neurite length quantified using IP Lab 3.6.5 software (Scanalytics). At least 30 randomly chosen neurons from different cultures were evaluated for each treatment group.

**Intracellular Ca<sup>2+</sup> monitoring.** Cerebrocortical neurons grown in 96-well plates were used for intracellular Ca<sup>2+</sup> concentration ( $[Ca^{2+}]_i$ ) measurements as described previously (Dravid et al., 2005). Briefly, the growth medium was removed and replaced with dye-loading medium (100  $\mu$ l per well) containing 4  $\mu$ M fluo-3 AM and 0.04% pluronic acid in Locke's buffer. After 1 h of incubation in dye-loading medium, the neurons were washed four times in fresh Locke's buffer (200  $\mu$ l per well, 22°C) using an automated microplate washer (Bio-Tek Instruments) and transferred to a FLEX Station II (Molecular Devices) benchtop scanning fluorometer chamber. The final volume of Locke's buffer in each well was 150  $\mu$ l. Fluorescence measurements were performed at 37°C. The neurons were excited at 488 nm and Ca<sup>2+</sup>-bound fluo-3 emission was recorded at 538 nm at 1.2 s intervals. After recording baseline fluorescence for 60 s, 50  $\mu$ l of a 4 $\times$  concentration of NMDA, PbTx-2, or both were added to the cells at a rate of 26  $\mu$ l/s, yielding a final volume of 200  $\mu$ l/well; the fluorescence was monitored for an additional 140–240 s. The fluo-3 fluorescence was expressed as  $(F_{max} - F_{min})/F_{min}$  where  $F_{max}$  was the maximum,  $F_{min}$  the minimum fluorescence measured in each well.

**Intracellular sodium concentration ( $[Na^+]_i$ ) measurement.**  $[Na^+]_i$  measurement and full *in situ* calibration of SBFI fluorescence ratio was performed as described previously (Cao et al., 2008). Cells grown in 96-well plates were washed four times with Locke's buffer (in mM: 8.6 HEPES, 5.6 KCl, 154 NaCl, 5.6 glucose, 1.0 MgCl<sub>2</sub>, 2.3 CaCl<sub>2</sub>, 0.1 glycine, pH 7.4) using an automated microplate washer (Bio-Tek Instruments). The background fluorescence of each well was measured and averaged before dye loading. Cells were then incubated for 1 h at 37°C with dye-loading buffer (100  $\mu$ l/well) containing 10  $\mu$ M SBFI-AM and 0.02% pluronic F-127. After 1 h incubation in dye-loading medium, cells were washed five times with Locke's buffer, leaving a final volume of 150  $\mu$ l in each well. The plate was then transferred to the chamber of a FLEXstation II (Molecular Devices). Cells were excited at 340 and 380 nm, and Na<sup>+</sup>-

bound SBFI emission was detected at 505 nm. Fluorescence readings were taken once every 4 s for 60 s to establish the baseline, and then 50  $\mu$ l PbTx-2 at final concentrations ranging from 5 to 1000 nM were added to each well from the compound plate at a rate of 26  $\mu$ l/s, yielding a final volume of 200  $\mu$ l/well. The raw emission data at each excitation wavelength were exported to an Excel work sheet and corrected for background fluorescence. The SBFI fluorescence ratios (340 of 380) versus time were then analyzed, and time–response and concentration–response graphs were generated using GraphPad Prism (GraphPad Software).

Full *in situ* calibration of the SBFI fluorescence ratio was done using calibration media containing the following (in mM): 0.6 MgCl<sub>2</sub>, 0.5 CaCl<sub>2</sub>, 10 HEPES, Na<sup>+</sup> and K<sup>+</sup> such that [Na<sup>+</sup>] plus [K<sup>+</sup>] = 130, 100 gluconate, and 30 Cl<sup>-</sup> (titrated with 10 mol/l KOH to pH 7.4). Gramicidin D (5  $\mu$ M) (Na<sup>+</sup> ionophore), monensin (10  $\mu$ M) (Na<sup>+</sup>/H<sup>+</sup> carrier), and ouabain (100  $\mu$ M) (Na<sup>+</sup>/K<sup>+</sup>-ATPase inhibitor) were added to equilibrate the intracellular and extracellular sodium concentration. After five washes, the Locke's buffer was replaced by 150  $\mu$ l sodium-containing calibration solution (0–130 mM). The plate was then loaded onto the FLEXstation chamber for recording of emitted fluorescence during excitation at 340 and 380 nm. Fluorescence data were converted to a ratio (340 of 380) after background correction. To convert the fluorescence ratio of emitted SBFI signals into a [Na<sup>+</sup>]<sub>i</sub> value, the following equation was used: [Na<sup>+</sup>] =  $\beta K_d [(R - R_{min}) / (R_{max} - R)]$  (1), where  $\beta$  is the ratio of the fluorescence of the free (unbound) dye to bound dye at the second excitation wavelength (380 nm),  $K_d$  is the apparent dissociation constant of SBFI for Na<sup>+</sup>,  $R$  is the background-subtracted SBFI fluorescence ratio, and  $R_{min}$  and  $R_{max}$  are, respectively, the minimum and maximum fluorescence values. The data relating [Na<sup>+</sup>]<sub>i</sub> to  $R$  were fitted by a three-parameter hyperbolic equation having the following form:  $R = R_{min} + [a([Na^+]_i)/(b + [Na^+]_i)]$  (2), where  $a$  and  $b$  are constants and equal to  $R_{max} - R_{min}$  and  $\beta K_d$ , respectively (Diarra et al., 2001; Cao et al., 2008). These data relating [Na<sup>+</sup>]<sub>i</sub> to  $R$  (see Fig. 5B) were well described ( $r^2 = 0.98$ ) by Equation 2. The derived parameters were  $R_{min} = 1.45 \pm 0.03$ ,  $a = 2.073 \pm 0.06$ , and  $b = 30.75 \pm 1.9$ . The value for  $R_{min}$  obtained by this method was identical to the value of  $R_{min}$  derived experimentally at [Na<sup>+</sup>] = 0 mM. The corresponding values for  $R_{max}$  and  $\beta K_d$  were, therefore,  $R_{max} = 3.52 \pm 0.09$  and  $\beta K_d = 30.75 \pm 1.9$  mM. We compared the values of  $R_{max}$  and  $\beta K_d$  obtained from a Hanes plot (Cao et al., 2008) to those derived from the three-parameter hyperbolic fit. The equation was rearranged to generate a Hanes plot such that  $[Na^+]_i / (R - R_{min}) = \{[Na^+]_i / (R_{max} - R_{min})\} + \{\beta K_d / (R_{max} - R_{min})\}$  (3).

The plotting of  $[Na^+]_i / (R - R_{min})$  versus  $[Na^+]_i$  as a Hanes function yielded a straight line ( $r^2 = 0.997$ ) (data not shown). The slope  $\{1 / (R_{max} - R_{min})\}$  provides a means to estimate of  $R_{max}$ , whereas the intercept on the abscissa is equal to  $-\beta K_d$ . The value for  $R_{min}$  was obtained from the experimental data. The values of  $R_{max}$  and  $\beta K_d$  calculated from Hanes plot were  $3.55 \pm 0.09$  and  $32.96 \pm 1.9$  mM, respectively, and were not significantly different from the values derived from the three-parameter hyperbolic fit which were  $3.52 \pm 0.09$  ( $R_{max}$ ) and  $30.75 \pm 1.9$  mM ( $\beta K_d$ ).

**Western blotting.** Western blot analysis was performed in cells grown in 12-well plates as described previously (Cao et al., 2007). Cells were washed three times with Locke's buffer and then allowed to equilibrate in Locke's buffer for 30 min. Cultures were then treated with the indicated drugs at 37°C for specified times. Cultures were then transferred to ice slurry to terminate drug exposure. After washing with ice-cold PBS, cells were harvested in ice-cold lysis buffer containing 50 mM Tris, 50 mM NaCl, 2 mM EDTA, 2 mM EGTA, 1% NP-40, 0.1% SDS, 2.5 mM sodium pyrophosphate, and 1 mM sodium orthovanadate. Phenylmethylsulfonyl fluoride (1 mM) and 1 $\times$  protease inhibitor mixture were then added and the lysate incubated for 20 min at 4°C. Cell lysates then underwent sonication and were centrifuged at 13,000  $\times$  g for 15 min at 4°C. The supernatant was assayed by Bradford method to determine protein content. Equal amounts of protein were mixed with the Laemmli sample buffer and boiled for 5 min. The samples were loaded onto a 10% SDS-PAGE gel and transferred to a nitrocellulose membrane by electroblotting. The membranes were blocked in TBST (20 mM Tris, 150 mM NaCl, 0.1% Tween 20) with 5% skim milk for 1 h at room temperature. After blocking, membranes were incubated overnight at 4°C in primary antibody

diluted in TBST containing 5% skim milk. The blots were washed and incubated with the secondary antibody conjugated with horseradish peroxidase for 1 h, washed four times in TBST, and exposed with ECL Plus for 4 min. Blots were exposed to Kodak hyperfilm and developed. Blots were subsequently stripped (63 mM Tris base, 70 mM SDS, 0.0007% 2-mercaptoethanol, pH 6.8) and reprobed for further use. Western blot densitometry data were obtained using MCID Basic 7.0 software (Imaging Research). ANOVA and graphing were completed using GraphPad Prism (GraphPad Software).

**Membrane potential assay fluorescence monitoring.** Membrane potential in the cerebrocortical neuron cultures was determined using the FLIPR membrane potential (FMP) assay (Molecular Devices). In this method, we used the FMP blue dye to assess the membrane potential of neurons in culture. Quantification of the changes in membrane potential was derived using KCl as a reference. The FMP blue dye is a lipophilic, anionic, bis-oxonol-based dye that distributes across the cell membrane as a function of membrane potential and displays enhanced fluorescence emission after binding to intracellular proteins (Whiteaker et al., 2001; Baxter et al., 2002). This kit also contains a proprietary extracellular fluorescence quencher that eliminates the need to wash neurons after the dye-loading incubation. In preliminary experiments, we determined that, with cerebrocortical neurons in culture, an optimum dye concentration was one-eighth of the suggested manufacturer concentration. The dye stock solution (1 $\times$ ) was prepared by dissolving 10 ml Locke's buffer to the content of each vial. For loading the cells, eightfold diluted stock solutions were used. After removing the culture medium, 180  $\mu$ l of assay buffer was added to the neurons, and the plate was incubated at 37°C in a 5% CO<sub>2</sub> and 95% humidity atmosphere for 30 min. For KCl calibration measurements, varying concentrations of 10 $\times$  KCl standard solutions in assay buffer were prepared. After 30 min equilibration incubation, the plate was transferred to a Flex Station II chamber, and the fluorescence measurements were performed at 37°C. Neurons were excited at 530 nm, and emission was recorded at 565 nm at 2 s intervals. After recording the baseline for 60 s, either 20  $\mu$ l KCl or PbTx-2 was added to a final volume of 200  $\mu$ l at a rate of 26  $\mu$ l/s, and the fluorescence was monitored for an additional 440 s. This protocol was executed by alternate column-by-column addition of KCl and PbTx-2 in the same 96-well plate using the Flex Station II pipettor.

A linear regression analysis of the log concentration of K<sup>+</sup> versus FMP blue fluorescence area under the curve (AUC) was generated. Because the membrane potential of isolated neurons is mainly the result of the K<sup>+</sup> equilibrium potential (Hille, 1992), we used the Goldman–Hodgkin–Katz equation to generate a standard curve for the estimation of membrane potential ( $E_M$ ) at various concentrations of extracellular K<sup>+</sup>:

$$E_M K_x Na_{1-x} Cl = \frac{RT}{F} \ln \left( \frac{P_{Na^+} [Na^+]_{out} + P_{K^+} [K^+]_{out} + P_{Cl^-} [Cl^-]_{in}}{P_{Na^+} [Na^+]_{in} + P_{K^+} [K^+]_{in} + P_{Cl^-} [Cl^-]_{out}} \right), \quad (4)$$

where  $E_M$  is membrane potential,  $R$  is universal gas constant,  $T$  is temperature using the Kelvin scale, and  $P_{K^+}$ ,  $P_{Na^+}$ , and  $P_{Cl^-}$  are permeabilities for K<sup>+</sup>, Na<sup>+</sup>, and Cl<sup>-</sup>, respectively.  $[K^+]_{out}$ ,  $[Na^+]_{out}$ , and  $[Cl^-]_{out}$  and  $[K^+]_{in}$ ,  $[Na^+]_{in}$ , and  $[Cl^-]_{in}$  are the respective extracellular and intracellular concentrations of K<sup>+</sup>, Na<sup>+</sup>, and Cl<sup>-</sup>. A 2 d *in vitro* (DIV-2) neuronal [Cl<sup>-</sup>]<sub>in</sub> value of 140 mM was used for these calculations (Kuner and Augustine, 2000). The regression for the  $[K^+]_{out}$  versus  $\Delta$  fluorescence and  $E_M$  was used for estimating PbTx-2-induced change in membrane potential.

**Electrophysiology.** Single-channel currents were recorded at 23°C in the cell-attached configuration (Hamill et al., 1981). Patch pipettes were pulled from borosilicate glass capillaries (Warner Instruments), coated with Sylgard 184 (Dow Corning) and fire-polished to a resistance of 10–15 M $\Omega$  when filled with the pipette solution. The external recording solution consisted of Mg<sup>2+</sup>-free Locke's buffer with 20  $\mu$ M EDTA to chelate trace amounts of divalent cations. PbTx-2 was always applied in the bath. The patch pipette solution consisted of extracellular Locke's buffer without MgCl<sub>2</sub> and with either 3 or 10  $\mu$ M NMDA and 100  $\mu$ M glycine. In some experiments, 10  $\mu$ M strychnine, 10  $\mu$ M bicuculline methiodide and 10  $\mu$ M DNQX were included in the external solution to

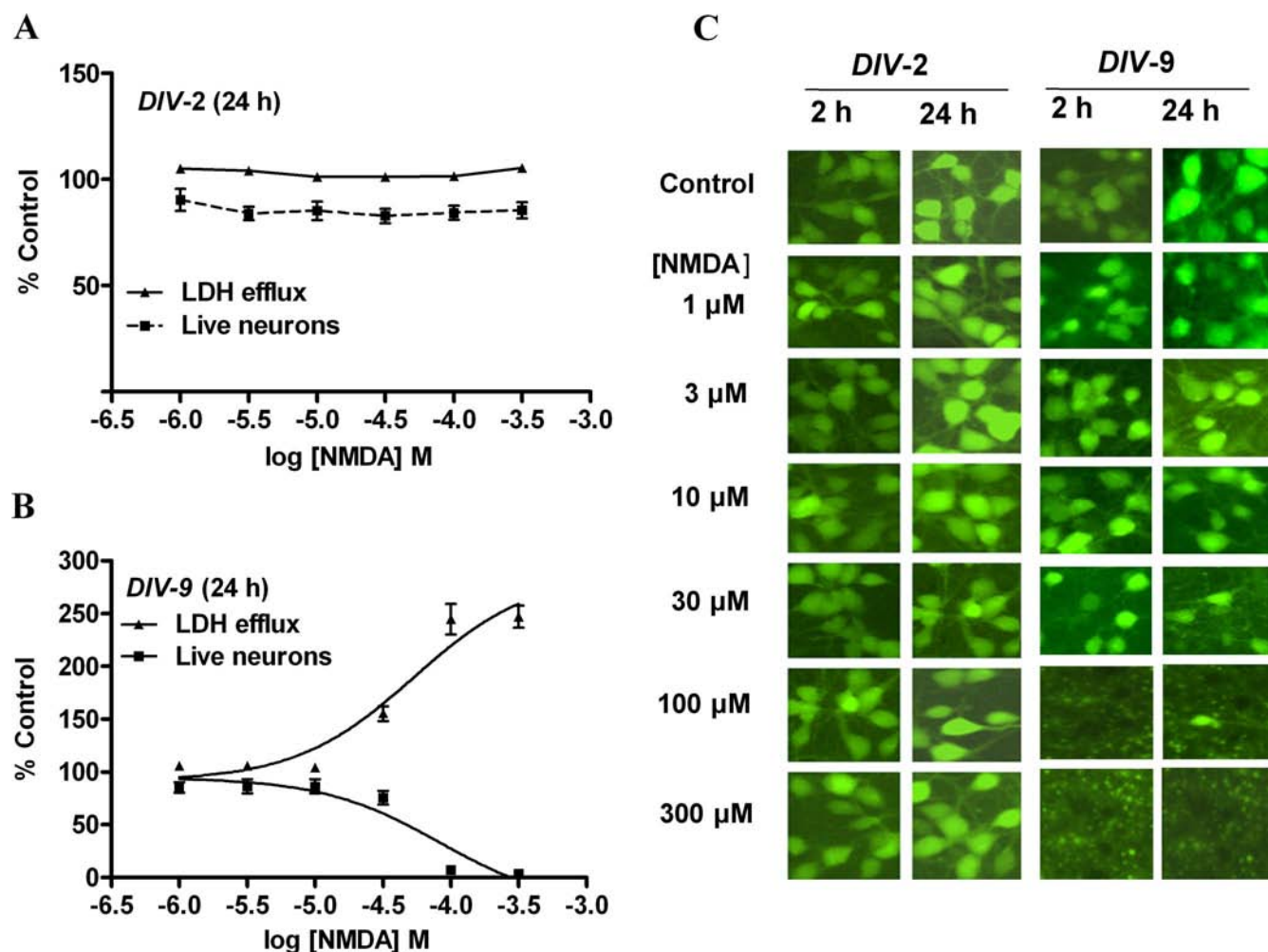


**Figure 1.** NMDA-induced excitotoxicity in immature cerebocortical neurons. **A, B**, Comparison of LDH efflux and estimation of viable neurons by using fluorescein diacetate staining in DIV-2 (**A**) and DIV-9 (**B**) cerebocortical neurons at 24 h after initiation of a 2 h NMDA exposure. Mean  $\pm$  SEM of LDH efflux values and viable cell count are represented as percentage of control. Experiment was repeated six times each with triplicate values. **C**, Representative images of fluorescein diacetate staining of cerebocortical neurons at 2 and 24 h time points.

block nonspecific components. All recordings were done from DIV-2 cerebocortical neurons. Cell-attached patch recordings were done using an Axopatch 200B amplifier (Molecular Devices), filtered at 8 kHz ( $-3$  dB, 8-pole Bessel), and digitized at 40 kHz digitized with Axon pClamp 10.2 software. The pipette potential was  $+60$  mV. Records were idealized with a segmental k-means algorithm (Qin, 2004) using QUB software ([www.qub.buffalo.edu](http://www.qub.buffalo.edu)). All conductance levels were assumed to be equal for the analysis. Dwell-time histograms were generated and fitted using Channelab (Synaptosoft) with an imposed dead time of  $100 \mu\text{s}$ . The open probability ( $P_o$ ), mean open time, and amplitude were compared by paired  $t$  test. For representation in figures, the  $P_o$ , mean open time, and amplitude were normalized to the average of respective control values. The corresponding PbTx-2-treated values were normalized to their paired control values.

## Results

### Immature cerebocortical neurons show decreased vulnerability to NMDA-induced excitotoxicity

Because NMDA receptors have been shown to be a crucial mediator of excitotoxicity (Berman and Murray, 2000; Hardingham and Bading, 2003) and immature neurons exhibit decreased vulnerability to excitotoxicity both *in vivo* (Liu et al., 1996) and *in vitro* (Choi et al., 1987; Mizuta et al., 1998; Cheng et al., 1999; Marks et al., 2005; King et al., 2006), we examined the influence of cerebocortical culture age on vulnerability to NMDA-induced

excitotoxicity. We assessed NMDA-induced LDH efflux, a biochemical index for neuronal injury, as a function of development in culture. Cerebocortical neurons were exposed to a range of NMDA concentrations for 2 h and assayed for LDH efflux at 2 and 24 h after the initiation of exposure. At 2, 4, and 6 DIV, cerebocortical cultures showed little sensitivity to NMDA-induced LDH efflux assessed immediately after either the 2 h exposure or at 24 h after exposure; however, DIV-9 cerebocortical neurons showed sensitivity to NMDA. In DIV-9 cultures, the assessment of NMDA toxicity at 24 h after initiation of exposure resulted in substantial levels of LDH efflux as reflected in a maximal LDH efflux value of  $247 \pm 10.5\%$  of control (Fig. 1). In DIV-9 neurons, the NMDA  $EC_{50}$  value with 95% confidence intervals (CI) for LDH efflux was  $53.1 \mu\text{M}$  ( $27.9$ – $101 \mu\text{M}$ ). The insensitivity to NMDA-induced excitotoxicity in DIV-2, -4, and -6 cultures agrees with previous reports. Studies with primary cerebocortical cultures have reported a decreased vulnerability to excitotoxicity in 2–7 DIV cultures compared with 11–14 DIV cultures after challenge with glutamate or NMDA (Choi et al., 1987; Mizuta et al., 1998; Cheng et al., 1999; King et al., 2006). Similarly, sensitivity to excitatory amino acid-induced toxicity in neocortical neurons has been shown to emerge at DIV-7–9 but not in DIV-2 (Frandsen and Schousboe, 1990; Griffiths et al.,

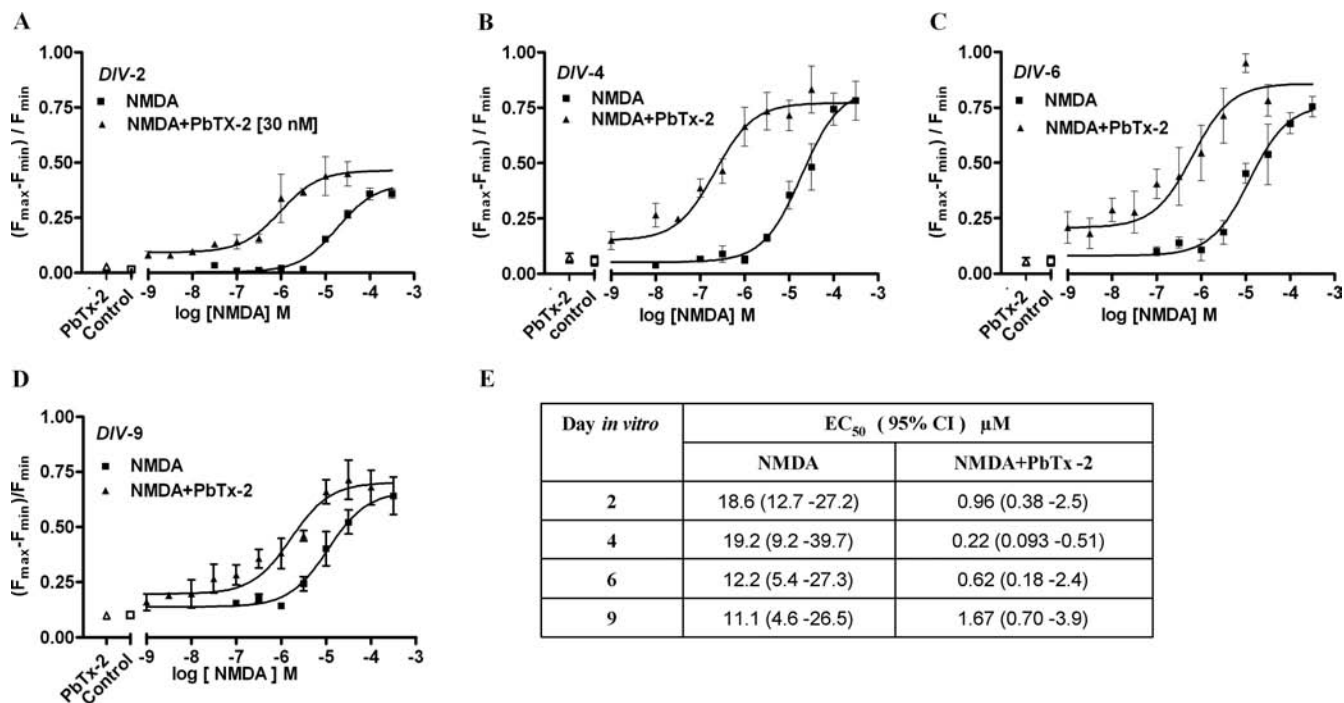


**Figure 2.** PbTx-2 augments NMDA-induced  $\text{Ca}^{2+}$  influx in immature cerebrocortical neurons as a function of culture age. **A–D**, Nonlinear regression analysis of the fractional increase  $[(F_{\max} - F_{\min})/F_{\min}]$  in  $\text{Ca}^{2+}$  influx as a function of NMDA concentration in the culture ages of 2, 4, 6, and 9 DIV. Each point represents mean  $\pm$  SEM of sextuplicate values. Experiment was repeated six times with sextuplicate determinations in six independent cultures. **E**,  $\text{EC}_{50}$  and 95% CI derived from the NMDA concentration–response (depicted in **A–D**) in the presence and absence of 30 nM PbTx-2.

1997). To confirm our LDH efflux data, fluorescein diacetate staining was used to allow visualization and quantification of viable neurons. As depicted in Figure 1, in DIV-2 and DIV-9 cerebrocortical neurons, the viable cell count data derived from fluorescein diacetate staining was well correlated with the LDH efflux data and provided confirmation of NMDA-induced excitotoxicity in DIV-9 but not DIV-2 cerebrocortical neurons. The NMDA  $\text{EC}_{50}$  value for decreasing the live neuron count was 82.2  $\mu\text{M}$  (95% CI 38.4–176  $\mu\text{M}$ ). Based on this insensitivity to NMDA-induced excitotoxicity, DIV-2 cerebrocortical cultures were selected as a model system to explore the influence of sodium on NMDA receptor signaling.

#### PbTx-2 augments NMDA-induced $\text{Ca}^{2+}$ influx in immature cerebrocortical neurons

Previous studies have indicated that activity-dependent neuronal development is primarily triggered through  $\text{Ca}^{2+}$ -dependent signaling pathways (Chen and Ghosh, 2005; Konur and Ghosh, 2005). Although NMDA receptors represent a key source of  $\text{Ca}^{2+}$  entry, the underlying mechanisms responsible for NMDAR regulation of activity-dependent development remain to be fully delineated. Because synaptic activity has been shown to elevate  $[\text{Na}^+]_i$  (Rose and Konnerth, 2001) and sodium acts as a positive regulator of NMDAR function (Yu and Salter, 1998), we used the sodium channel activator, PbTx-2, as a probe to further explore the influence of sodium on NMDAR signaling. A quantitative assessment of the increments in neuronal sodium concentration produced by an array of VGSC activators has demonstrated that brevetoxins such as PbTx-2 elevate  $[\text{Na}^+]_i$  to concentrations as high as 50 mM (Cao et al., 2008). Before the investigation of the influence of PbTx-2 on NMDA-induced  $\text{Ca}^{2+}$  influx, we first assessed the effect of PbTx-2 alone on  $\text{Ca}^{2+}$  dynamics in DIV-2 cerebrocortical neurons. The concentration dependence of the increase in  $[\text{Ca}^{2+}]_i$  stimulated by PbTx-2 was examined in fluo-

3-loaded DIV-2 cerebrocortical neurons. PbTx-2 produced a rapid and concentration-dependent increase in  $[\text{Ca}^{2+}]_i$  (supplemental Fig. S1A, available at [www.jneurosci.org](http://www.jneurosci.org) as supplemental material). Nonlinear regression analysis of the concentration dependence of the PbTx-2-induced integrated fluo-3 response indicated that the  $\text{EC}_{50}$  for PbTx-2-stimulated increase in  $[\text{Ca}^{2+}]_i$  was 244 nM (119–498 nM, 95% CI). A concentration of 30 nM PbTx-2 was found to be subthreshold in DIV-2 neurons in that this concentration did not increase fluo-3 fluorescence (supplemental Fig. S1A, available at [www.jneurosci.org](http://www.jneurosci.org) as supplemental material). This PbTx-2 concentration response profile generalized to DIV-4, -6, and -9 neurons in that a 30 nM concentration of PbTx-2 did not alter  $[\text{Ca}^{2+}]_i$  (data not shown).

Given that 30 nM PbTx-2 was without effect on  $\text{Ca}^{2+}$  dynamics in cerebrocortical neurons, we investigated NMDA-induced  $\text{Ca}^{2+}$  influx in the presence and absence of this concentration of PbTx-2 in DIV-2, -4, -6, and -9 cerebrocortical cultures. NMDA produced a concentration-dependent elevation of  $[\text{Ca}^{2+}]_i$  in all four ages of cerebrocortical neuron cultures. Analysis of the NMDA-concentration response data, in the absence of 30 nM PbTx-2, for DIV-2, -4, -6, and -9 revealed a leftward shift in these concentration–response curves as a function of development (Fig. 2). The  $\text{EC}_{50}$  value for NMDA-induced  $\text{Ca}^{2+}$  influx ranged from 19.2  $\mu\text{M}$  in DIV-4 neurons to 11.1  $\mu\text{M}$  in DIV-9 neurons. The presence of 30 nM PbTx-2 produced a robust potentiation of NMDA-induced  $\text{Ca}^{2+}$  influx in cultures of all ages (Figs. 2, 3; supplemental Fig. S2, available at [www.jneurosci.org](http://www.jneurosci.org) as supplemental material). The NMDA concentration–response curves for  $\text{Ca}^{2+}$  influx were significantly leftward shifted by 30 nM PbTx-2. Nonlinear regression analysis of these data indicated that NMDA  $\text{EC}_{50}$  values were significantly lower in the presence of PbTx-2 (Fig. 2E). These data suggest that PbTx-2 sensitizes cerebrocortical neurons to NMDA-induced  $\text{Ca}^{2+}$  influx. The PbTx-2 potentiation of NMDA-induced  $\text{Ca}^{2+}$  influx was most prominent

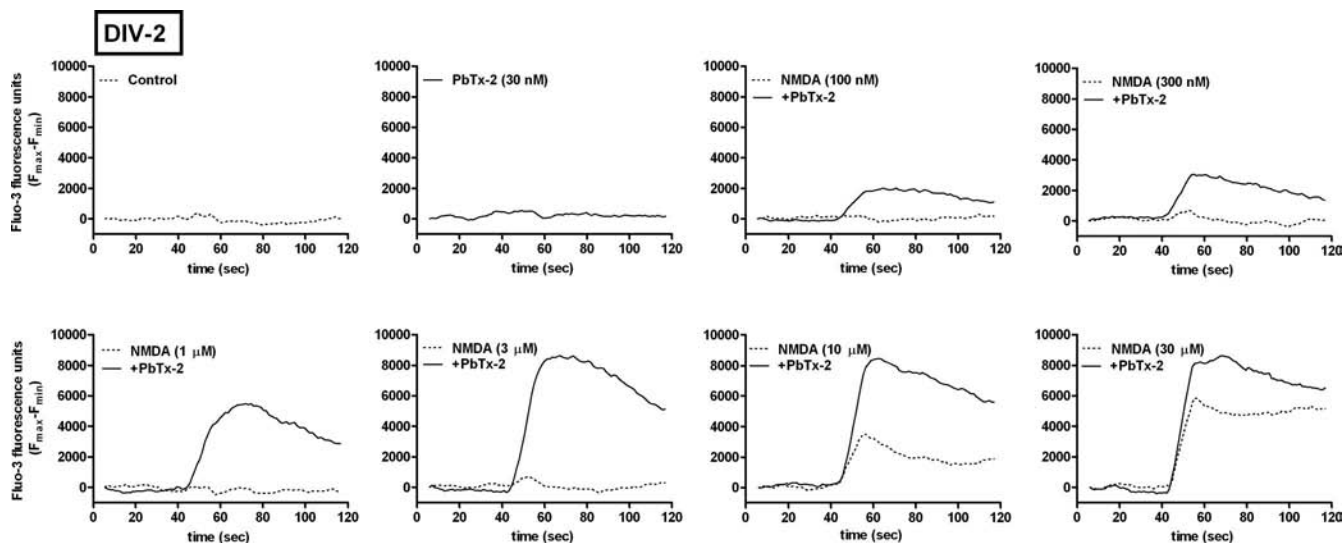


**Figure 3.** Effect of 30 nM PbTx-2 on NMDA-induced  $Ca^{2+}$  influx in immature cerebrocortical neurons. Representative time–response data using DIV-2 cerebrocortical neurons. Cerebrocortical neurons were treated with a range of NMDA concentrations in the presence and absence of 30 nM PbTx-2. The presence of 30 nM PbTx-2 produced a robust augmentation of NMDA-induced  $Ca^{2+}$  influx in DIV-2 neurons.

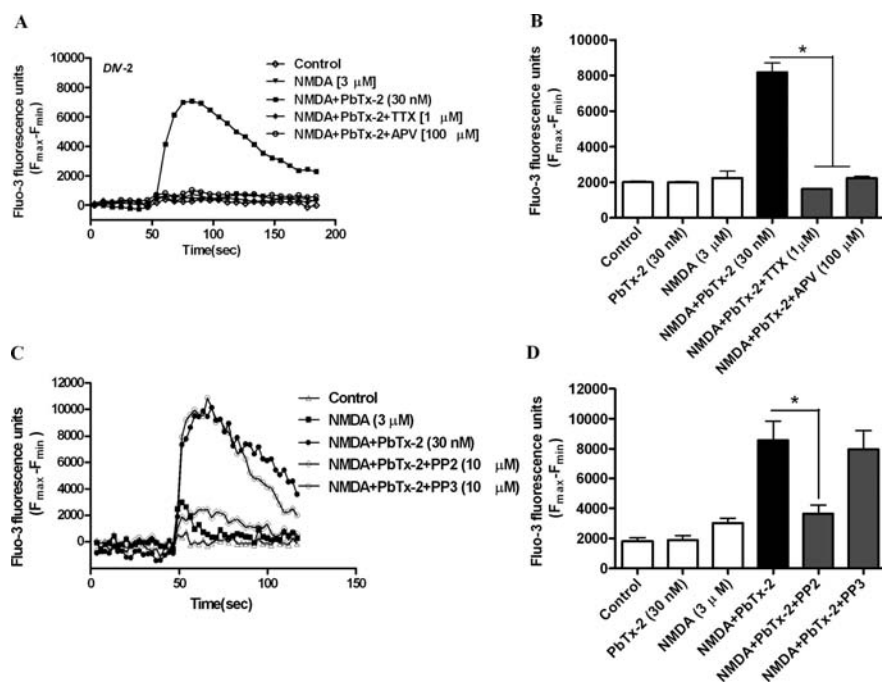


**Figure 4.** Pharmacological evaluation of PbTx-2-induced potentiation of NMDA-induced  $Ca^{2+}$  influx in DIV-2 cerebrocortical neurons. **A**, Time–response data are from representative experiment performed in sextuplicate and repeated four times. Cerebrocortical neurons were treated with either 1  $\mu M$  TTX or 100  $\mu M$  APV before the addition of 3  $\mu M$  NMDA and 30 nM PbTx-2. **B**, Each bar represents mean  $\pm$  SEM ( $n = 4$ ). Both 1  $\mu M$  TTX and 100  $\mu M$  APV completely blocked PbTx-2 potentiation of NMDA-induced  $Ca^{2+}$  influx.  $*p < 0.01$  (ANOVA followed by Dunnett’s multiple comparison test). **C**, Effect of PP2, a specific Src-family kinase inhibitor, on PbTx-2-induced potentiation of NMDA-induced  $Ca^{2+}$  influx in DIV-2 cerebrocortical neurons. Time–response data are from representative experiment performed in sextuplicate and repeated six times. Cerebrocortical neurons were exposed to 10  $\mu M$  PP2 or PP3 15 min before the addition of 3  $\mu M$  NMDA and 30 nM PbTx-2. **D**, Each bar represents mean  $\pm$  SEM ( $n = 6$ ).  $*p < 0.01$ , paired  $t$  test.

at an NMDA concentration of 3  $\mu M$  in DIV-2 neurons as depicted in Figure 3. NMDA at a concentration of 3  $\mu M$  alone did not affect  $[Ca^{2+}]_i$  but in the presence of 30 nM PbTx-2 elicited a robust increment in  $[Ca^{2+}]_i$ . Although not as strong as the effect in DIV-2 cultures, 30 nM PbTx-2 augments NMDA-induced  $Ca^{2+}$  influx in all ages of cerebrocortical cultures (the response of

DIV-9 neurons is shown in supplemental Fig. S2, available at [www.jneurosci.org](http://www.jneurosci.org) as supplemental material). Based on these results, a concentration of 30 nM PbTx-2 was selected to further probe the potential influence of sodium on NMDAR signaling.

**PbTx-2 potentiation of NMDA-induced  $Ca^{2+}$  influx requires VGSCs and activation of a Src family kinase**

To confirm the involvement of VGSCs and NMDARs in the PbTx-2 enhancement of NMDA-induced  $[Ca^{2+}]_i$ , we conducted a pharmacological evaluation of the response to a fixed concentration of 3  $\mu M$  NMDA in DIV-2 cerebrocortical neurons. The role of NMDARs and VGSCs in the response to NMDA in the presence and absence of PbTx-2 was assessed by pre-treating cerebrocortical neurons with 100  $\mu M$  D-APV, a competitive NMDA receptor antagonist or 1  $\mu M$  TTX, a VGSC pore blocker. These compounds both abrogated ( $p < 0.01$ ) NMDA-induced  $Ca^{2+}$  influx in the presence of PbTx-2 (Fig. 4A,B). These results, therefore, confirm the requirement for activation of NMDARs and VGSCs in this response. Because the upregulation of NMDAR function by  $[Na^+]_i$  has been shown to involve Src kinase activation, we next examined the role of Src family kinases in the PbTx-2 potentiation of NMDA-induced  $Ca^{2+}$  influx using the specific Src family kinase inhibitor, PP2 (10  $\mu M$ ) (Fig. 4C,D). PP2 dramatically reduced ( $p < 0.01$ ) the PbTx-2-induced potentiation of NMDA-induced  $Ca^{2+}$  influx in cerebrocortical neurons. In contrast, PP3 (10  $\mu M$ ), the inactive congener of PP2, did not affect the PbTx-2 potentiation of NMDA-induced  $Ca^{2+}$  influx, supporting the involvement of a Src family kinase in this re-

sponse. The activation of Src family kinases are tightly and dynamically controlled by autophosphorylation and dephosphorylation of specific tyrosine residues. The phosphorylation of a tyrosine residue (Y416) within the activation loop of Src kinase has been identified as important for its activation (Salter and Kalia, 2004). We therefore assessed tyrosine phosphorylation of Src using an anti-phospho-Y416 Src antibody. Western blot analysis revealed that the combination of 30 nM PbTx-2 and 3  $\mu$ M NMDA produced an activation of Src kinase as reflected by a significant increase in the phosphorylation of tyrosine 416 (supplemental Fig. S3, available at [www.jneurosci.org](http://www.jneurosci.org) as supplemental material).

### PbTx-2 increases intracellular sodium levels in immature cerebrocortical neurons

Given the role of  $[Na^+]_i$  as a putative regulator of NMDAR-mediated signaling, it was important to quantify the magnitude of PbTx-2-induced elevation of  $[Na^+]_i$  in immature cerebrocortical neurons. We therefore assessed PbTx-2-induced elevation of  $[Na^+]_i$  in DIV-2 cerebrocortical neurons loaded with SBFI. As described previously for the assay of  $[Na^+]_i$  in mature cerebrocortical neurons, we performed a full *in situ* calibration of the relationship between the ratiometric SBFI signal and  $[Na^+]_i$  in DIV-2 neurons (Cao et al., 2008). The emitted fluorescence intensities were recorded during excitation at 340 and 380 nm and were converted to a ratio (340 of 380) after background correction (Fig. 5A). These calibration data relating SBFI fluorescence ratio to  $[Na^+]_i$  were adequately described by a three-parameter hyperbolic curve fit as described in Materials and Methods (Fig. 5B). PbTx-2 treatment of DIV-2 cerebrocortical neurons produced a concentration-dependent decrease in SBFI fluorescence emitted by excitation at 380 nm, whereas emitted fluorescence during excitation at 340 nm was unaffected, indicating no significant cell swelling after PbTx-2 exposure in DIV-2 neurons (data not shown). As shown in Figure 5C, PbTx-2 produced concentration-dependent increments in  $[Na^+]_i$ . The *in situ* SBFI calibration showed that the basal  $[Na^+]_i$  in DIV-2 cerebrocortical neurons was  $8.1 \pm 0.32$  mM. This value is in reasonable agreement with those determined previously in more mature neuronal cultures: a basal level  $[Na^+]_i$  of 8.9 mM in cultured hippocampal neurons (Rose and Ransom, 1997),  $9 \pm 2$  mM in either cultured spinal dorsal horn or hippocampal neurons (Yu and Salter, 1998), and  $10.3 \pm 0.22$  mM in DIV-9 cerebrocortical neurons (Cao et al., 2008). Further analysis of the concentration–response profile for PbTx-2-induced elevation of  $[Na^+]_i$  indicated that the  $EC_{50}$  value for PbTx-2 was 43.3 nM (23.5–79.9 nM, 95% CI), and the maximum elevation of  $[Na^+]_i$  was  $36.6 \pm 0.9$  mM (Fig. 5D). Because a 30 nM concentration of PbTx-2 was sufficient to augment NMDA-induced  $Ca^{2+}$  influx, it was important to quantify the  $[Na^+]_i$  increment associated with this treatment. The 30 nM PbTx-2 treatment produced a maximum  $[Na^+]_i$  of  $16.9 \pm 1.5$  mM, representing an increment of  $8.8 \pm 1.8$  mM over basal. Previous reports in hippocampal neurons suggested that an incre-

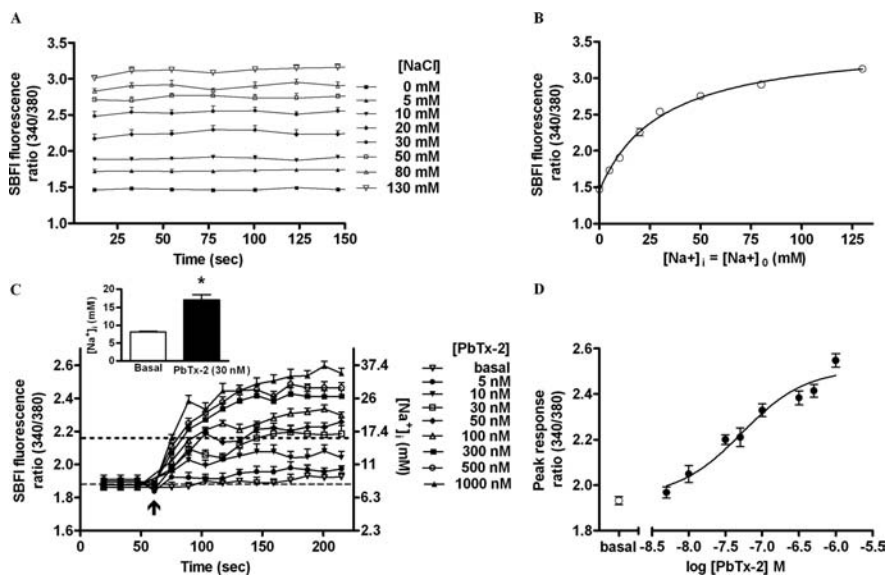


**Figure 5.** PbTx-2 increases intracellular sodium levels in DIV-2 cerebrocortical neurons. *A*, *In situ* calibration of SBFI fluorescence ratio (340 of 380). Time–response data show stepwise changes in SBFI fluorescence ratio values evoked by successive increments in extracellular sodium ion concentration. *B*, Three parameter hyperbolic curve fit adequately describes calibration data. SE bars are contained within each data point. *C*, Time–response profile for PbTx-2-induced  $[Na^+]_i$  elevation as represented by the SBFI fluorescence ratio. Data represent the mean  $\pm$  SEM of three separate experiments, each with six to eight replicates. The scale on the right ordinate depicts the calibrated  $[Na^+]_i$  corresponding to SBFI fluorescence ratio values. The basal  $[Na^+]_i$  was found to be  $8.1 \pm 0.32$  mM. A maximum elevation of  $[Na^+]_i$  to  $16.9 \pm 1.5$  mM was determined after addition of PbTx-2 (30 nM) corresponding to a  $[Na^+]_i$  increment of  $8.8 \pm 1.8$  mM. ( $*p < 0.001$ , unpaired *t* test). *D*, Nonlinear regression analysis of the PbTx-2 concentration–response data ( $EC_{50} = 43.3$  nM; 23.5–79.9 nM, 95% CI).

ment of  $[Na^+]_i$  of 10 mM was sufficient to produce significant increases in NMDAR channel activity (Yu and Salter, 1998; Yu, 2006). It has, moreover, been reported that increments of  $[Na^+]_i$  of  $>5$  mM may represent a critical threshold required to regulate NMDAR-mediated  $Ca^{2+}$  influx in primary cultures of hippocampal neurons (Xin et al., 2005). Consistent with these findings, the increment of  $[Na^+]_i$  detected in immature cerebrocortical neurons appears sufficient to upregulate NMDAR signaling.

### PbTx-2 augmentation of NMDA receptor signaling does not involve depolarization-induced relief of $Mg^{2+}$ blockade

The ability of PbTx-2 to potentiate NMDA-induced  $Ca^{2+}$  influx could be a consequence of either the elevation of  $[Na^+]_i$  or neuronal depolarization with attendant relief of the  $Mg^{2+}$  block of NMDAR. To ascertain the magnitude of PbTx-2-induced membrane depolarization, we assessed PbTx-2-induced membrane potential changes in DIV-2 cerebrocortical neurons using a membrane-potential sensitive fluorescence dye, FMP blue. The changes in membrane potential measured with FMP blue are well correlated with those determined by patch-clamp analysis (Baxter et al., 2002). To document that FMP blue behaved as a Nernstian fluorescent indicator of membrane potential in cerebrocortical neurons, we determined the relationship between extracellular  $K^+$  concentration and fluorescence intensity. To equate changes in membrane potential to alteration in FMP blue fluorescence, a KCl concentration–response calibration curve was generated to establish that fluorescent intensity was directly proportional to the extracellular  $K^+$  concentration (Fig. 6A). Extracellular  $K^+$  produced a concentration-dependent increase in maximum FMP blue fluorescence consistent with a depolarization-induced redistribution of the lipophilic anion dye and attendant increase in fluorescence quantum efficiency. As depicted in Figure 6B, the regression analysis of the  $K^+$

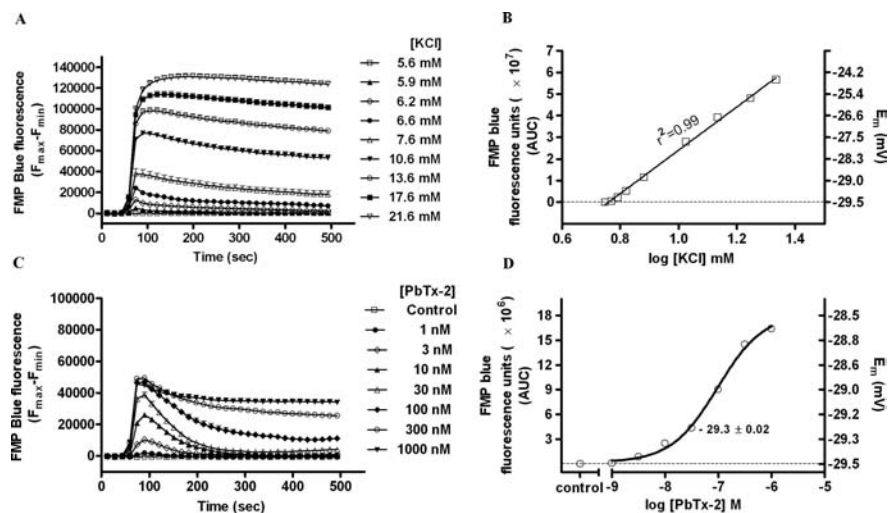


**Figure 6.** PbTx-2-evoked change in membrane potential in DIV-2 cerebocortical neurons. **A**, Concentration–response profile for KCl-evoked FMP blue fluorescence change as a function of time. Each point represents mean  $\pm$  SEM of 12 values. Experiment was repeated three times on independent cultures. **B**, The integrated time–response data for the increment in FMP blue fluorescence (AUC) was plotted as a function of  $K^+$  concentration. The displayed regression and correlation coefficient ( $r^2 = 0.99$ ) were derived from linear regression analysis. The right ordinate scale shows membrane potential for each  $[K^+]$  which was calculated using Goldman–Hodgkin–Katz equation as described in Materials and Methods. The resting membrane potential was  $-29.5 \pm 0.01$  mV. **C**, Concentration–response of PbTx-2-induced changes in membrane potential as determined by changes in FMP blue fluorescence. Each point represents the mean  $\pm$  SEM of 12 values. This experiment was repeated three times on independent cultures. **D**, Nonlinear regression analysis of the integrated time–response data for the increment in FMP blue fluorescence (AUC) as a function of PbTx-2 concentration. The membrane potential values were determined by performing  $K^+$  calibration regressions in the same culture plate. The membrane potential change evoked by 30 nM PbTx-2 was  $0.2 \pm 0.02$  mV.

concentration-dependent changes FMP blue fluorescence showed marked linear correlation ( $r^2 = 0.99$ ). For a Nernstian fluorescent indicator of membrane potential, the ratio of fluorescence inside to the outside of the cell should be related to the membrane potential as described by the Nernst equation (Ehrenberg et al., 1988). This prediction is based on the principal that the membrane potential of isolated neurons is mainly the result of the  $K^+$  diffusion potential (Hille, 1992). We, therefore, used the Goldman–Hodgkin–Katz equation to generate a standard curve for the estimation of membrane potential ( $E_M$ ) at various concentrations of extracellular  $K^+$ . The membrane potential of cerebocortical neurons was dependent on the external concentration of  $K^+$  (Hille, 1992). The concordance of the  $[K^+]_{out}$  versus membrane fluorescence and  $[K^+]_{out}$  versus  $E_M$  regressions indicates that changes in cerebocortical neuron FMP blue fluorescence can be used to estimate membrane potential. Therefore, the relationship between fluorescence change and  $E_M$  depicted in Figure 6B was generated to determine PbTx-2-induced changes in membrane potential of cerebocortical neurons. The resting membrane potential of DIV-2 cerebocortical neurons was found to be  $-29.5 \pm 0.01$  mV. This is consistent with previous demonstrations of relatively depolarized resting membrane potentials of immature neurons that later become more hyperpolarized as neurons mature (Ramo and McCormick, 1994; Kim et al., 1995). As shown in Figure 6C, PbTx-2 produced a rapid and concentration-dependent increment in FMP blue fluorescence in DIV-2 cerebocortical neurons. Nonlinear regression analysis of the PbTx-2 concentration–response relationship yielded an  $EC_{50}$  value of 96.7 nM (71.2–131.5 nM, 95% CI) (Fig. 6D). Because the 30 nM concentration of PbTx-2 was sufficient to augment NMDA-induced  $Ca^{2+}$  influx and to elevate  $[Na^+]_i$ , it was important to assess the

membrane potential changes associated with this treatment. The 30 nM PbTx-2 treatment produced a transient increase in FMP blue fluorescence that was roughly equivalent to the fluorescence change produced by an extracellular  $K^+$  concentration of 7.6 mM. The corresponding membrane potential change was accordingly found to be negligible, representing only a  $0.2 \pm 0.02$  mV depolarization (from  $29.5 \pm 0.01$  to  $29.3 \pm 0.02$  mV). This change in membrane potential would, therefore, not be sufficient to influence voltage-dependent  $Mg^{2+}$  block of NMDARs (Mayer et al., 1984). We confirmed the membrane potential and lack of influence of PbTx-2 (30 nM) in DIV-2 neurons using noninvasive single-channel recordings (Tyzio et al., 2003). Measurement of single-channel NMDA receptor currents in cell-attached mode indicated that the membrane potential was  $-28$  mV (19–38, 95% CI), and 30 nM PbTx-2 did not affect this measure in DIV-2 neurons (supplemental Fig. S4, available at [www.jneurosci.org](http://www.jneurosci.org) as supplemental material).

#### PbTx-2 increases NMDA single-channel open probability and mean open time

To gain insight into the effect of PbTx-2 on single-channel properties of NMDA receptors, unitary currents were recorded from DIV-2 cerebocortical neurons. Cell-attached patch recording was performed with  $3 \mu M$  NMDA and  $100 \mu M$  glycine in the patch pipette at a patch potential of  $+60$  mV. Experiments were performed in the nominal absence of extracellular  $Mg^{2+}$  in the recording buffer supplemented with  $20 \mu M$  EDTA to chelate trace amounts of divalent ions. In the majority of patches, we observed only single openings with no apparent simultaneous double openings. The absence of double openings was presumably attributable to the submaximal concentration of NMDA used in the patch pipette and the low expression of NMDA receptors in immature cerebocortical neurons. Patches in which we observed simultaneous double openings were not further analyzed. Single-channel recordings were idealized using the QUB and analyzed using ChannelLab with an imposed resolution of  $100 \mu s$ . Bath application of 30 nM PbTx-2 significantly increased the open probability ( $P_o$ ) of NMDA receptors from  $0.0054 \pm 0.002$  under control conditions to  $0.031 \pm 0.008$  ( $443 \pm 102\%$  of control) after 30 nM PbTx-2 ( $n = 5$ ,  $p < 0.05$ , paired  $t$  test) (Fig. 7A, B). The mean open time was also increased by PbTx-2 application from  $1.99 \pm 0.26$  ms without PbTx-2 to  $2.95 \pm 0.34$  ms ( $153 \pm 20\%$  of control) after PbTx-2 ( $n = 5$ ,  $p < 0.05$ , paired  $t$  test) (Fig. 7B). PbTx-2 did not modulate the amplitude of single-channel currents (control,  $6.4 \pm 0.3$  pA; PbTx-2,  $6.8 \pm 0.4$  pA;  $n = 5$ ) (Fig. 7B). The composite open and shut dwell-time histograms were generated and fitted using ChannelLab. The open time histogram could be fitted by the sum of two exponential components with time constants of 1.2 (81%) and 3.1 (19%). The time constants after PbTx-2 application were 1.6 (65%) and 4.1 (35%). Thus, PbTx-2 increased the area of the longer time constant. The composite shut time histograms could be fitted by sum of four exponential com-

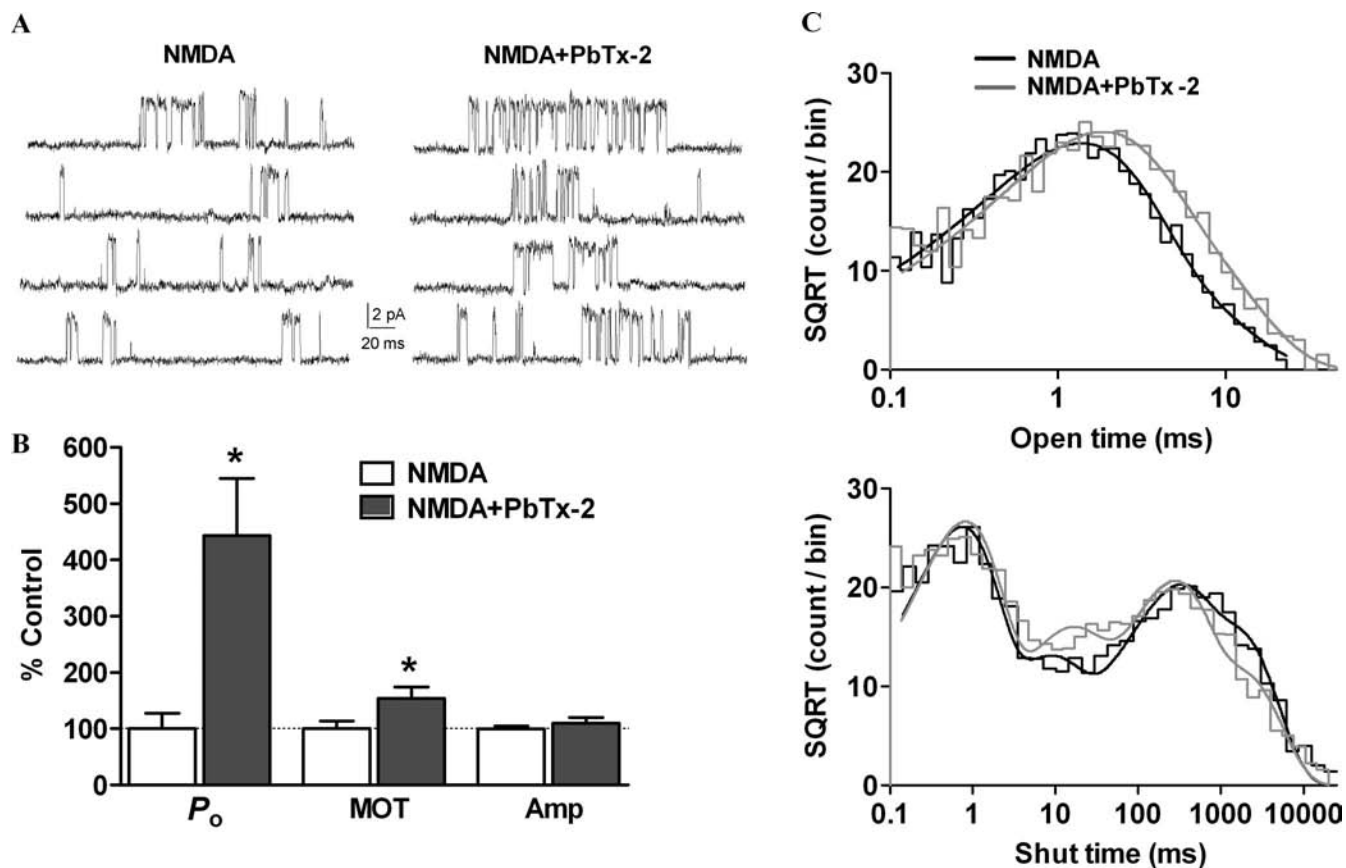


**Figure 7.** Increase in NMDA receptor channel open probability by PbTx-2. **A**, Cell-attached patch recording from DIV-2 cerebocortical neurons. NMDA receptor unitary currents were evoked by  $3 \mu\text{M}$  NMDA and  $100 \mu\text{M}$  glycine in the patch pipette (pipette potential =  $+60$  mV, filtered at 5 kHz for representation, digitized at 40 kHz). Enhancement of NMDA receptor activity by bath application of  $30 \text{ nM}$  PbTx-2. **B**, Bath application of  $30 \text{ nM}$  PbTx-2 increased the NMDA receptor channel open probability ( $P_o$ ) and mean open time (MOT) ( $n = 5$ ,  $p < 0.05$ , paired  $t$  test) but not the mean amplitude (Amp) ( $n = 5$ ). **C**, Pooled dwell-time histograms were fitted using ChannelLab. The open time histogram was fitted by the sum of two Gaussian components, and the shut time histogram was fitted by the sum of four Gaussian components. The time constants and area are described in Results.

ponents with time constants of 0.63 (47%), 7.4 (12%), 211 (22%), and 1410 (19%). The time constants were essentially same after PbTx-2 application 0.63 (45%), 10.0 (16%), 180 (28%), and 1361 (11%), except that the area of the slowest time constant was lowered by PbTx-2, which may underlie the increase in  $P_o$  by PbTx-2 (Fig. 7C).

To address the requirement for  $\text{Na}^+$  influx in the PbTx-2-mediated enhancement of NMDA receptor function, PbTx-2 was applied when external  $\text{Na}^+$  was substituted by equimolar concentrations of the impermeant cation *N*-methyl *D*-glucamine (NMDG). PbTx-2 failed to enhance NMDA receptor function under these conditions (Fig. 8A). The  $P_o$  before and after PbTx-2 application were  $0.004 \pm 0.002$  and  $0.005 \pm 0.002$ , respectively ( $n = 4$ ). The mean open time was also unaltered (before:  $1.21 \pm 0.14$  ms; after: PbTx-2,  $1.28 \pm 0.22$  ms;  $n = 4$ ). Resubstitution with a  $\text{Na}^+$ -containing extracellular solution with PbTx-2 lead to a significant increase in both  $P_o$  and mean open time compared with control condition [ $P_o$ ,  $0.011 \pm 0.003$  (275  $\pm$  36% of control); mean open time,  $1.97 \pm 0.22$  ms (166  $\pm$  20% of control);  $p < 0.05$ , paired  $t$  test]. These results suggest that PbTx-2 (30 nM)-induced influx of  $\text{Na}^+$  is crucial for augmentation of NMDA receptor function.

We further addressed the role of a Src family kinase in PbTx-2-induced augmentation of NMDA receptor function. Recordings were performed after 15 min preincubation with PP2 (Fig. 8B,C). PbTx-2 failed to increase  $P_o$  [control (PP2),  $0.0047 \pm 0.0005$ ; PbTx-2 (PP2),  $0.0045 \pm 0.0005$ ;  $n = 4$ ] (Fig. 8B) or

mean open time [control (PP2),  $1.95 \pm 0.32$  ms; PbTx-2 (PP2),  $1.89 \pm 0.29$ ;  $n = 4$ ] (Fig. 8C) when Src kinase was inhibited by PP2. To address any nonspecific effects of PP2, single-channel recordings were performed using PP3. PbTx-2-mediated enhancement of NMDA receptor function persisted in the presence of PP3 with both the  $P_o$  [control (PP3),  $0.0032 \pm 0.0005$ ; PbTx-2 (PP3),  $0.013 \pm 0.003$ ;  $n = 4$ ;  $p < 0.05$ , paired  $t$  test] (Fig. 8B) and mean open time [control (PP3),  $1.39 \pm 0.09$  ms; PbTx-2 (PP3),  $3.87 \pm 0.15$ ;  $n = 4$ ;  $p < 0.05$ , paired  $t$  test] (Fig. 8C) showing significant increases compared with PP3 controls. These results suggest a critical role for a Src family kinase in the  $\text{Na}^+$ -mediated regulation of NMDA receptor activity.

#### PbTx-2 enhances neurite outgrowth in immature cerebocortical neurons

We next sought to determine the functional consequences of PbTx-2 augmentation of NMDAR function in immature cerebocortical neurons. We, therefore, examined the influence of PbTx-2 on neurite outgrowth. A range of PbTx-2 concentrations were added to cerebocortical cultures 3 h after plating, and the total neurite length was assessed at 15, 24, 40, or 108 h later. The PbTx-2 concentration–response for total neurite outgrowth at the 15, 24, 40, and 108 h time points exhibited a bidirectional, or hormetic, profile. The 24-h exposure data depicted in Figure 9A reveal that PbTx-2 concentrations between 1 and 30 nM produced a graded increase in neurite outgrowth, whereas concentrations  $>30$  nM had progressively smaller responses. In all experiments,

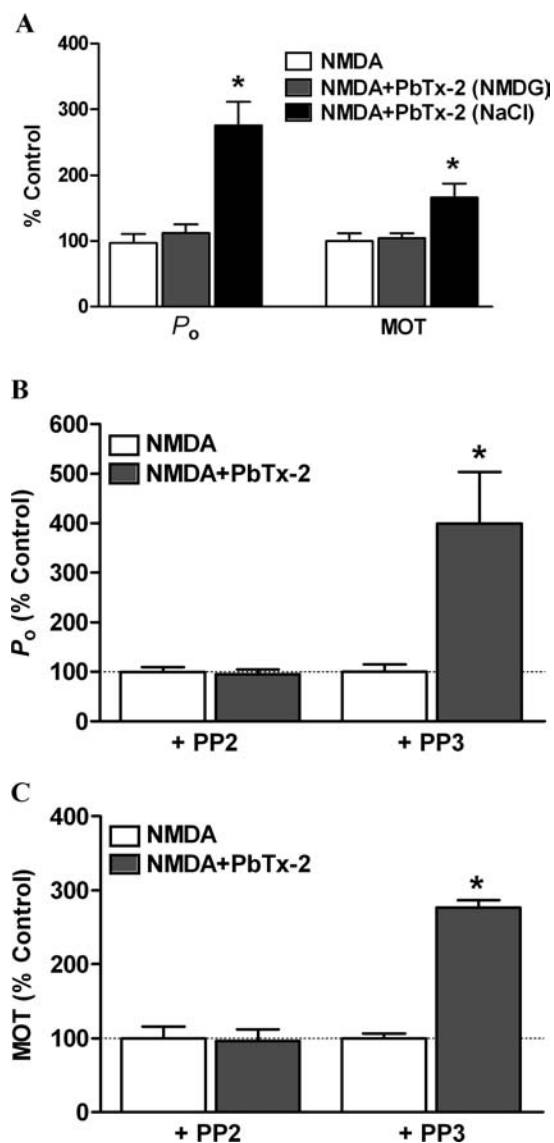


**Figure 8.** Augmentation of NMDA receptor unitary currents by PbTx-2 is dependent on sodium influx and Src kinase. Single-channel NMDA receptor currents were recorded as described in Figure 7. **A**, Replacement of extracellular  $\text{Na}^+$  with impermeant cation NMDG prevented PbTx-2-induced increase in the  $P_o$  and mean open time of NMDA receptors ( $n = 4$ ). Resubstitution with  $\text{Na}^+$ -containing Locke's buffer restored PbTx-2-mediated increase in the  $P_o$  and mean open time of NMDA receptors ( $n = 4$ ,  $*p < 0.05$ , paired  $t$  test). **B**, A 15 min preincubation with the Src kinase inhibitor PP2 (10  $\mu\text{M}$ ), but not the inactive analog PP3 (10  $\mu\text{M}$ ), blocked PbTx-2-induced enhancement of NMDA receptor  $P_o$  ( $n = 4$ ). **C**, PP2, but not PP3, blocked PbTx-2-induced enhancement of NMDA receptor mean open time ( $n = 4$ ,  $*p < 0.05$ , paired  $t$  test).

the 30 nM PbTx-2 concentration produced the largest effect on neurite outgrowth (Fig. 9A–C). This dramatic effect of 30 nM PbTx-2 on neurite length could be seen at all time points (~1.5-fold at 15 h,  $p < 0.05$ ; 2.0-fold at 24 h,  $p < 0.01$ ; 1.8-fold at 40 h,  $p < 0.01$ ; 1.4-fold at 108 h,  $p < 0.05$ ).

Using selective pharmacological inhibitors, we next sought to explore the signaling mechanisms underlying the enhanced neurite outgrowth produced by PbTx-2. We used the selective VGSC antagonist TTX to document the role of sodium channels in this response. Coincubation of TTX (1  $\mu\text{M}$ ) with 30 nM PbTx-2 completely blocked (control,  $187.5 \pm 15.5 \mu\text{m}$ ; PbTx-2,  $265.8 \pm 20.86 \mu\text{m}$ ; TTX,  $185 \pm 13.2 \mu\text{m}$ ; TTX plus PbTx-2,  $190.2 \pm 10.7 \mu\text{m}$ ) the influence of PbTx-2 on total neurite length (Fig. 10A,B),

indicating that the PbTx-2 response is mediated by activation of VGSCs. The role of NMDARs in the response to PbTx-2 was assessed using the uncompetitive NMDA receptor antagonist, MK-801. MK-801 pretreatment similarly abrogated PbTx-2-enhanced neurite development (control,  $101.5 \pm 7.51 \mu\text{m}$ ; PbTx-2,  $166.5 \pm 17.9 \mu\text{m}$ ; PbTx-2 plus MK-801,  $83.1 \pm 5.26 \mu\text{m}$ ). Inhibition of Src kinase with PP2 also eliminated the effect of PbTx-2 on neurite outgrowth (supplemental Fig. S5, available at [www.jneurosci.org](http://www.jneurosci.org) as supplemental material). In contrast, nifedipine, an L-type calcium channel blocker, did not affect ( $156.6 \pm 12.5 \mu\text{m}$ ) PbTx-2-enhanced neurite length (Fig. 10C,D).

Because CaMKK represents a common upstream activator of both calmodulin kinase I (CaMKI), CaMKIV, and MAPKs, the major signaling mediators for  $\text{Ca}^{2+}$ -dependent stimulation of neurite development, we determined the influence of the selective, cell-permeable CaMKK inhibitor, STO-609 (1,8-naphthoylethylene benzimidazole-3-carboxylic acid) (Tokumitsu et al., 2002, 2003; Wayman et al., 2004) on the response to PbTx-2. STO-609 (2.6  $\mu\text{M}$ ) treatment completely blocked PbTx-2-enhanced neurite outgrowth (Fig. 10C,D). These results suggest that PbTx-2-induced neurite outgrowth is dependent on NMDAR-mediated  $\text{Ca}^{2+}$  entry with subsequent activation of a CaMKK pathway. Together, these data indicate that PbTx-2 enhancement of the neurite outgrowth sequentially involves an increase in  $\text{Na}^+$  influx, upregulation of NMDAR function, and engagement of a  $\text{Ca}^{2+}$ -dependent CaMKK pathway (supplemental Fig. S7, available at [www.jneurosci.org](http://www.jneurosci.org) as supplemental material).

## Discussion

Activation of NMDA receptors plays an essential role in brain development including the control of dendritic growth (Cline, 2001; Ewald et al., 2008). NMDA receptor-mediated responses promote dendritic arbor growth, whereas pharmacological blockade of NMDA receptors reduce dendritic growth rate (Rajan and Cline, 1998; Lee et al., 2005). Additionally, the effects of neuronal activity on dendritic development are mediated by calcium-dependent signaling events (Konur and Ghosh, 2005). In the present study, we used a sodium channel activator to mimic the influence of neuronal activity in an effort to explore the relationship between intracellular  $[\text{Na}^+]_i$  and NMDAR-dependent development. The findings of this study in immature murine cerebrocortical cultures provide compelling evidence in support of a role for  $[\text{Na}^+]_i$  in activity-dependent processes of neuronal development.

VGSCs are vital for normal CNS functioning, and recent studies have additionally shown that intracellular sodium may act as a signaling molecule. Based on the original work of Hodgkin and Huxley (1952) with squid axons, a single action potential was calculated to minimally change the  $\text{Na}^+$  electrochemical gradient (Hille, 1992). The situation in mammalian neurons with fine axons, dendrites, and spines is, however, much different, attributable to greater surface-to-volume ratios. Thus, a single action potential may elevate  $[\text{Na}^+]_i$  substantially (Hille, 1992). Using two-photon imaging to measure  $\text{Na}^+$  transients in spines and dendrites of CA1 pyramidal neurons in hippocampal slices, Rose et al. (1999) demonstrated action potential-induced  $[\text{Na}^+]_i$  increments reached values of 3–4 mM after a train of just 20 action potentials.

We have previously found that the sodium channel activator PbTx-2 augments NMDA receptor-mediated  $\text{Ca}^{2+}$  influx in both spontaneously oscillating mature and nonoscillatory immat-

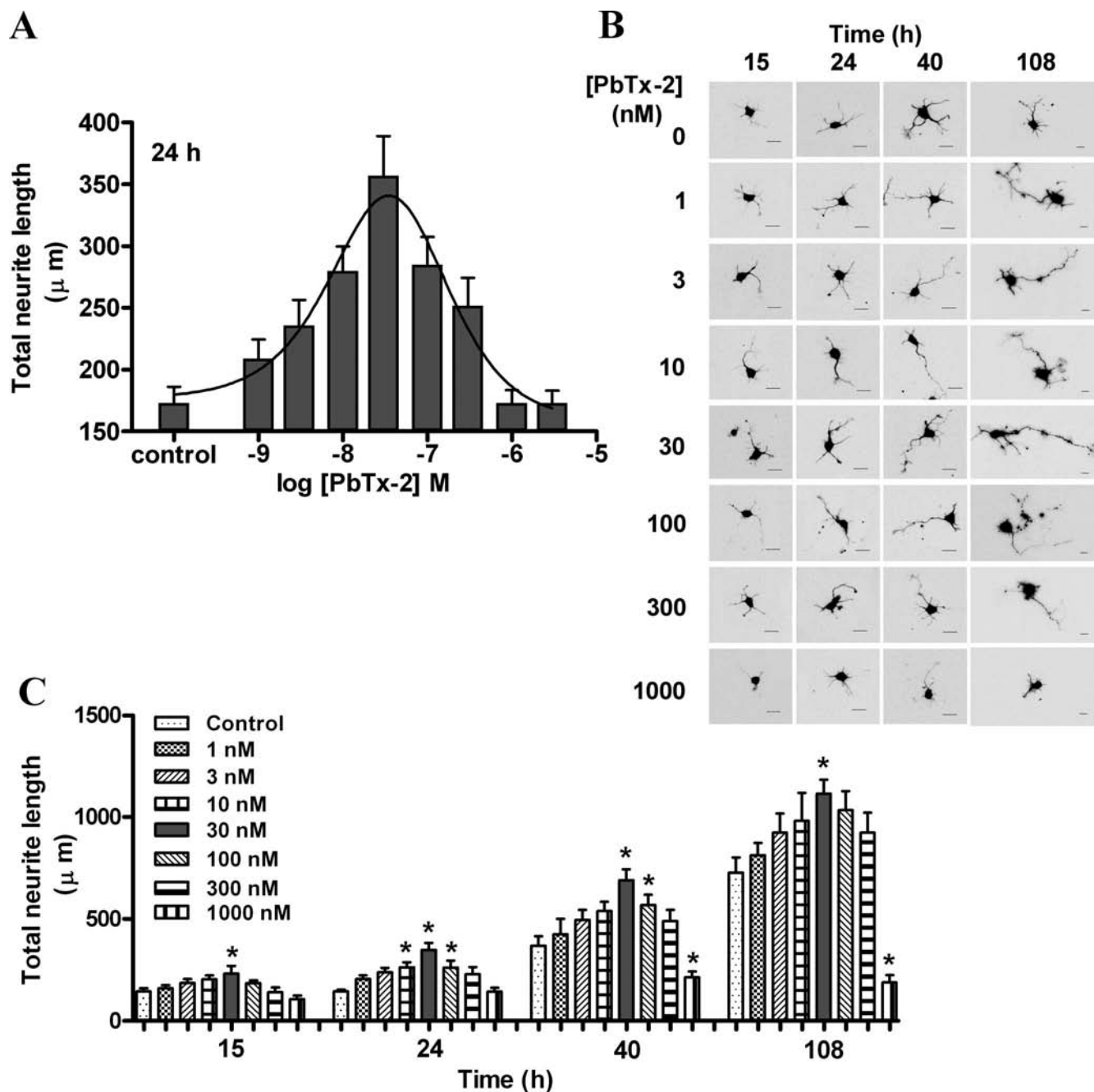


**Figure 9.** Effect of PbTx-2 on neurite outgrowth of cerebrocortical neurons. *A*, Concentration–response profile of PbTx-2 on neurite outgrowth at 24 h after plating. Various concentrations of PbTx-2 were added to the culture medium at 3 h after plating. The maximum enhancement of neurite extension was seen with 30 nM PbTx-2. Each value represents mean  $\pm$  SEM of 120 cells.  $*p < 0.05$ – $0.01$  (ANOVA followed by Dunnett’s multiple comparison test). PbTx-2-enhanced neurite extension displayed a hormetic concentration–response relationship with the peak response at 30 nM. *B*, *C*, Representative images (*B*) and quantification (*C*) of neurite length of cerebrocortical neurons at 15, 24, 40, and 108 h after plating.

ture cerebrocortical neurons (Dravid et al., 2005). PbTx-2 also enhanced the effect of bath applied NMDA on extracellular signal-regulated kinase 2 activation in cerebrocortical neurons. The influence of  $[\text{Na}^+]_i$  dynamics on NMDA receptor function has been demonstrated in hippocampal neurons where elevation of  $[\text{Na}^+]_i$  increased the open probability of NMDA receptors (Yu and Salter, 1998; Yu, 2006). An increment of  $[\text{Na}^+]_i$  of 10 mM was sufficient to produce significant increases in NMDA receptor single-channel activity. This  $\text{Na}^+$ -dependent regulation of NMDA receptor function was, moreover, shown to be controlled by Src-induced phosphorylation of the receptor (Yu and Salter, 1998; Yu, 2006). These results were confirmed and extended in

the present study using the sodium channel activator PbTx-2 as a probe to elevate intracellular  $\text{Na}^+$ . To unambiguously demonstrate the enhancement of NMDA receptor function by PbTx-2, we recorded single-channel currents from cell-attached patches. The shut time histogram with slow time constants resemble NR2B-containing receptors (Erreger et al., 2005), consistent with the expression of NR1/NR2B-containing receptors in immature neurons (Williams et al., 1993). PbTx-2 treatment increased both the mean open time and open probability of NMDA receptors. These effects of PbTx-2 on NMDA receptor function were dependent on extracellular  $\text{Na}^+$  and activation of Src kinase. An increase in intracellular  $\text{Na}^+$  and Src activation have previously

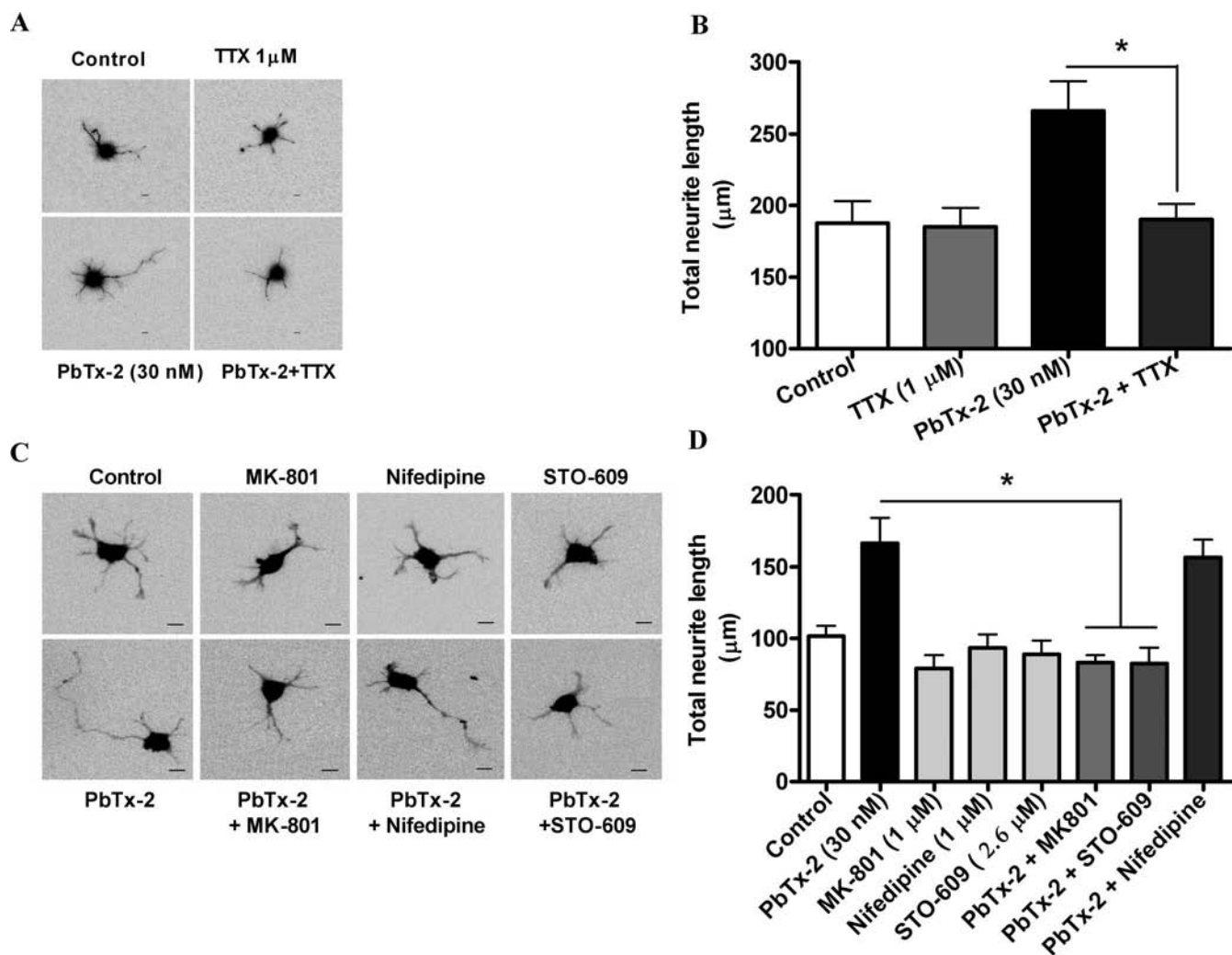


**Figure 10.** Pharmacological evaluation of signaling pathways involved in PbTx-2-induced neurite outgrowth. **A**, Representative images (scale bar, 10  $\mu\text{m}$ ) and respective quantification (**B**) of neurite extension at 24 h. The cerebrocortical neurons were treated with 30 nM PbTx-2 in the presence and absence of 1  $\mu\text{M}$  TTX at 3 h after plating. Bars represent mean  $\pm$  SEM of 30 cells.  $*p < 0.05$ , unpaired *t* test. **C, D**, Representative images (scale bar, 10  $\mu\text{m}$ ) (**C**) and quantification (**D**) of neurite extension at 24 h after plating. The 30 nM PbTx-2 exposure was examined in the presence or absence of MK-801 (1  $\mu\text{M}$ ), STO-609 (2.6  $\mu\text{M}$ ), or nifedipine (1  $\mu\text{M}$ ) beginning at 3 h after plating. Each bar represents the mean  $\pm$  SEM of 30 cells. PbTx-2-enhanced neurite extension was significantly blocked by MK-801 and STO-609 ( $*p < 0.05$ , ANOVA followed by Dunnett's multiple comparison test).

been shown to increase the mean open time and open probability of NMDA receptors in hippocampal neurons (Yu et al., 1997; Yu and Salter, 1998). An increase in apparent mean open time may represent increased stability of the open conformation rather than a change in agonist affinity, because the apparent mean open time appears to be independent of agonist concentration at NR1/NR2A receptors (Schorge et al., 2005). PbTx-2 exposure changed the area of certain shut time constants with no apparent shift in the time constants themselves, suggesting that the sodium channel activator may act by reducing the probability that the channel enters a long-lived shut state. Because the single-channel recordings were done in the absence of extracellular  $\text{Mg}^{2+}$ , these results additionally argue against relief of  $\text{Mg}^{2+}$ -dependent block in the actions of PbTx-2. These data, therefore, confirm the regulatory influence of  $\text{Na}^+$  on NMDAR channel activity in hippocampal neurons described previously (Yu and Salter, 1998) and extend this relationship between  $[\text{Na}^+]_i$  and NMDA receptor function to cerebrocortical neurons.

A key finding of this study is that a functional consequence of the regulatory influence of  $[\text{Na}^+]_i$  on NMDAR channel activity was established. Using immature cerebrocortical neurons, we found that PbTx-2 concentrations between 3 and 300 nM en-

hance neurite outgrowth. Thus, the ability of PbTx-2 to augment NMDAR channel activity translated into an enhancement of the trophic influence of NMDAR on developing cerebrocortical neurons. Accepting the premise that the effects of neuronal activity on the development and structural plasticity of dendritic arbors are primarily mediated by engagement of NMDA receptors (Tolias et al., 2005), our results suggest that PbTx-2 activation of sodium channels with attendant enhancement of NMDA receptor signaling mimics the response to neuronal activity.

An inverted-U model describes the relationship between NMDA receptor activity and neuronal survival and outgrowth (Lipton and Nakanishi, 1999; Hardingham and Bading, 2003). This inverted-U concentration–response relationship has primarily, but not exclusively, been regressed to intracellular  $\text{Ca}^{2+}$  regulation. An optimal window for  $[\text{Ca}^{2+}]_i$  is required for activity-dependent neurite extension and branching, with lower levels stabilizing growth cones and higher levels stalling them, in both cases preventing extension (Gomez and Spitzer, 2000; Hui et al., 2007). It is noteworthy that the concentration dependence for KCl-induced neurite outgrowth in PC12 cells also displays an inverted-U profile (Solem et al., 1995).

The PbTx-2 concentration–response profile for neurite outgrowth reproducibly produced a comparable bidirectional or hormetic relationship (Fig. 9). Although we have reported previously that the PbTx-2 concentration–response relationship for neuronal  $\text{Ca}^{2+}$  influx does not produce an inverted-U response (Berman and Murray, 2000), the pathways for  $\text{Ca}^{2+}$  influx did differ for low (100 nM) versus high (1000 nM) concentrations of PbTx-2 in DIV-2 cerebrocortical neurons (supplemental Fig. S1, available at [www.jneurosci.org](http://www.jneurosci.org) as supplemental material). The  $\text{Ca}^{2+}$  influx pathway stimulated by 100 nM PbTx-2 was primarily through NMDA receptors, whereas 1000 nM PbTx-2 stimulates influx through both L-type calcium channels and NMDA receptors (supplemental Fig. S1, available at [www.jneurosci.org](http://www.jneurosci.org) as supplemental material). The more sustained depolarization associated with exposure to 1000 nM PbTx-2 may produce greater activation of L-type calcium channels in these immature neurons (Fig. 6C). NMDA receptor-dependent and L-type  $\text{Ca}^{2+}$  channel-dependent  $\text{Ca}^{2+}$  influx pathways may differentially contribute to the observed stimulation of neurite outgrowth.  $\text{Ca}^{2+}$ -signaling pathways resulting from L-type  $\text{Ca}^{2+}$  channels and NMDA receptors have been shown to differ (Bading et al., 1993). Wayman et al. (2006) have shown that activity-dependent dendritic arborization in DIV-9 hippocampal neurons involves a  $\text{Ca}^{2+}$ -signaling pathway downstream of the NMDA receptor through activation of a CaMKK and CaMKI. These authors used 16 mM KCl to induce neuronal activity and demonstrated that the observed increase in total dendritic length and branching was eliminated by treatment with an NMDA receptor antagonist. In contrast, evidence for the involvement of L-type  $\text{Ca}^{2+}$  channels in dendritic growth and arborization of DIV-4 cortical neurons exposed to 50 mM KCl has been reported previously (Redmond et al., 2002). The explanation for the discordant results of these previously published studies most likely resides in the differing strengths of depolarizing stimuli produced by 16 versus 50 mM KCl: only the latter would be sufficient to activate L-type  $\text{Ca}^{2+}$  channels in mature cultures. Similarly, only 1000 nM PbTx-2 in the present study was capable of stimulating  $\text{Ca}^{2+}$  influx through L-type  $\text{Ca}^{2+}$  channels. Given that the resting membrane potential of DIV-2 cerebrocortical neurons was found to be in the  $-28$  to  $-30$  mV range and that L-type  $\text{Ca}^{2+}$  channels have an activation threshold at membrane voltages positive to  $-30$  mV (Trombley and Westbrook, 1991), the small depolarization produced by 1000 nM PbTx-2 may have been sufficient to activate L-type channels in these immature cultures. Although these data collectively do not provide an explanation for the inverted-U concentration–response curve for neurite outgrowth, they do illustrate the importance of the strength of a depolarizing stimulus as a determinant of the  $\text{Ca}^{2+}$ -signaling pathways activated.

Although the exact mechanism underlying the inverted-U response remains to be determined, high concentrations of PbTx-2 might promote slow inactivation of VGSCs with attendant reduction in sodium influx (Mitrovic et al., 2000; Ong et al., 2000). Alternatively, high concentrations of PbTx-2 could increase VGSC internalization, which has been shown to be a consequence of  $\text{Na}^+$  influx in immature neuronal tissue (Dargent et al., 1994). Consistent with these provisional explanations for the inverted-U PbTx-2 concentration–response relationship, quantification of cerebrocortical  $[\text{Na}^+]_i$  after 24-h exposure to PbTx-2 also exhibited a hormetic profile (supplemental Fig. S6, available at [www.jneurosci.org](http://www.jneurosci.org) as supplemental material). These data suggest that cerebrocortical neuron  $[\text{Na}^+]_i$  may shape the PbTx-2 concentration–response curve by upregulating NMDAR signaling.

We have recently shown that an array of sodium channel-gating modifiers produce  $[\text{Na}^+]_i$  increments that are of sufficient magnitude to increase NMDA receptor channel activity (Cao et al., 2008). Sodium channel activators, therefore, appear capable of mimicking activity-dependent control of neuronal development by upregulating NMDA receptor signaling pathways that influence neuronal growth and plasticity. Voltage-gated sodium channel activators may accordingly represent a novel pharmacologic strategy to regulate neuronal plasticity through an NMDA receptor and Src family kinase-dependent mechanism.

## References

- Bading H, Ginty DD, Greenberg ME (1993) Regulation of gene expression in hippocampal neurons by distinct calcium signaling pathways. *Science* 260:181–186.
- Baxter DF, Kirk M, Garcia AF, Raimondi A, Holmqvist MH, Flint KK, Bojanic D, Distefano PS, Curtis R, Xie Y (2002) A novel membrane potential-sensitive fluorescent dye improves cell-based assays for ion channels. *J Biomol Screen* 7:79–85.
- Berman FW, Murray TF (2000) Brevetoxin-induced autocrine excitotoxicity is associated with manifold routes of  $\text{Ca}^{2+}$  influx. *J Neurochem* 74:1443–1451.
- Cao Z, George J, Baden DG, Murray TF (2007) Brevetoxin-induced phosphorylation of Pyk2 and Src in murine neocortical neurons involves distinct signaling pathways. *Brain Res* 1184:17–27.
- Cao Z, George J, Gerwick WH, Baden DG, Rainier JD, Murray TF (2008) Influence of lipid soluble gating modifier toxins on sodium influx in neocortical neurons. *J Pharmacol Exp Ther* 326:604–613.
- Catterall WA, Gainer M (1985) Interaction of brevetoxin A with a new receptor site on the sodium channel. *Toxicol* 23:497–504.
- Chen Y, Ghosh A (2005) Regulation of dendritic development by neuronal activity. *J Neurobiol* 64:4–10.
- Cheng C, Fass DM, Reynolds IJ (1999) Emergence of excitotoxicity in cultured forebrain neurons coincides with larger glutamate-stimulated  $[\text{Ca}^{2+}]_i$  increases and NMDA receptor mRNA levels. *Brain Res* 849:97–108.
- Choi DW, Maulucci-Gedde M, Kriegstein AR (1987) Glutamate neurotoxicity in cortical cell culture. *J Neurosci* 7:357–368.
- Cline HT (2001) Dendritic arbor development and synaptogenesis. *Curr Opin Neurobiol* 11:118–126.
- Dargent B, Paillart C, Carlier E, Alcaraz G, Martin-Eauclaire MF, Couraud F (1994) Sodium channel internalization in developing neurons. *Neuron* 13:683–690.
- Diarra A, Sheldon C, Church J (2001) In situ calibration and  $[\text{H}^+]$  sensitivity of the fluorescent  $\text{Na}^+$  indicator SBFI. *Am J Physiol Cell Physiol* 280:C1623–C1633.
- Dravid SM, Baden DG, Murray TF (2005) Brevetoxin augments NMDA receptor signaling in murine neocortical neurons. *Brain Res* 1031:30–38.
- Ehrenberg B, Montana V, Wei MD, Wuskell JP, Loew LM (1988) Membrane potential can be determined in individual cells from the nernstian distribution of cationic dyes. *Biophys J* 53:785–794.
- Erreger K, Dravid SM, Banke TG, Wyllie DJ, Traynelis SF (2005) Subunit-specific gating controls rat NR1/NR2A and NR1/NR2B NMDA channel kinetics and synaptic signalling profiles. *J Physiol* 563:345–358.
- Ewald RC, Van Keuren-Jensen KR, Aizenman CD, Cline HT (2008) Roles of NR2A and NR2B in the development of dendritic arbor morphology *in vivo*. *J Neurosci* 28:850–861.
- Frandsen A, Schousboe A (1990) Development of excitatory amino acid induced cytotoxicity in cultured neurons. *Int J Dev Neurosci* 8:209–216.
- Gomez TM, Spitzer NC (2000) Regulation of growth cone behavior by calcium: new dynamics to earlier perspectives. *J Neurobiol* 44:174–183.
- Griffiths R, Malcolm C, Ritchie L, Frandsen A, Schousboe A, Scott M, Rumsby P, Meredith C (1997) Association of c-fos mRNA expression and excitotoxicity in primary cultures of mouse neocortical and cerebellar neurons. *J Neurosci Res* 48:533–542.
- Hamill OP, Marty A, Neher E, Sakmann B, Sigworth FJ (1981) Improved patch-clamp techniques for high-resolution current recording from cells and cell-free membrane patches. *Pflügers Arch* 391:85–100.
- Hardingham GE, Bading H (2003) The Yin and Yang of NMDA receptor signalling. *Trends Neurosci* 26:81–89.

- Hille B (1992) Ionic channels of excitable membranes, pp 403–411. Sunderland, MA: Sinauer.
- Hodgkin AL, Huxley AF (1952) Currents carried by sodium and potassium ions through the membrane of the giant axon of *Loligo*. *J Physiol* 116:449–472.
- Hui K, Fei GH, Saab BJ, Su J, Roder JC, Feng ZP (2007) Neuronal calcium sensor-1 modulation of optimal calcium level for neurite outgrowth. *Development* 134:4479–4489.
- Jeglitsch G, Rein K, Baden DG, Adams DJ (1998) Brevetoxin-3 (PbTx-3) and its derivatives modulate single tetrodotoxin-sensitive sodium channels in rat sensory neurons. *J Pharmacol Exp Ther* 284:516–525.
- Kim HG, Fox K, Connors BW (1995) Properties of excitatory synaptic events in neurons of primary somatosensory cortex of neonatal rats. *Cereb Cortex* 5:148–157.
- King AE, Chung RS, Vickers JC, Dickson TC (2006) Localization of glutamate receptors in developing cortical neurons in culture and relationship to susceptibility to excitotoxicity. *J Comp Neurol* 498:277–294.
- Koh JY, Choi DW (1987) Quantitative determination of glutamate mediated cortical neuronal injury in cell culture by lactate dehydrogenase efflux assay. *J Neurosci Methods* 20:83–90.
- Konur S, Ghosh A (2005) Calcium signaling and the control of dendritic development. *Neuron* 46:401–405.
- Kuner T, Augustine GJ (2000) A genetically encoded ratiometric neurotechnique indicator for chloride: Capturing chloride transients in cultured hippocampal neurons. *Neuron* 27:447–459.
- Lee LJ, Lo FS, Erzurumlu RS (2005) NMDA receptor-dependent regulation of axonal and dendritic branching. *J Neurosci* 25:2304–2311.
- Lipton SA, Nakanishi N (1999) Shakespeare in love—with NMDA receptors? *Nat Med* 5:270–271.
- Liu Z, Stafstrom CE, Sarkisian M, Tandon P, Yang Y, Hori A, Holmes GL (1996) Age-dependent effects of glutamate toxicity in the hippocampus. *Brain Res Dev Brain Res* 97:178–184.
- Marks JD, Boriboun C, Wang J (2005) Mitochondrial nitric oxide mediates decreased vulnerability of hippocampal neurons from immature animals to NMDA. *J Neurosci* 25:6561–6575.
- Mayer ML, Westbrook GL, Guthrie PB (1984) Voltage-dependent block by Mg<sup>2+</sup> of NMDA responses in spinal cord neurones. *Nature* 309:261–263.
- McAllister AK (2000) Cellular and molecular mechanisms of dendrite growth. *Cereb Cortex* 10:963–973.
- Miller FD, Kaplan DR (2003) Signaling mechanisms underlying dendrite formation. *Curr Opin Neurobiol* 13:391–398.
- Mitrovic N, George AL Jr, Horn R (2000) Role of domain 4 in sodium channel slow inactivation. *J Gen Physiol* 115:707–718.
- Mizuta I, Katayama M, Watanabe M, Mishina M, Ishii K (1998) Developmental expression of NMDA receptor subunits and the emergence of glutamate neurotoxicity in primary cultures of murine cerebral cortical neurons. *Cell Mol Life Sci* 54:721–725.
- Ong BH, Tomaselli GF, Balsler JR (2000) A structural rearrangement in the sodium channel pore linked to slow inactivation and use dependence. *J Gen Physiol* 116:653–662.
- Poli MA, Mende TJ, Baden DG (1986) Brevetoxins, unique activators of voltage-sensitive sodium channels, bind to specific sites in rat brain synaptosomes. *Mol Pharmacol* 30:129–135.
- Qin F (2004) Restoration of single-channel currents using the segmental k-means method based on hidden Markov modeling. *Biophys J* 86:1488–1501.
- Rajan I, Cline HT (1998) Glutamate receptor activity is required for normal development of tectal cell dendrites *in vivo*. *J Neurosci* 18:7836–7846.
- Ramoas AS, McCormick DA (1994) Developmental changes in electrophysiological properties of LGNd neurons during reorganization of retinogeniculate connections. *J Neurosci* 14:2089–2097.
- Redmond L, Kashani AH, Ghosh A (2002) Calcium regulation of dendritic growth via CaM kinase IV and CREB-mediated transcription. *Neuron* 34:999–1010.
- Rose CR, Konnerth A (2001) NMDA receptor-mediated Na<sup>+</sup> signals in spines and dendrites. *J Neurosci* 21:4207–4214.
- Rose CR, Ransom BR (1997) Regulation of intracellular sodium in cultured rat hippocampal neurones. *J Physiol* 499:573–587.
- Rose CR, Kovalchuk Y, Eilers J, Konnerth A (1999) Two-photon Na<sup>+</sup> imaging in spines and fine dendrites of central neurons. *Pflugers Arch* 439:201–207.
- Salter MW, Kalia LV (2004) Src kinases: a hub for NMDA receptor regulation. *Nat Rev Neurosci* 5:317–328.
- Saneyoshi T, Wayman G, Fortin D, Davare M, Hoshi N, Nozaki N, Natsume T, Soderling TR (2008) Activity-dependent synaptogenesis: regulation by a CaM-kinase kinase/CaM-kinase I/betaPIX signaling complex. *Neuron* 57:94–107.
- Schmitt JM, Wayman GA, Nozaki N, Soderling TR (2004) Calcium activation of ERK mediated by calmodulin kinase I. *J Biol Chem* 279:24064–24072.
- Schorge S, Elenes S, Colquhoun D (2005) Maximum likelihood fitting of single channel NMDA activity with a mechanism composed of independent dimers of subunits. *J Physiol* 569:395–418.
- Sin WC, Haas K, Ruthazer ES, Cline HT (2002) Dendrite growth increased by visual activity requires NMDA receptor and Rho GTPases. *Nature* 419:475–480.
- Solem M, McMahon T, Messing RO (1995) Depolarization-induced neurite outgrowth in PC12 cells requires permissive, low level NGF receptor stimulation and activation of calcium/calmodulin-dependent protein kinase. *J Neurosci* 15:5966–5975.
- Tokumitsu H, Inuzuka H, Ishikawa Y, Ikeda M, Saji I, Kobayashi R (2002) STO-609, a specific inhibitor of the Ca(2+)/calmodulin-dependent protein kinase kinase. *J Biol Chem* 277:15813–15818.
- Tokumitsu H, Inuzuka H, Ishikawa Y, Kobayashi R (2003) A single amino acid difference between alpha and beta Ca2+/calmodulin-dependent protein kinase kinase dictates sensitivity to the specific inhibitor, STO-609. *J Biol Chem* 278:10908–10913.
- Tolias KF, Bikoff JB, Burette A, Paradis S, Harrar D, Tavazoie S, Weinberg RJ, Greenberg ME (2005) The Rac1-GEF Tiam1 couples the NMDA receptor to the activity-dependent development of dendritic arbors and spines. *Neuron* 45:525–538.
- Trombley PQ, Westbrook GL (1991) Voltage-gated currents in identified rat olfactory receptor neurons. *J Neurosci* 11:434–444.
- Tyzio R, Ivanov A, Bernard C, Holmes GL, Ben-Ari Y, Khazipov R (2003) Membrane potential of CA3 hippocampal pyramidal cells during postnatal development. *J Neurophysiol* 90:2964–2972.
- Ulanir SK, Kim JE, Hall BJ, Deerinck T, Ellisman M, Ghosh A (2007) Regulation of spine morphology and spine density by NMDA receptor signaling *in vivo*. *Proc Natl Acad Sci U S A* 104:19553–19558.
- Wayman GA, Kaech S, Grant WF, Davare M, Impey S, Tokumitsu H, Nozaki N, Banker G, Soderling TR (2004) Regulation of axonal extension and growth cone motility by calmodulin-dependent protein kinase I. *J Neurosci* 24:3786–3794.
- Wayman GA, Impey S, Marks D, Saneyoshi T, Grant WF, Derkach V, Soderling TR (2006) Activity-dependent dendritic arborization mediated by CaM-kinase I activation and enhanced CREB-dependent transcription of Wnt-2. *Neuron* 50:897–909.
- West AE, Griffith EC, Greenberg ME (2002) Regulation of transcription factors by neuronal activity. *Nat Rev Neurosci* 3:921–931.
- Whiteaker KL, Gopalakrishnan SM, Groebe D, Shieh CC, Warrior U, Burns DJ, Coghlan MJ, Scott VE, Gopalakrishnan M (2001) Validation of FLIPR membrane potential dye for high throughput screening of potassium channel modulators. *J Biomol Screen* 6:305–312.
- Williams K, Russell SL, Shen YM, Molinoff PB (1993) Developmental switch in the expression of NMDA receptors occurs *in vivo* and *in vitro*. *Neuron* 10:267–278.
- Wong RO, Ghosh A (2002) Activity-dependent regulation of dendritic growth and patterning. *Nat Rev Neurosci* 3:803–812.
- Xin WK, Kwan CL, Zhao XH, Xu J, Ellen RP, McCulloch CA, Yu XM (2005) A functional interaction of sodium and calcium in the regulation of NMDA receptor activity by remote NMDA receptors. *J Neurosci* 25:139–148.
- Yu XM (2006) The role of intracellular sodium in the regulation of NMDA-receptor-mediated channel activity and toxicity. *Mol Neurobiol* 33:63–80.
- Yu XM, Salter MW (1998) Gain control of NMDA-receptor currents by intracellular sodium. *Nature* 396:469–474.
- Yu XM, Askalan R, Keil GJ 2nd, Salter MW (1997) NMDA channel regulation by channel-associated protein tyrosine kinase Src. *Science* 275:674–678.

## Supplemental Data

# **Sodium channel activation augments NMDA receptor function and promotes neurite outgrowth in immature cerebrocortical neurons**

**Joju George,<sup>1</sup> Shashank M. Dravid,<sup>1</sup> Anand Prakash,<sup>1</sup> Jun Xie,<sup>1,2</sup> Jennifer Peterson,<sup>3</sup> Sairam V. Jabba,<sup>1</sup> Daniel G. Baden,<sup>4</sup> and Thomas F. Murray<sup>1</sup>**

## **Supplemental Experimental Procedures**

Resting membrane potential was measured non-invasively by recording unitary NMDA receptor currents in cell-attached mode at different pipette potentials as described previously (Tyzio et al., 2003) (Fig. S4). Under conditions where NMDA receptors exhibit linear current-voltage relationship and reverse at 0 mV, the expected membrane potential of the cell will be equal to the pipette holding potential at which the NMDA channel reverses polarity. This approach provided an independent confirmation of the DIV-2 cerebrocortical neuron resting membrane potential determined with the Nernstian dye, FMP Blue.

We used a modified procedure to measure  $[Na^+]_i$  increments following a 24 h PbTx-2 exposure (Fig. S6). A range of PbTx-2 concentrations (10  $\mu$ l (16X)) were added to wells (150 $\mu$ l) at 3 h post plating. At the 24 h time point, 40  $\mu$ l (5X) of SBFI-AM dye (15  $\mu$ M final concentration) was added with 1X corresponding PbTx-2 concentrations per well to yield a final volume of 200  $\mu$ l/well. This procedure maintained constant PbTx-2 exposure during the dye-loading step. Following a one-hour incubation, the neurons were washed

as described using an automated microplate washer prior to placement in the FLEX Station™ II.

### **Figure S1**

#### **PbTx-2-induced Ca<sup>2+</sup> influx in DIV-2 cerebrocortical neurons.**

A. PbTx-2 concentration-response data for the increment in fluo-3 fluorescence as a function of time. Each point represents mean ± SEM of sextuplicate values. Experiment was repeated four times with sextuplicate determinations in three independent cultures. B. Comparison of the Ca<sup>2+</sup> influx pathways triggered by either 100 nM (a) or 1,000 nM (b) PbTx-2. TTX (voltage-gated sodium channel blocker), APV (NMDA receptor competitive antagonist), nifedidine (L-type calcium channel antagonist), NBQX (AMPA receptor antagonist) and KBR-7943 (blocker of reverse mode of sodium-calcium exchanger) were used to block individual calcium influx pathways. C. Analysis of data depicted in S1.B.

### **Figure S2**

#### **Effect of 30 nM PbTx-2 on NMDA-induced Ca<sup>2+</sup> influx in DIV-9 cerebrocortical neurons.**

DIV-9 time-response data. Although these cultures exhibit prominent spontaneous Ca<sup>2+</sup> oscillations, the sustained Ca<sup>2+</sup> influx produced by NMDA is augmented by PbTx-2 (30 nM).

### **Figure S3**

#### **PbTx-2 enhances phosphorylation of Src kinase.**

**A.** Tyrosine phosphorylation (416) of Src kinase was determined by immunoblotting. Cerebrocortical neurons were treated with 30 nM PbTx-2 and/or 3  $\mu$ M NMDA and phosphorylation assessed at the indicated times. A representative blot is shown. The experiment was repeated four times in independent cultures. **B.** Quantitative analysis of the relative band densities of immunoblot. Each point represents mean  $\pm$  SEM of four values.

\* $p < 0.05$  (ANOVA followed by Bonferroni's multiple comparison test).

### **Figure S4**

#### **Membrane potential of DIV-2 cerebrocortical neurons determined from cell-attached recordings of NMDAR channels.**

Assessment of membrane potential of DIV-2 neurons and the effect of PbTx-2 was performed using NMDA receptor cell-attached recordings as a voltage sensor. Current-voltage relationship of single channel NMDA receptor currents was performed in cell-attached mode (see methods for details). The currents through NMDA channels reverse at pipette holding potential of -28mV. PbTx-2 application did not affect the reversal potential of NMDA channels indicating a lack of effect on membrane potential. These data confirm the results obtained using a membrane potential sensitive dye (Fig.6).

## Figure S5

### Effect of Src family kinase inhibitor PP2 and the inactive congener PP3 on PbTx-2-induced neurite outgrowth

A. Representative images (scale bar, 10  $\mu\text{m}$ ) and respective quantification (**B**) of neurite extension at 24 h. The cerebrocortical neurons were treated with 30 nM PbtX-2 in the presence and absence of either 2  $\mu\text{M}$  PP2 or PP3 at 3 h after plating. Bars represent mean  $\pm$  SEM of 20 cells.  $*p < 0.05$ , unpaired t-test.

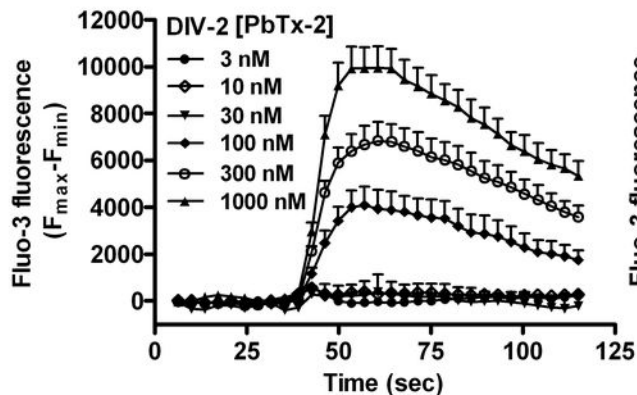
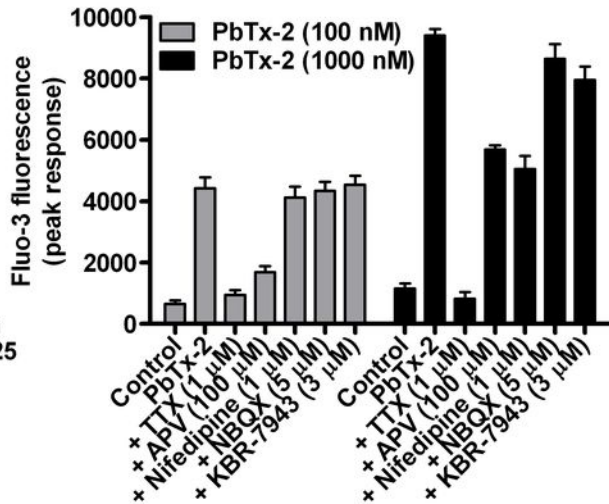
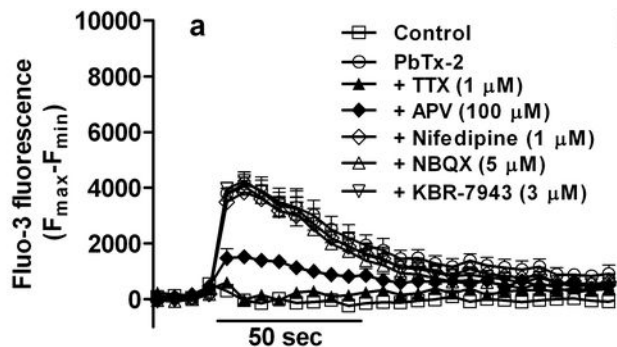
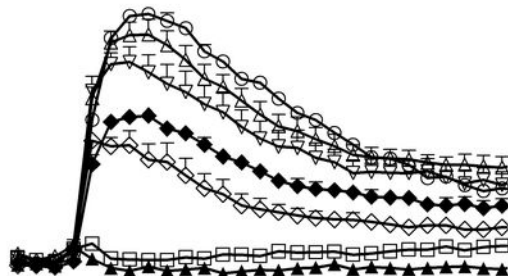
## Figure S6

### $[\text{Na}^+]_i$ levels increase in cerebrocortical neurons following 24 h exposure to PbTx-2.

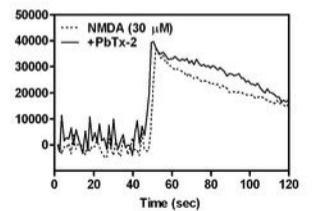
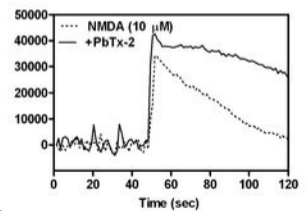
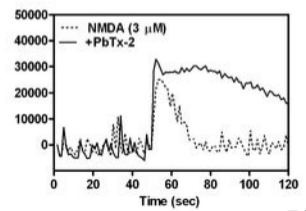
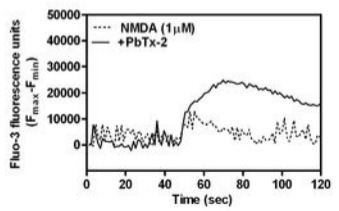
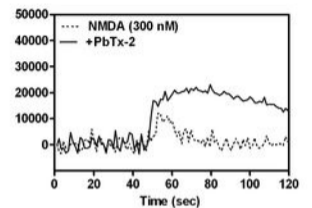
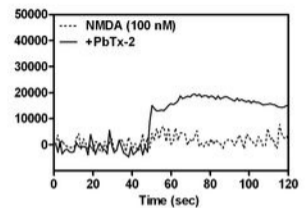
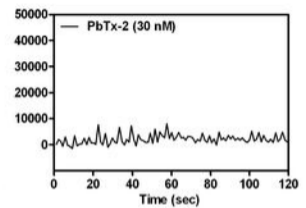
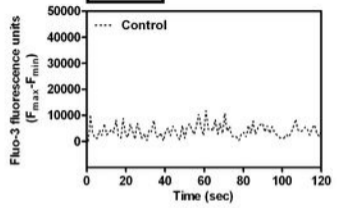
Measurement of  $[\text{Na}^+]_i$  at 24 h following a similar treatment paradigm as used for neurite outgrowth assays. Mean peak values  $\pm$  SEM for SBFI fluorescence (340/380) from three independent cultures each with triplicate determinations. The right ordinate shows the estimated  $[\text{Na}^+]_i$  values from *in situ* calibration.  $*p < 0.05$  (ANOVA followed by Dunnett's multiple comparison test).

## Figure S7

### Schematic diagram for pathways involved in PbTx-2 stimulation of neurite outgrowth.

**A****C****B****b**

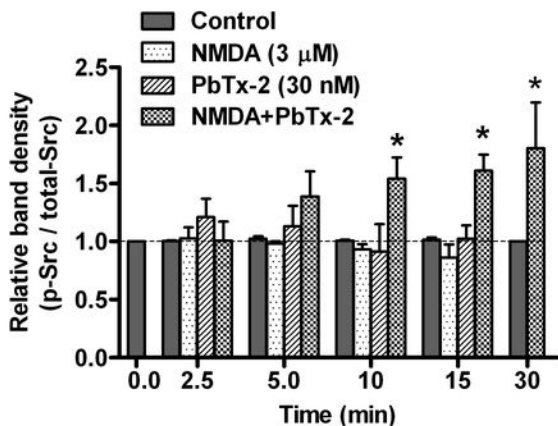
**DIV-9**

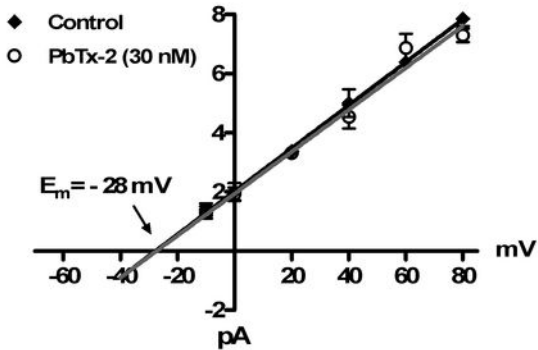


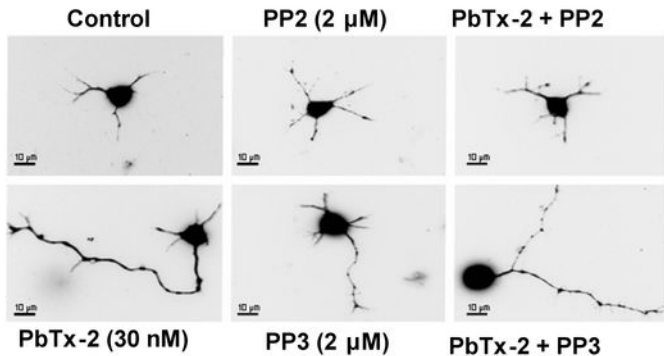
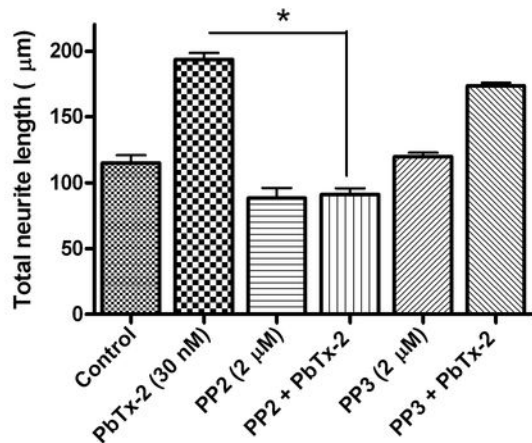
A

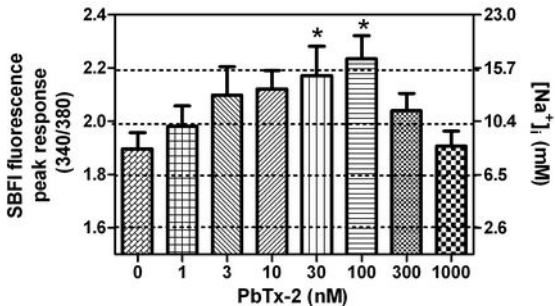


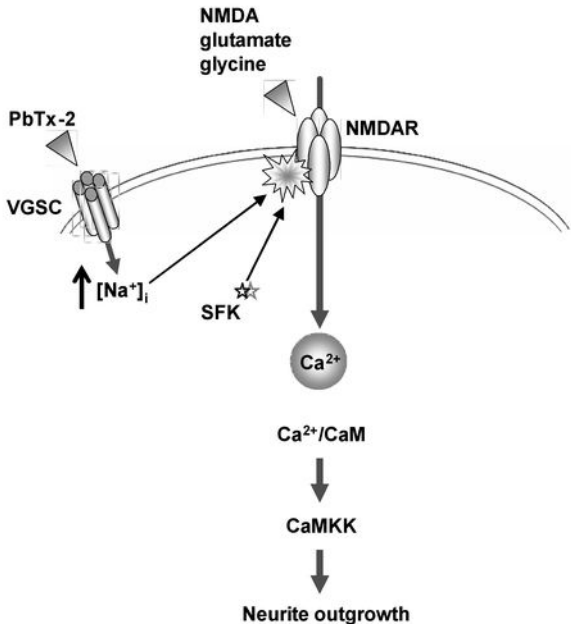
B





**A****B**





## CHAPTER 3

### **Intracellular sodium regulation of NMDA receptor-dependent neuronal plasticity.**

#### **Introduction:**

Activity-dependent neuronal development is becoming an important area of research in neuroscience and it has been shown conclusively that neuronal activity plays a key role in regulation of dendritic development (McAllister, 2000; Chen and Ghosh, 2005). The influence of neuronal activity on dendritic arborization has been demonstrated in several studies using activity deprivation experiments and blockade or attenuation of activity is shown to result in long lasting deficits in dendritic arborization (Sin et al., 2002; Wong and Ghosh, 2002; Faherty et al., 2003). Spontaneous activity is a characteristic feature of developing neurons and it is proposed that this activity facilitates the refinement of coarse wiring laid out by predetermined genetic programs. Spontaneous activity also has been shown to have a profound influence on enhancing dendritic growth and development (Redmond et al., 2002). Moreover, several studies suggest that neuronal activity can regulate spine morphology (Yuste and Bonhoeffer, 2004). Although activity-induced changes in dendritic structure is most pronounced during development (Kalb, 1994), activity-induced changes in dendrite morphology also have been reported to occur outside the limits of the developmental time window. Induction of long-term potentiation (LTP) and the associated changes in dendritic arbor and spine dynamics is the best example of activity dependent structural plasticity in adults. The effects of neuronal activity on dendritic development are mediated by intracellular calcium signals, and

recent studies indicate that calcium-induced signaling events have both cytoplasmic and nuclear targets (Chen and Ghosh, 2005).

NMDARs play a critical role in activity-dependent development and plasticity, dendritic arborization, spine morphogenesis, and synapse formation by stimulating calcium-dependent signaling pathways (Rajan and Cline, 1998; Sin et al., 2002; West et al., 2002; Wong and Ghosh, 2002; Miller and Kaplan, 2003; Tolia et al., 2005). NMDAR-dependent CaMKK/calmodulin kinase I-signaling cascades have been shown to regulate neurite/axonal outgrowth (Wayman et al., 2004), activity-dependent synaptogenesis (Saneyoshi et al., 2008) and  $Ca^{2+}$ -dependent ERK activation and dendritic outgrowth (Schmitt et al., 2004; Wayman et al., 2006). CaMK and ERK pathways have been implicated in mediating activity-dependent transcriptional control of dendritic complexity. The CaMK pathway contributes to a fast early phase of CREB phosphorylation, whereas the ERK pathway mediates a later prolonged phosphorylation state. Brain derived neurotrophic factor (BDNF) has been shown to regulate axonal and dendritic branching and synaptogenesis (Figurov et al., 1996; Kang and Schuman, 1996). BDNF gene expression is shown to be regulated by CREB-dependent transcription, and BDNF is found to be secreted in an activity dependent manner from presynaptic nerve terminals (Pang et al., 2004). The neuronal effects of BDNF are primarily mediated via a high affinity neurotrophin receptor, TrkB. Surface expression of TrkB is reported to be regulated by neuronal activity (Du et al., 2000) and BDNF-TrkB signaling complex initiates signal transduction mechanisms that enhance dendritic morphogenesis (Takemoto-Kimura et al., 2007). Inasmuch as neuronal activity involves voltage gated sodium channels primarily, the surface expression of voltage gated sodium channels has

been reported to be regulated in an activity dependent manner (Dargent et al., 1994). Similarly, trafficking and surface expression of NMDARs also is tightly regulated via phosphorylation of the NR2B subunit (Snyder et al., 2005), which is shown to be highly expressed in developing young neurons (Hall et al., 2007). A better understanding of the activity-dependent regulation of surface expression of these channels and receptors is necessary to investigate the manifold signaling mechanisms recruited in activity-dependent structural plasticity.

The ability of NMDARs to engage diverse signaling mechanisms that converge at the level of actin dynamics make them the best candidate for mediating complex structural plasticity. NMDAR- interacts (directly or indirectly) with several guanylyl nucleotide exchange factors (GEFs) like Rac1, Cdc42, Tiam1 and  $\beta$ PIX that function as intermediate candidates for regulating actin dynamics and control dendritic growth and spine morphogenesis (Saneyoshi et al., 2008). PSD-95 is a multi-domain post-synaptic density protein that clusters glutamate receptors and the associated signaling complexes, and the amount of PSD-95 is reported to determine the size and strength of synapses (Kim and Sheng, 2004). It has been shown that local NMDAR-BDNF stimulation can produce increase in dendritic arbor development and PSD-95 transported to synapses localizes the actin-remodeling GTPases like Rac, which has been shown to interact with NMDARs. All these reports strongly agree on the ability of NMDAR signaling to engage diverse signal transduction pathways to enhance synaptic strengthening.

Various studies have indicated that changes in  $[Na^+]_i$  produced in the soma and dendrites as a result of neuronal activity may act as a signaling molecule and play a role in activity-dependent synaptic plasticity (Yu and Salter, 1998; Yu, 2006). These findings

were confirmed and extended in our study using the sodium channel activator PbTx-2 as a probe to elevate intracellular  $\text{Na}^+$ . In our previous report (George et al., 2009), we showed that PbTx-2 produced a concentration-dependent increment in  $[\text{Na}^+]_i$  ( $\text{EC}_{50}$  -43.3 nM with 23.5-79.9 nM, 95 % CI) and that 30 nM PbTx-2 produced a maximum  $[\text{Na}^+]_i$  of  $16.9 \pm 1.5$  mM, representing an increment of  $8.8 \pm 1.8$  mM over basal. This concentration of PbTx-2 was also found to augment NMDA-induced  $\text{Ca}^{2+}$  influx. Moreover, single channel recordings from cell-attached patches showed that PbTx-2 (30 nM) treatment upregulated NMDAR channel activity without altering the resting membrane potential. These effects of PbTx-2 on NMDA receptor function were dependent on extracellular  $\text{Na}^+$  and activation of Src kinases. In light of this evidence, we hypothesized that exposure to PbTx-2 can modulate complex aspects of structural plasticity like dendritogenesis, spinogenesis and synaptogenesis, by mimicking neuronal activity. In this study, exposure to PbTx-2 was found to promote dendritogenesis, spinogenesis and synaptogenesis via NMDAR dependent signaling pathways. Consistent with these results, Antillatoxin, a potent activator of VGSC has also been shown to enhance NMDAR-dependent neurite outgrowth in cerebrocortical neurons (Jabba et al., 2010). The findings presented in this report indicate that sodium channel activation induced NMDAR-mediated signaling influences dendritic arborization by increasing the total number of dendritic branches, enhances spinogenesis by stimulating dendritic filopodia formation and increasing synapse formation in cerebrocortical neurons. These NMDAR-dependent effects are recruited through activation of both a transcriptional program that involves CREB-mediated gene expression and local signaling that involves Rac/Cdc-42 regulation of actin dynamics, primarily via a CaM kinase-dependent signaling pathway. Moreover,

PbTx-2-induced total neurite outgrowth, dendritic arbor development and synapse formation exhibited a biphasic concentration-response profile with 30 and 100 nM of PbTx-2 having the most robust effect. Altogether these data indicate that PbTx-2, an activator of voltage-gated sodium channels, mimics activity-dependent control of neuronal development by elevating intracellular sodium levels and augmenting NMDAR function for downstream signaling events. These signaling events involve primarily a CaMK signaling pathway with downstream activation of CREB dependent transcription of BDNF and enhance denritogenesis, spinogenesis and synaptogenesis in developing cerebrocortical neurons.

### **Materials:**

Trypsin, penicillin, streptomycin, heat-inactivated fetal bovine serum, horse serum and soybean trypsin inhibitor were obtained from Atlanta Biologicals (Norcross, GA). Minimum essential medium (MEM), Deoxyribonuclease (DNase), poly-L-lysine, poly-D-lysine hydrobromide, cytosine arabinoside, NMDA, Protease inhibitor cocktail, D (-)-2-Amino-5-phosphono-pentanoic acid (APV),  $\beta$ -glycerophosphate, Fluoromount™ aqueous mounting medium were purchased from Sigma (St. Louis, MO). Pluronic acid, fluo-3 AM and SBFI AM were purchased from Molecular Probes (Eugene, OR). STO-609 was purchased from Calbiochem (La Jolla, CA). ECL Plus kit was purchased from Amersham Biosciences (Piscataway, NJ). Rhodamine-conjugated phalloidin and DAPI were purchased from Cytoskeleton, Inc.  $\omega$ -conotoxin and nimodipine were purchased from Tocris Bioscience (Ellisville, MO). Alexa fluor-488 and Alexa fluor-568 were purchased from The Jackson Laboratory (Sacramento, CA). Rac activation assay kit was purchased from NewEast Biosciences (Malvern, PA). Brevetoxin-2 (PbTx-2) was isolated and

purified from *Karinia breve* cultures at the Center for Marine Sciences at the University of North Carolina (Wilmington, NC).

## **Methods:**

### **Cerebrocortical Neuron Culture:**

Cerebrocortical neurons were harvested from embryos of Swiss-Webster mice on embryonic day 16 and cultured as described previously (Cao et al., 2008). Cells were plated onto poly-L-lysine-coated 96-well (9 mm) (Costar), 24-well (15.6 mm), 12-well (22 mm) or 6-well (35-mm) culture plates (TPP-Midscience) and incubated at 37°C in a 5% CO<sub>2</sub> and 95% humidity atmosphere. Cytosine arabinoside (10 µM) was added to the culture medium on day 2 after plating to prevent proliferation of non-neuronal cells. All animal use protocols were approved by the Institutional Animal Care and Use Committee of Creighton University.

### **Intracellular Ca<sup>2+</sup> Monitoring:**

Cerebrocortical neurons grown in 96-well plates (1.5 x 10<sup>5</sup> cells per well) were used for intracellular Ca<sup>2+</sup> concentration ([Ca<sup>2+</sup>]<sub>i</sub>) measurements. The growth medium was removed and replaced with dye loading medium (100 µl per well) containing 4 µM fluo-3 AM and 0.04% Pluronic acid in Locke's buffer. After 1 h of incubation in dye loading medium, the neurons were washed four times with fresh Locke's buffer (200 µl per well, 22°C) using an automated microplate washer (Bio-Tek Instruments Inc, VT, USA) and transferred to a FLEX Station<sup>TM</sup> II (Molecular Devices, Sunnyvale, USA) benchtop scanning fluorometer chamber. The final volume of Locke's buffer in each well was 150

$\mu$ l. Fluorescence measurements were carried out at 37°C. The neurons were excited at 488 nm and Ca<sup>2+</sup>-bound fluo-3 emission was recorded at 538 nm at 1.2 s intervals. After recording baseline fluorescence for 60 s, 50  $\mu$ l of a 4 times concentration of drugs were added to the cells at a rate of 26  $\mu$ l/s, yielding a final volume of 200  $\mu$ l/well; the fluorescence was monitored for an additional 140-240 s. The fluo-3 fluorescence was expressed as (F<sub>max</sub>-F<sub>min</sub>) where F<sub>max</sub> was the maximum and F<sub>min</sub> the minimum fluorescence measured in each well.

### **Immunoblotting:**

Immunoblot analysis was performed in cells grown in 12-well plates (2.0 x 10<sup>6</sup> cells per well) within 24 h post plating. Cells were washed two times with Locke's incubation buffer (154 mM NaCl, 5.6 mM KCl, 1.0 mM MgCl<sub>2</sub>, 2.3 mM CaCl<sub>2</sub>, 8.6 mM HEPES, 5.6 mM glucose, 0.1 mM glycine, pH 7.4) and then allowed to equilibrate in Locke's buffer for 30 min. Cultures were then treated with the indicated drugs at 37° C for specified times. In some experiments, time points more than 4 h were done in serum-free Neurobasal medium without B-27. Cultures were then transferred to ice slurry. After washing with ice cold Locke's buffer, cells were harvested in ice cold lysis buffer containing 50 mM Tris, 150 mM NaCl, 2 mM EDTA, 2 mM EGTA, 1% NP-40, 0.1% SDS, 2 mM sodium pyrophosphate, 1 mM sodium orthovanadate, 25 mM  $\beta$ -glycerophosphate. Phenylmethylsulfonyl fluoride (1mM) and Protease inhibitor cocktail were then added and the lysate incubated for 15 min at 4°C. Cell lysates then underwent sonication and were centrifuged at 12,000 $\times$ g for 15 min at 4° C. The supernatant was assayed by the Bradford method to determine protein content. Equal amounts of protein

were mixed with Laemmli sample buffer and boiled for 5 min. The samples were loaded onto a 12% SDS-PAGE gel and transferred to a nitrocellulose membrane by electroblotting. The membranes were blocked in TBST (20 mM Tris, 150 mM NaCl, 0.1% Tween 20) with 5% non-fat dry milk or BSA for 1 h at room temperature. After blocking, membranes were incubated overnight at 4 °C in primary antibody diluted in TBST containing either 5% non-fat dry milk or BSA. The blots were washed and incubated with the secondary antibody conjugated with horseradish peroxidase for 2 h, washed three times in TBST and exposed with ECL Plus for 4 min. Blots were exposed to Kodak hyperfilm and developed. Blots were subsequently stripped (63 mM Tris base, 70 mM SDS, 0.0007% 2-mercaptoethanol, pH=6.8) and reprobed. Immunoblot densitometry data was obtained using MCID Basic 7.0 software® (Imaging Research, Inc.). Graphing and statistical analysis were completed using GraphPad Prism® (GraphPad Software, Inc., San Diego, CA).

### **Antibodies:**

CaMKIV (dilution used, 1:2000), Phospho-CREB (Ser133) (1:3000), CREB (86B10) (1:3000), Phospho-CaMKII (Thr286) (1:2000), Phospho-Akt (Ser473) (1:1000), Phospho-Akt (Thr308) (1:1000) and Akt (1:2000), Phospho-p44/42 and p44/42 (1:2000) were purchased from Cell signaling Technology, Inc (Danvers, MA); p-CaMKI (Thr177) (1:2000), CaMKI (M-20) (1:2000) and P-CaMKIV (Thr 196)(1:1000) were purchased from Santa Cruz Biotechnology, Inc ( Santa Cruz, CA); CaMKII (1:10,000) was purchased from Novus Biologicals ( Littleton, CO).

**Double Immunofluorescence:**

Neurons ( $1.0 \times 10^6$  cells/ml) grown on Poly-D-lysine coated cover glass ( $22 \text{ mm}^2$ ) placed inside 6 well plates were used. PbTx-2 at different concentrations was added to the culture medium at 3 h after plating. The neurons on the cover glass were initially fixed with 2% PFA for 2 min following 4% PFA post-fixing for 5 min. After washing with PBS, the neurons were permeabilized with 0.2% Triton X-100 in PBS for 10 min, followed by blocking with 6% normal serum for 30 min. Primary antibodies, synaptophysin [1:800, Invitrogen (Carlsbad, CA)] and PSD-95 [1:400, Thermo Fisher Scientific (Rockford, IL)], in 3% serum in PBS were added and incubated overnight at  $4^\circ\text{C}$ . Following washing, the neurons were incubated in secondary antibodies conjugated with Alexa fluor 488 (1:1000) and Alexa fluor 568 (1:1000) at room temperature for 2 h. The neurons were washed with PBS and the cover glasses were mounted onto subbed slides in aqueous medium.

**Image acquisition and colocalization analysis:**

Images were acquired using an Olympus spinning disk confocal microscope with 60X oil immersion objective in  $1344 \times 1024$  pixel ( $144 \times 110 \mu\text{m}$ ) frames and scanned at  $0.2 \mu\text{m}$  intervals along the Z-axis with a depth of  $5 \mu\text{m}$  (25 planes). For each condition about 20-30 image frames were taken from each independent experiment and repeated at least three times. Double immunostaining with synaptophysin (green), a pre-synaptic marker and PSD-95 (red), a post-synaptic marker yielded a reliable quantification of colocalized punctae (yellow) as an indication of a functional synapse. Automated colocalization analysis was performed using Slide book (4.2) digital microscopy software, which

analyze entire two channel confocal stacks by measuring the intensity of each label, voxel by voxel. For quantification of colocalized puncta, initially the confocal stacks were deconvolved and backgrounds of the images were corrected using the same threshold values for all images to be analyzed. A mask segmentation of fluorescent objects was created in both channel images and the merged image was statistically analyzed using cross mask and cross channel functions. To exclude neuronal soma, a size exclusion limit was defined. Pearson's correlation coefficient ( $\geq 0.7$ ) was used to determine colocalized puncta. Pearson's correlation coefficient indicates the extent to which the intensity of the two labels increases together in the same voxels. It varies between +1 and -1, with positive values indicating a positive correlation, values near 0 indicating no correlation, and negative values indicating an inverse correlation. To determine synapse density, total dendritic length 5  $\mu\text{m}$  away from neuronal soma was measured in each frame and normalized to the number of synapses per 20  $\mu\text{m}$  dendritic length.

### **Diolistic labeling:**

Neurons grown on Poly-D-lysine coated glass coverslips placed inside 24 well culture plates ( $0.1 \times 10^6$  cells per well) were used. The media was removed and the neurons were pre-fixed in 1.5% (w/v) Paraformaldehyde (PFA) in PBS for 15 min. Following a brief wash with PBS, tungsten particles (1.1  $\mu\text{m}$  diameter, Bio-Rad) coated with the lipophilic carbocyanine dye DiI (Invitrogen) were delivered diolistically into the neurons at 100 psi using a Helios Gene Gun system (Bio-Rad) fitted with a polycarbonate filter with 20  $\mu\text{m}$  pore size (Sterlitech). DiI was allowed to diffuse along neuron dendrites and axons in PBS containing 0.01 % (w/v) thimerosal for 48 h at 4°C, and then labeled neurons were

post fixed in 4% PFA for 10 min. The fixed neurons were again washed with PBS and the coverslips were mounted onto subbed slides in aqueous medium.

Z-stacked images were acquired using an Olympus spinning disk confocal microscope attached to a Hamamatsu ORCA-ER digital camera. DiI was excited using a mercury arc discharge light source and the images were captured with a 60X oil-immersion objective using Slide Book 4.2 software. Each neuron was scanned at 0.2  $\mu\text{m}$  intervals along the z-axis with a depth of 5  $\mu\text{m}$  (25 planes).

### **Measurement of dendritic branching and filopodia/spine density:**

For quantitative analysis, a three-dimensional perspective was rendered by the surpass module of Imaris software (Biplane Scientific solutions). For the analysis of dendritic arbor development, the dendritic tracings were quantified by sholl analysis (Sholl, 1953). Dendritic arborization was also measured by counting the total number of dendritic branches (branching, indicated, Y bifurcated) or dendritic branch points at each order away from the cell body or dendritic shaft. The quantification on dendritic protrusions was commenced after the first branch point and the values were normalized based on number and length of the dendrites quantified within each individual neuron. The rendered image after Gaussian smoothing was thresholded manually such that all visually discernable neuronal protrusions in 3D were identified. We employed filament module of Imaris software that quantifies spine density and head diameter. The minimum end segment diameter (spine head) was set at  $\geq 0.215 \mu\text{m}$  (i.e the thinnest quantifiable spines were 0.215  $\mu\text{m}$  in diameter). For automatic quantification of neuronal protrusions, the following algorithm was used; Total number of protrusions from dendrites  $\geq 0.215$

$\mu\text{m}$  head diameter and  $\leq 10 \mu\text{m}$  length; number of Spines  $\Rightarrow 0.430 \mu\text{m}$  head diameter and  $\leq 5.375 \mu\text{m}$  length; number of filopodia = Total number of protrusions minus number of spines.

### **Whole Cell Binding Assay:**

Whole cell binding assay of primary neuronal cultures was done by our previously described method (Li et al., 2001). Neurons were plated in 6 well ( $5 \times 10^6$  /well) culture plates and exposed to various concentrations of PbTx-2 at 3 h post plating. At the indicated times, the cells were rinsed with Buffer A (140 mM choline chloride, 5 mM KCl, 1.8 mM  $\text{CaCl}_2$ , 0.8 mM  $\text{MgSO}_4$ , and 10 mM HEPES (pH 7.4 with 1 M Tris). Cells were incubated for 4 h at  $4^\circ\text{C}$  in the presence of buffer B (buffer A plus 2 mg/ml BSA) containing  $\sim 2$  nM [ $^3\text{H}$ ] BTX, 300 nM PbTx-2 and 10  $\mu\text{M}$  deltamethrin (PbTx-2 and deltamethrin were used to increase specific binding). Nonspecific binding of [ $^3\text{H}$ ] BTX was determined as [ $^3\text{H}$ ] BTX bound in the presence of 100  $\mu\text{M}$  veratridine. QX-314 (1 mM), a quaternary lidocaine derivative was used to define cell surface binding. After incubation, cells were rinsed with buffer A before lysis with 1 ml of 1% Triton X-100 under a condition of constant shaking overnight. A 750- $\mu\text{l}$  aliquot of the resulting lysate was collected, and [ $^3\text{H}$ ] BTX bound was measured by liquid scintillation counting.

### **Rac or Cdc42 activation assay:**

Cells grown in 6 well plates ( $5 \times 10^6$  cells per well) were used to measure Rac or Cdc42-GTP levels following PbTx-2 exposure. After removing the media, the cells were pre-incubated in sterile filtered Locke's buffer for 3 h and then PbTx-2 was added for 30 min. Following drug exposure, the cells were transferred to ice-slurry and washed two

times with ice-cold PBS. Cells were lysed using lysis buffer containing 50 mM Tris-HCl (pH-8.0), 150 mM NaCl, 10 mM MgCl<sub>2</sub>, 1 mM EDTA, 1% Triton-100 (Neweast Biosciences) and the lysate was cleared by centrifugation for 10 min (12,000×g at 4°C). Samples were collected for total Rac or Cdc42 from each sample. Aliquoted equal volumes of cell lysate and diluted twice with lysis buffer. Briefly, anti-active Rac mouse monoclonal antibody (1:1000) with protein A/G agarose beads were incubated with cell lysates for 1 h at 4°C with gentle agitation. For *in vitro* GTPγS/GDP protein loading for positive and negative controls, cell lysates were incubated with either GTPγS (100 μM, final concentration) or GDP (1 mM) for 30 min at 30°C with gentle agitation in the presence of 20 mM EDTA. The loading was stopped by placing the cell lysates on an ice-slurry and adding 60 mM MgCl<sub>2</sub> (final concentration) followed by the same procedure used for active Rac or Cdc42 pull-down. After the incubation, the pellet was collected by centrifugation at 5000×g for 1 min and the beads were washed three times in lysis buffer. The precipitated active Rac or Cdc42 was detected by immunoblot (16% SDS-PAGE) analysis using anti-Rac or Cdc42 rabbit polyclonal antibody (1:2000).

#### **Reverse transcription of RNA and polymerase chain reaction (RT-PCR):**

Briefly, 2 μg RNA purified from DIV-1 cerebrocortical neuron cultures was reverse transcribed into cDNA in a 10 μl reaction and the cDNA obtained was subjected to either a conventional RT PCR or real time PCR amplification. In each case, RNA samples were verified as free of DNA contamination using an RT-PCR negative control lacking reverse transcriptase. From the 10 μl cDNA, 5 μl was used for the PCR reaction with BDNF primers and 5 μl was used for the PCR reaction with GAPDH (glyceraldehyde phosphate

dehydrogenase) primers. For the conventional PCR, a total of 25 cycles were employed with annealing at 60<sup>0</sup>C and extension at 72<sup>0</sup>C. 12 µl of each sample's PCR product was separated by 2% agarose gel electrophoresis and the gels were imaged using a UV image analyzer. For the real time PCR, we employed 40 cycles with annealing at 60<sup>0</sup>C and extension at 72<sup>0</sup>C and the fold change in gene expression was calculated using the formula  $2^{-\Delta\Delta ct}$  where  $\Delta\Delta ct$  is (Ct of test BDNF-Ct of test GAPDH)-(Ct of control BDNF-Ct of control GAPDH).

#### **F-actin staining and quantification of growth cone collapse:**

The response of neuronal growth cones following either PbTx-2 or NSC23766 treatment was assessed in three independent experiments (n=60 neurons per group from each experiment). Drugs were added 3 h post plating and then neurons were fixed at 16 h and stained for F-actin with Rhodamine-conjugated phalloidin (Cytoskeleton, Inc) to visualize growth cone morphology. At this time point, more than 70 % of the neurons (control, n=174) displayed distinct growth cones  $\geq 3$  per neuron. The collapsed growth cones of each neuron, which were defined as those with no lamellipodia and not more than two filopodia (Kapfhammer et. al., 2007), were counted and expressed as the percentage of the total growth cones of that neuron.

#### **Biotinylation assay of surface expressed NR2B subunit of NMDA receptors, TrkB receptors and VGSCs:**

Biotinylation assay of cultured cortical neurons was performed as described previously (Tnag, et al., 2009). DIV-1 neurons grown on 6 well plates ( $5 \times 10^6$  cells per well) were allowed to equilibrate in Locke's buffer for 30 min after removing the media.

The neurons were then treated with various concentrations of PbTx-2 at 37° C for 30 min. Cultures were then transferred to an ice slurry. Neurons were washed three times with ice-cold PBS containing 1 mM MgCl<sub>2</sub>, 0.1 mM CaCl<sub>2</sub>, and 5 mM EDTA (PBS+), and incubated with 1 mg/ml EZ-Link Sulfo-NHS-LC-biotin (Pierce) in PBS+ with protease inhibitors for 20 min at 4°C with gentle agitation. Cells were washed 3 times with ice-cold quenching buffer (50 mM glycine in PBS+) for 5 min each. The cells were then sonicated and centrifuged at 40,000 rpm for 20 min at 4°C to obtain the crude membrane fraction. The crude membrane fraction was first lysed in 1% SDS for 30 min at 37°C and then in 1% TX-100 at 4°C, both in PBS with 5 mM EDTA and protease inhibitors. The lysate was centrifuged at 14, 000 rpm for 20 min and then incubated with streptavidin-Sepharose beads (Pierce) for 2 h at 4°C with gentle rotation. Beads were washed four times in washing buffer containing 1% TX-1000 and then twice in PBS. Bound proteins were eluted in Laemmli sample buffer and immunoblotted with antibodies against NR2B (1:1000) and  $\alpha$ -tubulin (1: 10,000)

## **Results:**

### **PbTx-2 enhanced neurite outgrowth exhibits a hormetic profile similar to that of NMDA.**

In our previous report, we have shown that PbTX-2, a sodium channel activator, elevates intracellular sodium levels, augments NMDA-induced  $\text{Ca}^{2+}$  influx and increases both mean open time and open probability of NMDARs in developing cerebrocortical neurons (George et al., 2009). Subsequent assessment of functional consequences of PbTx-2 augmented NMDAR function showed that PbTx-2 concentrations between 3 and 300 nM enhanced neurite outgrowth with peak response at 30 nM. PbTx-2-enhanced neurite outgrowth exhibited a biphasic or hormetic concentration-response profile ( $\text{EC}_{50}$ ~31.6 nM;  $\text{IC}_{50}$ ~50.1 nM). Pharmacological studies showed that PbTx-2 enhanced neurite outgrowth was primarily dependent on VGSCs and NMDARs. Inasmuch as we excluded the possibility of PbTx-2 to be a depolarizing stimulus to influence NMDAR function, we reasoned that an increase in  $[\text{Na}^+]_i$  may act as a positive regulator of NMDAR-dependent developmental plasticity in immature cerebrocortical neurons. Lipton *et al* (1999) described an inverted U model for the relationship between NMDAR activity and neurite outgrowth, with too much or too little NMDAR activity resulting in regressed growth or neuronal death, similar to the pattern that we observed for PbTx-2 enhanced neurite outgrowth. In the light of this evidence and PbTx-2 augmented NMDAR activity, we compared PbTx-2 enhanced neurite outgrowth with that of the NMDA-induced response in DIV-1 neurons. NMDA concentration-response curve for neurite outgrowth was also found to exhibit a hormetic profile ( $\text{EC}_{50}$ ~25.1 nM;  $\text{IC}_{50}$ ~25  $\mu\text{M}$ ) (Fig 1 A, B). This finding suggests that PbTx-2 enhanced neurite outgrowth

involves an NMDAR dependent mechanism and indicates its ability to cause activation of sodium channels with attendant increase in  $[Na^+]_i$  that is capable of regulating and shaping NMDAR signaling for neurite outgrowth.

Inasmuch as the actions of PbTx-2 mimic neuronal activity and activity dependent neuronal development is triggered through  $Ca^{2+}$ - dependent signaling pathways (Konur and Ghosh, 2005), we next sought to determine whether concentrations of PbTx-2 that produced effects on neurite outgrowth were also capable of elevating  $[Ca^{2+}]_i$  in DIV-1 cerebrocortical neurons. Intracellular  $Ca^{2+}$  dynamics were imaged in cells loaded with the  $Ca^{2+}$ -sensitive fluorescent dye Fura2/AM. PbTx-2 produced a rapid and concentration-dependent increase in  $[Ca^{2+}]_i$  (Fig. 2A). Non-linear regression analysis of the concentration dependence of PbTx-2-induced integrated Fura2 response yielded an  $EC_{50}$  of 360 nM (133 nM~969 nM, 95% CI) (Fig. 2B). Concentrations of PbTx-2 that elicited an enhanced effect on neurite outgrowth (10-300 nM), produced an increase in  $[Ca^{2+}]_i$ , indicating that PbTx-2-induced neurite outgrowth is primarily mediated through  $Ca^{2+}$ -dependent signaling pathways.

In order to delineate the  $Ca^{2+}$  influx pathways triggered by PbTx-2, a pharmacological evaluation of the  $[Ca^{2+}]_i$  response to 100 nM PbTx-2 was performed in neuronal cultures loaded with fluo-3/AM. Neurons were pretreated with specific antagonists-TTX (VGSCs), APV (NMDARs), nifedipine (VGCC), NBQX (AMPA receptors) and KBR-7943 ( $Na^+/Ca^{2+}$  exchanger)-to evaluate the role of these channels in PbTx-2-induced  $Ca^{2+}$  influx (Fig. 2C, D). TTX (1  $\mu$ M) completely blocked the response to PbTx-2, indicating the involvement of VGSCs in the PbTx-2 induced increase in  $[Ca^{2+}]_i$ . The competitive antagonist of NMDARs, APV (100  $\mu$ M), significantly reduced

PbTx-2-induced  $\text{Ca}^{2+}$  influx, suggesting that NMDAR channels are the major  $\text{Ca}^{2+}$  influx pathway stimulated by 100 nM PbTx-2.

### **PbTx-2 exposure regulates channel and receptor cell surface expression.**

To explore the mechanism underlying the hormetic profile of PbTx-2 induced neurite outgrowth, we investigated the influence of PbTx-2 on cell surface expression of VGSCs and NMDARs. Initially, we exposed DIV-1 cerebrocortical cultures acutely to PbTx-2 and assessed the cell surface expression of VGSCs, NMDARs and TrkB receptors using a surface biotinylation assay. TrkB receptors mediate the actions of brain derived neurotrophic factor (BDNF), and BDNF-TrkB signaling complex is proven to have a profound neurotrophic effect on developing neurons (Lindsay et al., 1994). In addition, BDNF and its receptor TrkB have been implicated in NMDAR dependent LTP and synapse formation (McAllister et al., 1999; Poo, 2001). As the NR2B subunit containing NMDAR has been shown to predominate in immature developing neurons (Monyer et al., 1994) and cell surface expression of NMDARs are primarily regulated by NR2B subunits (Roche et al., 2001; Groc et al., 2006), we evaluated the cell surface expression of the NR2B subunit following acute exposure to PbTx-2. Biotinylated proteins from crude membrane lysates were extracted, pulled-down with streptavidin-Sepharose beads, resolved by SDS-PAGE, and probed with antibodies (Fig. 3 A, B). The cell surface expressing endogenous NR2B subunits were  $18.13 \pm 5.25$  % and PbTx-2 exposure increased surface expression of NR2B subunits (PbTx-2 (30 nM),  $26.65 \pm 4.35$  %; 100 nM,  $39.88 \pm 1.2$  % 1  $\mu\text{M}$ ,  $49.21 \pm 10.02$ % compared to control,  $18.13 \pm 5.25$  %). We further assessed the regulation of TrkB receptors on neuronal cell surface following PbTx-2 exposure. Cell surface expression of TrkB is regulated by neuronal activity at

multiple levels including increased insertion into the plasma membrane (Du et al., 2000), enhanced endocytosis of BDNF-TrkB signaling complex, and activation of transcription of the TrkB gene (Nagappan and Lu, 2005). Cell surface expression of TrkB receptors ( $23.6 \pm 3.4$  %) was increased substantially within 30 min of PbTx-2 exposure (PbTx-2 (30 nM),  $62.87 \pm 7.84$  %; 100 nM,  $40.26 \pm 10.57$  %; 1  $\mu$ M,  $62.74 \pm 14.7$  % compared to control,  $23.6 \pm 3.4$  %). This is direct evidence for upregulation of NMDAR and TrkB surface expression following PbTx-2 exposure that could contribute to the neurotogenic actions of PbTx-2 on cerebrocortical neurons.

Because we were unable to find a difference in cell surface expression of VGSCs following acute exposure to PbTx-2, we performed a whole cell binding assay to evaluate surface expression of VGSCs after chronically exposing the cultures to PbTx-2 for 12 and 24 h. Cells were incubated with [ $^3$ H] BTX (batrachotoxin), a radioligand probe that labels receptor site 2 on VGSCs, for assessment of the total pool of receptors. This ligand binds preferentially to the active or open state of the channel, and the specific binding is sensitive to conformational changes induced by the binding of neurotoxins at other receptor sites on VGSCs. Hence, we used PbTx-2 (300 nM) and deltamethrin (10  $\mu$ M) to increase the specific binding of [ $^3$ H] BTX through positive allosteric interactions. Consistent with our previous report (Li et al., 2001), the specific binding of [ $^3$ H] BTX was increased ( $56 \pm 7$  % vs control) in the presence of PbTx-2 and deltamethrin. QX-314 (1 mM), a quaternary lidocaine derivative, was used to define the cell surface component of [ $^3$ H] batrachotoxin binding. To prevent recycling of the sequestered receptors to the cell membrane, binding reactions were performed at 4°C. Cerebrocortical neurons were treated with 30 and 1000 nM PbTx-2 at 3 h after plating and the cell surface fraction of

VGSCs was assessed at 12 h and 24 h time points (Fig. 3 C). In preliminary experiments, we determined that a 4 h incubation period was an optimum duration required to reach equilibrium of specific binding in primary neuronal cultures. The cell surface fraction at 12 h post treatment was  $50.7 \pm 9.4$  % and exposure to 30 nM PbTx-2 significantly increased cell surface expression of VGSC by  $\sim 50\%$  ( $101 \pm 9.4$  %, P value=0.015, Student t test) whereas 1  $\mu$ M PbTx-2 reduced cell surface expressing VGSCs ( $24.6 \pm 7.7$  %) (Fig. 3 C). The sequestered fraction of VGSC surface receptors increased ( $10.6 \pm 4.8$  %, P value < 0.001, Student t test) significantly at 24 h. The ability of PbTx-2 to increase the cell surface expression of VGSCs at low concentration (30 nM) and decrease the cell surface expression at high concentration (1  $\mu$ M) explains the biphasic concentration-response profile when measuring neurite outgrowth.

### **PbTx-2 enhances dendritic arbor development and stimulates filopodia formation.**

NMDARs play a critical role in activity-regulated neuronal structural plasticity of dendritic arbors through  $\text{Ca}^{2+}$ -dependent signaling cascades (Wong and Ghosh, 2002; Tolia et al., 2005). Inasmuch as PbTx-2 augments NMDAR function and enhances neurite outgrowth, we further investigated the effect of PbTx-2 on dendritic arbor development and spinogenesis. Low density ( $0.1 \times 10^6$  cells per ml) cerebrocortical neuron cultures were exposed to PbTx-2 3 h after plating and the effects of PbTx-2 on various aspects of structural plasticity during development were assessed. We used a Helios Gene Gun to diolistically label the neurons by intracellular delivery of tungsten particles coated with lipophilic carbocyanine (DiI) dyes. To measure dendritic arborization, we performed an automated three-dimensional sholl analysis (Sholl, 1953), where a set of concentric spheres (1  $\mu$ m apart) centered at the cell body is drawn and the number of

dendritic branch intersections at each sphere is counted, to analyze arbor complexity. At DIV-4, control neurons showed a gradual increase in branch density closer to the neuronal soma with a maximum number of  $7.5 \pm 0.6$  intersections which started to decline approximately 10  $\mu\text{m}$  away from the soma (Fig. 4 A, B). PbTx-2 (30 nM and 100 nM) exposed neurons showed a robust increase in dendritic complexity and a shift in the sholl curve to the right compared to control neurons (Fig. 4 B). Area under the curve (AUC) analysis of sholl data showed a significant increase in dendritic complexity following 30 and 100 nM PbTx-2 compared to control (ANOVA, P value=0.0008 Dunnett's post hoc test) (Fig. 4 C). Similar to the neurite outgrowth, this data also showed a hormetic profile, with 10 and 300 nM PbTx-2 showing a minimal effect on dendritic arborization. Using selective pharmacological inhibitors, we next explored the signaling mechanisms underlying enhanced dendritic arborization produced by PbTx-2. As depicted in Fig. 4 (E, F), coincubation of TTX (1 $\mu\text{M}$ ) and MK-801 (1  $\mu\text{M}$ ) with 30 nM PbTx-2 markedly blocked PbTx-2 enhanced dendritic complexity, indicating that the PbTx-2 response is mediated by activation of VGSCs and NMDARs. In contrast, nimodipine (1 $\mu\text{M}$ ), an L-type calcium channel blocker and STO-609 (2.6  $\mu\text{M}$ ), a CaMKK inhibitor did not attenuate the PbTx-2 enhancement of response on dendritic arborization. (Rajan and Cline, 1998) have shown that early synaptic currents in tectal neurons are mediated principally by NMDARs and that blocking NMDAR early in the period of dendritic arbor development prevents the initial elaboration of the arbor. In agreement with this report, our results suggest that PbTx-2 activation of sodium channels with attendant enhancement of NMDAR signaling is responsible for the initial triggering of neurite outgrowth and development of dendritic arbors.

PbTx-2 (30 nM) treated neurons on DIV-5 showed increased density of dendritic protrusions ( $32.4 \pm 3.3$  protrusions per 50  $\mu\text{m}$  dendrite vs Control ( $9.6 \pm 1.1$ ) (Fig. 5). Further analysis of these protrusions with a defined algorithm for length and head diameter (see *Methods and Materials*) in PbTx-2 treated neurons showed that most of these protrusions are filopodial-like rather than thin or stubby spine-like (length  $\leq 5.375\mu\text{m}$ ; head diameter  $\geq 0.430 \mu\text{m}$ ) (Fig. 5 A,D). PbTx-2 exposed neurons on DIV-6 revealed a shift in the nature of protrusions from filopodial-type ( $12.5 \pm 3.04$ ) to thin or stubby- spine like protrusions ( $20 \pm 3.5$ ) without a change in total protrusion density ( $32.5 \pm 4.2$  protrusions per 50  $\mu\text{m}$  dendrite) than DIV-5 (Fig. 5 B, E). Dendritic filopodia are defined as the precursors of spines and they are predominantly active in the early phase of neuronal development and further transform to functional spines and initiate the process of excitatory synapse formation (Tada and Sheng, 2006; Yoshihara et al., 2009). Evidence indicates that it is the smaller weaker spines that preferentially undergo long-term potentiation (LTP), whereas larger spines are more stable and show less plasticity (Matsuzaki et al., 2004). Such observations have led to the idea that thin spines might represent ‘plasticity spines’ and large mushrooms’ represent memory spines’ (Kasai et al., 2003). Taken together, our data suggest that PbTx-2 triggered NMDA-mediated signaling play a key role in facilitating the maturation process of dendritogenesis by stimulating dendritic arbor development and filopodia formation in cerebrocortical neurons.

**PbTx-2 enhances neuronal connectivity by accelerating the appearance of spontaneous calcium oscillations and increasing synapse formation.**

Next, we investigated the influence of PbTx-2 on spontaneous  $\text{Ca}^{2+}$  oscillations which is a manifestation of neuronal connectivity. We used fluo-3 loaded cerebrocortical

neuronal cultures to study the ontogeny of these  $\text{Ca}^{2+}$  oscillations. These spontaneous  $\text{Ca}^{2+}$  oscillations become prominent from DIV-6 both in amplitude ( $3391 \pm 173.4$ ) and frequency ( $11 \pm 1.5 / 300 \text{ sec}$ ) (Fig. 6 A, B, C). For evaluating the influence of PbTx-2 on  $\text{Ca}^{2+}$  oscillation ontogeny, we co-incubated PbTx-2 (30 nM) in alternate column-by-column with controls in the same culture plate 3 h after plating. We scanned for spontaneous  $\text{Ca}^{2+}$  oscillations from DIV-2 onwards at 12 h intervals (Fig. 7). PbTx-2 accelerated the emergence of spontaneous  $\text{Ca}^{2+}$  oscillations by 24 h (DIV-5), shifting the curves of both amplitude and frequency of spontaneous  $\text{Ca}^{2+}$  oscillation to the left (Fig. 7 B, C). As depicted in Fig. 7 A, control oscillations became prominent only by 148 h (DIV-6) exhibiting an increase in fluorescence of above 3000 while PbTx-2 exposed neurons began to exhibit similar peaks from 124 h (DIV-5) (124 h,  $4209.6 \pm 692$ ; 136 h,  $4077.8 \pm 793$ ; 148 h,  $4981.5 \pm 836$ ). Analysis of frequency (number of spikes / 300 sec) also showed a significant increase from 124 h compared to control (Control vs PbTx-2;  $4.8 \pm 2$  vs  $10.5 \pm 1.8$  (124 h),  $4.8 \pm 2.2$  vs  $13 \pm 2.5$  (136 h), and  $9 \pm 1.1$  vs  $15.8 \pm 2.7$  (148 h). Inasmuch as spontaneous calcium oscillations contribute to maturation of synapses and development of pattern generating circuits (Blankenship and Feller), these data suggest that accelerated appearance of spontaneous calcium oscillations in PbTx-2 exposed cerebrocortical neurons might be a reflection of the process of early synaptogenesis.

Inasmuch as synchronized  $\text{Ca}^{2+}$  oscillations reflect formation of functional synapses and neuronal networks and PbTx-2 accelerated the appearance of spontaneous calcium oscillations, we assessed the effect of PbTx-2 on formation of synapses in cerebrocortical neuron cultures. We performed double immunofluorescence using antibodies against

synaptophysin (pre-synaptic marker) and PSD-95 (post-synaptic marker) to quantify synapse density as indicated by colocalized fluorescent puncta. Neurons were exposed to PbTx-2 at 3 h post plating and double immunostained on DIV-6. Confocal Z-stack images were deconvolved, background subtracted and quantified for colocalized puncta using Slidebook software, which analyzes entire two channel confocal stacks by measuring the intensity of each label, voxel by voxel. Pearson's correlation coefficient  $\geq 0.7$  was set to determine colocalized puncta. Concentration-response analysis of PbTx-2 effects on synaptic density showed that PbTx-2 (30 nM) and (100 nM) produced a significant (ANOVA P value  $> 0.0001$ , Dunnett's post hoc test) increase in synaptic density (number of puncta per 20  $\mu\text{m}$ ) compared to control cultures, whereas 300 nM and 1000 nM PbTx-2 showed a progressive decline in synaptic density (Fig. 8). (Control,  $0.95 \pm 0.2$ ; PbTx-2 (30 nM),  $3.99 \pm 0.24$ ; PbTx-2 (100 nM),  $3.8 \pm 0.34$ ; PbTx-2 (300 nM),  $2.53 \pm 0.24$ ; PbTx-2 (1000 nM),  $0.79 \pm 0.27$ ) (Fig. 8 B). The reduced response with higher concentrations of PbTx-2 on synaptic density is consistent with the observed hormetic profile for neurite outgrowth and dendritic arbor development.

### **Sodium channel activation mimics activity-dependent signaling mechanisms for neuronal development.**

Studies to date have shown that activity-dependent neuronal development is primarily regulated by calcium-dependent signaling events (Konur and Ghosh, 2005). NMDAR-dependent CaMKK/CaMKI signaling cascade has moreover been shown to regulate neurite/axonal outgrowth (Wayman et al., 2006), activity-dependent synaptogenesis (Saneyoshi et al., 2008), and  $\text{Ca}^{2+}$ -dependent extracellular regulated kinase (ERK) activation and dendritic outgrowth (Wayman et al., 2006). NMDAR mediated  $\text{Ca}^{2+}$ -

dependent signaling events impart both local and global effects on neuronal structural plasticity. We have shown that PbTx-2 induced intracellular  $[Na^+]$  augments NMDAR function and elevates intracellular calcium levels. Inasmuch as  $Ca^{2+}$ / Calmodulin-kinases (CaMKs), a family of serine/threonine protein kinases, mediate many of these activity-dependent intracellular responses, we investigated phosphorylation and activation of members of the CaMK family, such as CaMKII, CaMKK, CaMKI and CaMKIV following PbTx-2 exposure. We performed immunoblot analysis in neuronal cultures within 24 h post plating. Cultures were treated with drugs for specified times in Locke's incubation buffer after removing the media. This approach enabled us to evaluate the acute response produced by PbTx-2 exposure for triggering downstream signaling cascades. Preliminary pharmacological evaluation has shown that PbTx-2 enhanced neurite outgrowth engages the CaMKK signaling pathway. As a first step we screened for activation of CaMKK substrates, CaMKI, CaMKIV and protein kinase B (PKB/Akt). PbTx-2 (100 nM) exposure showed phosphorylation and activation of CaMKI at Thr177, but not CaMKIV (Thr196) or Akt (Thr308 and Ser473) (Fig. 9 C). Phosphorylation of CaMKI at Thr177 occurred within 5 min and was sustained up to 120 min following PbTx-2 exposure. The NMDAR-dependent cross-talk between CaMKK/CaMKI and MEK/ERK appears to be an important component of early LTP (Schmitt et al., 2005) and activity-dependent dendritic arborization (Wayman et al., 2006). Moreover, CaMK and ERK pathways have been implicated in mediating activity-dependent transcriptional control of dendritic complexity (Wu et al., 2001). We therefore assessed phosphorylation of ERK with 100 nM PbTx-2 treatment. Time course analysis of ERK activation exhibited a bimodal pattern with early peak phosphorylation detected within 5 min of

PbTx-2 exposure followed by a progressive decline reaching basal levels at 60 min before going up again (Fig. 9 C, D). Although previous reports (Chandler et al., 2001; Dravid et al., 2004) have shown this bidirectional pattern of NMDAR-mediated ERK1/2 activation in primary cortical neurons, the exact mechanism of the bimodal activation of ERK1/2 in developing cerebrocortical neurons is unknown.

We also evaluated PbTx-2 induced CaMKII activation. Activation of CaMKII by  $\text{Ca}^{2+}$ /CaM allows intramolecular autophosphorylation of several sites, including Thr286, Thr305 and Thr306. Autophosphorylation of Thr286 has been implicated in autonomous and prolonged activation of CaMKII even with transient elevations of intracellular  $\text{Ca}^{2+}$  levels. Immunoblotting analysis showed that PbTx-2 (100 nM) exposure produced marked phosphorylation of CaMKII at Thr286 and exhibited sustained activation for the entire 2 h period of exposure (Fig. 9 C, D).

Inasmuch as CaMKs, including CaMKI, CaMKII and CaMKIV as well as Ras/MAPK signaling events play major roles in activity-dependent nuclear phosphorylation of CREB at Ser133, we examined the effect of PbTx-2 on CREB phosphorylation at Ser133. PbTx-2 (100 nM) exposure was found to increase CREB (Ser133) phosphorylation (Fig. 9 C, D).

We also assessed the phosphorylation and activation of CaMKs with 30 and 300 nM of PbTx-2 in a similar fashion. Increased phosphorylation of CaMKII at Thr286 occurred with 30 nM PbTx-2 exposure (Fig. 9 A, B), but the involvement of other CaMKs was not detected. 30 nM PbTx-2 also produced transient phosphorylation of CREB at Ser133 with a sustained peak effect lasting for only about 30 min (Fig. 9 A, B). Following 300

nM PbTx-2 exposure, besides activation of CaMKII (Thr286) and CaMKI (Thr177), we also detected phosphorylation and activation of CaMKIV (Thr196) and Akt (Ser473) (Fig. 9 E, F). In this case, ERK showed a sustained activation rather than the bimodal profile observed with 100 nM PbTx-2 (Fig. 9 E, F).

Altogether these data demonstrate that the strength of the signal induced by different concentrations of PbTx-2 may trigger various signaling cascades with differing effects on neuronal development. Therefore we extended and assessed complete time course profile of PbTx-2 induced CREB (Ser133) phosphorylation with 30, 100 and 300 nMPbTx-2. As depicted in Fig.10 A, 30 nM PbTx-2 exposure induced an increase in CREB (Ser133) phosphorylation which started to decline at 60 min and returned to basal by about 90 min whereas 100 nM PbTx-2 treatment showed sustained phosphorylation for about 2 h. Higher concentration of PbTx-2 (300 nM) exhibited a further prolonged activation (6-18 h) of CREB. This data strengthens our argument of strength of the stimuli determining the signaling pathway and pattern of activation.

We next examined PbTx-2 induced CREB phosphorylation using various pharmacological inhibitors. As shown in Fig.10 B, TTX (1  $\mu$ M) completely abrogated PbTx-2 (30 nM)-induced CREB phosphorylation indicating primary involvement of VGSCs (Fig.10 B). APV (100  $\mu$ M), a competitive inhibitor of NMDARs and STO-609 (2.6  $\mu$ M), a CaMKK inhibitor significantly attenuated (P value < 0.05) PbTx-2 induced CREB phosphorylation. The L-type VGCC blocker nimodipine (1  $\mu$ M) had no effect. In a similar fashion, pharmacological analysis of PbTx-2 (100 nM)-induced CREB phosphorylation also showed primary involvement of VGSCs. Significant attenuation by APV and STO-609 suggest the contribution of NMDARs and CaMKK in PbTx-2

induced CREB phosphorylation. NBQX (5  $\mu$ M), an AMPA receptor blocker, nimodipine (1  $\mu$ M) and  $\omega$ -conotoxin (1  $\mu$ M), an N-type  $\text{Ca}^{2+}$  channel blocker did not suppress PbTx-2 induced CREB phosphorylation. N-type calcium channels have been associated primarily with neurotransmitter release at synaptic sites (Dunlap et al., 1995). These data indicate that NMDARs make a greater contribution than L-type VGCC to PbTx-2-induced CREB phosphorylation and they also engage CaMKK mediated signaling with less pronounced involvement of neurotransmitter release from presynaptic sites. The ability of NMDARs to drive changes in CREB dependent gene expression is a developmentally regulated event (West et al., 2001). It has also been reported that in young neurons, activation of calcium influx through NMDARs leads to robust CREB-dependent transcription whereas in mature neurons, calcium influx through L-type VGCC leads to sustained CREB (Ser133) phosphorylation (Sala et al., 2000).

BDNF is an activity-regulated gene and its expression is regulated by CREB-dependent transcription (Shieh et al., 1998; Tao et al., 1998). BDNF has been shown to mediate dendritic elaboration (McAllister et al., 1995; Dijkhuizen and Ghosh, 2005). The activity-induced transcriptional initiation of new BDNF mRNA occurs rapidly and without the need for new protein synthesis (Lauterborn et al., 1996) through the posttranslational modification of preexisting transcription factors (West et al., 2001). Therefore, we assessed PbTx-2-induced BDNF transcription with conventional RT-PCR in DIV-1 cerebrocortical neurons. BDNF mRNA expression level increased in a time- and concentration-dependent manner with PbTx-2 exposure (Fig. 11A). Moreover, we confirmed the PbTx-2 increase in BDNF mRNA levels by performing real-time PCR. PbTx-2 (30 nM) displayed a temporal pattern of fold change in gene expression (Fig. 11

B) with a 4 fold increase at 1 h exposure and 6 fold increase at 2 h. BDNF, a small secreted protein, acts through binding to two different receptors: TrkB and p75. Binding to the high affinity tyrosine kinase receptor TrkB, mediates most of the neuronal effects of BDNF (McAllister, 2002). As shown above, acute PbTx-2 exposure increased cell surface expression of TrkB receptors (Fig. 3 A, B), indicating that PbTx-2 sensitizes cerebrocortical neurons for the neurotrophic effect of the TrkB-BDNF signaling complex. These findings suggest that effects of this sodium channel activator (PbTx-2) on neuronal development involve NMDAR-mediated CaMK signaling with downstream activation of CREB-dependent transcription of BDNF.

#### **Involvement of Rho family GTPases:**

Besides the activity-dependent nuclear signaling, it has been shown that local signaling events control the dynamics of the cytoskeleton and thereby regulate the growth and development of dendrites, axons and spines (Saneyoshi et al.; Wong and Ghosh, 2002). Rho family GTPases play a very important role in the regulation of actin dynamics. The best characterized members of Rho family GTPases, Rac1 and Cdc42 have been shown to facilitate dendritic and axonal growth through several signal transduction pathways. To explore their role in neuronal growth cone formation, we performed a concentration-response analysis of growth cone dynamics by using a Rac1 inhibitor, NSC23799. After exposing NSC23799 to neurons at 3 h post plating, we fixed neurons at 16 h and then stained for F-actin with Rhodamine-conjugated phalloidin to visualize growth cone morphology (Fig.12 A). At this time point, more than 70 % of neurons (control, n=174) displayed distinct growth cones  $\geq 3$  per neuron. The collapsed growth cones of each neuron, which were defined as those with no lamellipodia and not

more than two filopodia (Kapfhammer et. al., 2007), were counted and expressed as a percentage of the total growth cones of the neuron. NSC23799 (5  $\mu$ M) significantly increased neuronal growth cone collapse, indicating the requirement of Rac1 in growth cone dynamics (Fig. 12 B). We therefore confirmed the activation of Rac1 in DIV-1 neurons following PbTx-2 exposure by performing Rac-GTP pull down assays. As shown in Fig. 12 C, PbTx-2 (100 nM) exposure for 30 min increased Rac-GTP levels by 4 fold compared to control. Using pull down assays, we also evaluated the effect of PbTx-2 on Cdc42. Fold changes of 2-2.5 were detected in Cdc-42 GTP levels after 30 min PbTx-2 exposure (Fig. 12 D). These data suggest that PbTx-2 induced activation of both Rac and Cdc42 signaling together with nuclear signaling may engage in the regulation of dendritic development. Altogether these results suggest that enhancing NMDAR activity through elevation of intracellular sodium promotes neuronal structural plasticity by engaging manifold signaling mechanisms acting in concert.

## **Discussion:**

In this study, we report that sodium channel activation induced NMDAR-mediated signaling positively influences different aspects of neuronal connectivity such as dendritic arborization, spinogenesis and synaptogenesis. We demonstrate that this is achieved by engaging both the transcriptional program that involves CREB-mediated gene expression and local signaling that involves Rac/Cdc-42 regulation of actin dynamics, primarily through a CaM kinase-dependent signaling pathway. Surprisingly, PbTx-2-induced total neurite outgrowth, dendritic arbor development and synapse formation exhibited a biphasic concentration response profile with 30 and 100 nM of PbTx-2 having the most robust effect. PbTx-2 exposure accelerated the appearance of spontaneous calcium oscillations in cerebrocortical neurons reflecting an early formation of functional synapses. PbTx-2 exposure was also found to regulate receptor cell surface expression of VGSCs, NR2B and TrkB. We have shown previously that 30 nM PbTx-2 elevates  $[Na^+]_i$  above the threshold for upregulating NMDAR function and augments NMDAR function by increasing both mean open time and open probability through a Src-dependent mechanism without affecting resting membrane potential. Altogether these data indicate that PbTx-2, an activator of voltage-gated sodium channels, mimics activity-dependent control of neuronal development by elevating intracellular sodium levels and augmenting NMDAR function for downstream signaling events. This provides compelling evidence to support the hypothesis that elevation of  $[Na^+]_i$  following neuronal activity plays a critical role in modulating activity-dependent signaling for neuronal plasticity.

Recent studies have indicated that changes in  $[Na^+]_i$  produced in the soma and dendrites as a result of neuronal activity may act as a signaling molecule and play a role in activity-dependent synaptic plasticity. The influence of  $[Na^+]_i$  dynamics on NMDA receptor function has been demonstrated in hippocampal neurons where elevation of  $[Na^+]_i$  increased the open probability of NMDA receptors (Yu and Salter, 1998; Yu, 2006). An increment of  $[Na^+]_i$  of 10 mM was sufficient to produce significant increases in NMDAR single-channel activity. This  $Na^+$ -dependent regulation of NMDAR function was, moreover, shown to be controlled by Src-induced phosphorylation of the receptor (Yu and Salter, 1998; Yu, 2006). Additionally it has been reported that increments of  $[Na^+]_i$  of  $> 5$  mM may represent a critical threshold required to regulate NMDAR-mediated  $Ca^{2+}$  influx in primary cultures of hippocampal neurons (Xin et al., 2005). These results were confirmed and extended in our study using the sodium channel activator, PbTx-2 as a probe to elevate intracellular  $Na^+$  to study its effects on NMDAR-mediated structural plasticity during development. In our previous report (George et al., 2009), we have shown that PbTx-2 produced concentration-dependent increments in  $[Na^+]_i$  ( $EC_{50}$  43.3 nM with 23.5-79.9 nM, 95 % CI) and that 30 nM of PbTx-2 produced a maximum  $[Na^+]_i$  of  $16.9 \pm 1.5$  mM, representing an increment of  $8.8 \pm 1.8$  mM over basal. This concentration of PbTx-2 was also found to augment NMDA-induced  $Ca^{2+}$  influx. Moreover, single channel recordings from cell-attached patches showed that PbTx-2 treatment increased both the mean open time and open probability of NMDA receptors. These effects of PbTx-2 on NMDA receptor function were dependent on extracellular  $Na^+$  and activation of Src kinases.

PbTx-2 did not alter the resting membrane potential at a concentration (30 nM) that promotes dendritogenesis. Consistent with these results, Antillatoxin, a potent activator of VGSCs has also been shown to enhance NMDAR-dependent neurite outgrowth in cerebrocortical neurons (Jabba et al., 2010).

The presence of sodium channels in neuronal spines has been recently demonstrated (Araya et al., 2007) and these spine sodium channels in neocortical pyramidal neurons have been shown to boost synaptic potentials and facilitate action potential backpropagation. Recent reports have shown that synaptic stimulation causes  $[Na^+]_i$  increments of up to 10 mM in dendrites and of up to 35-40 mM in dendritic spines (Rose et al., 1999; Rose and Konnerth, 2001). Lorincz and Nusser (2010) have determined different dendritic sodium channel subunit compositions in neocortical and hippocampal pyramidal cells and have shown that characteristic subcellular distributions of  $Na_v1.6$  are the key substrates enabling dendritic excitability. The significance of the increase in  $[Na^+]_i$  in dendritic spines following synaptic stimulations is relatively understudied. Our study indicates that beginning from neurite outgrowth, this signaling molecule can regulate even more complex aspects of neuronal connectivity via engaging NMDAR dependent signaling mechanisms, suggesting a crucial role for  $[Na^+]_i$  in mediating structural plasticity.

NMDARs are essential mediators of many forms of synaptic plasticity and also mediate several aspects of development (Bliss and Collingridge, 1993; Aamodt and Constantine-Paton, 1999). However, when excessively activated, NMDARs can cause cell death and result in many neuropathological scenarios (Arundine and Tymianski,

2004). Consistent with this concept, Lipton and Nakanishi (1999) described an inverted U model for the relationship between NMDA receptor activity and neurite outgrowth. In agreement with this study, concentration-response analysis of neurite outgrowth data for NMDA and PbTx-2 exhibited biphasic response profiles in our study. We also observed a similar pattern of response for PbTx-2 induced dendritic arbor development and synaptic density. In our study, we can tentatively regress the biphasic concentration response profile of PbTx-2 on neuronal plasticity to the differences in the expression pattern of VGSCs following chronic exposure to PbTx-2. Although, acute treatment with PbTx-2 resulted in increased cell surface expression of the NR2B subunit of NMDARs and TrkB receptors with higher concentrations of PbTx-2, the pattern of expression following chronic exposure has not been investigated. Sequestration or internalization of VGSCs induced by higher concentration of PbTx-2 is in agreement with previous reports that showed higher concentrations of PbTx-2 promoting slow inactivation (Mitrovic et al., 2000; Ong et al., 2000) or increasing internalization (Dargent et al., 1994) of VGSCs with attendant reduction in sodium influx. It is also reported that in the developing central neurons (hippocampus and cortex), activity triggered by sodium channel agonists causes rapid internalization of sodium channel proteins and down regulation of  $\alpha$ -subunit mRNAs. This phenomenon occurs only at early stages of development and is specific for sodium channels. The loss of sodium channel sensitivity to activity-induced internalization with development parallels the appearance of the  $\beta$ 1 subunit during development, implying a protective or stabilizing role for the  $\beta$ 1 subunit (Alcaraz et al., 1997).

In hippocampus and cortex, NMDARs are typically NR1/NR2B heteromers early in development, but the subunit composition is developmentally regulated with NR2A expression increasing over time (Monyer et al., 1994; Sans et al., 2000). Thus, NMDARs formed exclusively by NR1 and NR2B dominate during late embryogenesis and early postnatal development, a time of rapid synaptogenesis in cortex and a period of low synaptic AMPAR/NMDAR ratio (Hall et al., 2007). It has been shown that NR2B-containing NMDAR have higher surface mobility than NR2A-containing receptors (Groc et al., 2006). NR2B-containing NMDARs are more involved in the regulation of endocytosis than NR2A-containing receptors and preferentially traffic through recycling endosomes (Roche et al., 2001). NR2B also contains three tyrosine phosphorylation sites (Y1252, Y1336 and Y1472) (Nakazawa et al., 2001). Y1472 is within a tyrosine-based internalization motif and phosphorylation of NR2B Y1472 facilitates inhibition of NR2B-mediated endocytosis (Roche et al., 2001), whereas dephosphorylation promotes increased endocytosis of NMDARs (Snyder et al., 2005). Considering these important roles of NR2B subunits in receptor trafficking and endocytosis, the increased surface expression of the NR2B subunit of NMDAR by PbTx-2 exposure in immature cerebrocortical neurons could possibly be contributing to increased sensitivity of NMDARs to activate downstream signaling events. We have previously demonstrated that PbTx-2 is capable of sensitizing these neurons to NMDA-induced  $Ca^{2+}$  influx. The NMDA concentration-response curves for  $Ca^{2+}$  influx were significantly leftward shifted by 30 nM PbTx-2 in DIV-2,-4,-6 and -9 cerebrocortical cultures (George et al., 2009) and this supports our argument that PbTx-2 sensitizes neocortical neurons to NMDAR mediated signaling events.

Surface expression of TrkB, the receptor for BDNF, is regulated by neuronal activity at multiple levels including increased insertion into the plasma membrane (Du et al., 2000), enhanced endocytosis of the BDNF-TrkB signaling complex, and activation of transcription of the TrkB gene (Nagappan and Lu, 2005). The predominant Trk receptors expressed in mammalian CNS are TrkB and TrkC, whereas the expression of TrkA is limited in the CNS and is not significantly detected in the cortex (Valenzuela et al., 1993; Knusel et al., 1994). There are three major TrkB isoforms, the full-length isoform and two truncated isoforms, T1 and T2, which both lack cytoplasmic tyrosine-kinase domains (Barbacid, 1994). Many neuronal populations, including hippocampal and cortical neurons, express both full-length and truncated receptors (Escandon et al., 1994). Relative levels of expression of these isoforms are dramatically regulated during development. The full-length TrkB predominates in early CNS development, and the truncated forms exceed full length TrkB at later stages of development (Escandon et al., 1994; Fryer et al., 1996). Mechanistically, truncated receptors might function as negative regulators of full-length TrkB as is demonstrated *in vitro* (Escandon et al., 1994; Fryer et al., 1996; Fryer et al., 1997). These TrkB isoforms have differential effects on dendritic arborization, that is, full-length TrkB increased proximal dendritic branching whereas truncated TrkB promoted net elongation of distal dendrites. PbTx-2 exposure at low concentration increased the cell surface expression of TrkB receptors, causing the system to be more responsive to neurotrophic effects of BDNF and thereby positively influencing different aspects of neuronal structural plasticity.

In addition, the intracellular calcium response following PbTx-2 exposure at increasing concentrations also helps to explain the biphasic nature of the different aspects

of neuronal structural plasticity. This inverted U concentration-response relationship has been documented previously in relation to intracellular  $\text{Ca}^{2+}$  regulation. An optimal window for  $[\text{Ca}^{2+}]_i$  is required for activity-dependent neurite extension and branching, with lower levels stabilizing growth cones and higher levels stalling them, in both cases preventing extension (Gomez and Spitzer, 2000; Hui et al., 2007). Our  $\text{Ca}^{2+}$  imaging studies exhibited a concentration-dependent increment in intracellular  $\text{Ca}^{2+}$  levels by exposure to PbTx-2. Thirty nM and 100 nM PbTx-2 produced a substantial increase in  $[\text{Ca}^{2+}]_i$  suggesting that the PbTx-2 induced increase in  $[\text{Ca}^{2+}]_i$  may be optimal to impart a trophic influence on dendritic development. Although the higher (1000 nM) concentration of PbTx-2 produced robust elevation of  $[\text{Ca}^{2+}]_i$ , it did not enhance dendritic development as compared with 30 and 100 nM PbTx-2. In our study, we found that increased  $[\text{Ca}^{2+}]_i$  is primarily mediated via NMDAR channels. (Takasu et al., 2002) have demonstrated NR1, NR2 subunits of NMDARs and glutamate stimulated NMDAR-mediated  $\text{Ca}^{2+}$  influx in E18+1 DIV rat cerebrocortical cultures indicating the presence of a functional glutamatergic system in DIV-1 neurons.

Several studies have shown that  $\text{Ca}^{2+}$  influx through VGCCs and NMDARs leads to the activation of distinct signaling pathways. It has been reported that in young cortical neurons, activation of calcium influx through NMDARs, but not L-type VGCC, leads to robust CREB-dependent transcription whereas in mature neurons, L-type VGCC drives sustained CREB (Ser133) phosphorylation (Sala et al., 2000). The ability of NMDARs to drive changes in CREB dependent gene expression is also explained as a developmentally regulated event (West et al., 2002). Studies in mature neurons have shown that  $\text{Ca}^{2+}$  influx through the NMDAR channel is tightly regulated by activation of

protein phosphatase1 (Westphal et al., 1999) associated with NMDAR that dephosphorylates CREB at Ser133, but this type of regulation has not been reported for L-type VGCC. These reports highlight the importance of NMDAR channels as the major mediators of developmental structural plasticity. Consistent with this observation, PbTx-2 produced a concentration-dependent activation of NMDAR-mediated CREB (Ser133) phosphorylation. Moreover, our data provide clear experimental evidence and support the concept that different stimulus paradigms induce different CREB activation profiles and hence distinct signaling pathways. Higher concentration of PbTx-2 (300 nM) exhibited a prolonged activation of CREB whereas lower concentration of PbTx-2 (30 nM) produced only a transient activation.

Activation of the transcription factor CREB is shown to regulate BDNF gene transcription (Shieh et al., 1998; Tao et al., 1998). BDNF regulates axonal and dendritic growth, efficacy of synaptic transmission and synaptic plasticity (Kang and Schuman, 1996). BDNF gene expression was found to be upregulated by exposure to PbTx-2, indicating the involvement of a NMDAR-activated CREB dependent signaling mechanism involving BDNF. BDNF plays a major role in activity dependent neuronal development as BDNF can be secreted from presynaptic terminals in an activity-dependent manner and the level of BDNF mRNA is positively regulated by neuronal activity (Zafra et al., 1990).

During the critical period of development, it may be presumed that the signaling mechanisms operate in an orchestrated or concerted manner. Phosphorylation and activation of CaMKII (Thr286) was detected with 30 nM PbTx-2, while 100 nM PbTx-2 exposure additionally produced activation of CaMKI (Thr177) and ERK. Moreover,

activation of CaMKIV (Thr196) and Akt (Ser473) were also found after exposure to 300 nM PbTx-2. This differential activation of intracellular signaling mechanisms with varying stimuli lends insight into how neurons decode different patterns of neuronal activity into distinct cellular responses. Consistent with our data, 30 and 100 nM PbTx-2 produced striking effects on neurite outgrowth and dendritic arborization; however, they evoked only a transient increase in FMP blue fluorescence in our membrane potential assay that was roughly equivalent to the fluorescence change produced by an extracellular  $K^+$  concentration of 7.6 and 8.5 mM. Previous studies have shown that differing strengths of depolarizing stimuli produced by 16 versus 50 mM KCl preferentially engage NMDAR compared to L-type  $Ca^{2+}$  channel-dependent signaling for dendritic growth, with L-type  $Ca^{2+}$  channels beginning to be recruited from 50 mM KCl. Wayman et al (2006) have shown that activity-dependent dendritic arborization in DIV-9 hippocampal neurons involves a  $Ca^{2+}$ -mediated signaling pathway downstream of the NMDA receptor through activation of a CaMKK and CaMKI. Redmond et al (2002) showed evidence for the involvement of L-type  $Ca^{2+}$  channels in dendritic growth and arborization of DIV-4 cortical neurons exposed to 50 mM KCl. Despite the channel specificity induced by different depolarization stimuli, Brosenitsch and Katz (2001) have demonstrated that phasic and chronic depolarizing stimuli act through distinct mechanisms to induce neuronal gene expression. Both presynaptic and postsynaptic signaling mechanisms may underlie in depolarization stimuli induced by KCl. It is mostly that 30 nM and 100 nM PbTx-2 -induced signaling is engaging a post synaptic mechanism. In support of this hypothesis,  $\omega$ -conotoxin, an N-type  $Ca^{2+}$  channel blocker, did not significantly attenuate PbTx-2-induced CREB activation, indicating less

pronounced involvement of presynaptic mechanisms. Altogether our data provide important insights into the regulation of NMDAR activity by  $[\text{Na}^+]_i$  and its functional consequences during development.

The ERK activation profile showed a bimodal pattern consistent with previous reports (Chandler et al., 2001; Dravid et al., 2004). Although the exact mechanism for this bimodal response is not yet known, this implies the presence of multiple regulatory networks during neuronal development. Previous reports have shown that MAPK is activated in a stimulus-dependent fashion and helps support neuronal excitability, synapse potentiation, nuclear signaling and memory formation (Finkbeiner et al., 1997; Martin et al., 1997; Winder et al., 1999). CaMK and ERK pathways have been implicated in mediating activity-dependent transcriptional control of dendritic complexity. The CaMK pathway contributes to a fast early phase of CREB phosphorylation, whereas the ERK pathway mediates a later prolonged phosphorylation state (Wu et al., 2001). The difference in ERK activation dynamics results in different cellular outcomes such as differentiation or proliferation. In hippocampal neurons, stabilization of ERK activity for an hour has been implicated in mediating local effects of calcium signaling on filopodia formation (Wu et al., 2001). In cortical neurons, Ha and Redmond (2008) have shown that sustained ERK activation for more than an hour displayed greater dendritic complexity than ERK activity that was not sustained. It is possible that both transient activation of ERK that lasted less than an hour and sustained activation of ERK that lasted for several hours might be recruiting distinct intracellular signaling mechanisms that can impart local as well as global effects on actin dynamics. One of the upstream activators of the MAPK pathway, Ras, is activated by increases in intracellular  $\text{Ca}^{2+}$

(Ghosh and Greenberg, 1995). Once activated, Ras appears to associate with and activate the serine/threonine kinase, Raf and trigger sequential downstream activation of MEK-1, MAP kinases and ribosomal S6 kinases, which in turn contributes to local and nuclear effects. In cultured hippocampal neurons or acute slices, NMDA-stimulated activation of ERK is predominantly mediated through CaMKK/CaMKI (Schmitt et al., 2005). Furthermore, this pathway appears to be important for dendritic arborization where activity-dependent NMDAR activation of the  $\gamma$  isoform of CaMKI results in MEK/ERK-mediated CREB-regulated transcription of Wnt-2 (Wayman et al., 2006) and microRNA132 (Wayman et al., 2008b).

The activated signaling mechanisms described herein with 30 and 100 nM PbTx-2 demonstrate that CaMKII and CaMKI have primary roles in NMDAR-dependent developmental plasticity. The predominant activation of CaMKII but not CaMKI in DIV-1 cerebrocortical neurons with 30 nM PbTx-2 indicates that CaMKII plays a key role in early induction of NMDAR-mediated trophic signaling during dendritic development. It is widely accepted that CaMKII has a key role in synaptic plasticity, learning and memory. NMDAR-dependent LTP in hippocampal CA1 region triggers  $\text{Ca}^{2+}$ /CaM-dependent rapid activation of CaMKII. The elevated spine  $\text{Ca}^{2+}$ /CaM also activates CaMKK to phosphorylate and activate CaMKI. The characteristic autonomous activity of CaMKII and CaMKK-dependent activation of CaMKI contribute to rapid induction of synaptic potentiation (Wayman et al., 2008a). CaMKII is unique in its structural and biochemical properties and has been widely implicated in synaptic plasticity and learning and memory (Wayman et al., 2008a). The intramolecular autophosphorylation of CaMKII at Thr286 and its  $\text{Ca}^{2+}$ -independent autonomous activity can result in prolonged

CaMKII activity even with transient elevations of intracellular  $\text{Ca}^{2+}$  levels. Moreover, interaction of CaMKII with NMDAR-NR2B subunits and PSD-95 has been documented. In hippocampal neurons, a brief stimulus promotes a transient and reversible interaction of CaMKII with NR2B, whereas stronger stimulus results in persistent translocation of CaMKII (Bayer et al., 2006). The association of CaMKII with PSD has been shown to correlate with synaptic strength of individual spines (Asrican et al., 2007). The role of CaMKII $\alpha$  and  $\beta$  isoforms have been examined in dendritic growth and elaboration and the studies indicate that CaMKII $\alpha$  plays a role in stabilization of dendritic arbors in mature neurons whereas in young neurons, active CaMKII $\alpha$  leads to attenuation of dendritic arbors (Redmond, 2008). CaMKII $\beta$  specifically binds and bundles F-actin to promote dendritic branching and increase filopodial motility in DIV-3 hippocampal neurons (Fink et al., 2003). The ability of CaMKII $\beta$  to promote an increase in dendrites decreased with age and by 11 DIV it was found to have an inhibitory effect. CaMKII-dependent activation of kalirin 7, a GTP exchange factor for Rac1, enhances the development of complex dendrites and the formation and maturation of spines (Xie et al., 2007). Considering all these findings, our data suggest that CaMKII may play an early dominant role in triggering signaling cascades for neurite outgrowth, dendritic arborization and synapse strengthening.

The CaMK cascade also includes CaMKK and downstream components CaMKI and CaMKIV. The CaMKK/CaMKI signaling pathway has been shown to regulate morphology and motility of axonal growth cones and basal axonal outgrowth (Wayman et al., 2004). Because CaMKK/CaMKI exerts  $\text{Ca}^{2+}$ -dependent cross-talk with the MAP-kinase ERK (Schmitt et al., 2004), this signaling pathway accounts for ERK-mediated

LTP (Schmitt et al., 2005) as well as for activity-dependent dendritic arborization (Wayman et al., 2006). These multiple functions, however, appear to be mediated by different CaMKI isoforms. Regulation of ERK activation and CREB-dependent dendritic arborization is mediated by the  $\gamma$  isoform of CaMKI. Saneyoshi et al., (2008), showed the interaction of  $\beta$ PIX, a Rac1 GEF, forms a signaling complex containing CaMKK/CaMKI/ $\beta$ PIX/Rac that regulates the morphogenesis of spines in an activity-dependent manner. Upon CaMKK activation, CaMKIV regulates nuclear function by modulating the phosphorylation of CREB and CBP (Soderling, 2000). CaMKIV can form a complex with protein phosphatase 2A, which may account for its relatively transient activation in cells by CaMKK (Anderson et al., 2004). Studies show that CaMKIV expression is upregulated during the peak period of dendritic development which induces significant elaboration of dendrites when it is over expressed in cortical neurons (Redmond et al., 2002).

Recent studies indicate that Akt (also known as Protein kinase B/PKB), a serine threonine kinase, plays an important role in several aspects of neurite outgrowth. In our study, a stronger stimulus (300 nM PbTx-2 exposure) was required to demonstrate Akt phosphorylation (Ser-473) Akt-mediated neurite outgrowth has been shown to involve glycogen synthase kinase (GSK)  $3\beta$ , peripherin, mammalian target of rapamycin (mTOR),  $\delta$ -catenin and Hsp27. As in neurite outgrowth, the PI3K-Akt-GSK pathway has been shown to regulate the early stages of dendrite formation in hippocampal neurons stimulated with hepatocyte growth factor (Lim and Walikonis, 2008). The co-ordinated PI3K-Akt and Ras-MAPK signaling pathways have been shown to increase dendritic

complexity in dissociated postnatal hippocampal CA1/CA3 neuronal cultures (Kumar et al., 2005).

A growing body of evidence indicates the prominent role of NMDAR in structural plasticity because of its ability to engage diverse signaling pathways that converge at the level of actin dynamics to enhance dendritogenesis, spinogenesis and synaptogenesis. Consistent with these reports, we observed activation of Rac and Cdc42 following exposure to 30 and 100 nM PbTx-2. Recent studies reveal that NMDAR-mediated CaMK and Rac GEF signaling converge and control dendritic growth and spine morphogenesis. The activation of CaMKII following NMDAR activation is important for activity-dependent spine plasticity (Tolias et al., 2005) by involving a specific GEF, Tiam-1 in young neurons. The NMDAR-mediated CaMKK-CaMKI cascade has also been shown to regulate hippocampal spine plasticity through activation of the Rac GEF  $\beta$ PIX (Pak-interacting exchange factor). It has moreover been shown that NMDAR-dependent activation of CaMKI $\gamma$  and its Rac-mediated downstream effects require the activity of Rac GEF STEF (Sif-and Tiam1-like exchange factor) in dendritogenesis of young neurons. The presence of multiple signaling networks and induction of distinct signaling events with varying stimuli indicate that growth and development of neurons involves complex regulatory signaling networks with each signaling pathway compensating for the loss of other signaling, as required during this critical period.

## **References:**

- Aamodt SM, Constantine-Paton M (1999) The role of neural activity in synaptic development and its implications for adult brain function. *Adv Neurol* 79:133-144.
- Aid T, Kazantseva A, Piirsoo M, Palm K, Timmusk T (2007) Mouse and rat BDNF gene structure and expression revisited. *J Neurosci Res* 85:525-535.
- Alcaraz G, Sampo B, Tricaud N, Giraud P, Martin-Eauclaire MF, Couraud F, Dargent B (1997) Down-regulation of voltage-dependent sodium channels coincides with a low expression of alphabeta1 subunit complexes. *Brain Res Mol Brain Res* 51:143-153.
- Anderson KA, Noeldner PK, Reece K, Wadzinski BE, Means AR (2004) Regulation and function of the calcium/calmodulin-dependent protein kinase IV/protein serine/threonine phosphatase 2A signaling complex. *J Biol Chem* 279:31708-31716.
- Araya R, Nikolenko V, Eisenthal KB, Yuste R (2007) Sodium channels amplify spine potentials. *Proc Natl Acad Sci U S A* 104:12347-12352.
- Arundine M, Tymianski M (2004) Molecular mechanisms of glutamate-dependent neurodegeneration in ischemia and traumatic brain injury. *Cell Mol Life Sci* 61:657-668.
- Asrican B, Lisman J, Otmakhov N (2007) Synaptic strength of individual spines correlates with bound Ca<sup>2+</sup>-calmodulin-dependent kinase II. *J Neurosci* 27:14007-14011.

- Baden DG (1989) Brevetoxins: unique polyether dinoflagellate toxins. *FASEB J* 3:1807-1817.
- Baden DG, Bourdelais AJ, Jacocks H, Michelliza S, Naar J (2005) Natural and derivative brevetoxins: historical background, multiplicity, and effects. *Environ Health Perspect* 113:621-625.
- Bamji SX (2005) Cadherins: actin with the cytoskeleton to form synapses. *Neuron* 47:175-178.
- Bannister AJ, Kouzarides T (1996) The CBP co-activator is a histone acetyltransferase. *Nature* 384:641-643.
- Barbacid M (1994) The Trk family of neurotrophin receptors. *J Neurobiol* 25:1386-1403.
- Bayer KU, LeBel E, McDonald GL, O'Leary H, Schulman H, De Koninck P (2006) Transition from reversible to persistent binding of CaMKII to postsynaptic sites and NR2B. *J Neurosci* 26:1164-1174.
- Benarroch EE (2007) Rho GTPases: role in dendrite and axonal growth, mental retardation, and axonal regeneration. *Neurology* 68:1315-1318.
- Berninger B, Marty S, Zafra F, da Penha Berzaghi M, Thoenen H, Lindholm D (1995) GABAergic stimulation switches from enhancing to repressing BDNF expression in rat hippocampal neurons during maturation in vitro. *Development* 121:2327-2335.
- Blankenship AG, Feller MB Mechanisms underlying spontaneous patterned activity in developing neural circuits. *Nat Rev Neurosci* 11:18-29.
- Bliss TV, Collingridge GL (1993) A synaptic model of memory: long-term potentiation in the hippocampus. *Nature* 361:31-39.

- Boiko T, Rasband MN, Levinson SR, Caldwell JH, Mandel G, Trimmer JS, Matthews G (2001) Compact myelin dictates the differential targeting of two sodium channel isoforms in the same axon. *Neuron* 30:91-104.
- Brosenitsch TA, Katz DM (2001) Physiological patterns of electrical stimulation can induce neuronal gene expression by activating N-type calcium channels. *J Neurosci* 21:2571-2579.
- Cao Z, George J, Gerwick WH, Baden DG, Rainier JD, Murray TF (2008) Influence of lipid soluble gating modifier toxins on sodium influx in neocortical neurons. *J Pharmacol Exp Ther*.
- Castren E, Zafra F, Thoenen H, Lindholm D (1992) Light regulates expression of brain-derived neurotrophic factor mRNA in rat visual cortex. *Proc Natl Acad Sci U S A* 89:9444-9448.
- Catterall WA, Gainer M (1985) Interaction of brevetoxin A with a new receptor site on the sodium channel. *Toxicon* 23:497-504.
- Catterall WA, Goldin AL, Waxman SG (2003) International Union of Pharmacology. XXXIX. Compendium of voltage-gated ion channels: sodium channels. *Pharmacol Rev* 55:575-578.
- Catterall WA, Perez-Reyes E, Snutch TP, Striessnig J (2005) International Union of Pharmacology. XLVIII. Nomenclature and structure-function relationships of voltage-gated calcium channels. *Pharmacol Rev* 57:411-425.
- Cestele S, Catterall WA (2000) Molecular mechanisms of neurotoxin action on voltage-gated sodium channels. *Biochimie* 82:883-892.

- Chandler LJ, Sutton G, Dorairaj NR, Norwood D (2001) N-methyl D-aspartate receptor-mediated bidirectional control of extracellular signal-regulated kinase activity in cortical neuronal cultures. *J Biol Chem* 276:2627-2636.
- Chang L, Jones Y, Ellisman MH, Goldstein LS, Karin M (2003) JNK1 is required for maintenance of neuronal microtubules and controls phosphorylation of microtubule-associated proteins. *Dev Cell* 4:521-533.
- Chen BS, Roche KW (2007) Regulation of NMDA receptors by phosphorylation. *Neuropharmacology* 53:362-368.
- Chen Y, Ghosh A (2005) Regulation of dendritic development by neuronal activity. *J Neurobiol* 64:4-10.
- Chowdhury S, Shepherd JD, Okuno H, Lyford G, Petralia RS, Plath N, Kuhl D, Huganir RL, Worley PF (2006) Arc/Arg3.1 interacts with the endocytic machinery to regulate AMPA receptor trafficking. *Neuron* 52:445-459.
- Ciani L, Salinas PC (2005) WNTs in the vertebrate nervous system: from patterning to neuronal connectivity. *Nat Rev Neurosci* 6:351-362.
- Cline HT (2001) Dendritic arbor development and synaptogenesis. *Curr Opin Neurobiol* 11:118-126.
- Cobos I, Borello U, Rubenstein JL (2007) Dlx transcription factors promote migration through repression of axon and dendrite growth. *Neuron* 54:873-888.
- Cohen S, Greenberg ME (2008) Communication between the synapse and the nucleus in neuronal development, plasticity, and disease. *Annu Rev Cell Dev Biol* 24:183-209.

- Colbran RJ, Brown AM (2004) Calcium/calmodulin-dependent protein kinase II and synaptic plasticity. *Curr Opin Neurobiol* 14:318-327.
- Cull-Candy SG, Leszkiewicz DN (2004) Role of distinct NMDA receptor subtypes at central synapses. *Sci STKE* 2004:re16.
- Dargent B, Paillart C, Carlier E, Alcaraz G, Martin-Eauclaire MF, Couraud F (1994) Sodium channel internalization in developing neurons. *Neuron* 13:683-690.
- Dijkhuizen PA, Ghosh A (2005) BDNF regulates primary dendrite formation in cortical neurons via the PI3-kinase and MAP kinase signaling pathways. *J Neurobiol* 62:278-288.
- Dingledine R, Borges K, Bowie D, Traynelis SF (1999) The glutamate receptor ion channels. *Pharmacol Rev* 51:7-61.
- Docherty RJ, Farmer CE (2009) The pharmacology of voltage-gated sodium channels in sensory neurones. *Handb Exp Pharmacol*:519-561.
- Dolmetsch RE, Pajvani U, Fife K, Spotts JM, Greenberg ME (2001) Signaling to the nucleus by an L-type calcium channel-calmodulin complex through the MAP kinase pathway. *Science* 294:333-339.
- Dravid SM, Baden DG, Murray TF (2004) Brevetoxin activation of voltage-gated sodium channels regulates Ca dynamics and ERK1/2 phosphorylation in murine neocortical neurons. *J Neurochem* 89:739-749.
- Du J, Feng L, Yang F, Lu B (2000) Activity- and Ca(2+)-dependent modulation of surface expression of brain-derived neurotrophic factor receptors in hippocampal neurons. *J Cell Biol* 150:1423-1434.

- Dunlap K, Luebke JI, Turner TJ (1995) Exocytotic Ca<sup>2+</sup> channels in mammalian central neurons. *Trends Neurosci* 18:89-98.
- Ernfors P, Bengzon J, Kokaia Z, Persson H, Lindvall O (1991) Increased levels of messenger RNAs for neurotrophic factors in the brain during kindling epileptogenesis. *Neuron* 7:165-176.
- Escandon E, Soppet D, Rosenthal A, Mendoza-Ramirez JL, Szonyi E, Burton LE, Henderson CE, Parada LF, Nikolics K (1994) Regulation of neurotrophin receptor expression during embryonic and postnatal development. *J Neurosci* 14:2054-2068.
- Ewald RC, Van Keuren-Jensen KR, Aizenman CD, Cline HT (2008) Roles of NR2A and NR2B in the development of dendritic arbor morphology in vivo. *J Neurosci* 28:850-861.
- Faherty CJ, Kerley D, Smeyne RJ (2003) A Golgi-Cox morphological analysis of neuronal changes induced by environmental enrichment. *Brain Res Dev Brain Res* 141:55-61.
- Figurov A, Pozzo-Miller LD, Olafsson P, Wang T, Lu B (1996) Regulation of synaptic responses to high-frequency stimulation and LTP by neurotrophins in the hippocampus. *Nature* 381:706-709.
- Fink CC, Bayer KU, Myers JW, Ferrell JE, Jr., Schulman H, Meyer T (2003) Selective regulation of neurite extension and synapse formation by the beta but not the alpha isoform of CaMKII. *Neuron* 39:283-297.

- Finkbeiner S, Tavazoie SF, Maloratsky A, Jacobs KM, Harris KM, Greenberg ME (1997) CREB: a major mediator of neuronal neurotrophin responses. *Neuron* 19:1031-1047.
- Fryer RH, Kaplan DR, Kromer LF (1997) Truncated trkB receptors on nonneuronal cells inhibit BDNF-induced neurite outgrowth in vitro. *Exp Neurol* 148:616-627.
- Fryer RH, Kaplan DR, Feinstein SC, Radeke MJ, Grayson DR, Kromer LF (1996) Developmental and mature expression of full-length and truncated TrkB receptors in the rat forebrain. *J Comp Neurol* 374:21-40.
- Furukawa H, Singh SK, Mancusso R, Gouaux E (2005) Subunit arrangement and function in NMDA receptors. *Nature* 438:185-192.
- Furutani Y, Matsuno H, Kawasaki M, Sasaki T, Mori K, Yoshihara Y (2007) Interaction between telencephalin and ERM family proteins mediates dendritic filopodia formation. *J Neurosci* 27:8866-8876.
- Gawley RE, Rein KS, Kinoshita M, Baden DG (1992) Binding of brevetoxins and ciguatoxin to the voltage-sensitive sodium channel and conformational analysis of brevetoxin B. *Toxicon* 30:780-785.
- George J, Dravid SM, Prakash A, Xie J, Peterson J, Jabba SV, Baden DG, Murray TF (2009) Sodium channel activation augments NMDA receptor function and promotes neurite outgrowth in immature cerebrocortical neurons. *J Neurosci* 29:3288-3301.
- Ghosh A, Greenberg ME (1995) Calcium signaling in neurons: molecular mechanisms and cellular consequences. *Science* 268:239-247.

- Glantz LA, Lewis DA (2000) Decreased dendritic spine density on prefrontal cortical pyramidal neurons in schizophrenia. *Arch Gen Psychiatry* 57:65-73.
- Gomez TM, Spitzer NC (2000) Regulation of growth cone behavior by calcium: new dynamics to earlier perspectives. *J Neurobiol* 44:174-183.
- Groc L, Heine M, Cousins SL, Stephenson FA, Lounis B, Cognet L, Choquet D (2006) NMDA receptor surface mobility depends on NR2A-2B subunits. *Proc Natl Acad Sci U S A* 103:18769-18774.
- Ha S, Redmond L (2008) ERK mediates activity dependent neuronal complexity via sustained activity and CREB-mediated signaling. *Dev Neurobiol* 68:1565-1579.
- Hall BJ, Ripley B, Ghosh A (2007) NR2B signaling regulates the development of synaptic AMPA receptor current. *J Neurosci* 27:13446-13456.
- Hand R, Bortone D, Mattar P, Nguyen L, Heng JI, Guerrier S, Boutt E, Peters E, Barnes AP, Parras C, Schuurmans C, Guillemot F, Polleux F (2005) Phosphorylation of Neurogenin2 specifies the migration properties and the dendritic morphology of pyramidal neurons in the neocortex. *Neuron* 48:45-62.
- Honkura N, Matsuzaki M, Noguchi J, Ellis-Davies GC, Kasai H (2008) The subspine organization of actin fibers regulates the structure and plasticity of dendritic spines. *Neuron* 57:719-729.
- Horch HW, Katz LC (2002) BDNF release from single cells elicits local dendritic growth in nearby neurons. *Nat Neurosci* 5:1177-1184.
- Hui K, Fei GH, Saab BJ, Su J, Roder JC, Feng ZP (2007) Neuronal calcium sensor-1 modulation of optimal calcium level for neurite outgrowth. *Development* 134:4479-4489.

- Inglis FM, Zuckerman KE, Kalb RG (2000) Experience-dependent development of spinal motor neurons. *Neuron* 26:299-305.
- Isackson PJ, Huntsman MM, Murray KD, Gall CM (1991) BDNF mRNA expression is increased in adult rat forebrain after limbic seizures: temporal patterns of induction distinct from NGF. *Neuron* 6:937-948.
- Jabba SV, Prakash A, Dravid SM, Gerwick WH, Murray TF Antillatoxin, a novel lipopeptide, enhances neurite outgrowth in immature cerebrocortical neurons through activation of voltage-gated sodium channels. *J Pharmacol Exp Ther* 332:698-709.
- Jaffe AB, Hall A (2005) Rho GTPases: biochemistry and biology. *Annu Rev Cell Dev Biol* 21:247-269.
- Jan YN, Jan LY (2003) The control of dendrite development. *Neuron* 40:229-242.
- Jaworski J, Spangler S, Seeburg DP, Hoogenraad CC, Sheng M (2005) Control of dendritic arborization by the phosphoinositide-3'-kinase-Akt-mammalian target of rapamycin pathway. *J Neurosci* 25:11300-11312.
- Jeglitsch G, Rein K, Baden DG, Adams DJ (1998) Brevetoxin-3 (PbTx-3) and its derivatives modulate single tetrodotoxin-sensitive sodium channels in rat sensory neurons. *J Pharmacol Exp Ther* 284:516-525.
- Kalb RG (1994) Regulation of motor neuron dendrite growth by NMDA receptor activation. *Development* 120:3063-3071.
- Kang H, Schuman EM (1996) A requirement for local protein synthesis in neurotrophin-induced hippocampal synaptic plasticity. *Science* 273:1402-1406.

- Kaplan MR, Cho MH, Ullian EM, Isom LL, Levinson SR, Barres BA (2001) Differential control of clustering of the sodium channels Na(v)1.2 and Na(v)1.6 at developing CNS nodes of Ranvier. *Neuron* 30:105-119.
- Kasai H, Matsuzaki M, Noguchi J, Yasumatsu N, Nakahara H (2003) Structure-stability-function relationships of dendritic spines. *Trends Neurosci* 26:360-368.
- Kaufmann WE, Moser HW (2000) Dendritic anomalies in disorders associated with mental retardation. *Cereb Cortex* 10:981-991.
- Kim E, Sheng M (2004) PDZ domain proteins of synapses. *Nat Rev Neurosci* 5:771-781.
- Klein ME, Impey S, Goodman RH (2005) Role reversal: the regulation of neuronal gene expression by microRNAs. *Curr Opin Neurobiol* 15:507-513.
- Knusel B, Rabin SJ, Hefti F, Kaplan DR (1994) Regulated neurotrophin receptor responsiveness during neuronal migration and early differentiation. *J Neurosci* 14:1542-1554.
- Konur S, Ghosh A (2005) Calcium signaling and the control of dendritic development. *Neuron* 46:401-405.
- Kornhauser JM, Cowan CW, Shaywitz AJ, Dolmetsch RE, Griffith EC, Hu LS, Haddad C, Xia Z, Greenberg ME (2002) CREB transcriptional activity in neurons is regulated by multiple, calcium-specific phosphorylation events. *Neuron* 34:221-233.
- Kuczewski N, Porcher C, Lessmann V, Medina I, Gaiarsa JL (2009) Activity-dependent dendritic release of BDNF and biological consequences. *Mol Neurobiol* 39:37-49.

- Kumar V, Zhang MX, Swank MW, Kunz J, Wu GY (2005) Regulation of dendritic morphogenesis by Ras-PI3K-Akt-mTOR and Ras-MAPK signaling pathways. *J Neurosci* 25:11288-11299.
- Lauterborn JC, Rivera S, Stinis CT, Hayes VY, Isackson PJ, Gall CM (1996) Differential effects of protein synthesis inhibition on the activity-dependent expression of BDNF transcripts: evidence for immediate-early gene responses from specific promoters. *J Neurosci* 16:7428-7436.
- Lavezzari G, McCallum J, Lee R, Roche KW (2003) Differential binding of the AP-2 adaptor complex and PSD-95 to the C-terminus of the NMDA receptor subunit NR2B regulates surface expression. *Neuropharmacology* 45:729-737.
- Lee HK (2006) Synaptic plasticity and phosphorylation. *Pharmacol Ther* 112:810-832.
- Lee LJ, Lo FS, Erzurumlu RS (2005) NMDA receptor-dependent regulation of axonal and dendritic branching. *J Neurosci* 25:2304-2311.
- Li WI, Berman FW, Okino T, Yokokawa F, Shioiri T, Gerwick WH, Murray TF (2001) Antillatoxin is a marine cyanobacterial toxin that potently activates voltage-gated sodium channels. *Proc Natl Acad Sci U S A* 98:7599-7604.
- Li Z, Okamoto K, Hayashi Y, Sheng M (2004) The importance of dendritic mitochondria in the morphogenesis and plasticity of spines and synapses. *Cell* 119:873-887.
- Lim CS, Walikonis RS (2008) Hepatocyte growth factor and c-Met promote dendritic maturation during hippocampal neuron differentiation via the Akt pathway. *Cell Signal* 20:825-835.
- Lipton SA, Nakanishi N (1999) Shakespeare in love--with NMDA receptors? *Nat Med* 5:270-271.

- Lohmann C, Wong RO (2005) Regulation of dendritic growth and plasticity by local and global calcium dynamics. *Cell Calcium* 37:403-409.
- Lohmann C, Bonhoeffer T (2008) A role for local calcium signaling in rapid synaptic partner selection by dendritic filopodia. *Neuron* 59:253-260.
- Lohmann C, Finski A, Bonhoeffer T (2005) Local calcium transients regulate the spontaneous motility of dendritic filopodia. *Nat Neurosci* 8:305-312.
- Lohof AM, Ip NY, Poo MM (1993) Potentiation of developing neuromuscular synapses by the neurotrophins NT-3 and BDNF. *Nature* 363:350-353.
- Lorincz A, Nusser Z Molecular identity of dendritic voltage-gated sodium channels. *Science* 328:906-909.
- Martin KC, Michael D, Rose JC, Barad M, Casadio A, Zhu H, Kandel ER (1997) MAP kinase translocates into the nucleus of the presynaptic cell and is required for long-term facilitation in *Aplysia*. *Neuron* 18:899-912.
- Matsuzaki M, Honkura N, Ellis-Davies GC, Kasai H (2004) Structural basis of long-term potentiation in single dendritic spines. *Nature* 429:761-766.
- McAllister AK (2000) Cellular and molecular mechanisms of dendrite growth. *Cereb Cortex* 10:963-973.
- McAllister AK (2002) Bdnf. *Curr Biol* 12:R310.
- McAllister AK, Lo DC, Katz LC (1995) Neurotrophins regulate dendritic growth in developing visual cortex. *Neuron* 15:791-803.
- McAllister AK, Katz LC, Lo DC (1999) Neurotrophins and synaptic plasticity. *Annu Rev Neurosci* 22:295-318.

- Michelliza S, Abraham WM, Jacocks HM, Schuster T, Baden DG (2007) Synthesis, modeling, and biological evaluation of analogues of the semisynthetic brevetoxin antagonist beta-naphthoyl-brevetoxin. *Chembiochem* 8:2233-2239.
- Miller FD, Kaplan DR (2003) Signaling mechanisms underlying dendrite formation. *Curr Opin Neurobiol* 13:391-398.
- Mitrovic N, George AL, Jr., Horn R (2000) Role of domain 4 in sodium channel slow inactivation. *J Gen Physiol* 115:707-718.
- Monyer H, Burnashev N, Laurie DJ, Sakmann B, Seeburg PH (1994) Developmental and regional expression in the rat brain and functional properties of four NMDA receptors. *Neuron* 12:529-540.
- Morgan JI, Cohen DR, Hempstead JL, Curran T (1987) Mapping patterns of c-fos expression in the central nervous system after seizure. *Science* 237:192-197.
- Murphy TH, Corbett D (2009) Plasticity during stroke recovery: from synapse to behaviour. *Nat Rev Neurosci* 10:861-872.
- Naeve GS, Ramakrishnan M, Kramer R, Hevroni D, Citri Y, Theill LE (1997) Neurtin: a gene induced by neural activity and neurotrophins that promotes neuritogenesis. *Proc Natl Acad Sci U S A* 94:2648-2653.
- Nagappan G, Lu B (2005) Activity-dependent modulation of the BDNF receptor TrkB: mechanisms and implications. *Trends Neurosci* 28:464-471.
- Nakazawa T, Komai S, Tezuka T, Hisatsune C, Umemori H, Semba K, Mishina M, Manabe T, Yamamoto T (2001) Characterization of Fyn-mediated tyrosine phosphorylation sites on GluR epsilon 2 (NR2B) subunit of the N-methyl-D-aspartate receptor. *J Biol Chem* 276:693-699.

- Nedivi E (1999) Molecular analysis of developmental plasticity in neocortex. *J Neurobiol* 41:135-147.
- Nikonenko I, Boda B, Steen S, Knott G, Welker E, Muller D (2008) PSD-95 promotes synaptogenesis and multiinnervated spine formation through nitric oxide signaling. *J Cell Biol* 183:1115-1127.
- Ong BH, Tomaselli GF, Balsler JR (2000) A structural rearrangement in the sodium channel pore linked to slow inactivation and use dependence. *J Gen Physiol* 116:653-662.
- Ooms LM, Fedele CG, Astle MV, Ivetac I, Cheung V, Pearson RB, Layton MJ, Forrai A, Nandurkar HH, Mitchell CA (2006) The inositol polyphosphate 5-phosphatase, PIPP, Is a novel regulator of phosphoinositide 3-kinase-dependent neurite elongation. *Mol Biol Cell* 17:607-622.
- Pang PT, Teng HK, Zaitsev E, Woo NT, Sakata K, Zhen S, Teng KK, Yung WH, Hempstead BL, Lu B (2004) Cleavage of proBDNF by tPA/plasmin is essential for long-term hippocampal plasticity. *Science* 306:487-491.
- Paoletti P, Neyton J (2007) NMDA receptor subunits: function and pharmacology. *Curr Opin Pharmacol* 7:39-47.
- Pierce RH, Henry MS, Blum PC, Hamel SL, Kirkpatrick B, Cheng YS, Zhou Y, Irvin CM, Naar J, Weidner A, Fleming LE, Backer LC, Baden DG (2005) Brevetoxin composition in water and marine aerosol along a Florida beach: Assessing potential human exposure to marine biotoxins. *Harmful Algae* 4:965-972.

- Poli MA, Mende TJ, Baden DG (1986) Brevetoxins, unique activators of voltage-sensitive sodium channels, bind to specific sites in rat brain synaptosomes. *Mol Pharmacol* 30:129-135.
- Poo MM (2001) Neurotrophins as synaptic modulators. *Nat Rev Neurosci* 2:24-32.
- Qiu Z, Ghosh A (2008) A brief history of neuronal gene expression: regulatory mechanisms and cellular consequences. *Neuron* 60:449-455.
- Rajan I, Cline HT (1998) Glutamate receptor activity is required for normal development of tectal cell dendrites in vivo. *J Neurosci* 18:7836-7846.
- Ramos B, Gaudilliere B, Bonni A, Gill G (2007) Transcription factor Sp4 regulates dendritic patterning during cerebellar maturation. *Proc Natl Acad Sci U S A* 104:9882-9887.
- Read DE, Gorman AM (2009) Involvement of Akt in neurite outgrowth. *Cell Mol Life Sci* 66:2975-2984.
- Redmond L (2008) Translating neuronal activity into dendrite elaboration: signaling to the nucleus. *Neurosignals* 16:194-208.
- Redmond L, Kashani AH, Ghosh A (2002) Calcium regulation of dendritic growth via CaM kinase IV and CREB-mediated transcription. *Neuron* 34:999-1010.
- Rial Verde EM, Lee-Osbourne J, Worley PF, Malinow R, Cline HT (2006) Increased expression of the immediate-early gene *arc/arg3.1* reduces AMPA receptor-mediated synaptic transmission. *Neuron* 52:461-474.
- Roche KW, Standley S, McCallum J, Dune Ly C, Ehlers MD, Wenthold RJ (2001) Molecular determinants of NMDA receptor internalization. *Nat Neurosci* 4:794-802.

- Rose CR, Konnerth A (2001) NMDA receptor-mediated Na<sup>+</sup> signals in spines and dendrites. *J Neurosci* 21:4207-4214.
- Rose CR, Kovalchuk Y, Eilers J, Konnerth A (1999) Two-photon Na<sup>+</sup> imaging in spines and fine dendrites of central neurons. *Pflugers Arch* 439:201-207.
- Sala C, Rudolph-Correia S, Sheng M (2000) Developmentally regulated NMDA receptor-dependent dephosphorylation of cAMP response element-binding protein (CREB) in hippocampal neurons. *J Neurosci* 20:3529-3536.
- Salter MW, Kalia LV (2004) Src kinases: a hub for NMDA receptor regulation. *Nat Rev Neurosci* 5:317-328.
- Saneyoshi T, Fortin DA, Soderling TR Regulation of spine and synapse formation by activity-dependent intracellular signaling pathways. *Curr Opin Neurobiol* 20:108-115.
- Saneyoshi T, Wayman G, Fortin D, Davare M, Hoshi N, Nozaki N, Natsume T, Soderling TR (2008) Activity-dependent synaptogenesis: regulation by a CaM-kinase kinase/CaM-kinase I/betaPIX signaling complex. *Neuron* 57:94-107.
- Sans N, Petralia RS, Wang YX, Blahos J, 2nd, Hell JW, Wenthold RJ (2000) A developmental change in NMDA receptor-associated proteins at hippocampal synapses. *J Neurosci* 20:1260-1271.
- Schmitt JM, Wayman GA, Nozaki N, Soderling TR (2004) Calcium activation of ERK mediated by calmodulin kinase I. *J Biol Chem* 279:24064-24072.
- Schmitt JM, Guire ES, Saneyoshi T, Soderling TR (2005) Calmodulin-dependent kinase kinase/calmodulin kinase I activity gates extracellular-regulated kinase-dependent long-term potentiation. *J Neurosci* 25:1281-1290.

- Schratt G (2009) microRNAs at the synapse. *Nat Rev Neurosci* 10:842-849.
- Schratt GM, Tuebing F, Nigh EA, Kane CG, Sabatini ME, Kiebler M, Greenberg ME (2006) A brain-specific microRNA regulates dendritic spine development. *Nature* 439:283-289.
- Segal M (2005) Dendritic spines and long-term plasticity. *Nat Rev Neurosci* 6:277-284.
- Shepherd JD, Rumbaugh G, Wu J, Chowdhury S, Plath N, Kuhl D, Huganir RL, Worley PF (2006) Arc/Arg3.1 mediates homeostatic synaptic scaling of AMPA receptors. *Neuron* 52:475-484.
- Shieh PB, Hu SC, Bobb K, Timmusk T, Ghosh A (1998) Identification of a signaling pathway involved in calcium regulation of BDNF expression. *Neuron* 20:727-740.
- Sholl DA (1953) Dendritic organization in the neurons of the visual and motor cortices of the cat. *J Anat* 87:387-406.
- Sin WC, Haas K, Ruthazer ES, Cline HT (2002) Dendrite growth increased by visual activity requires NMDA receptor and Rho GTPases. *Nature* 419:475-480.
- Snyder EM, Nong Y, Almeida CG, Paul S, Moran T, Choi EY, Nairn AC, Salter MW, Lombroso PJ, Gouras GK, Greengard P (2005) Regulation of NMDA receptor trafficking by amyloid-beta. *Nat Neurosci* 8:1051-1058.
- Soderling TR (2000) CaM-kinases: modulators of synaptic plasticity. *Curr Opin Neurobiol* 10:375-380.
- Spitzer NC, Lautermilch NJ, Smith RD, Gomez TM (2000) Coding of neuronal differentiation by calcium transients. *Bioessays* 22:811-817.

- Tada T, Sheng M (2006) Molecular mechanisms of dendritic spine morphogenesis. *Curr Opin Neurobiol* 16:95-101.
- Takasu MA, Dalva MB, Zigmond RE, Greenberg ME (2002) Modulation of NMDA receptor-dependent calcium influx and gene expression through EphB receptors. *Science* 295:491-495.
- Takemoto-Kimura S, Terai H, Takamoto M, Ohmae S, Kikumura S, Segi E, Arakawa Y, Furuyashiki T, Narumiya S, Bito H (2003) Molecular cloning and characterization of CLICK-III/CaMKIgamma, a novel membrane-anchored neuronal Ca<sup>2+</sup>/calmodulin-dependent protein kinase (CaMK). *J Biol Chem* 278:18597-18605.
- Takemoto-Kimura S, Ageta-Ishihara N, Nonaka M, Adachi-Morishima A, Mano T, Okamura M, Fujii H, Fuse T, Hoshino M, Suzuki S, Kojima M, Mishina M, Okuno H, Bito H (2007) Regulation of dendritogenesis via a lipid-raft-associated Ca<sup>2+</sup>/calmodulin-dependent protein kinase CLICK-III/CaMKIgamma. *Neuron* 54:755-770.
- Tao X, Finkbeiner S, Arnold DB, Shaywitz AJ, Greenberg ME (1998) Ca<sup>2+</sup> influx regulates BDNF transcription by a CREB family transcription factor-dependent mechanism. *Neuron* 20:709-726.
- Tian L, Stefanidakis M, Ning L, Van Lint P, Nyman-Huttunen H, Libert C, Itohara S, Mishina M, Rauvala H, Gahmberg CG (2007) Activation of NMDA receptors promotes dendritic spine development through MMP-mediated ICAM-5 cleavage. *J Cell Biol* 178:687-700.

- Tolias KF, Bikoff JB, Burette A, Paradis S, Harrar D, Tavazoie S, Weinberg RJ, Greenberg ME (2005) The Rac1-GEF Tiam1 couples the NMDA receptor to the activity-dependent development of dendritic arbors and spines. *Neuron* 45:525-538.
- Tongiorgi E (2008) Activity-dependent expression of brain-derived neurotrophic factor in dendrites: facts and open questions. *Neurosci Res* 61:335-346.
- Trainer VL, Baden DG, Catterall WA (1994) Identification of peptide components of the brevetoxin receptor site of rat brain sodium channels. *J Biol Chem* 269:19904-19909.
- Ueda T, Sakagami H, Abe K, Oishi I, Maruo A, Kondo H, Terashima T, Ichihashi M, Yamamura H, Minami Y (1999) Distribution and intracellular localization of a mouse homologue of Ca<sup>2+</sup>/calmodulin-dependent protein kinase I $\beta$ 2 in the nervous system. *J Neurochem* 73:2119-2129.
- Ultanir SK, Kim JE, Hall BJ, Deerinck T, Ellisman M, Ghosh A (2007) Regulation of spine morphology and spine density by NMDA receptor signaling in vivo. *Proc Natl Acad Sci U S A* 104:19553-19558.
- Urbanska M, Blazejczyk M, Jaworski J (2008) Molecular basis of dendritic arborization. *Acta Neurobiol Exp (Wars)* 68:264-288.
- Valenzuela DM, Maisonpierre PC, Glass DJ, Rojas E, Nunez L, Kong Y, Gies DR, Stitt TN, Ip NY, Yancopoulos GD (1993) Alternative forms of rat TrkC with different functional capabilities. *Neuron* 10:963-974.

- Vissel B, Krupp JJ, Heinemann SF, Westbrook GL (2001) A use-dependent tyrosine dephosphorylation of NMDA receptors is independent of ion flux. *Nat Neurosci* 4:587-596.
- Vo N, Klein ME, Varlamova O, Keller DM, Yamamoto T, Goodman RH, Impey S (2005) A cAMP-response element binding protein-induced microRNA regulates neuronal morphogenesis. *Proc Natl Acad Sci U S A* 102:16426-16431.
- Wayman GA, Lee YS, Tokumitsu H, Silva AJ, Soderling TR (2008a) Calmodulin-kinases: modulators of neuronal development and plasticity. *Neuron* 59:914-931.
- Wayman GA, Impey S, Marks D, Saneyoshi T, Grant WF, Derkach V, Soderling TR (2006) Activity-dependent dendritic arborization mediated by CaM-kinase I activation and enhanced CREB-dependent transcription of Wnt-2. *Neuron* 50:897-909.
- Wayman GA, Kaech S, Grant WF, Davare M, Impey S, Tokumitsu H, Nozaki N, Banker G, Soderling TR (2004) Regulation of axonal extension and growth cone motility by calmodulin-dependent protein kinase I. *J Neurosci* 24:3786-3794.
- Wayman GA, Davare M, Ando H, Fortin D, Varlamova O, Cheng HY, Marks D, Obrietan K, Soderling TR, Goodman RH, Impey S (2008b) An activity-regulated microRNA controls dendritic plasticity by down-regulating p250GAP. *Proc Natl Acad Sci U S A* 105:9093-9098.
- West AE, Griffith EC, Greenberg ME (2002) Regulation of transcription factors by neuronal activity. *Nat Rev Neurosci* 3:921-931.

- West AE, Chen WG, Dalva MB, Dolmetsch RE, Kornhauser JM, Shaywitz AJ, Takasu MA, Tao X, Greenberg ME (2001) Calcium regulation of neuronal gene expression. *Proc Natl Acad Sci U S A* 98:11024-11031.
- Westenbroek RE, Merrick DK, Catterall WA (1989) Differential subcellular localization of the RI and RII Na<sup>+</sup> channel subtypes in central neurons. *Neuron* 3:695-704.
- Westphal RS, Tavalin SJ, Lin JW, Alto NM, Fraser ID, Langeberg LK, Sheng M, Scott JD (1999) Regulation of NMDA receptors by an associated phosphatase-kinase signaling complex. *Science* 285:93-96.
- Winder DG, Martin KC, Muzzio IA, Rohrer D, Chruscinski A, Kobilka B, Kandel ER (1999) ERK plays a regulatory role in induction of LTP by theta frequency stimulation and its modulation by beta-adrenergic receptors. *Neuron* 24:715-726.
- Wong RO, Ghosh A (2002) Activity-dependent regulation of dendritic growth and patterning. *Nat Rev Neurosci* 3:803-812.
- Wu GY, Deisseroth K, Tsien RW (2001) Activity-dependent CREB phosphorylation: convergence of a fast, sensitive calmodulin kinase pathway and a slow, less sensitive mitogen-activated protein kinase pathway. *Proc Natl Acad Sci U S A* 98:2808-2813.
- Xie Z, Srivastava DP, Photowala H, Kai L, Cahill ME, Woolfrey KM, Shum CY, Surmeier DJ, Penzes P (2007) Kalirin-7 controls activity-dependent structural and functional plasticity of dendritic spines. *Neuron* 56:640-656.
- Xin WK, Kwan CL, Zhao XH, Xu J, Ellen RP, McCulloch CA, Yu XM (2005) A functional interaction of sodium and calcium in the regulation of NMDA receptor activity by remote NMDA receptors. *J Neurosci* 25:139-148.

- Yoshihara Y, De Roo M, Muller D (2009) Dendritic spine formation and stabilization. *Curr Opin Neurobiol* 19:146-153.
- Yu FH, Catterall WA (2003) Overview of the voltage-gated sodium channel family. *Genome Biol* 4:207.
- Yu X, Malenka RC (2003) Beta-catenin is critical for dendritic morphogenesis. *Nat Neurosci* 6:1169-1177.
- Yu XM (2006) The Role of Intracellular Sodium in the Regulation of NMDA-Receptor-Mediated Channel Activity and Toxicity. *Mol Neurobiol* 33:63-80.
- Yu XM, Salter MW (1998) Gain control of NMDA-receptor currents by intracellular sodium. *Nature* 396:469-474.
- Yuste R, Bonhoeffer T (2004) Genesis of dendritic spines: insights from ultrastructural and imaging studies. *Nat Rev Neurosci* 5:24-34.
- Zafra F, Hengerer B, Leibrock J, Thoenen H, Lindholm D (1990) Activity dependent regulation of BDNF and NGF mRNAs in the rat hippocampus is mediated by non-NMDA glutamate receptors. *EMBO J* 9:3545-3550.
- Zito K, Scheuss V, Knott G, Hill T, Svoboda K (2009) Rapid functional maturation of nascent dendritic spines. *Neuron* 61:247-258.

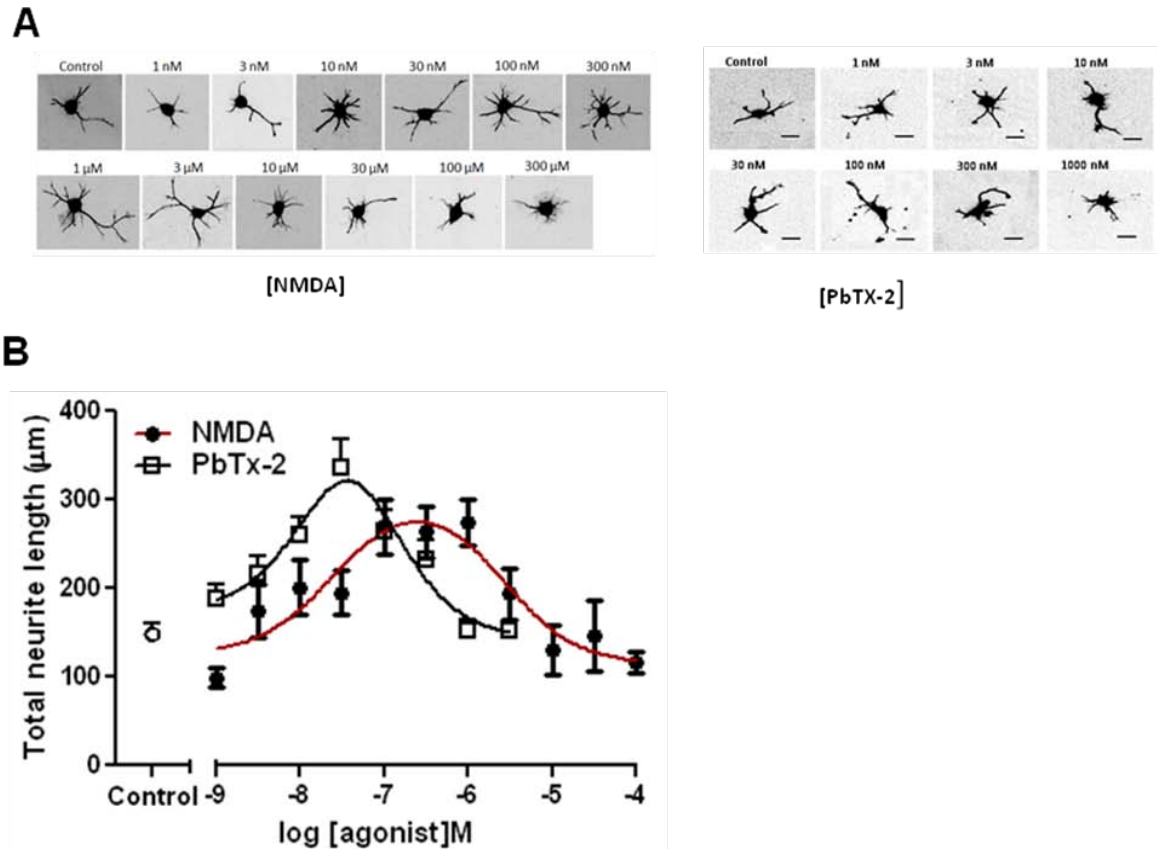


**Figure 1. PbTx-2 enhanced neurite outgrowth exhibits a hormetic profile similar to the NMDA response.**

(A) Representative images (scale bar, 10  $\mu\text{m}$ ) (B) and quantification of neurite outgrowth at 24 h after plating. Various concentrations of PbTx-2 or NMDA were added to the culture medium at 3 h post plating. Each value represents the mean  $\pm$  SEM of 120 neurons.

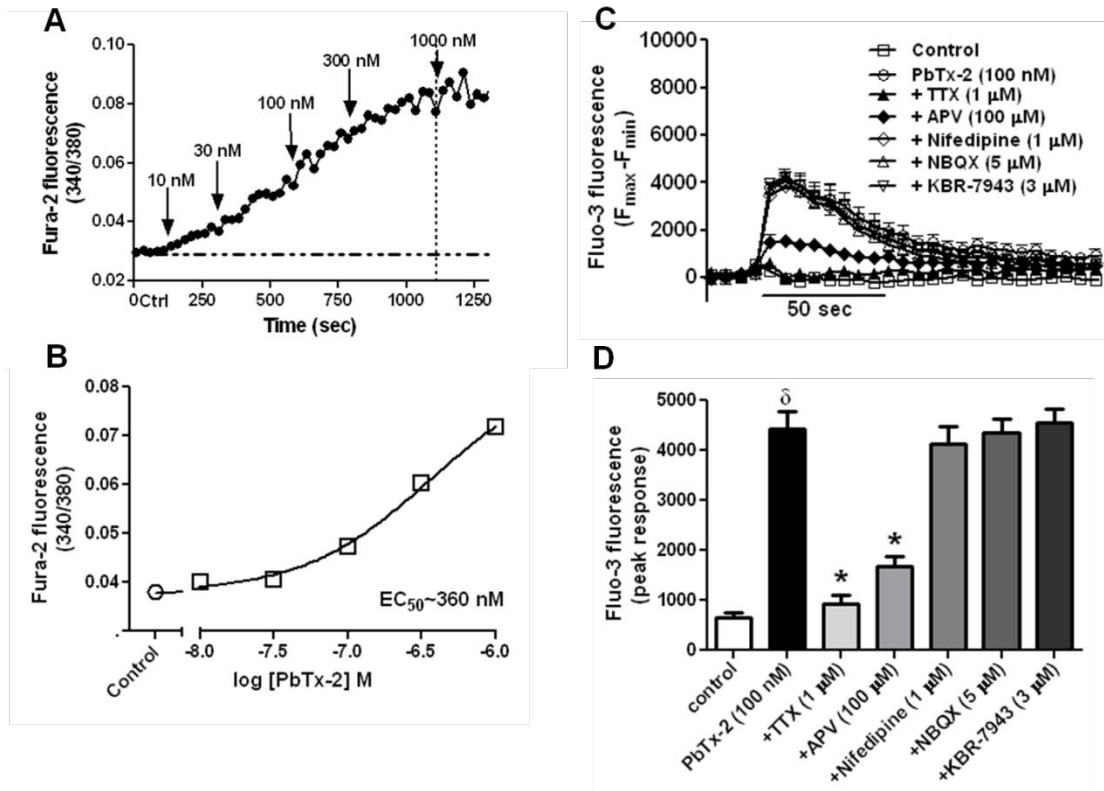


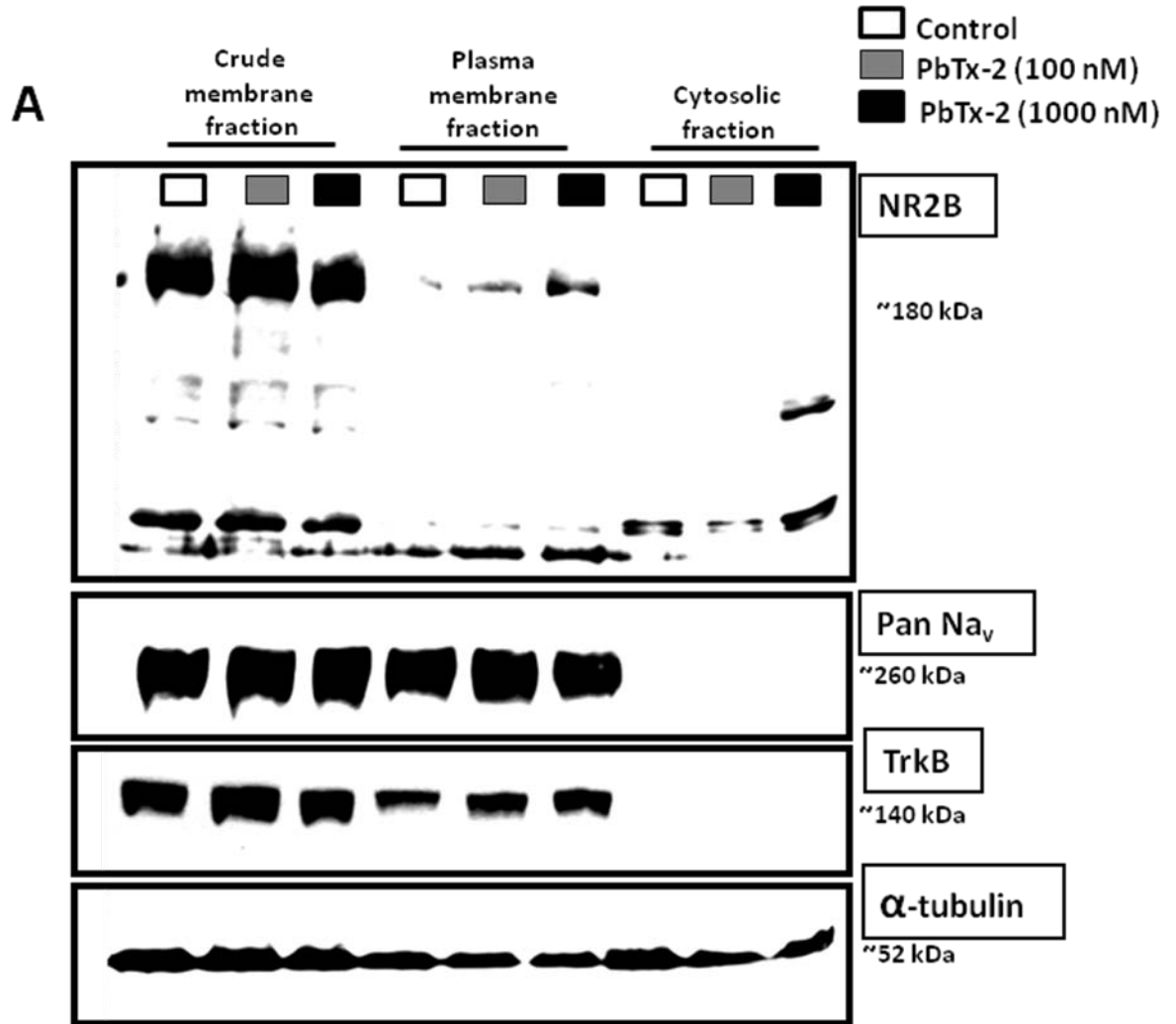
**Figure 2. PbTx-2-induced  $\text{Ca}^{2+}$  influx and pharmacological evaluation in cerebrocortical neurons.**

(A) Single cell imaging of Fura2/AM loaded neurons. Fluorescence intensities were measured using Slide book software. Time-response profile of PbTx-2 –induced  $\text{Ca}^{2+}$  influx in DIV-1 cerebrocortical neurons. Data shown are from a representative experiment (n=20-30 cells; n=2 independent experiments). Each concentration of PbTx-2 was added, as indicated by the arrow, after successive washing. PbTx-2 produced a concentration-dependent increment in  $\text{Ca}^{2+}$  influx in these cerebrocortical neurons.

(B) Non-linear regression analysis of the PbTx-2 concentration-response data ( $\text{EC}_{50}$ ~360 nM; 133 nM~969 nM, 95% CI)

**(C)** Pharmacological evaluation of PbTx-2 (100 nM) induced  $\text{Ca}^{2+}$  influx in DIV-2 cerebrocortical neuronal cultures. Data are from a representative experiment performed in triplicate and repeated thrice. TTX (VGSC blocker), APV (NMDAR competitive antagonist), nifedipine (L-type VGCC antagonist), NBQX (AMPA receptor antagonist) and KBR-7943 (blocker of reverse mode of sodium-calcium exchanger) were used to block individual calcium influx pathways.

**(D)** Histogram representing quantification of the data shown in C. TTX (1  $\mu\text{M}$ ), APV (100  $\mu\text{M}$ ) significantly blocked PbTx-2-induced  $\text{Ca}^{2+}$  influx.



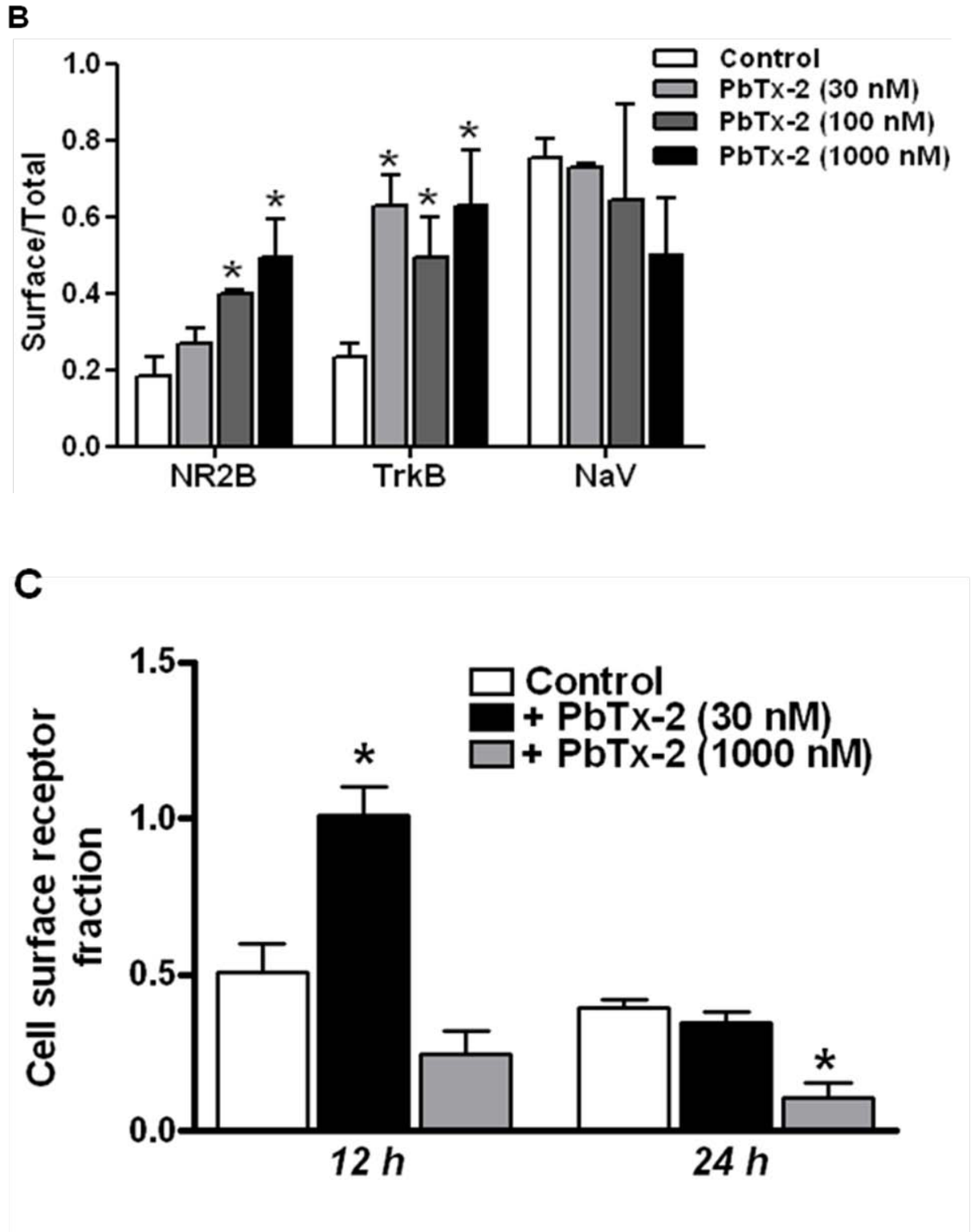
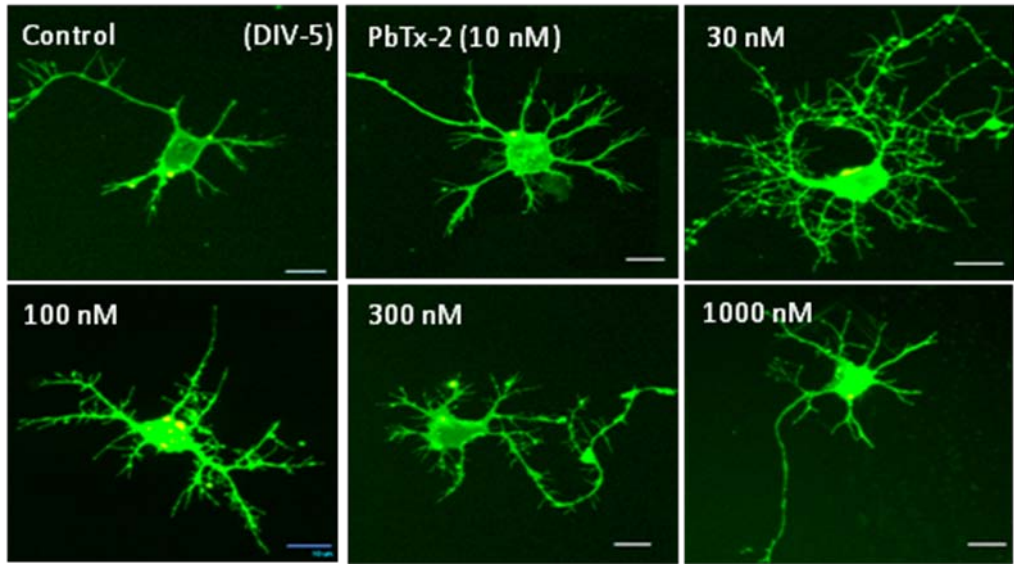
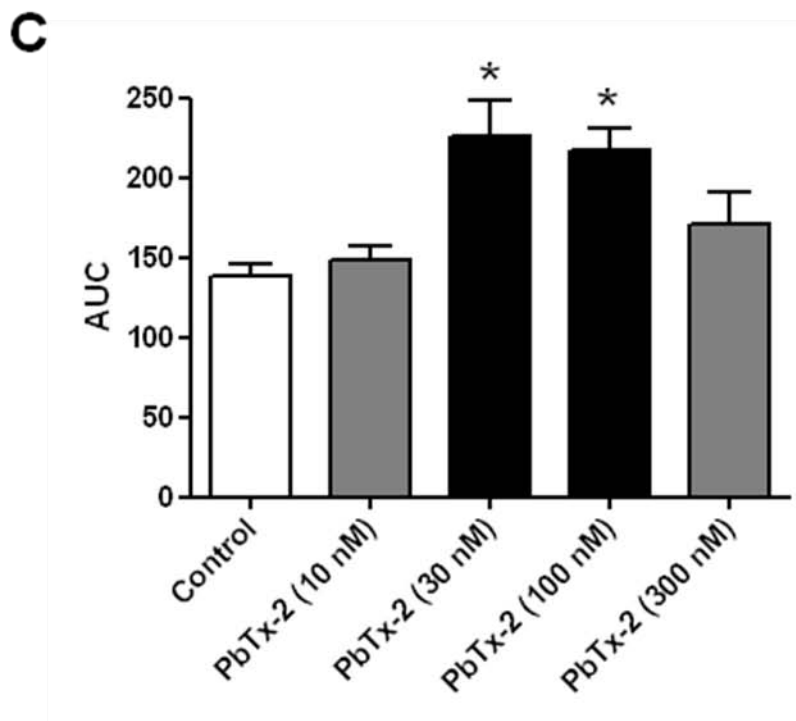
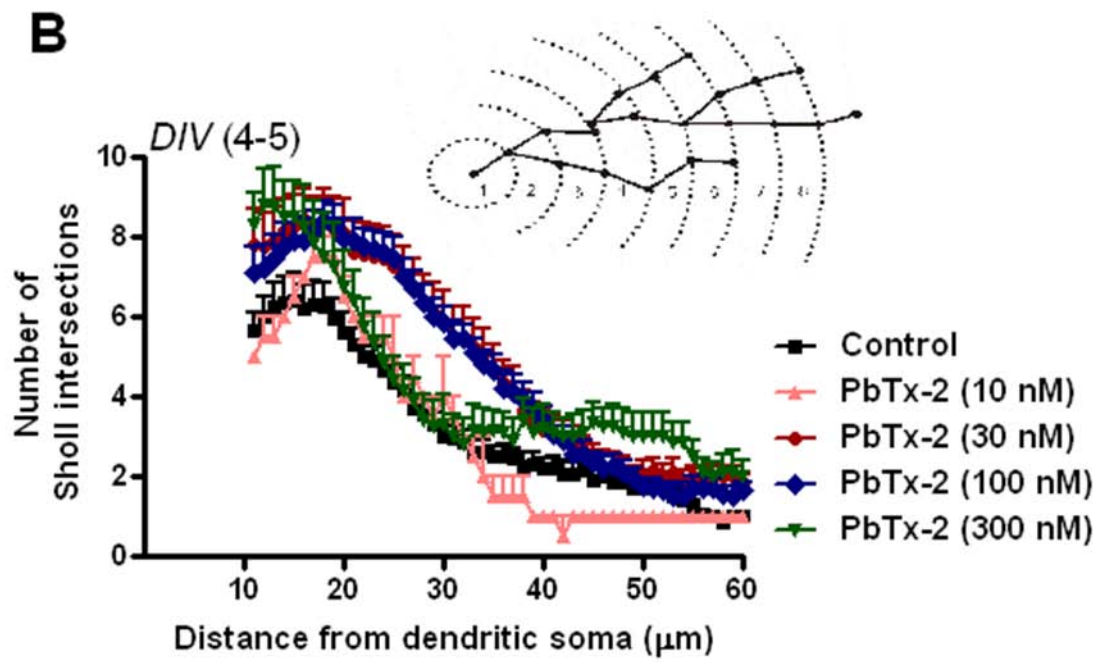


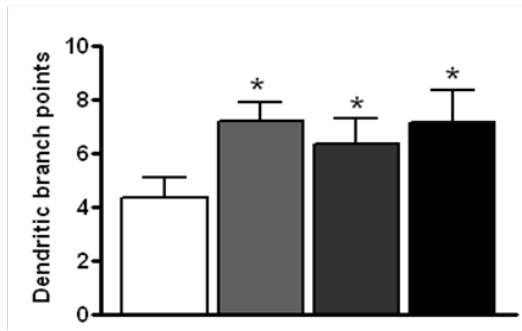
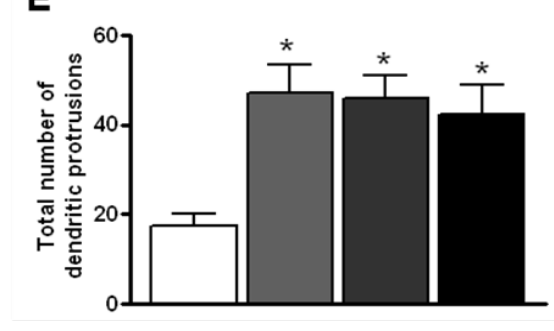
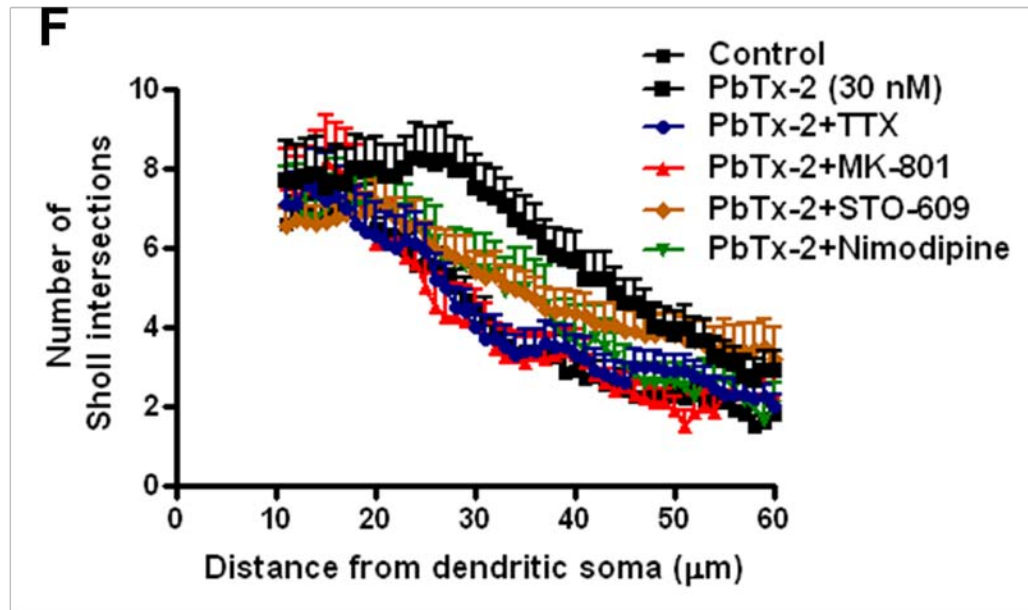
Figure 3. Influence of PbTx-2 on cell surface channel and receptor expression.

- (A)** Biotinylation assay for cell surface receptors on DIV-1 cerebrocortical neurons. Biotinylated surface proteins were isolated after 30 min of PbTx-2 exposure, resolved by SDS/PAGE, and probed with NR2B, pan Na<sub>v</sub>, TrkB and  $\alpha$ -tubulin antibodies. A representative blot is shown.  $n=3$  independent experiments.
- (B)** Quantification of the biotinylation experiments. The immuno-reactive signals for cell surface NR2B, Na<sub>v</sub> and TrkB were normalized to the respective crude membrane fraction and presented as a bar graph.  $n = 3$  independent experiments. Error bars, mean  $\pm$  SEM.; \*,  $P < 0.05$ , Student's  $t$  test.
- (C)** Effect of PbTx-2 exposure on cell surface expressing VGSCs in DIV-1 cerebrocortical neurons. PbTx-2 (30 nM) and 1000 nM were added at 3 h post plating and the cell surface fraction of VGSCs was assessed at 12 h and 24 h time points. Whole cell binding was assayed by binding at 4<sup>o</sup> C for 4 h in the presence of  $\sim 2$  nM [<sup>3</sup>H] BTX. QX-314 (1 mM), a quarternary lidocaine derivative, was used to define cell surface binding. The ratio of cell surface binding (in the presence of QX-314) to total cell binding was used to obtain a value representing the fraction of cell surface expressing VGSCs.  $n=3$  independent experiments. Error bars, mean  $\pm$  SEM.; \*,  $P < 0.05$ , Student's  $t$  test.

A





**D****E****F**

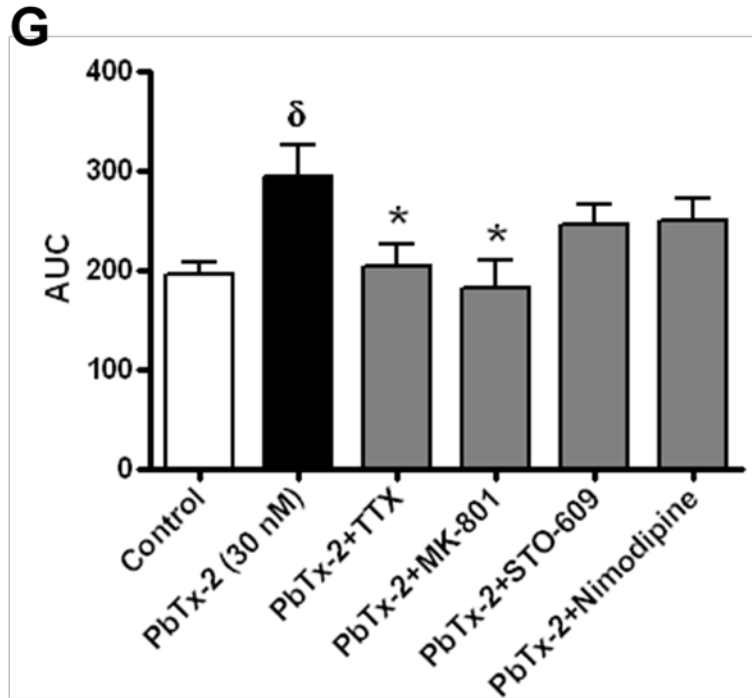


**Figure 4. PbTx-2 exposure enhances dendritic arborization.**

(A) Representative images of DiI-loaded cerebrocortical neurons at DIV-4 /-5.

Various concentrations of PbTx-2 were added to the culture medium at 3 h after plating.

Neurons were fixed and labeled diolistically using the Helios Gene gun system.

(B) Effect of PbTx-2 on dendritic arborization. Automated three-dimensional sholl analysis was performed using Imaris software which characterizes arbor structure and complexity.

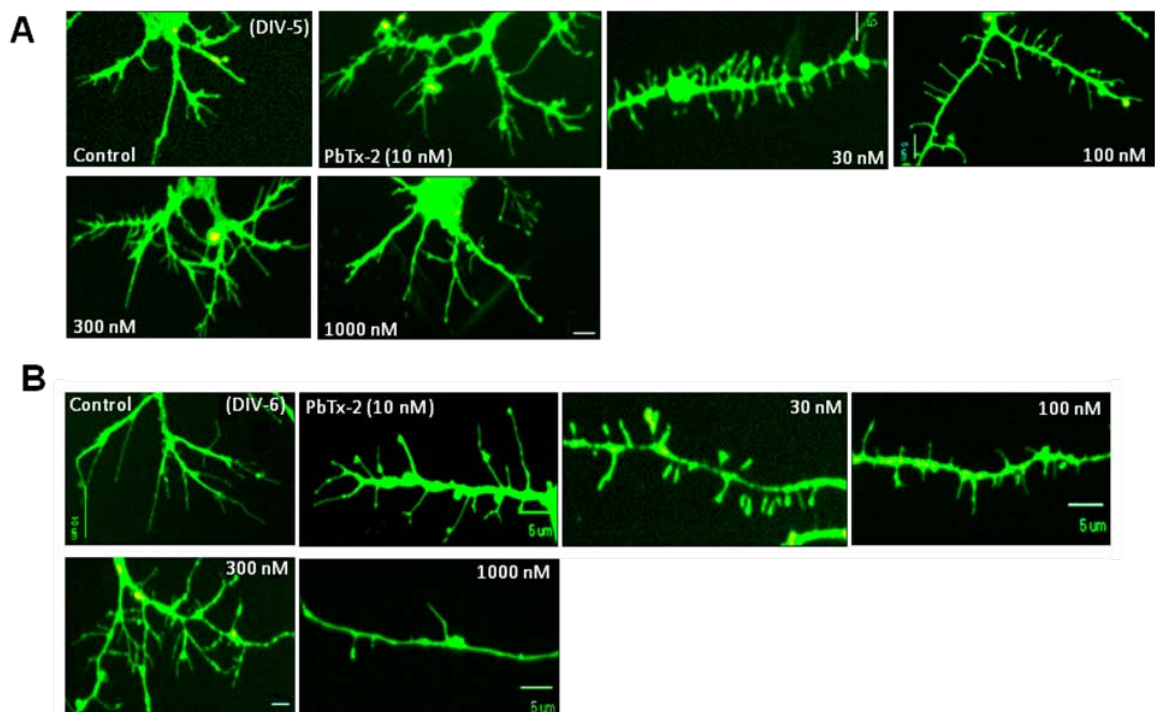
(C) Area under the curve (AUC) analysis of Sholl data shown in B. PbTx-2 30 and 100 nM significantly enhanced dendritic complexity compared to control neurons.

The experiment was performed thrice, and each point represents the mean value derived from analysis of 30-40 neurons. (ANOVA, P value=0.0008, Dunnett's post hoc test)

**(D)** Analysis of the number of dendritic branch points **(E)** and dendritic protrusions. Each value represents the mean  $\pm$  SEM of 20-30 neurons. \*,  $P < 0.05$ , Student's  $t$  test.

**(F)** Pharmacological evaluation of PbTx-2 (30 nM)-induced dendritic arborization. Sholl analysis of dendritic arbors. The 30 nM PbTx-2 exposure was examined in the presence of TTX (1  $\mu$ M), MK-801 (1  $\mu$ M), STO-609 (2.6  $\mu$ M), or nifedipine (1  $\mu$ M) beginning at 3 h after plating. Each data point represents mean  $\pm$  SEM of 50-60 neurons.

**(G)** AUC analysis of the data shown in *F*. PbTx-2 enhanced dendritic arbor development was significantly attenuated by MK-801 and TTX. \*,  $P < 0.05$ , Student's  $t$  test.



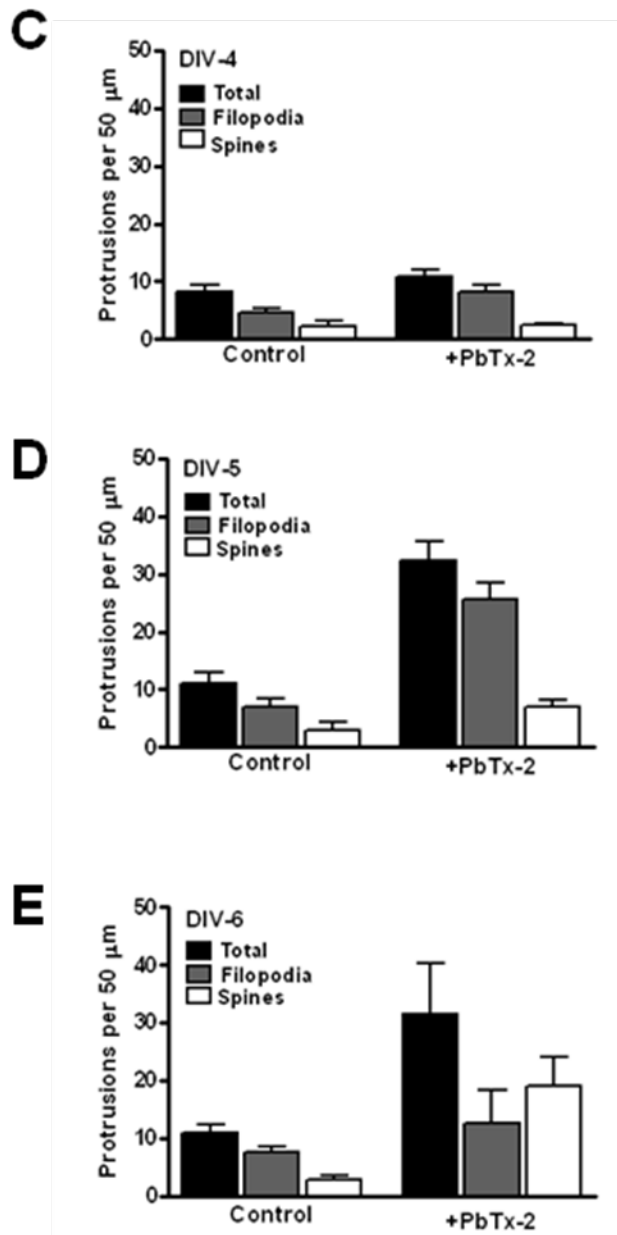


**Figure 5. PbTx-2 enhances spinogenesis by stimulating increased filopodia formation.**

(A) Representative images (Scale bar, 5  $\mu$ m) of DiI- labeled cerebrocortical neurons at DIV-5 (B) and DIV-6. PbTx-2 concentration- response relationship measuring dendritic protrusion density (protrusions per 50  $\mu$ m dendritic length) is shown. (C,D)

Analysis of dendritic protrusions with a defined algorithm (*See Methods*) for length and head diameter and classified as filopodial and thin or stubby spine-like protrusions compared to total protrusions. PbTx-2 exposed neurons (**D**) on DIV-6 show a shift from filopodial type to thin or stubby-like protrusions. Each bar represents the mean  $\pm$  SEM of 20-30 neurons.

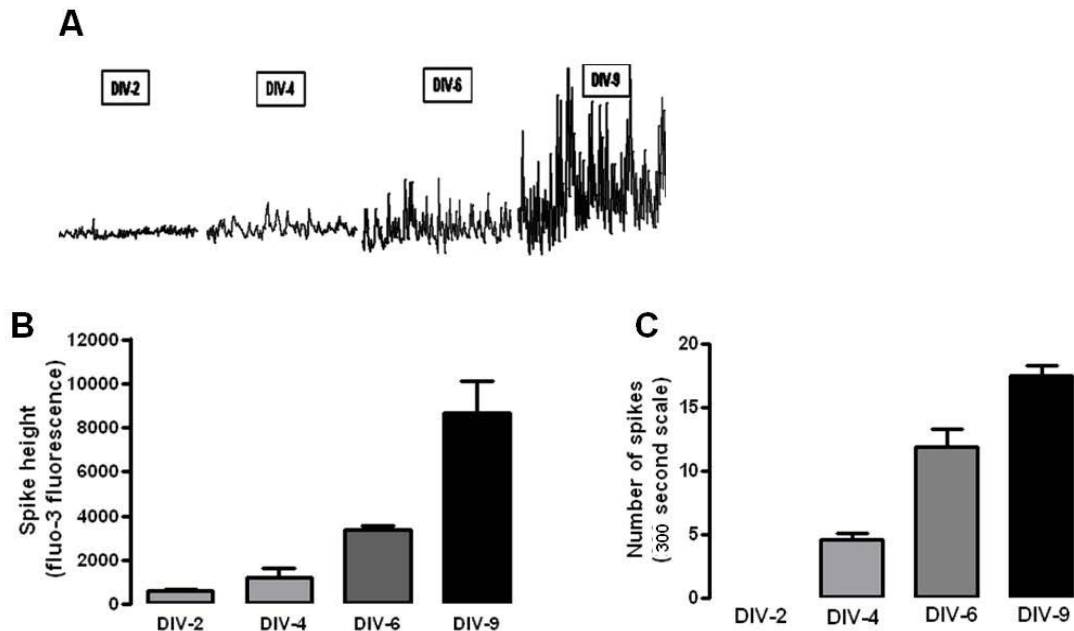


**Figure 6. Ontogeny of spontaneous Ca<sup>2+</sup> oscillations in cerebrocortical neurons.**

(A) Representative images showing spontaneous Ca<sup>2+</sup> oscillations at DIV-2,-4,-6 and -9 in Fluo-3 loaded neuronal cultures. (B, C) Bar graphs showing quantification of spontaneous Ca<sup>2+</sup> oscillations (B) mean  $\pm$ SEM of peak response (amplitude) (C) frequency of Ca<sup>2+</sup> oscillations (number of spikes per 300 sec, mean  $\pm$  SEM).  $n \geq 3$  independent experiments. These spontaneous Ca<sup>2+</sup> oscillations become prominent from DIV-6 onwards both in amplitude and frequency of oscillations.

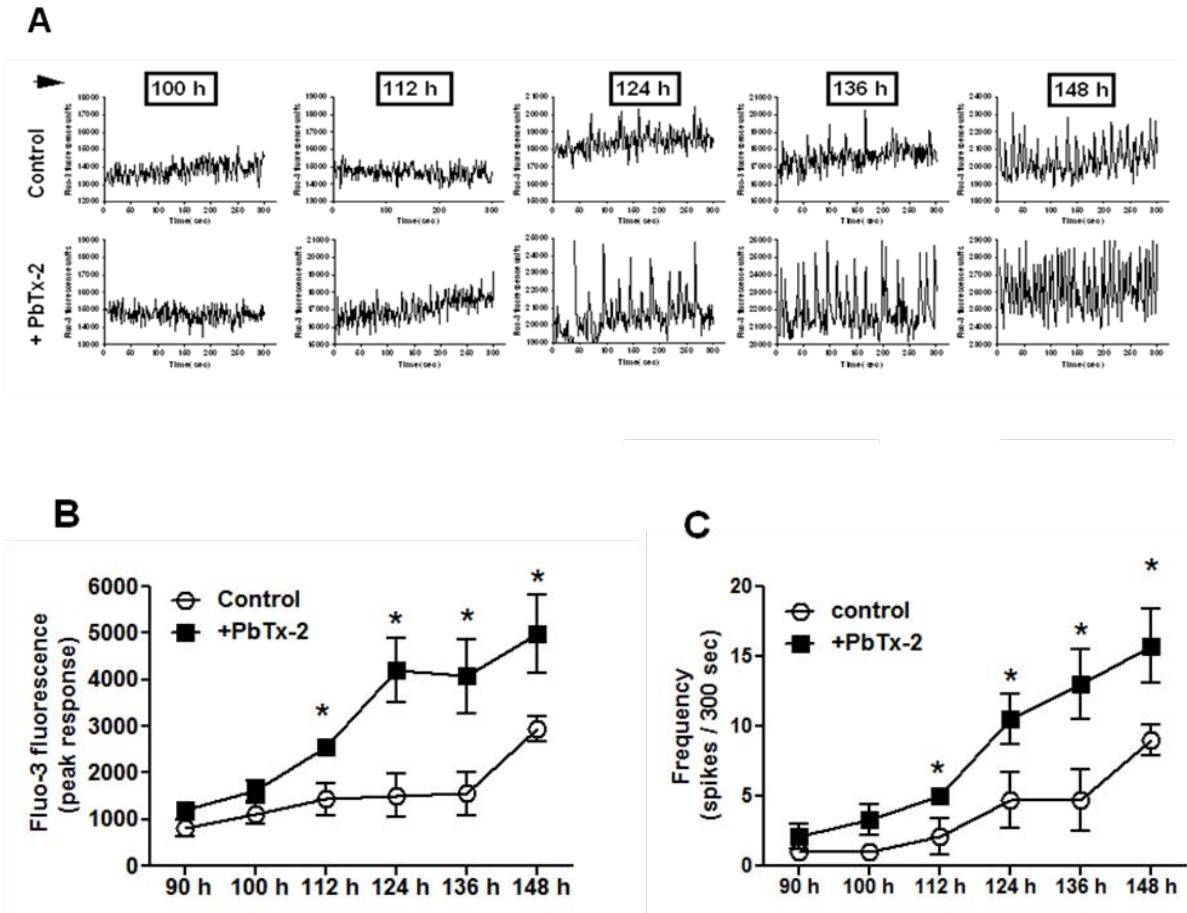
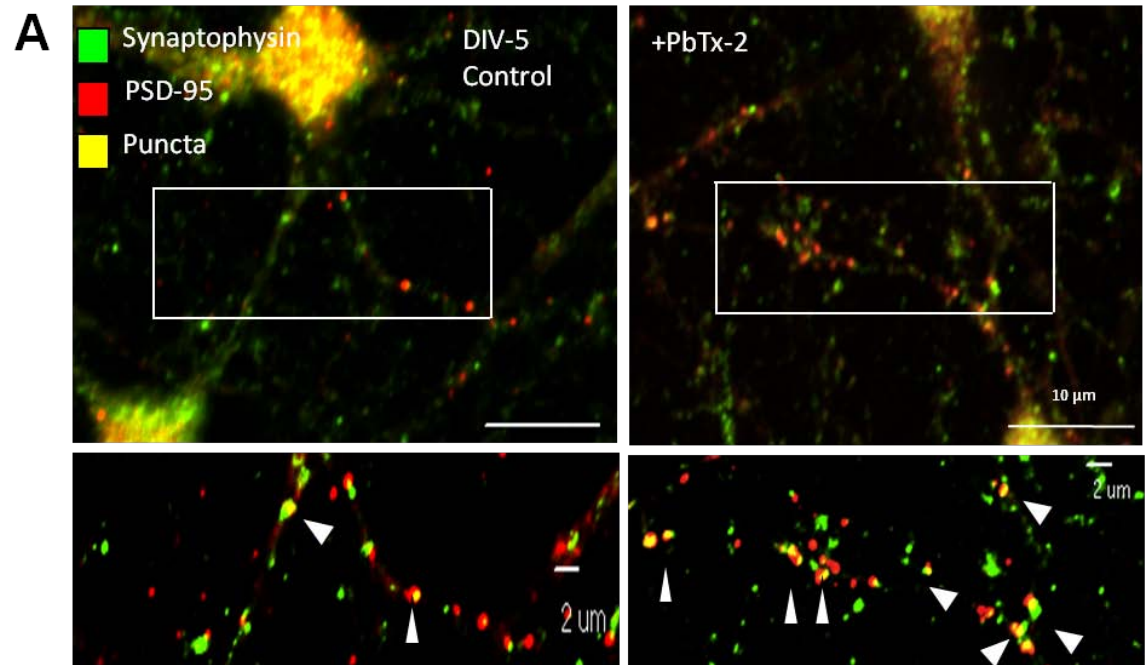


**Figure 7. PbTx-2 exposure accelerated the emergence of spontaneous  $\text{Ca}^{2+}$  oscillations.**

**(A)** Effect PbTx-2 (30 nM) on spontaneous  $\text{Ca}^{2+}$  oscillations. PbTx-2 was coincubated in alternate wells with controls in the same culture plate 3 h post plating and scanned for spontaneous  $\text{Ca}^{2+}$  oscillations in fluo-3 loaded neurons at the indicated time points. The data are a representative experiment performed in quadruplicate and repeated twice.

**(B, C)** Quantification of the data shown in **A**. **(B)** mean  $\pm$  SEM of peak response (amplitude) **(C)** frequency of  $\text{Ca}^{2+}$  oscillations (number of spikes per 300 sec, mean  $\pm$  SEM). PbTx-2 accelerated the emergence of spontaneous  $\text{Ca}^{2+}$  oscillations by 24 h

(DIV-5) by shifting both the amplitude and frequency of spontaneous  $\text{Ca}^{2+}$  oscillation curves to the left.



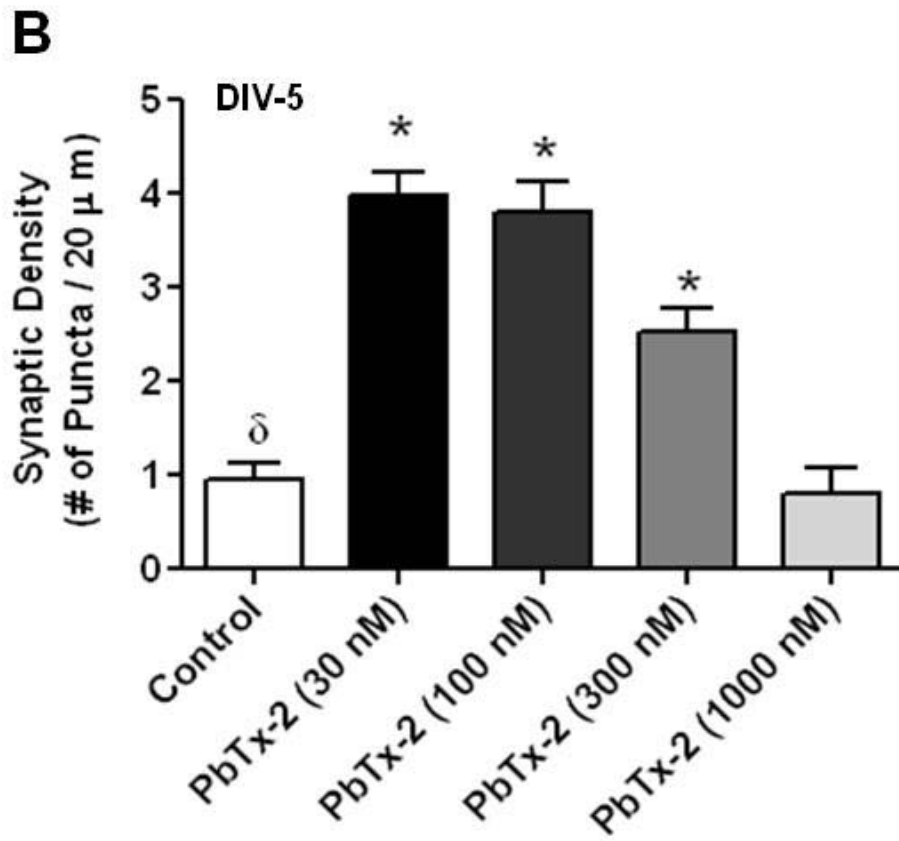
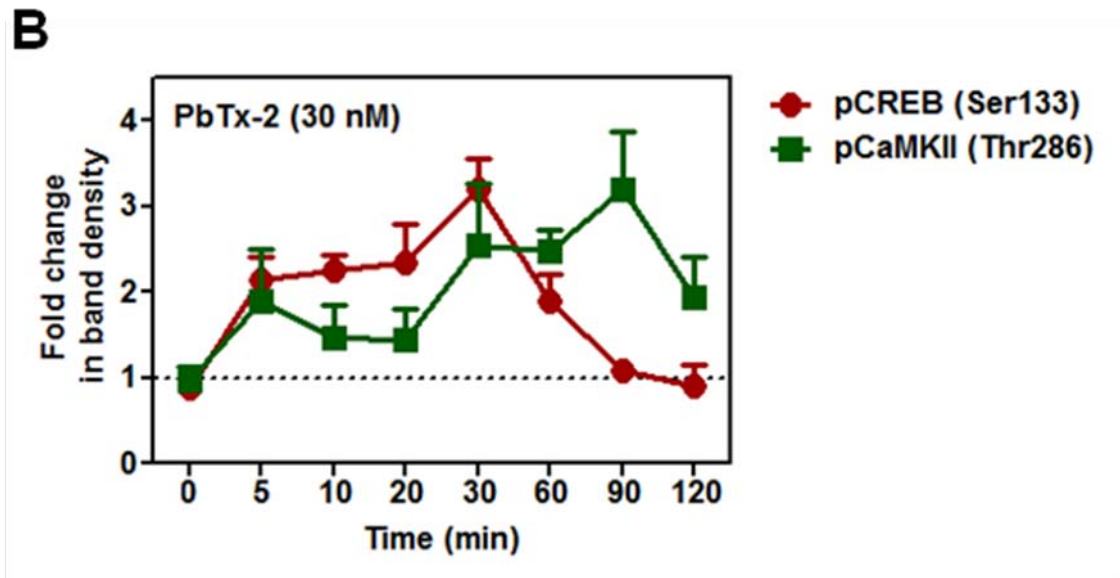
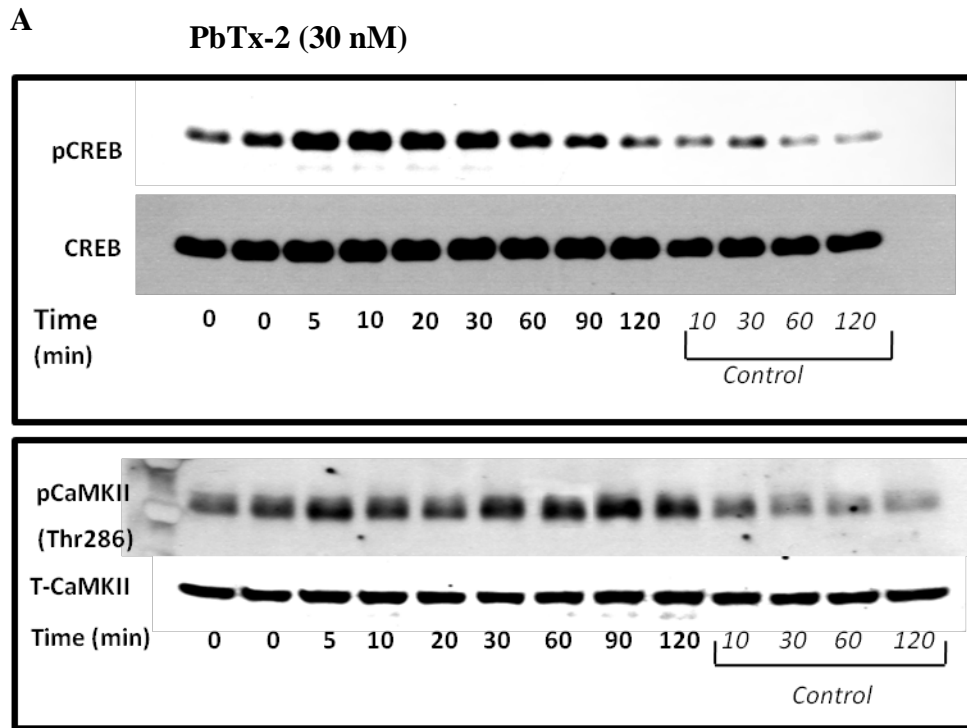


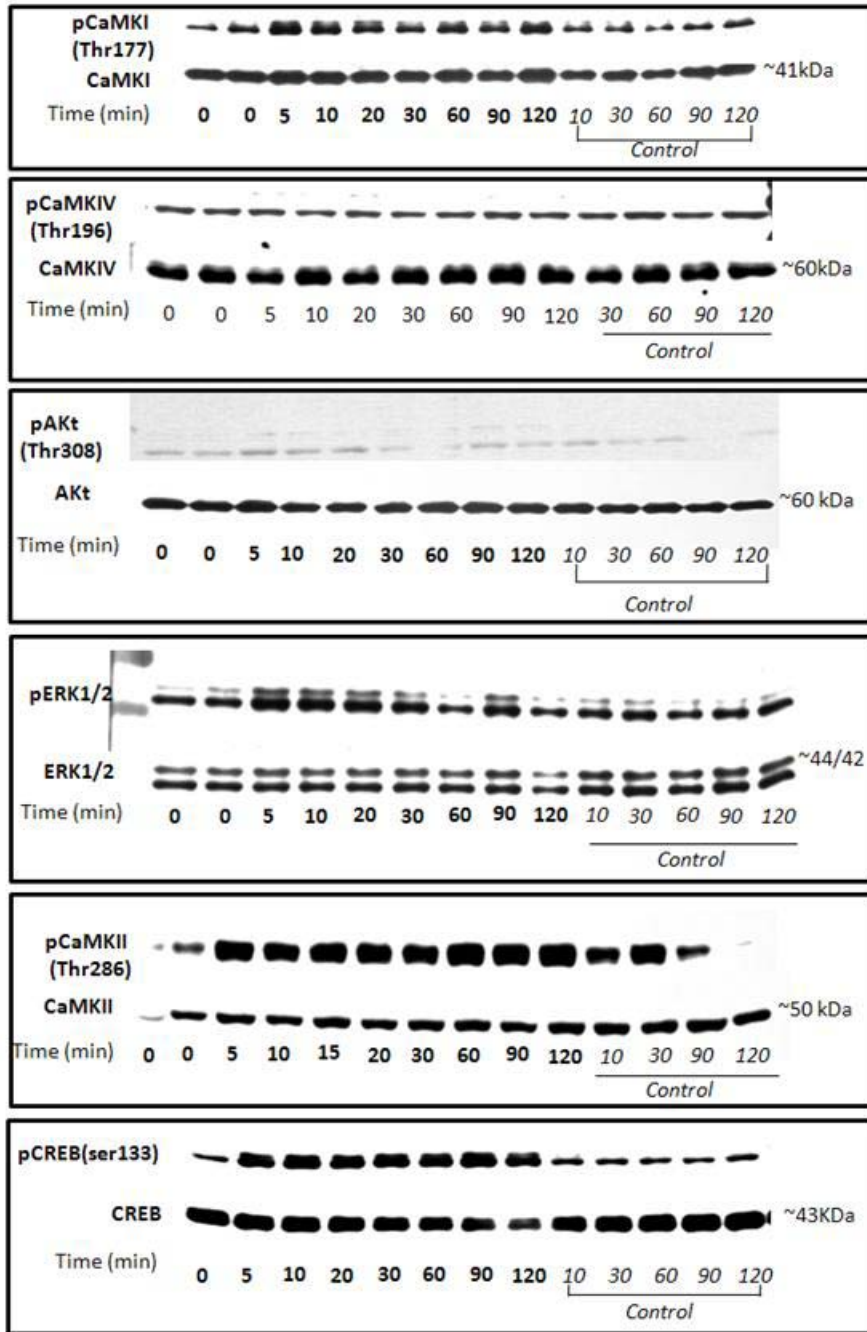
**Figure 8. Effect of PbTx-2 on formation of synapses in cerebrocortical neuron cultures.**

- (A) Representative images of double immunostained cerebrocortical neurons at DIV-6. Various concentrations of PbTx-2 were added to the culture medium at 3 h after plating. Antibodies against synaptophysin (presynaptic marker/green) and PSD-95 (post-synaptic marker/red) were used to quantify synapse density as indicated by colocalized fluorescent puncta (yellow). Confocal Z-stack images were deconvolved, background subtracted and quantified for colocalized puncta using slidebook® software.
- (B) Quantification of colocalized fluorescent puncta. To measure synapse density, total dendritic length 5  $\mu$ m away from the neuronal soma was measured in each frame and

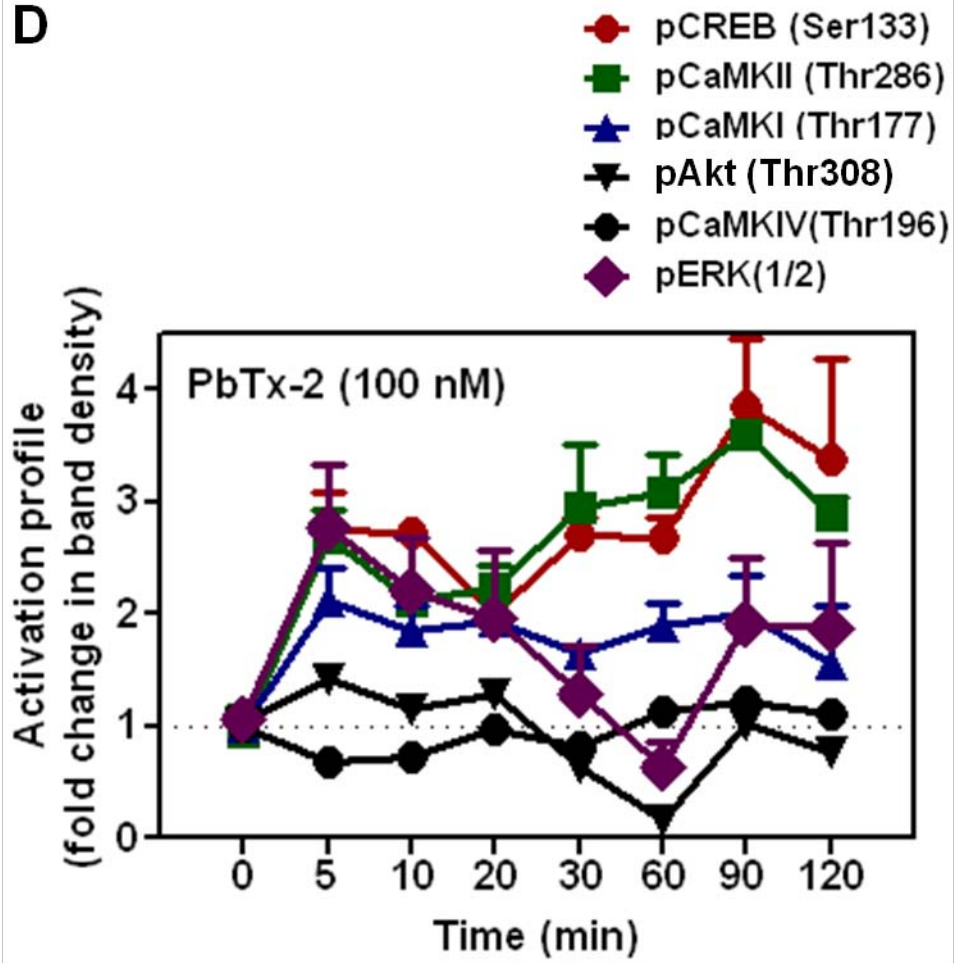
normalized to the number of synapses per 20  $\mu\text{m}$  dendritic length.  $n=3$  independent experiments with duplicate samples. (ANOVA  $P$  value  $>0.0001$ , Dunnett's post hoc test).

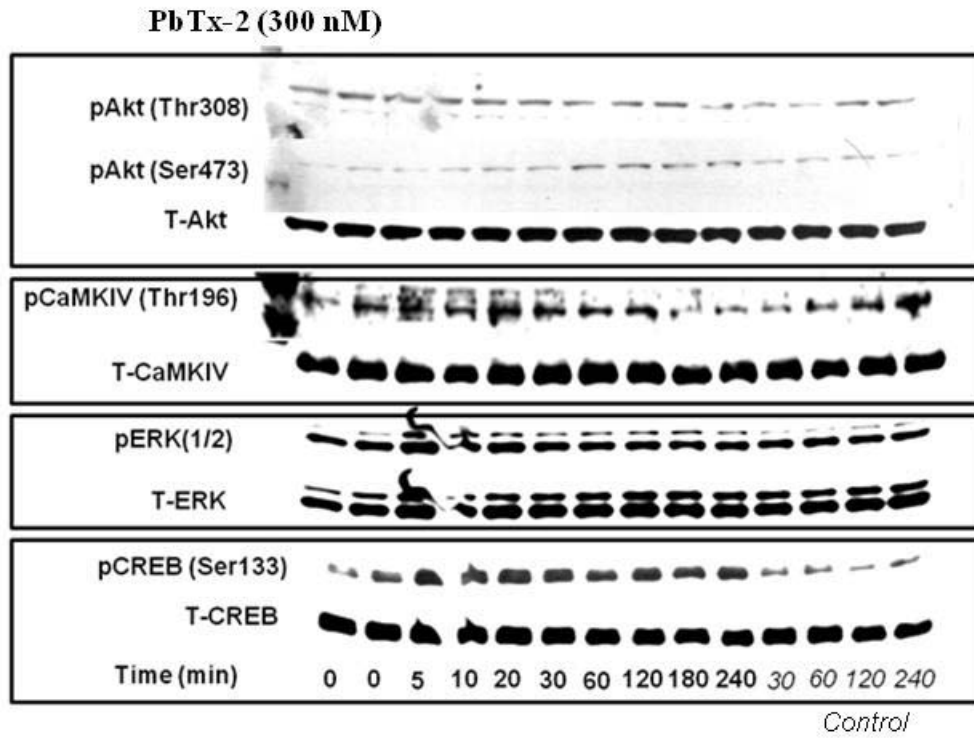
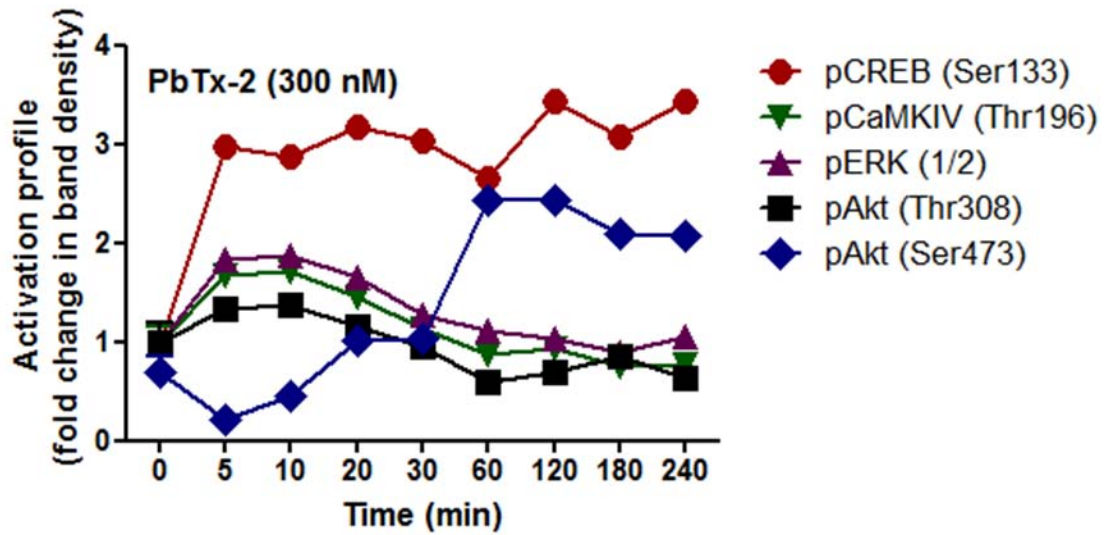


**C** PbTx-2 (100 nM)



D



**E****F**

**Figure 9. Signaling mechanisms underlying PbTx-2-induced neuronal plasticity.**

(A) Time-course analysis of PbTx-2 (30 nM)-induced phosphorylation and activation of CaMKII (Thr286) and CREB at Ser133 in DIV-1 cerebrocortical neurons. Representative Immunoblots are shown. (B) Quantitative analysis of relative band densities of immunoblots. n=3 independent experiments. Error bars, mean  $\pm$  SEM. (C)

Time-course profile of 100 nM PbTx-2-induced phosphorylation and activation of CaMKII (Thr286), CaMKI (Thr177), CaMKIV(Thr196), Akt (Ser473) and CREB (Ser133). Representative immunoblots are shown. (D) PbTx-2 (100 nM) induced activation profile of CaMKs and CREB. Relative band densities of immunoblots are plotted. Each point represents mean  $\pm$  SEM of 3 independent experiments. (E)

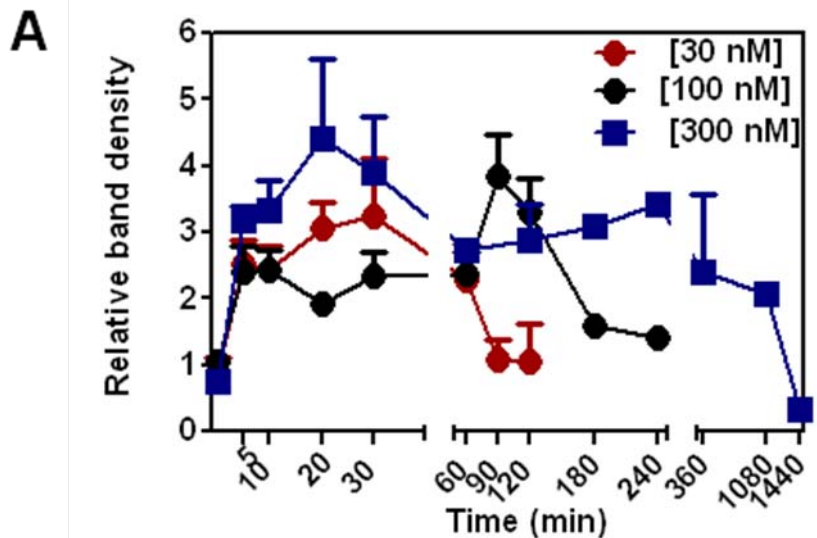
Immunoblot analysis and (F) quantification of 300 nM PbTx-2 induced phosphorylation and activation of Akt (Ser473), Akt (Thr308) and CaMKIV (Thr196). n=2 independent experiments.

Immunoblot analysis and (F) quantification of 300 nM PbTx-2 induced phosphorylation and activation of Akt (Ser473), Akt (Thr308) and CaMKIV (Thr196). n=2 independent experiments.

Immunoblot analysis and (F) quantification of 300 nM PbTx-2 induced phosphorylation and activation of Akt (Ser473), Akt (Thr308) and CaMKIV (Thr196). n=2 independent experiments.

Immunoblot analysis and (F) quantification of 300 nM PbTx-2 induced phosphorylation and activation of Akt (Ser473), Akt (Thr308) and CaMKIV (Thr196). n=2 independent experiments.

Immunoblot analysis and (F) quantification of 300 nM PbTx-2 induced phosphorylation and activation of Akt (Ser473), Akt (Thr308) and CaMKIV (Thr196). n=2 independent experiments.



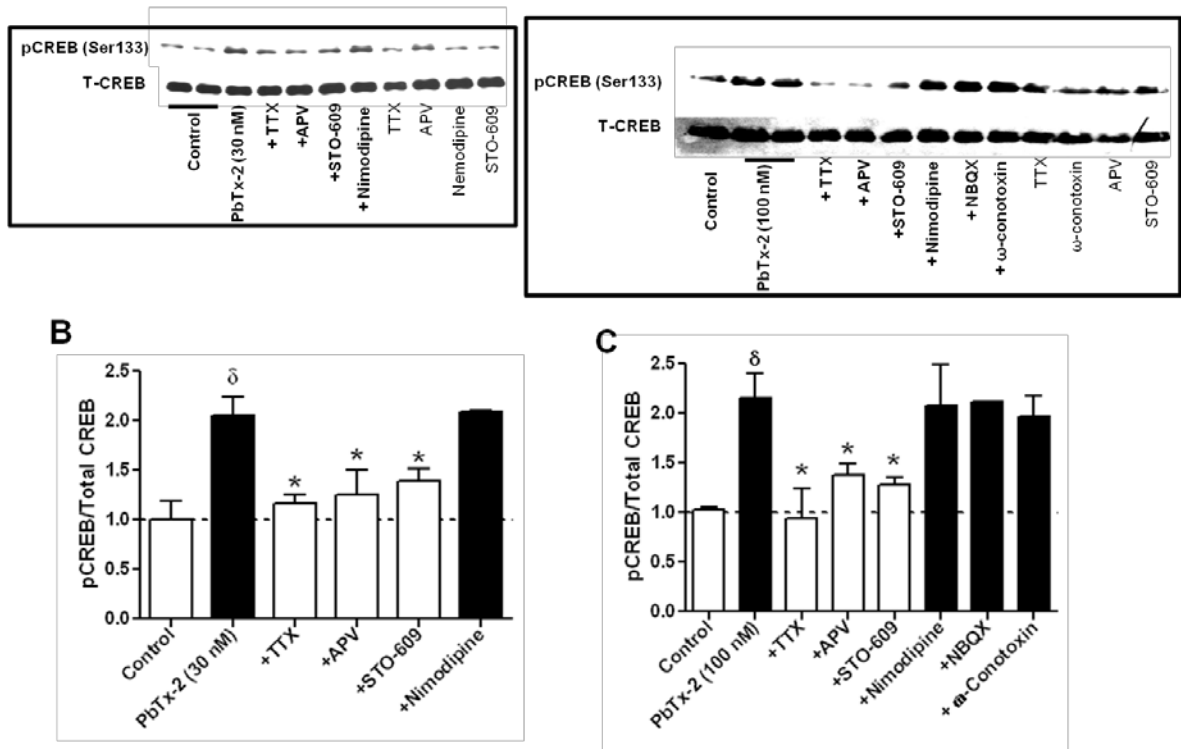
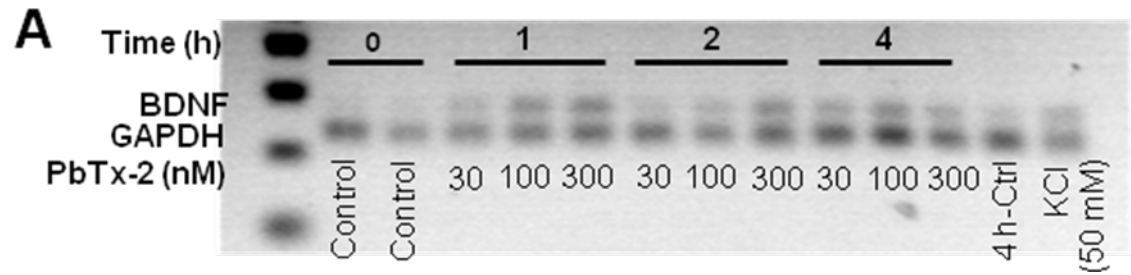


**Figure 10. PbTx-2-induced concentration-dependent activation of CREB (Ser133) and pharmacological evaluation of CREB phosphorylation**

(A) Time-response analysis of CREB (Ser133) phosphorylation following 30, 100 and 300 nM PbTx-2 exposure. Relative band densities were pooled from respective immunoblotting. Each point represents mean  $\pm$  SEM of 3 independent experiments.

(B, C) Pharmacological evaluation of (B) 30 nM and (C) 100 nM PbTx-2-induced CREB activation. Neuronal cultures were treated with either 30 nM PbTx-2 for 10 min or 100 nM PbTx-2 for 30 min in the presence and absence of TTX (1  $\mu$ M), MK-801 (1  $\mu$ M) or APV (100  $\mu$ M), NBQX (5  $\mu$ M), STO-609 (2.6  $\mu$ M), nimodipine (1  $\mu$ M) or  $\omega$ -conotoxin (1  $\mu$ M). Representative immunoblots and quantification of relative band densities are shown. Mean  $\pm$  SEM, n=2 independent experiments. \*, P value < 0.05 versus PbTx-2 response, Student t test.



**B**

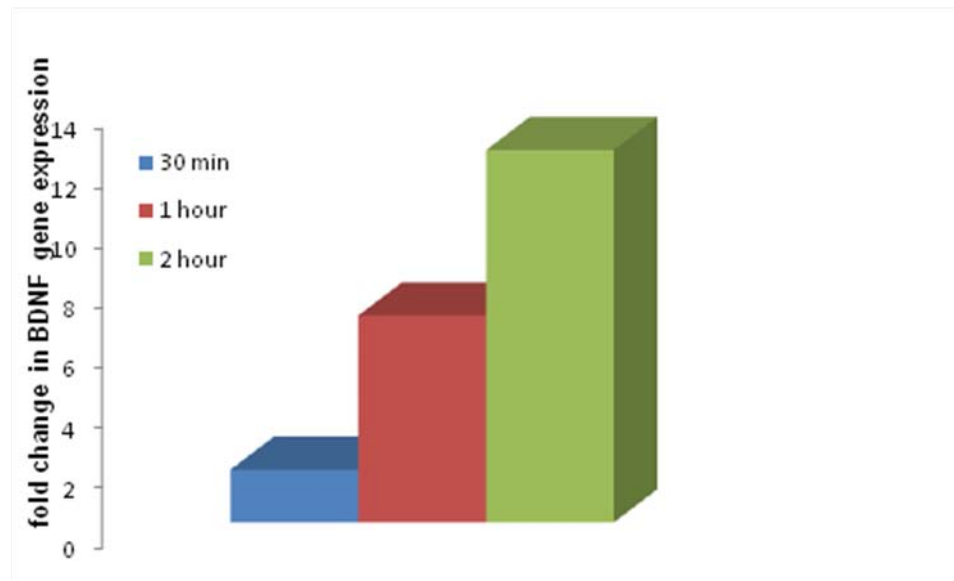


**Figure 11. PbTx-2 increases BDNF mRNA expression in a time and concentration-dependent manner.**

(A) Conventional RT-PCR in DIV-1 cerebrocortical neurons showed a time and concentration dependent increase in BDNF mRNA level expression.

(B) qRT-PCR revealed a time dependent increase in BDNF mRNA levels following exposure to 30 nM PbTx-2.

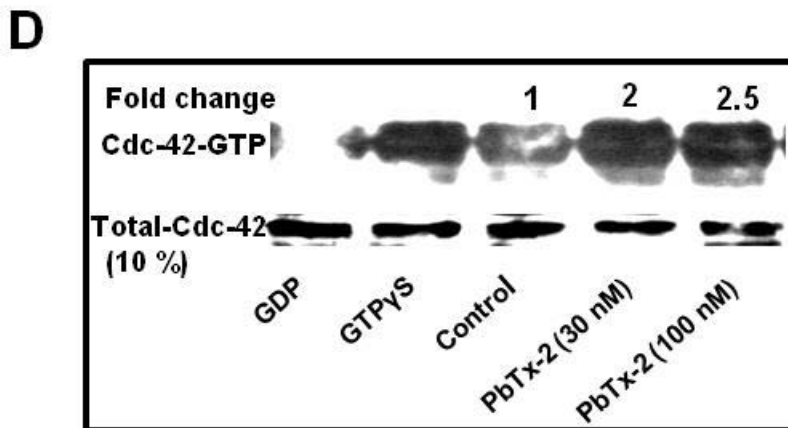
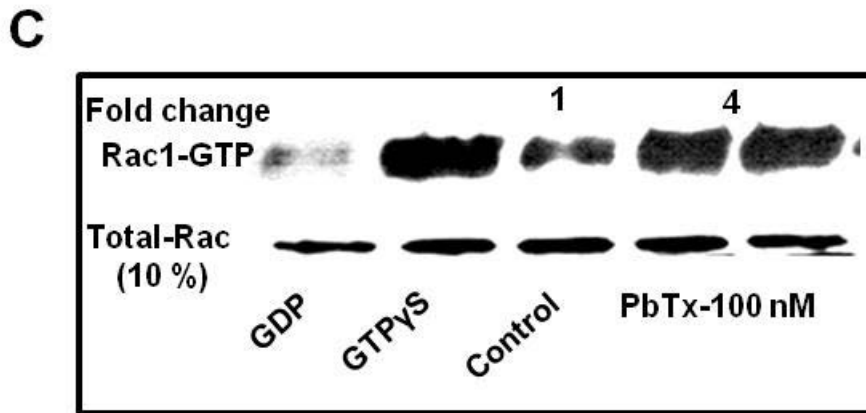
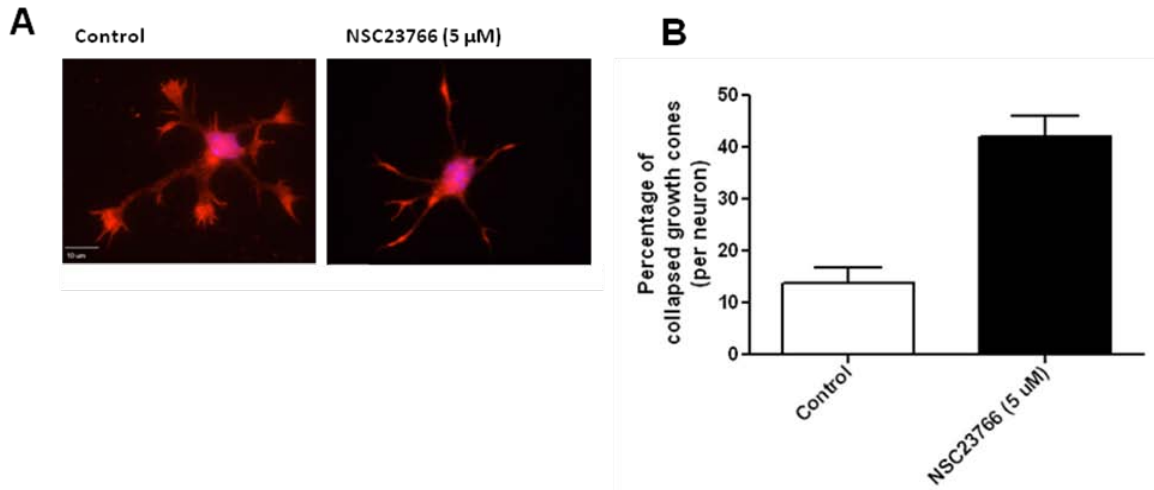


**Figure 12. Involvement of Rho family GTPases.**

- (A) NSC23799 (5  $\mu$ M) significantly increased neuronal growth cone collapse, indicating the requirement of Rac1 in growth cone dynamics. NSC23799 (5  $\mu$ M) was added to the culture medium 3 h post plating. Neurons were fixed at 16 h and stained for F-actin with Rhodamine- conjugated phalloidin to visualize growth cone morphology. Representative images are shown. (B) Quantification of growth cone collapse. Each bar represents Mean  $\pm$  SEM of 170-250 neurons from 2 independent experiments. \*, P value < 0.05, Student's *t* test.
- (C) Activation of Rac1 in DIV-1 neurons following PbTx-2 exposure was measured by performing Rac-GTP pull down assay. PbTx-2 (100 nM) exposure increased Rac-GTP levels by 4 fold compared to control within 30 min.
- (D) PbTx-2 induced Cdc-42 activation. PbTx-2 (30 nM and 100 nM) exposure increased Cdc42-GTP levels by 2-2.5 fold compared to control.

## CHAPTER 4

### Summary and conclusions

Neuronal activity regulates morphology and connectivity of neurons during development. The mechanisms by which neurons decode neuronal activity into activation of the signaling pathways that regulate morphological complexity are unclear. However, CaMKs and MAPKs are involved in mediating Ca<sup>2+</sup>-dependent signaling events, either by acting locally to modulate actin dynamics or by activation of nuclear signaling and gene transcription. Many aspects of activity-dependent neuronal development such as dendritic arborization, spinogenesis and synaptogenesis are mediated through NMDA receptor-dependent Ca<sup>2+</sup> signaling mechanisms.

NMDAR-mediated activation of CaMKII has been found to be important for activity-dependent spine plasticity, induction of LTP and in developing neurons, regulation of dendritic complexity. NMDA receptor-dependent CaMKK/CaMKI signaling cascades have moreover, been shown to regulate axonal growth and growth cone dynamics (Wayman et al., 2004), activity-dependent synaptogenesis (Saneyoshi et al., 2008), and Ca<sup>2+</sup>-dependent ERK activation and dendritic growth (Schmitt et al, 2004; Wayman et al, 2006). NMDARs, therefore, play a critical role in activity-dependent development and plasticity, dendritic arborization, spine morphogenesis, and synapse formation by stimulating these calcium-dependent pathways.

Recent studies have indicated that changes in intracellular sodium concentration produced in the soma and dendrites as a result of neuronal activity may act as a signaling

molecule and play a role in activity-dependent synaptic plasticity. It has been shown that synaptic stimulation causes  $[Na^+]_i$  increments of 10 mM in dendrites and of upto 35-40 mM in dendritic spines (Rose and Konnerth.,2001). A recent study has demonstrated the presence of spine sodium channels in neocortical pyramidal neurons (Araya et al., 2007). In hippocampal neurons intracellular  $[Na^+]_i$  increments have been demonstrated to increase NMDAR-mediated whole-cell currents and NMDAR single channel activity by increasing both channel open probability and mean open time. This  $[Na^+]_i$  mediated upregulation of NMDAR function has been shown to require Src kinase activation (Yu and Salter, 1998). Src family kinases act as a crucial point of convergence for signaling pathways that enhance NMDAR activity, and, by upregulating the function of NMDARs, Src gates the production of NMDAR-dependent synaptic potentiation and plasticity (Salter and Kalia, 2004).

We reasoned that  $[Na^+]_i$  may act as a positive regulator of developmental plasticity in immature cerebrocortical neurons. In the present study we used brevetoxin (PbTx-2), a voltage-gated sodium channel (VGSC) activator, to manipulate  $[Na^+]_i$  in immature murine cerebrocortical neurons. Brevetoxins interact with neurotoxin site 5 on the  $\alpha$ -subunit of VGSCs (Catterall and Gainer, 1985; Poli et al., 1986) and augment sodium influx through VGSCs by shifting the activation potential to more negative values, increasing the mean open time of the channel and inhibiting channel inactivation (Jeglitsch et al., 1998). The objectives of the present study were based on the central hypothesis that sodium channel activators are capable of mimicking activity-dependent regulation of neuronal development by upregulating NMDA receptor signaling pathways. Upregulation of NMDA receptor signaling pathways influence neuronal growth and

plasticity. Voltage-gated sodium channel activators may represent a novel pharmacologic strategy to regulate neuronal plasticity through NMDA receptor and Src family kinase-dependent mechanism.

The specific hypotheses of the present study were (1) Sodium channel activation augments NMDA receptor function and promotes neurite outgrowth in immature cerebrocortical neurons.

(2) Sodium channel activation regulates spontaneous  $\text{Ca}^{2+}$  oscillations, spinogenesis and synaptogenesis in cerebrocortical neurons. The specific aims under the first hypothesis were to (i)

Investigate the mechanisms underlying the influence of  $[\text{Na}^+]_i$  on NMDA receptor signaling in immature cerebrocortical neurons, (ii) Characterize the mechanisms underlying VGSC influence on neurite outgrowth, and under second hypothesis, (iii) Determine the temporal correlation between synchronous  $\text{Ca}^{2+}$  oscillations, spinogenesis and synaptogenesis in cerebrocortical neurons, (iv) Delineate the signaling pathways involved in PbTx-2 regulation of spinogenesis and synaptogenesis.

First, we assessed a model system to probe the interaction between voltage-gated sodium channels and NMDA receptors in immature cerebrocortical neurons. Inasmuch as immature neurons exhibited decreased vulnerability to excitotoxicity both *in vivo* and *in vitro*, we examined the vulnerability to NMDA-induced excitotoxicity as a function of cerebrocortical culture age. We assessed NMDA-induced LDH efflux, a biochemical index for neuronal injury, as a function of development in culture. At 2, 4 and 6 days *in vitro* (DIV) cerebrocortical cultures showed little sensitivity to NMDA-induced LDH efflux; however, DIV-9 cerebrocortical neurons showed marked sensitivity to LDH

efflux. To confirm the LDH efflux data, fluorescein diacetate staining was used to allow visualization and quantification of viable neurons. In DIV-2 and DIV-9 cerebrocortical neurons, the viable cell count data derived from fluorescein diacetate staining was well correlated with the LDH efflux data and provided confirmation of NMDA-induced excitotoxicity in DIV-9 cerebrocortical neurons. Due to their insensitivity to NMDA-induced excitotoxicity despite the presence of NMDARs and a functional glutamatergic system at this stage, DIV-2 cerebrocortical cultures were selected as a model system to explore the influence of sodium on NMDA receptor signaling.

Prior to the investigation of the influence of PbTx-2 on NMDA-induced  $\text{Ca}^{2+}$  influx, we assessed the effect of PbTx-2 alone on  $\text{Ca}^{2+}$  dynamics in DIV-2 cerebrocortical neurons. PbTx-2 alone, at a concentration of 30 nM, did not affect  $\text{Ca}^{2+}$  dynamics in DIV-2 cerebrocortical neurons; however, this treatment robustly potentiated NMDA-induced  $\text{Ca}^{2+}$  influx. The NMDA concentration-response curves for  $\text{Ca}^{2+}$  influx were significantly leftward shifted by 30 nM PbTx-2. These data suggest that PbTx-2 sensitizes cerebrocortical neurons to NMDA-induced  $\text{Ca}^{2+}$  influx. Based on these results, a concentration of 30 nM PbTx-2 was selected to further probe the potential influence of sodium on NMDAR signaling. Further pharmacological evaluation confirmed the involvement of VGSCs and NMDARs in PbTx-2 enhancement of NMDA-induced  $[\text{Ca}^{2+}]_i$ . We used the specific Src kinase inhibitor PP2 and immunoblotting for tyrosine phosphorylation of Src to demonstrate that PbTx-2 potentiation of NMDA-induced elevation of  $[\text{Ca}^{2+}]_i$  was dependent on Src. Inasmuch as  $[\text{Na}^+]_i$  act as a putative regulator of NMDAR-mediated signaling, we assessed PbTx-2-induced elevation of  $[\text{Na}^+]_i$  in DIV-2 cerebrocortical neurons loaded with SBFI. PbTx-2 produced concentration-dependent

increments in  $[Na^+]_i$ . The *in situ* SBFI calibration showed that the basal  $[Na^+]_i$  in DIV-2 cerebrocortical neurons was  $8.1 \pm 0.32$  mM. The 30 nM PbTx-2 treatment produced a maximum  $[Na^+]_i$  of  $16.9 \pm 1.5$  mM representing an increment of  $8.8 \pm 1.8$  mM over basal. Consistent with previous findings (Yu and Salter, 1998; Xin et al., 2005), the increment of  $[Na^+]_i$  detected in immature cerebrocortical neurons appears sufficient to upregulate NMDAR signaling. To ascertain the magnitude of PbTx-2-induced membrane depolarization, we assessed PbTx-2 induced membrane potential changes in DIV-2 cerebrocortical neurons using a membrane-potential sensitive fluorescence dye, FMP blue. The corresponding membrane potential change produced by 30 nM PbTx-2 was modest and therefore was insufficient to relieve the voltage-dependent  $Mg^{2+}$  block of NMDARs. To unambiguously demonstrate the enhancement of NMDA receptor function by PbTx-2, we recorded single-channel currents from cell-attached patches. PbTx-2 treatment was found to increase both the mean open time and open probability of NMDA receptors. These effects of PbTx-2 on NMDA receptor function were dependent on extracellular  $Na^+$  and activation of Src kinase. The functional consequences of PbTx-2-induced enhancement of NMDAR function were evaluated in immature cerebrocortical neurons. PbTx-2 concentrations between 3 and 300 nM enhanced neurite outgrowth. The PbTx-2 concentration-response curve for total neurite outgrowth exhibited a hormetic profile with the peak response at 30 nM. Pharmacological studies showed that the PbTx-2 enhanced neurite outgrowth involves elevation of  $[Na^+]_i$  following activation of sodium channels, enhancement of NMDA receptor signaling and engagement of the CaMKK pathway. Voltage-gated sodium channel activators may accordingly represent a novel

pharmacologic strategy to regulate neuronal plasticity through an NMDA receptor and Src family kinase-dependent mechanism.

We further assessed the influence of PbTx-2 on spontaneous synchronized  $\text{Ca}^{2+}$  oscillations as a measure of functional synaptogenesis and neuronal connectivity. Preliminary studies showed that these oscillations become prominent from DIV-6 onwards. Inasmuch as 30 nM PbTx-2 treatments produced augmentation of NMDA-induced  $\text{Ca}^{2+}$  dynamics with enhancement of neurite outgrowth, we investigated the influence of 30 nM PbTx-2 on spontaneous  $\text{Ca}^{2+}$  oscillations. PbTx-2 accelerated the emergence of synchronized  $\text{Ca}^{2+}$  oscillations by 24 h (DIV-5). Inasmuch as synchronized  $\text{Ca}^{2+}$  oscillations reflect formation of functional synapses and a neuronal network; we assessed the effect of PbTx-2 on neuronal morphology. For morphological studies, we employed Diolistic labeling using a Helios Gene Gun to randomly fill neurons by intracellular delivery of tungsten particles coated with lipophilic carbocyanine (DiI) dyes. PbTx-2 enhanced dendritic arbor development as well as, spinogenesis by stimulating dendritic filopodia formation. Further, we assessed the signaling mechanisms underlying PbTx-2 induced neuronal plasticity. Immunoblotting experiments revealed phosphorylation and activation of CaMKI (Thr177) and CaMKII (Thr286) following PbTx-2 exposure. PbTx-2 also induced ERK1/2 phosphorylation. CREB is known to be an activity-regulated transcription factor, and PbTx-2 exposure increased CREB phosphorylation at Ser133. As BDNF gene expression is regulated by CREB dependent transcription, we assessed the BDNF mRNA expression level and this was found to be increased in a time-and concentration-dependent manner with PbTx-2 exposure. We next assessed the effect of PbTx-2 on actin dynamics. Members of Rho

family GTPases, Cdc-42 and Rac1, were both activated within 30 min of PbTx-2 exposure. PbTx-2 induced neuronal plasticity therefore involves actin remodeling. These findings suggest that the influence of a sodium channel activator on neuronal development involves NMDAR-mediated CaMK signaling with downstream activation of CREB-dependent transcription of BDNF and Rac/Cdc-42 signaling for actin remodeling.

The PbTx-2 induced neurite outgrowth, dendritic arbor development and synapse formation- all exhibited biphasic concentration-response profiles with 30 and 100 nM PbTx-2 having the most robust effect. To explore the mechanism underlying this hormetic profile, we investigated the influence of PbTx-2 on cell surface expression of VGSCs and NMDARs. [<sup>3</sup>H] batrachotoxin binding to neurotoxin site2 was used to label VGSCs. QX-314, a quaternary lidocaine derivative, was used to define the cell surface component of [<sup>3</sup>H] batrachotoxin binding. Exposure to 30 nM PbTx-2 increased cell surface expression of VGSC at 12 h, whereas 1 μM PbTx-2 produced a sequestration of cell surface VGSCs. The ability of high PbTx-2 concentrations to promote VGSC internalization may contribute to the biphasic concentration response profiles. A biotinylation assay was then used to assess the acute effects of PbTx-2 on cell surface expression of NMDAR NR2B subunits and TrkB receptors. Cell surface expression of NR2B subunits and TrkB receptors were acutely increased following PbTx-2 exposure. PbTx-2 treatment might be therefore sensitizing neurons to the neurotrophic effects of glutamate and BDNF. These data suggest that enhancing NMDAR activity through elevation of intracellular sodium promotes neuronal structural plasticity in a biphasic profile by engaging manifold signaling mechanisms.